DOT/FAA/AR-02/35

Office of Aviation Research
Washington, D.C. 20591

Statistical Loads Data for the Airbus A-320 Aircraft in Commercial Operations

April 2002

Final Report

This document is available to the U.S. public through the National Technical Information Service (NTIS), Springfield, Virginia 22161.



U.S. Department of Transportation
Federal Aviation Administration

NOTICE

This document is disseminated under the sponsorship of the U.S. Department of Transportation in the interest of information exchange. The United States Government assumes no liability for the contents or use thereof. The United States Government does not endorse products or manufacturers. Trade or manufacturer's names appear herein solely because they are considered essential to the objective of this report. This document does not constitute FAA certification policy. Consult your local FAA aircraft certification office as to its use.

This report is available at the Federal Aviation Administration William J. Hughes Technical Center's Full-Text Technical Reports page: actlibrary.tc.faa.gov in Adobe Acrobat portable document format (PDF).

Technical Report Documentation Page

1. Report No.	2. Government Accession No.	3. Recipient's Catalog No.
DOT/FAA/AR-02/35		

4. Title and Subtitle	
STATISTICAL LOADS DATA FOR THE AIRBUS A-320 AIRCRAFT IN COMMERCIAL OPERATIONS	April 2002
	6. Performing Organization Code

7. Author(s)	8. Performing Organization Report No.
John W. Rustenburg, Donald A. Skinn, and Daniel O. Tipps	UDR-TR-2001-00080

9. Performing Organization Name and Address	10. Work Unit No. (TRAIS)
University of Dayton Research Institute Structural Integrity Division 300 College Park Dayton, OH 45469-0120	RPD-510
	11. Contract or Grant No. Grant No. 00-G-015

12. Sponsoring Agency Name and Address	13. Type of Report and Period Covered
U.S. Department of Transportation Federal Aviation Administration Office of Aviation Research Washington, DC 20591	Final Report
	14. Sponsoring Agency Code ANM-110

15. Supplementary Notes

The Federal Aviation Administration William J. Hughes Technical Center Technical Monitor was Thomas DeFiore

16. Abstract

The University of Dayton is supporting the Federal Aviation Administration (FAA) research on the structural integrity requirements for the U.S. commercial transport airplane fleet. The primary objective of this research is to develop new and improved methods and criteria for processing and presenting large commercial transport airplane flight and ground loads usage data. The scope of activities performed involves (1) defining the service-related factors that affect the operational life of commercial aircraft; (2) designing an efficient software system to reduce, store, and process large quantities of optical quick-access recorder data; and (3) reducing, analyzing, and providing processed data in statistical formats that will enable the FAA to reassess existing certification criteria. Equally important, these new data will also enable the FAA, the aircraft manufacturers, and the airlines to better understand and control those factors that influence the structural integrity of commercial transport aircraft. Presented herein are Airbus A-320 aircraft operational usage data collected from 10,066 flights, representing 30,817 flight hours, as recorded by a single U.S. airline operator. Statistical data are presented on the aircraft's usage, flight and ground loads data, and systems operational data. The data presented in this report will provide the user with information about the accelerations, speeds, altitudes, flight duration and distance, gross weights, speed brake/spoiler cycles, thrust reverser usage, and gust velocities encountered by the Airbus A-320 during actual operational usage.

17. Key Words	18. Distribution Statement
Optical quick access recorder, Flight profiles, Flight loads, Ground loads, Systems operational data, Statistical loads data	This document is available to the public through the National Technical Information Service (NTIS), Springfield, Virginia 22161.

19. Security Classif. (of this report)	20. Security Classif. (of this page)	21. No. of Pages	22. Price
Unclassified	Unclassified	116	N/A

PREFACE

This research was performed by the Flight Systems Integrity Group of the Structural Integrity Division of the University of Dayton Research Institute (URDI) under Federal Aviation Administration (FAA) Grant No. 00-G-015 entitled "An Assessment of A-320 Operational Loads and Usage Characteristics and Automated Systems Effects." The Program Manager for the FAA was Mr. Thomas DeFiore of the FAA William J. Hughes Technical Center at Atlantic City International Airport, New Jersey, and the Program Technical Advisor was Mr. Terence Barnes of the FAA Aircraft Certification Office. Mr. Daniel Tipps was the Principal Investigator for the University of Dayton, provided overall technical direction for this effort, and assisted in preparation of the final report. Mr. Donald Skinn developed the data reduction algorithms, programmed the data reduction criteria, and performed the data reduction. Mr. John Rustenburg performed the data analysis, created the graphical presentations, and assisted in preparation of the final report.

While UDRI tries to use the same data reduction criteria when processing data from different aircraft types, there are circumstances when the criteria must be revised in order to accurately retrieve data associated with a desired event. One of these occurred in the identification of the liftoff and touchdown events. Specifically, when the squat switch indication was used on the Airbus A-320 as the criteria to determine when liftoff and touchdown occurred, the processed data showed that the squat switch did not provide an accurate indication of when these events actually occurred. Thus, UDRI conducted a study to determine if a better criteria could be developed for determining when these events occurred. The newly developed criteria used radio altitude to identify when liftoff occurred and time (5-seconds) prior to when the squat switch indication came on to identify when touchdown occurred.

The application of these new criteria provided good results, but all statistical data involving the A-320 aircraft operations during liftoff and touchdown that had been previously processed had to be redone. Of particular importance, when the new touchdown criteria were used, it was discovered that the vertical load factor data associated with the touchdown event had been previously processed as having occurred during the approach phase of the flight instead of at touchdown. Consequently, the previously processed gust velocity flight data reflected the response to occurrences of vertical load factors that should have been attributed to landing impact.

Based on these findings from the A-320 program, UDRI investigated the statistical data it had previously processed at touchdown for other aircraft types such as the B-737, MD-80, and B-767, and concluded that the new criteria for touchdown could affect the data presented in published reports for those aircraft. Thus, the statistical data presented in those reports may need to be updated using the new touchdown criteria. It is also possible that the gust velocity data contained in some of the earlier FAA/NASA documents could be affected by UDRI's findings. A list of these reports is presented on the next page.

PRIOR FAA JET TRANSPORTATION LOADS DATA REPORTS

Report Number:	Report Title:
DOT/FAA/AR-00/10	Statistical Loads Data for B-767 Aircraft in Typical Overseas Service, May 2000
DOT/FAA/AR-98/65	Flight Loads Data for a Boeing MD-82 in Commercial Operations, December 1998
DOT/FAA/AR-98/28	Statistical Loads Data for Boeing 737-400 Aircraft in Commercial Operations, August 1998
DOT/FAA/AR-95/21	Flight Loads Data for a Boeing 737-400 in Commercial Operation, April 1996
DOT/FAA-CT-89/36 – Volume I	The NASA Digital VGH Program – Exploration of Methods and Final Results, Volume I – Development of Methods, December 1989
DOT/FAA-CT-89/36 – Volume II	The NASA Digital VGH Program – Exploration of Methods and Final Results, Volume II – L1011 Data 1978-1979: 1619 HOURS, December 1989
DOT/FAA-CT-89/36 – Volume III	The NASA Digital VGH Program – Exploration of Methods and Final Results, Volume III – B727 Data 1978-1980: 1765 HOURS, December 1989
DOT/FAA-CT-89/36 – Volume IV	The NASA Digital VGH Program – Exploration of Methods and Final Results, Volume IV – B747 Data 1978-1980: 1689 HOURS, December 1989
DOT/FAA-CT-89/36 – Volume V	The NASA Digital VGH Program – Exploration of Methods and Final Results, Volume V – DC10 Data 1981-1982: 129 HOURS, December 1989

TABLE OF CONTENTS

		Page
EXECUTIVE SUMMARY		xiii
1.	INTRODUCTION	1
2.	AIRCRAFT DESCRIPTION	1
3.	AIRLINE DATA COLLECTION AND EDITING SYSTEMS	3
3.1	Airline Data Collection System	3
3.2	Airline Data Editing System	4
4.	UNIVERSITY OF DAYTON RESEARCH INSTITUTE DATA PROCESSING	4
4.1	Recorded Data Parameters	4
4.2	Computed Parameters	5
4.2.1	Atmospheric Density	5
4.2.2	Equivalent Airspeed	5
4.2.3	Dynamic Pressure (q)	6
4.2.4	Derived Gust Velocity (U_{de})	6
4.2.5	Continuous Gust Intensity (U_{σ})	7
4.2.6	Flight Distance	8
4.2.7	Rate of Climb	8
4.3	Data Reduction Operations	8
4.3.1	Initial Quality Screening	8
4.3.2	Time History Files	9
4.3.3	Relational Database	10
4.3.4	Permanent Data Files	11
4.3.5	Loads Data Reduction	11
4.4	Data Reduction Criteria	11
4.4.1	Phases of Flight Profile	11
4.4.2	Specific Events	13
4.4.3	Sign Conventions	15
4.4.4	Peak Selection Technique	16
4.4.5	Separation of Maneuver and Gust Load Factors	17
4.4.6	Flap Detents	17

5. DATA PRESENTATION 17

5.1 Aircraft Usage Data 21

5.1.1 Weight and Flight Distance Data 21
5.1.2 Altitude and Speed Data 22
5.1.3 Attitude and Rate Data 23

5.2 Ground Loads Data 24

5.2.1 Lateral Load Factor Data 25
5.2.2 Longitudinal Load Factor Data 26
5.2.3 Vertical Load Factor Data 27

5.3 Flight Loads Data 28

5.3.1 Gust Vertical Load Factor Data 29
5.3.2 Derived Gust Velocity Data 29
5.3.3 Continuous Gust Intensity Data 29
5.3.4 Gust V-n Diagram Data 29
5.3.5 Maneuver Vertical Load Factor Data 30
5.3.6 Maneuver V-n Diagram Data 30
5.3.7 Combined Maneuver and Gust Vertical Load Factor Data 31
5.3.8 Combined Maneuver and Gust Lateral Load Factor Data 31
5.3.9 Ground-Air-Ground Cycle Data 31

5.4 Systems Operational Data 31

5.4.1 Flap Usage Data 32
5.4.2 Speed Brake Usage Data 32
5.4.3 Landing Gear Data 33
5.4.4 Thrust Reverser Data 33
5.4.5 Brake Application Data 33
5.4.6 Propulsion Data 33

6. CONCLUSIONS 34

7. REFERENCES 34

APPENDICES

A—Data Presentation
B—Great Circle Distance Calculation

LIST OF FIGURES

Figure		Page
1	Airbus A-320 Three-View Drawing	2
2	Airline Recording and Editing System	3
3	Data Processing Flow Chart	9
4	Description of Flight Profile Phases	11
5	Sketch of Ground Phases and Specific Events	13
6	Sign Convention for Airplane Accelerations	15
7	The Peak-Between-Means Classification Criteria	16

LIST OF TABLES

Table		Page
1	Airbus A-320 Aircraft Characteristics	2
2	Recorded Parameters Provided to UDRI	4
3	Parameter Editing Values	10
4	Flight Phase Criteria	12
5	Summary of Specific Events Criteria	14
6	Flap Detents (Airbus A-320)	17
7	Statistical Data Formats	18

LIST OF SYMBOLS AND ABBREVIATIONS

$\overline{A}$	aircraft PSD gust response factor
a	speed of sound (ft/sec)
a_0	speed of sound at sea level (ft/sec)
$\overline{c}$	wing mean geometric chord (ft)
$\overline{C}$	aircraft discrete gust response factor
C_{L_α}	aircraft lift curve slope per radian
$C_{L_{max}}$	maximum lift coefficient
CAS	calibrated air speed
c.g.	center of gravity
D	integrated flight distance
EAS	equivalent airspeed
F(PSD)	continuous gust alleviation factor
g	gravity constant, 32.17 ft/sec^2
H_p	pressure altitude, (ft)
K_g	discrete gust alleviation factor, $0.88\ \mu/(5.3 + \mu)$
KCAS	knots calibrated air speed
KEAS	knots equivalent air speed
kts	knots
L	turbulence scale length (ft)
M	Mach number
M_{MO}	Maximum Mach number at altitude
N	number of occurrences for U_σ (PSD gust procedure)
N_0	number of zero crossings per nautical mile (PSD gust procedure)
N_1	fan (low pressure compressor) rotor speed (percentage of normal maximum turbine speed.)
N_2	turbine (high pressure compressor) rotor speed (percentage of normal maximum turbine speed)
nm	nautical mile
n_x	longitudinal load factor (g)
n_y	lateral load factor (g)
n_z	vertical load factor (g)

q	dynamic pressure (lbs/ft^2)
RC	rate of climb (ft/sec)
S	wing area (ft^2)
TAS	true airspeed
U_{de}	derived gust velocity (ft/sec, EAS)
U_σ	continuous turbulence gust intensity (ft/sec, TAS)
V_B	design speed for maximum gust
V_C	design cruise speed
V_D	design dive speed
V_e	equivalent airspeed
V_{MO}	maximum airspeed at altitude
V_T	true airspeed
W	gross weight (lbs)
Δn_z	incremental vertical load factor, n_z - 1
$\Delta n_{z_{man}}$	incremental maneuver load factor
$\Delta n_{z_{gust}}$	incremental gust load factor
Δt	time increment
μ	airplane mass ratio, $\frac{2(W/S)}{\rho g \bar{c} C_{L_\alpha}}$
ρ	air density, slugs/ft^3 (at altitude)
ρ_0	standard sea level air density, 0.0023769 slugs/ft

LIST OF AIRPORT CODES

ABQ	Albuquerque	MCO	Orlando
ACA	Acapulco	MEX	Mexico City
AMA	Amarillo	MIA	Miami
ATL	Atlanta	MRY	Monterey
AUS	Austin	MSN	Madison
BDL	Windsor Locks	MSP	Minneapolis
BIL	Billings	MSY	New Orleans
BNA	Nashville	OAK	Oakland
BOS	Boston	OMA	Omaha
BUF	Buffalo	ONT	Ontario
BWI	Baltimore	ORD	Chicago
CCS	Caracas	ORF	Norfolk
CLE	Cleveland	PDX	Portland
CLT	Charlotte	PHL	Philadelphia
CMH	Columbus	PHX	Phoenix
COS	Colorado Springs	PIT	Pittsburgh
CVG	Covington/Cincinnati	PVD	Providence
CYVR	Vancouver	RDU	Raleigh/Durham
DCA	Washington National	RFD	Rockford
DEN	Denver	RIC	Richmond
DFW	Dallas/Fort Worth	RNO	Reno
DSM	Des Moines	SAL	San Salvador
DTW	Detroit	SAN	San Diego
EWR	Newark	SEA	Seattle
GRR	Grand Rapids	SFO	San Francisco
GSO	Greensboro	SJC	San Jose
GXY	Greeley	SJO	San Jose
IAD	Washington Dulles	SJU	San Juan
IAH	Houston	SLC	Salt Lake City
IDA	Idaho Falls	SMF	Sacramento
IND	Indianapolis	SNA	Santa Ana (Orange County)
JAC	Jackson	STL	St Louis
JFK	New York	STT	St Thomas
LAS	Las Vegas	TPA	Tampa
LAX	Los Angeles	TUL	Tulsa
LGA	New York	TUS	Tucson
LNK	Lincoln	YYC	Calgary
MCI	Kansas City	YYZ	Toronto International

EXECUTIVE SUMMARY

The University of Dayton is supporting the Federal Aviation Administration (FAA) research on the structural integrity requirements for the U.S. commercial transport airplane fleet. The primary objective of this research is to develop new and improved methods and criteria for processing and presenting large commercial transport airplane flight and ground loads usage data. The scope of activities performed involves (1) defining the service-related factors that affect the operational life of commercial aircraft; (2) designing an efficient software system to reduce, store, and process large quantities of optical quick-access recorder data; and (3) reducing, analyzing, and providing processed data in statistical formats that will enable the FAA to reassess existing certification criteria. Equally important, these new data will also enable the FAA, the aircraft manufacturers, and the airlines to better understand and control those factors that influence the structural integrity of commercial transport aircraft. Presented herein are Airbus A-320 aircraft operational usage data collected from 10,066 flights, representing 30,817 flight hours, as recorded by a single U.S. airline operator. Statistical data are presented on the aircraft's usage, flight and ground loads data, and systems operations. The data presented in this report will provide the user with information about the accelerations, speeds, altitudes, flight duration and distance, gross weights, speed brake/spoiler cycles, thrust reverser usage, and gust velocities encountered by the Airbus A-320 during actual operational usage.

1. INTRODUCTION.

The Federal Aviation Administration (FAA) has an ongoing airborne data monitoring systems research program to collect, process, and evaluate statistical flight and ground loads data from transport aircraft used in normal commercial airline operations. The objectives of this program are (a) to acquire, evaluate, and utilize typical operational in-service data for comparison with the prior data used in the design and qualification testing of civil transport aircraft and (b) to provide a basis to improve the structural criteria and methods of design, evaluation, and substantiation of future airplanes. The University of Dayton Research Institute (UDRI) supports the FAA's efforts by developing the technology for reducing, processing, analyzing, and reporting on the operational flight and ground loads data received from the airlines participating in the FAA program and by conducting research studies.

Since the inception of the FAA's Airborne Data Monitoring Systems Research Program, the scope of the Flight Loads Program has steadily expanded to include research on data collected from several aircraft operators and on aircraft models such as the B-737, B-767, MD-82/83, and BE-1900D. While current program research efforts are tailored primarily to support the FAA and the aircraft structural design community in evaluating design criteria related to the strength, durability, and damage tolerance of the basic airframe structure, much of the data that are available, when provided in meaningful statistical formats, can provide the aircraft operator with some valuable insight into how his aircraft and aircraft systems are being used during normal flight and ground operations. In an effort to improve the data content and to disseminate meaningful data to the larger community of designers, regulators, and aircraft operators, UDRI has made changes, deletions, and additions to the statistical data formats as presented in past reports. These changes occur throughout the data presentation section of this report.

This report presents flight and ground loads data obtained from 56 Airbus A-320 aircraft representing 10,066 flights and 30,817 hours of airline operations from one U.S. carrier.

2. AIRCRAFT DESCRIPTION.

The Airbus A-320 is the first subsonic commercial aircraft equipped with fly-by-wire control throughout the entire flight envelope, and the first aircraft to have sidestick controls instead of the standard control column and aileron wheel. The fly-by-wire system controls ailerons, elevators, spoilers, flaps, leading-edge devices, engine thrust, and rudder and tail surface trim. The flight control system incorporates features which will not allow the aircraft's structural and aerodynamic limits to be exceeded regardless of pilot input.

Table 1 presents certain operational characteristics and major physical dimensions of the Airbus A-320 aircraft, and figure 1 presents a three-view drawing showing front, top, and side views of the aircraft.

TABLE 1. AIRBUS A-320 AIRCRAFT CHARACTERISTICS

Maximum taxi weight Maximum takeoff weight Maximum landing weight Maximum zero-fuel weight	162,920 lb 162,038 lb 142,195 lb 133,378 lb
Fuel Capacity	40,551 lb @ 6.55 lb/ U.S. gallons
2 CFM 56-5-A1 or V2500	@ 25,000 lbs static thrust @ sea level each
Wing span Wing reference area Wing MAC Wing sweep	111.26 ft 1,317.5 ft^2 113.76 in 25 degrees
Length Height Tread Wheel base	123 ft 3 in 38 ft 8.5 in 24 ft 11 in 41 ft 5 in

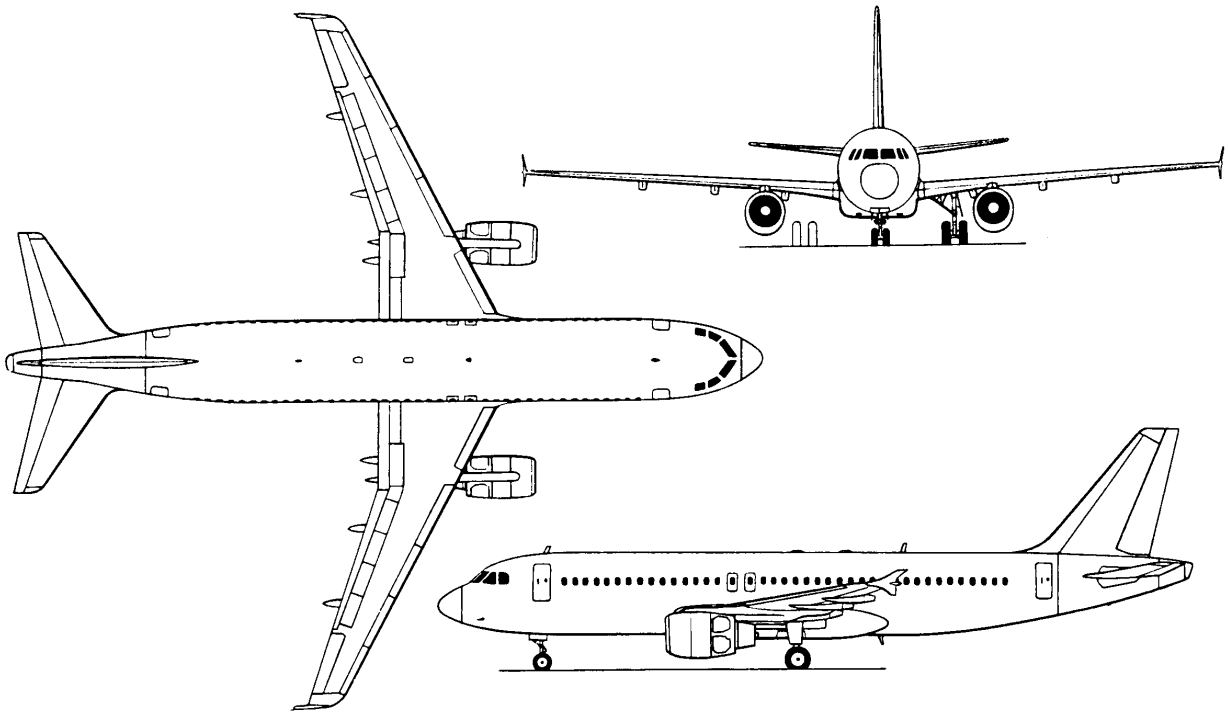


FIGURE 1. AIRBUS A-320 THREE-VIEW DRAWING

3. AIRLINE DATA COLLECTION AND EDITING SYSTEMS.

The airline data collection and editing system consists of two major components: (1) the data collection system installed on board the aircraft and (2) the ground data editing station. A schematic overview of the system is shown in figure 2. The data collection and editing systems are discussed in more detail below.

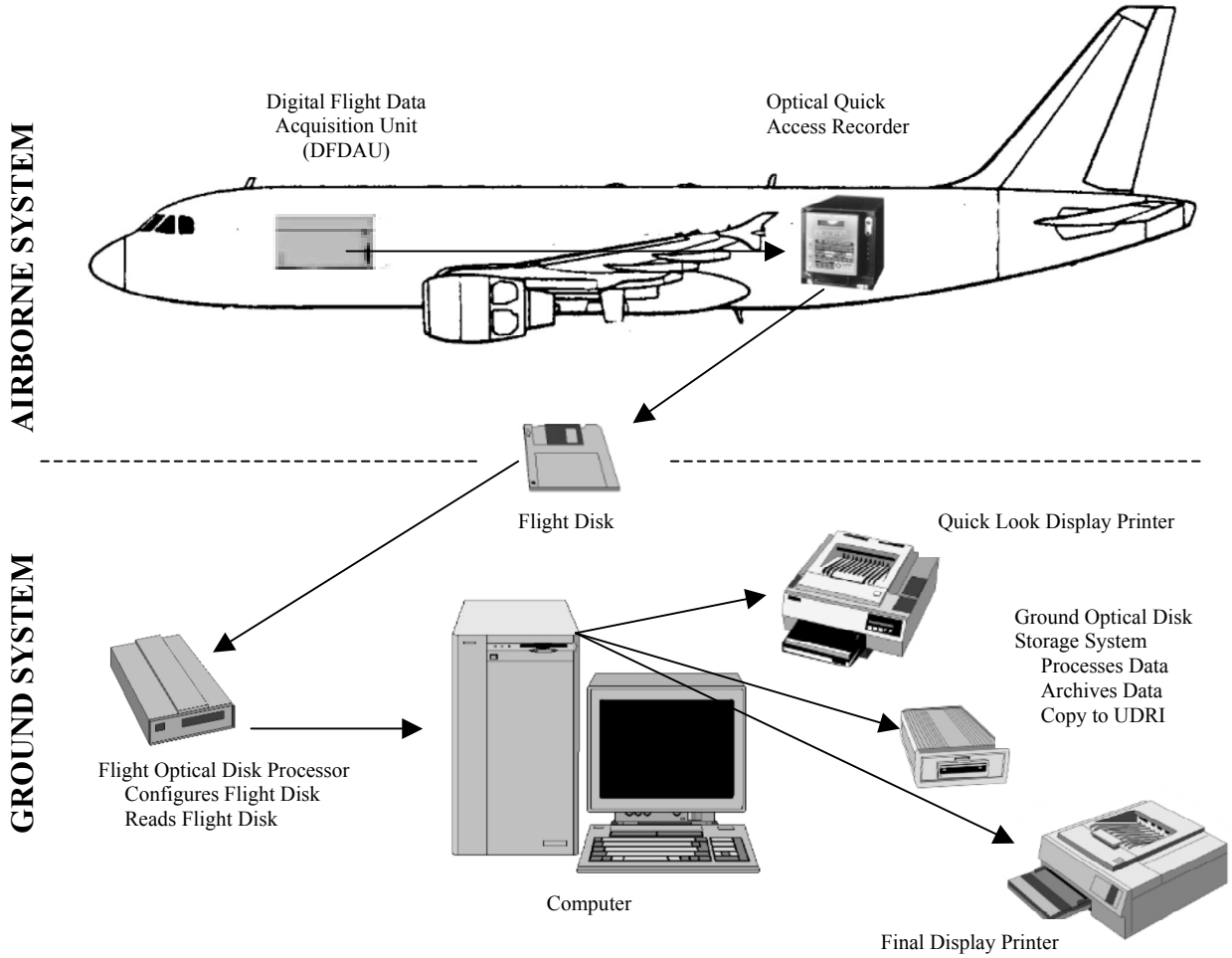


FIGURE 2. AIRLINE RECORDING AND EDITING SYSTEM

3.1 AIRLINE DATA COLLECTION SYSTEM.

The onboard data collection system for the Airbus A-320 consists of a Digital Flight Data Acquisition Unit (DFDAU), a Digital Flight Data Recorder (DFDR), and an Optical Quick-Access Recorder (OQAR). The DFDAU collects sensor signals and sends parallel data signals to both the DFDR and the OQAR. The OQAR is equipped with an optical disk, which can store up to 300 hours of flight data, whereas the DFDR uses a 25-hour looptape. The optical disk is periodically removed from the OQAR and forwarded to the ground processing station.

3.2 AIRLINE DATA EDITING SYSTEM.

The airline ground data editing station consists of a computer, a magneto-optical (MO) disk drive, and flight data editing software. The software performs a number of functions during the process of transferring the raw flight data into DOS file format onto the hard disk. The most important of these functions includes a data integrity check and removal of flight sensitive information. Data considered sensitive are those that can be used to readily identify a specific flight. The desensitized data are forwarded to UDRI for flight loads processing and analysis.

4. UNIVERSITY OF DAYTON RESEARCH INSTITUTE DATA PROCESSING.

The recorded flight and ground loads parameter data are provided by the airline to UDRI on magneto-optical disks containing binary files for multiple flights for different airplanes. This section lists the recorded parameters received from the airline, identifies those parameters processed by UDRI, describes the methods used to extract or compute parameters that are not recorded, and describes how these data are then processed by UDRI through a series of computer software programs to extract the final data required to develop the statistical data formats.

4.1 RECORDED DATA PARAMETERS.

Table 2 lists the recorded data parameters provided by the airline to UDRI for each recorded flight.

TABLE 2. RECORDED PARAMETERS PROVIDED TO UDRI

Parameter	Sampling Rate	Parameter	Sampling Rate
Vertical Acceleration	8 per second	Climb Rate	2 per second
Lateral Acceleration	4 per second	Mach Number	1 per second
Longitudinal Acceleration	4 per second	Pressure Altitude	1 per second
Aileron Position - Right and Left	1 per second each	Gross Weight	1 per 64 seconds
Elevator Position - Right and Left	1 per second each	Center of Gravity (%MAC)	1 per second
Rudder Position	2 per second	Fuel Flow - Right and Left	1 per second each
Rudder Trim	1 per second	Bank Angle	2 per second
Horizontal Stabilizer Position	1 per second	Pitch Angle	4 per second
Flap Position	1 per second	Roll Rate	4 per second
Slat Position	1 per second	Pitch Rate	4 per second
Slat/Flap Configuration	1 per second	Yaw Rate	1 per second
Spoiler/Speed Brake Position - 1, 2, 3, 4, 5 – Right and Left	1 per second each	Angle of Attack - Right and Left	1 per second each
N1 Engine - Right and Left	1 per second each	Magnetic Heading	1 per second
N2 Engine - Right and Left	1 per second each	True Heading	1 per second
Thrust Reverser Status - Engine 1 and 2	1 per second each	Magnetic Track	1 per second
Throttle Resolver Angle - Right and Left	1 per second each	Latitude	1 per second
Squat Switch - Main - Right and Left and Nose	1 per second each	Longitude	1 per second
Brake Pedal Angle - Right and Left	2 per second each	Total Air Temperature	1 per second
Calibrated Airspeed	1 per second	Radio Altitude Right and Left	4 per second each
True Airspeed	1 per second	Autopilot	1 per second
Ground Speed	1 per second	Inertial Vertical Velocity	2 per second

However, not all parameters listed in table 2 are used for statistical analysis and data presentation. Those recorded parameters that are used by UDRI to create time history files, compressed onto MO disks, and processed through the data reduction software for statistical analysis and data presentation are highlighted in table 2.

4.2 COMPUTED PARAMETERS.

Certain information and parameters needed in subsequent data reduction are not recorded and need to be extracted or derived from available time history data. Derived gust velocity, $U_{de,}$ and continuous gust intensity, $U_{\sigma,}$ are important statistical load parameters, which are derived from measured vertical accelerations. This derivation of U_{de} and U_{σ} requires knowledge of atmospheric density, equivalent airspeed, and dynamic pressure. These values are calculated using equations that express the rate of change of density as a function of altitude based on the International Standard Atmosphere.

4.2.1 Atmospheric Density.

For altitudes below 36,089 feet, the density ρ is expressed as a function of altitude by

$$\rho = \rho_0 \left(1 - 6.876 \times 10^{-6} \times H_p\right)^{4.256} \tag{1}$$

where ρ_0 is air density at sea level (0.0023769 slugs/ft^3) and H_p is pressure altitude (ft). Pressure altitude is a recorded parameter.

4.2.2 Equivalent Airspeed.

Equivalent air speed (V_e) is a function of true air speed (V_T) and the square root of the ratio of air density at altitude (ρ) to air density at sea level (ρ_0) and is expressed as

$$V_e = V_T \sqrt{\frac{\rho}{\rho_0}} \tag{2}$$

True airspeed (V_T) is derived from Mach number (M) and speed of sound (a):

$$V_T = Ma \tag{3}$$

Mach number is dimensionless and is a recorded parameter. The speed of sound (a) is a function of pressure altitude (H_p) and the speed of sound at sea level and is expressed as

$$a = a_0 \sqrt{\left(1 - 6.876 \times 10^{-6} \times H_p\right)} \tag{4}$$

Substituting equations 1 and 4 into equation 2 gives

$$V_e = M \times a_0 \times \left(1 - 6.876 \times 10^{-6} \times H_p\right)^{0.5} \times \left(1 - 6.876 \times 10^{-6} \times H_p\right)^{2.128} \tag{5}$$

which simplifies to

$$V_e = M \times a_0 \times \left(1 - 6.876 \times 10^{-6} \times H_p\right)^{2.626} \tag{6}$$

where the speed of sound at sea level a_0 is 1116.4 fps or 661.5 knots.

4.2.3 Dynamic Pressure (q).

The dynamic pressure (q) is calculated from the air density and velocity as

$$q = \frac{1}{2} \rho V^2 \tag{7}$$

where

ρ = air density at altitude (slugs/ft^3)
V = true air speed (ft/sec)

4.2.4 Derived Gust Velocity (U_{de}).

The derived gust velocity, U_{de}, is computed from the peak values of gust incremental vertical acceleration as

$$U_{de} = \frac{\Delta n_z}{\overline{C}} \tag{8}$$

where Δn_z is gust peak incremental vertical acceleration and $\overline{C}$ is the aircraft response factor, considering the plunge-only degree of freedom and is calculated from

$$\overline{C} = \frac{\rho_0 V_e C_{L_\alpha} S}{2W} K_g \tag{9}$$

where

ρ_0 = 0.002377 slugs/ft^3, standard sea level air density
V_e = equivalent airspeed (ft/sec)
C_{L_α} = aircraft lift-curve slope per radian
S = wing reference area (ft^2)
W = gross weight (lbs)
K_g = $\frac{0.88\mu}{5.3 + \mu}$ = gust alleviation factor

μ = $\frac{2W}{\rho g \overline{c} C_{L_\alpha} S}$

ρ = air density, slug/ft^3, at pressure altitude (Hp), from equation 1

g = 32.17 ft/sec^2
$\overline{c}$ = wing mean geometric chord (ft)

In this program, the lift-curve slope, C_{L_α}, is the untrimmed flexible lift-curve slope for the entire airplane. For the flaps retracted conditions, the lift-curve slope is given as a function of Mach number and altitude; for flaps extended, the lift-curve slope is a function of flap deflection and calibrated airspeed (CAS).

4.2.5 Continuous Gust Intensity (U_σ).

Power spectral density (PSD) functions provide a turbulence description in terms of the probability distribution of the root-mean-square (rms) gust velocities. The root-mean-square gust velocities or continuous gust intensities, U_σ, are computed from the peak gust value of vertical acceleration using the power spectral density technique as described in reference 1 as

$$U_\sigma = \frac{\Delta n_z}{\overline{A}} \tag{10}$$

where Δn_z = gust peak incremental vertical acceleration

$\overline{A}$ = aircraft PSD gust response factor = $\frac{\rho_0 V_e C_{L\alpha} S}{2W}$ F(PSD) in $\frac{1}{ft/sec}$ (11)

ρ_0 = 0.002377 slugs/ft^3, standard sea level air density
V_e = equivalent airspeed (ft/sec)
C_{L_α} = aircraft lift-curve slope per radian
S = wing reference area (ft^2)
W = gross weight (lbs)

$$F(PSD) = \frac{11.8}{\sqrt{\pi}}\left[\frac{\overline{c}}{2L}\right]^{\frac{1}{3}}\sqrt{\frac{\mu}{110+\mu}},\ dimensionless \tag{12}$$

$\overline{c}$ = wing mean geometric chord (ft)
L = turbulence scale length, 2500 ft

$$\mu = \frac{2W}{\rho g \overline{c} C_{L_\alpha} S},\ \text{dimensionless} \tag{13}$$

ρ = air density (slugs/ft^3)
g = 32.17 ft/sec^2

To determine the number of occurrences (N) for U_σ, calculate

$$N = \frac{N_0(o)_{ref}}{N_0(o)} = \frac{\pi\overline{c}}{203}\left[\frac{\rho}{\rho_0}\mu\right]^{0.46},\ \text{dimensionless} \tag{14}$$

where $\overline{c}$, ρ, ρ_0, and μ are defined above. Then each U_σ peak is counted as N counts at that U_σ value. This number of counts is used to determine the number of counts per nautical mile (*nm*), or

$$\frac{\text{counts}}{nm} = \left(\frac{N}{\text{distance flown in counting interval}}\right) \tag{15}$$

Finally, the number of such counts is summed from the largest plus or minus value toward the smallest to produce the cumulative counts per nautical mile.

4.2.6 Flight Distance.

The flight distance was obtained either by determining the stage length of the flight or by integrating the range with respect to changes in aircraft velocity as a function of time.

The stage length is defined as the distance from departure airport to destination airport and is determined as the great circle distance in nautical miles between the point of liftoff (departure) and the point of touchdown (destination). Appendix B describes the calculation of great circle distance. The time histories of longitude and latitude are matched against the UDRI generated phase of flight file to determine the geographical location of the aircraft at the point of liftoff and the point of touchdown.

The integrated flight distance D is obtained by the numerical integration from the time at liftoff (t_0) to the time of touchdown (t_n), and V_T is the average true velocity during Δt.

$$D = \sum_{t_0}^{t_n} \Delta t \cdot V_T \tag{16}$$

4.2.7 Rate of Climb.

Although the rate of climb was a recorded value on the Airbus A-320, it was not always a recorded value on other aircraft; therefore, UDRI continued its previous practice of calculating these values. The rate of climb is obtained by numerical differentiation of the change in pressure altitude with time.

$$RC = \sum_{t_1}^{t_2} \frac{\Delta H_p}{\Delta t} \tag{17}$$

4.3 DATA REDUCTION OPERATIONS.

The data reduction phase retrieves the data from the magneto-optical disks provided by the airline, processes it through a series of computer programs that convert the data to UDRI compatible formats, and provides statistical information on aircraft usage, ground loads, flight loads, and systems operation. The data processing flow chart is illustrated in figure 3, and the flow of the processed data is discussed in subsequent paragraphs.

4.3.1 Initial Quality Screening.

All incoming data files are screened for acceptability. Individual flights are edited to remove erroneous or meaningless data such as discontinuous elapsed time data, evidence of nonfunctional channels or sensors, incomplete flight phases, and duplicate data sets. Files with missing, incomplete, or duplicate data are identified. The A-320 data, as provided by the airline, were found to have randomly distributed frame gaps and/or repeated frames for all but 356 flights. The existence of the erroneous data frames prevented routine data processing. UDRI developed an intermediate process to provide usable flight time histories through deletion of the frame gaps or repeated frames. As a consequence, the flight times in the segments where the gaps or repeated frames occurred were slightly reduced. However, the effect of the frame

deletion on the final loads statistics is considered insignificant. Of the 15,046 flights provided by the airline, UDRI was able to extract 10,066 flights of usable data.

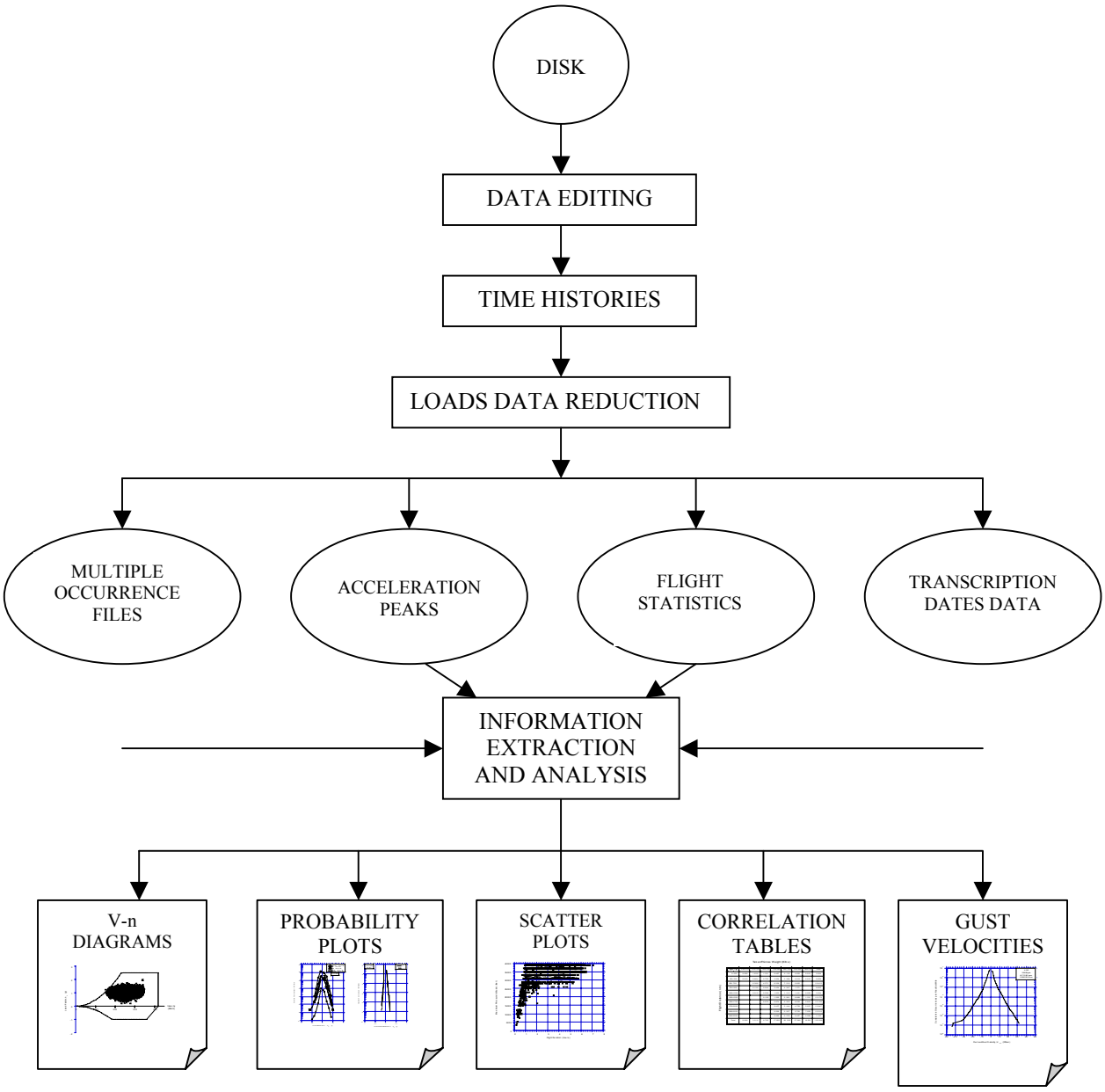


FIGURE 3. DATA PROCESSING FLOW CHART

4.3.2 Time History Files.

Each magneto-optical disk provided by the airline contains multiple flights for each airplane. The files on MO disks are separated into individual parameter time history files for each flight. Then these time history files are compressed and stored on the same 230-MB magneto-optical disks for later recall by the flight loads processing software. Data editing and verification are performed on the data as the time histories are being prepared. Message alerts indicate that

obviously erroneous data have been removed and/or that questionable data have been retained but need to be manually reviewed prior to their acceptance. Table 3 lists the limits against which the data are compared. Some of the parameters from table 1 are edited and retained even though they are not currently being used.

TABLE 3. PARAMETER EDITING VALUES

Item		Min	Max
1.	Gross Weight	38,000 kg	74,000 kg
2.	Pressure Altitude (Hp)	-2,000 ft	40,000 ft
3.	Calibrated Airspeed	0 kts	450 kts
4.	Vertical Acceleration	-2.0 g	+4.0 g
5.	Lateral Acceleration	-1.0 g	+1.0 g
6.	Longitudinal Acceleration	-1.0 g	+1.0 g
7.	Flap Handle Position	0°	40°
8.	Elevator Position	-31°	+20°
9.	Aileron Position	-26°	+26°
10.	Rudder Position	-60°	+60°
11.	Trim Position	-13.5°	+4°
12.	Speed Brake Position	-51°	0°
13.	Throttles 1 and 2	-25°	45°
14.	Engine N_1 and N_2	0%	120%
15.	Thrust Reverser Status	0	1
16.	Squat Switch (main gear)	0	1
17.	Pitch Attitude	-10°	+30°
18.	Bank Attitude	-40°	+40°
19.	Mach Number	0	0.9
20.	Ground Speed	0 kts	600 kts
21.	Brake Pedal Angle	-75°	+75°
22.	Fuel Flow	All	All
23.	Latitude	-90°	+90°
24.	Longitude	-180°	+180°
25.	Magnetic Heading	0°	360°
26.	Pitch Rate	All	All
27.	Radio Altitude	-20 ft	<2500 ft

4.3.3 Relational Database.

Important characteristics about each set of flights received from the airline are recorded in a relational database. The airline identifier, aircraft tail number, and disk identifier of the disk received from the airline are in the data. Each flight is assigned a unique flight sequence number. The flight sequence number assigned to the first flight of the set and the number of flights in the set are also entered. Also recorded is the disk identifier of the MO disk, which contains the compressed time history files of all flights in the set.

4.3.4 Permanent Data Files.

In addition to the time history files, two other files are created and permanently stored with the time history files. The first file contains the chronologically sorted list of the phases of flight and their corresponding starting times. This file provides the means to separate flight-by-flight phases in subsequent data analysis processing. The second file contains the accumulated time and distance for various combinations of phase of flight and altitude band. This file provides the capability to present data results in terms of normalized unit time and/or distance.

4.3.5 Loads Data Reduction.

The loads data reduction program uses the compressed time history files to derive statistical information on aircraft usage, ground loads, flight loads, and systems operations. These data are then reduced in accordance with specific data reduction criteria.

4.4 DATA REDUCTION CRITERIA.

To process the measured data into statistical loads formats, specific data reduction criteria were developed for separating the phases of ground and flight operations, identifying specific events associated with operation of the aircraft and its onboard systems, assigning sign conventions, determining maximum and minimum values and load cycles, and distinguishing between gust and maneuver load factors. These criteria are discussed in the following paragraphs.

4.4.1 Phases of Flight Profile.

The ground and flight phases were determined by UDRI from the recorded data. Each time history profile was divided into nine phases–four ground phases (taxi out, takeoff roll, landing roll with and without thrust reverser deployed, and taxi in) and five airborne phases (departure, climb, cruise, descent, and approach). Figure 4 shows these nine phases of a typical flight profile.

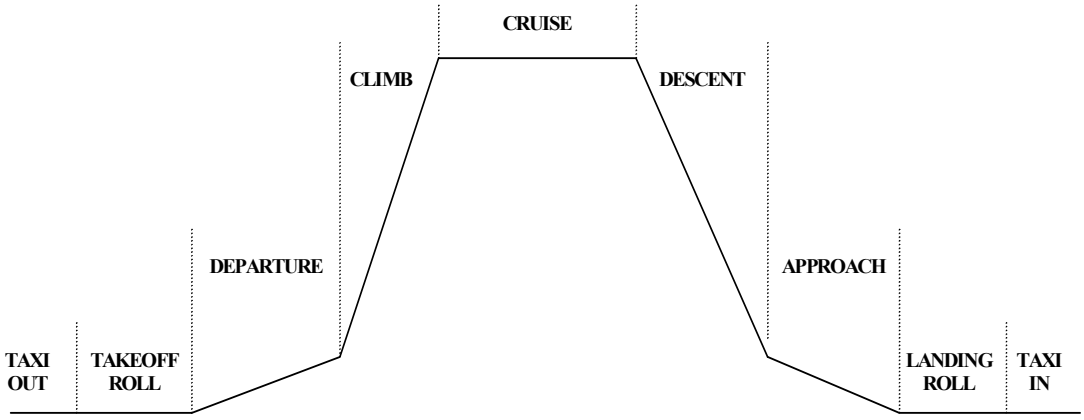


FIGURE 4. DESCRIPTION OF FLIGHT PROFILE PHASES

The criteria used to define each of these phases are summarized in table 4 and discussed in more detail in the following paragraphs.

TABLE 4. FLIGHT PHASE CRITERIA

Phase of Flight	Defining Condition at Start of Phase
Taxi Out	From initial aircraft movement
Takeoff Roll	Ground acceleration > 2kts/sec in a 20 second duration sequence
Departure	Liftoff, squat switch off
Climb	Rate of climb ≥ 250 ft/min maintained for at least 1 minute with flaps retracted
Cruise	Rate of climb is between ±250 ft/min and flaps retracted
Descent	Rate of descent ≥ 250 ft/min occurs for at least 1 minute and flaps retracted
Approach	Rate of descent ≤ 250 ft/min occurs for at least 1 minute with flaps extended
Landing Roll	Touchdown, squat switch on
Taxi In	End of runway turnoff to parked at the gate or recorder shutdown

4.4.1.1 Ground Phases.

Specific data reduction criteria were developed and used to identify the beginning and end of each ground phase of operation (taxi out, takeoff roll, landing roll with and without thrust reverser deployed, and taxi in).

The taxi out phase begins when the ground speed exceeds 1 knot. All aircraft movement until the aircraft begins its takeoff roll is defined as being taxi out.

The beginning of the takeoff roll is found by searching for ground speeds that accelerated at rates greater than 2 kts/sec for a minimum duration of 20 seconds. Then, when these values are found, the beginning of the takeoff roll is assigned as being the time slice where the first ground speed rate change greater than 2 kts/sec for that sequence occurred. The takeoff roll ends at liftoff with the squat switch off signal.

The landing roll phase is defined as beginning 1 second after the squat switch signaled that the landing touchdown had occurred and ending when the aircraft begins its turnoff from the active runway. The criterion for the turnoff is based on a change in the magnetic heading following landing and is discussed further in paragraph 4.4.2.4.

Taxi in is defined from the point where the aircraft completed its turnoff from the active runway after its landing roll to the point when the aircraft was either parked at the gate or the recorder has shut down. The criterion for completion of the turnoff uses magnetic heading to identify when the aircraft has either returned to taxiing in a straight line or has turned in the opposite direction and is also discussed further in paragraph 4.4.2.4.

4.4.1.2 Airborne Phases.

The airborne portion of each flight profile was separated into phases called departure, climb, cruise, descent, and approach. These phases occur between the time that the squat switch turns off at liftoff until it turns on again at landing touchdown. The beginning of each flight phase is

defined based on combinations of the squat switch position, flap settings, and/or the calculated rate of climb or descent over a period of at least 1 minute as shown in table 4. Also, by definition, the departure phase cannot be less than 1 minute in length.

It should be noted that an airborne phase could occur several times per flight because it is determined by the rate of climb and the position of the flaps. When this occurs, the flight loads data are combined and presented as a single flight phase. The UDRI software then creates a file that chronologically lists the phases of flight and their corresponding starting times.

4.4.2 Specific Events.

In addition to the ground and airborne phases, a unique set of criteria was also required to identify certain specific events such as liftoff, landing touchdown, thrust reverser deployment and stowage, and start and completion of turnoff from the active runway after landing. Figure 5 shows a sketch depicting these phases and events.

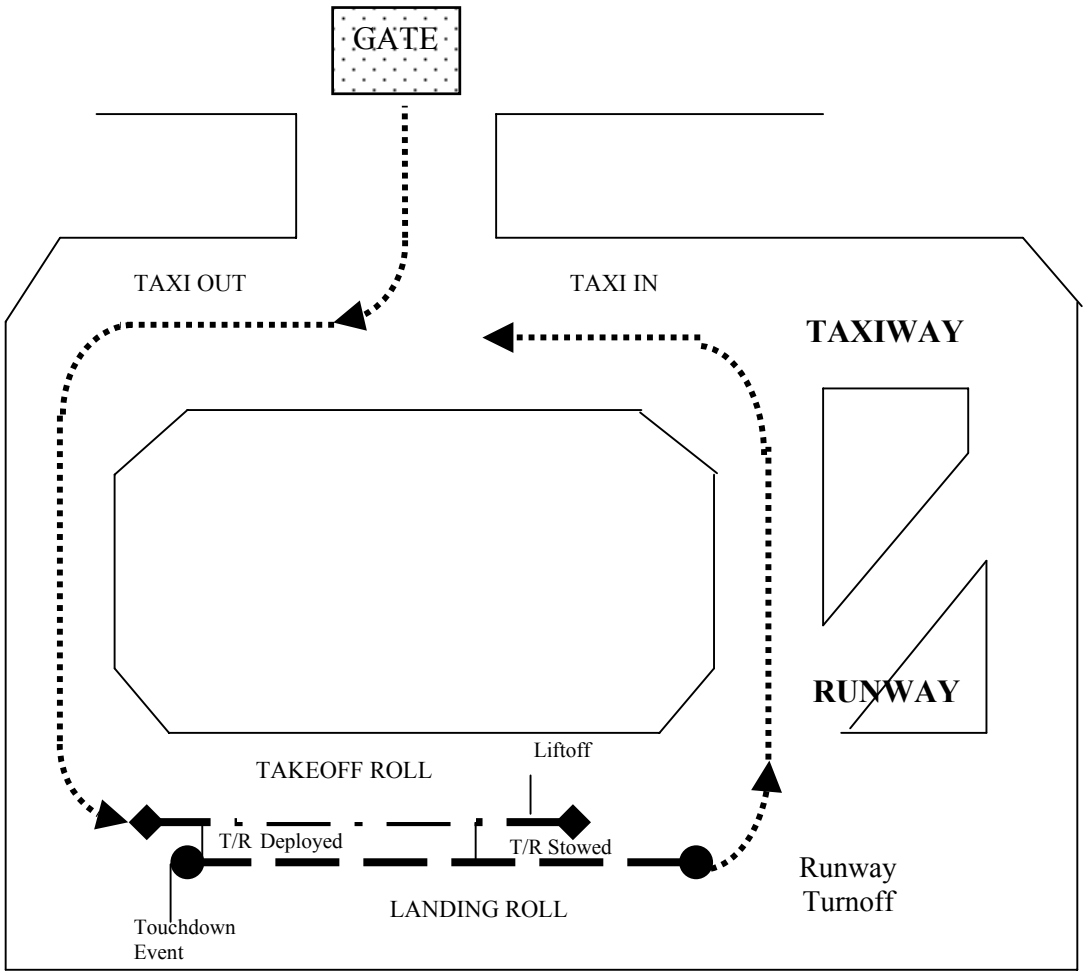


FIGURE 5. SKETCH OF GROUND PHASES AND SPECIFIC EVENTS

The criteria used to define each of the specific events are summarized in table 5 and discussed in more detail in reference 2 and the following paragraphs.

TABLE 5. SUMMARY OF SPECIFIC EVENTS CRITERIA

Phase/Event	Defining Conditions
Liftoff	Point of first reading in series of increasing radio altitude values greater than 4 feet higher than the average radio altitude value calculated during the takeoff roll.
Landing Touchdown	From 5 seconds prior to squat switch on to 1 second afterwards.
Thrust Reverser Deployment/Stowage	Thrust reverser switch on for deployment and pff for stowage.
Runway Turnoff	From first sequential magnetic heading change in same direction from runway centerline and heading sequence changes >13.5 degrees to a straight line heading or turn in opposite direction.

4.4.2.1 Liftoff.

During development of the statistical formats of pitch angle at liftoff and touchdown, UDRI concluded that the squat switch on the A-320 was not providing a reliable indication of when liftoff (or touchdown) was actually occurring. So, in order to determine when liftoff actually occurred, a new algorithm was developed that identifies the liftoff point as the first reading in the series of increasing radio altitude values that was greater than 4 feet higher than the average radio altitude value that it calculated during the takeoff roll.

4.4.2.2 Landing Touchdown.

For the determination of general landing statistics, the landing touchdown has been defined as the time when the landing gear touches down and the squat switch closes. However, as stated above, UDRI discovered that the squat switch on the A-320 was not an accurate indicator of when touchdown actually occurred. To ensure that the maximum vertical and side load factors associated with touchdown were identified, the actual touchdown event was deemed to occur within a time frame from 5 seconds prior to until 1 second following squat switch closure. UDRI decided that it was more important to ensure capturing the touchdown event even if the 5-second time prior to squat switch closure resulted in some minor loss of flight data. The 1-second time after squat switch was chosen somewhat arbitrarily but was intended to ensure that sufficient time was allowed for the aircraft to respond to the touchdown and for the vertical and side load accelerations to build to their maximum values.

4.4.2.3 Thrust Reverser Deployment/Stowage.

An on/off switch identifies when deployment or stowage of the thrust reverser occurs. Thus, by identifying when this occurs as a special event, load factor acceleration data can be obtained at the instant of thrust reverser deployment and during the time of thrust reverser usage and stowage.

4.4.2.4 Runway Turnoff.

Changes in the aircraft's magnetic heading were used to identify the beginning and end of the aircraft's turnoff from the active runway after the landing roll. After the aircraft touched down, subsequent magnetic heading readings were averaged and this average heading was defined as the runway centerline. Subsequent magnetic heading changes were then tested to identify continuous movement in the same direction away from this centerline. When the aircraft's sequential magnetic heading change exceeded 13.5 degrees from the direction of the landing centerline, the time slice associated with the first sequential heading change from the landing centerline in the direction of the turn was defined as the beginning of the turnoff from the runway.

An alternate method was used to identify flights involving "shallow" turns from the runway that did not exceed the 13.5 degree turn criteria. This method uses aircraft ground speed and magnetic heading to calculate the aircraft's position relative to the runway centerline by identifying when the aircraft's position perpendicular to the runway centerline exceeded 100 feet. The time slice associated with the first aircraft movement away from the landing centerline in the direction of the turn was defined as the beginning of the aircraft's turnoff from the runway.

The end point of the first turnoff from the active runway was also identified using magnetic heading readings. An algorithm was developed that uses the changes in magnetic heading, while the aircraft was in its turn, to identify when the aircraft had either returned to taxiing in a straight line or was turning in the opposite direction. The first point that provided this indication was then defined as the end point of the turnoff from the runway. This point is also the beginning of the taxi in phase.

4.4.3 Sign Conventions.

Acceleration data are recorded in three directions: vertical (z), lateral (y), and longitudinal (x). As shown in figure 6, the positive z direction is up; the positive y direction is airplane starboard; and the positive x direction is forward.

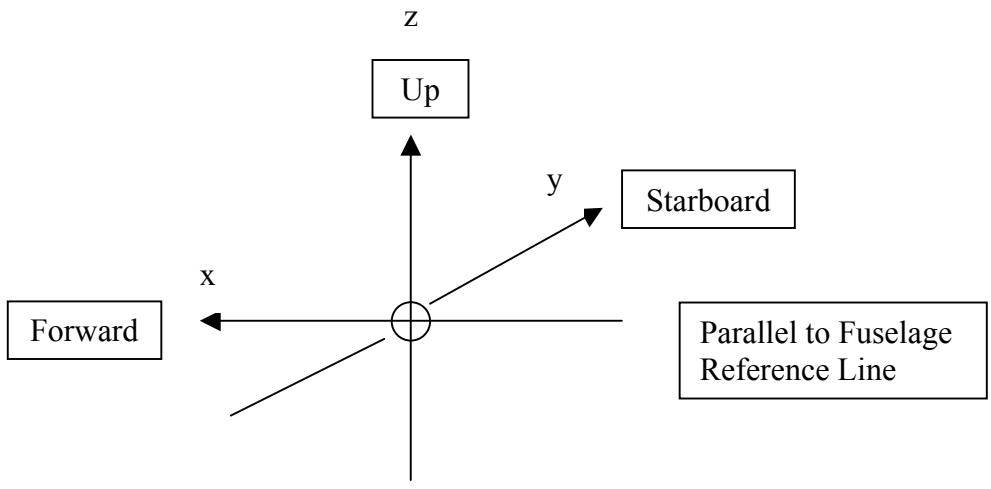


FIGURE 6. SIGN CONVENTION FOR AIRPLANE ACCELERATIONS

4.4.4 Peak Selection Technique.

The peak-between-means method presented in reference 1 is used to identify positive and negative peaks in the acceleration data. This method is consistent with past practices and pertains to all accelerations (n_x, n_y, Δn_z, $\Delta n_{z_{gust}}$, $\Delta n_{z_{man}}$). A brief description of the peak-between-means technique follows.

One peak is identified between each two successive crossings of the mean acceleration, which is the 0-g condition for lateral, longitudinal, and incremental vertical accelerations. Peaks greater than the mean are considered positive and those less than the mean negative. A threshold zone is defined around the mean, within which acceleration peaks are ignored because they have been shown to be irrelevant. The threshold zone is ±0.05 g for the vertical accelerations Δn_z, $\Delta n_{z_{gust}}$, $\Delta n_{z_{man}}$, ±0.005 g for lateral acceleration n_y, and ±0.0025 g for longitudinal acceleration n_x.

Figure 7 below demonstrates the acceleration peak selection technique. The sample acceleration trace contains 8 zero crossings, which are circled, set off by vertical dashed lines, and labeled as C_i, i = 0 to 7. For each of the seven intervals between successive mean crossings, C_{i-1} to C_i, i = 1 to 7, one peak, which is located at P_i, is identified. Those peaks lying outside of the threshold zone (P_1, P_2, P_5, P_6, and P_7) are accepted and retained; whereas, those peaks lying inside the threshold zone (P_3 and P_4) are ignored.

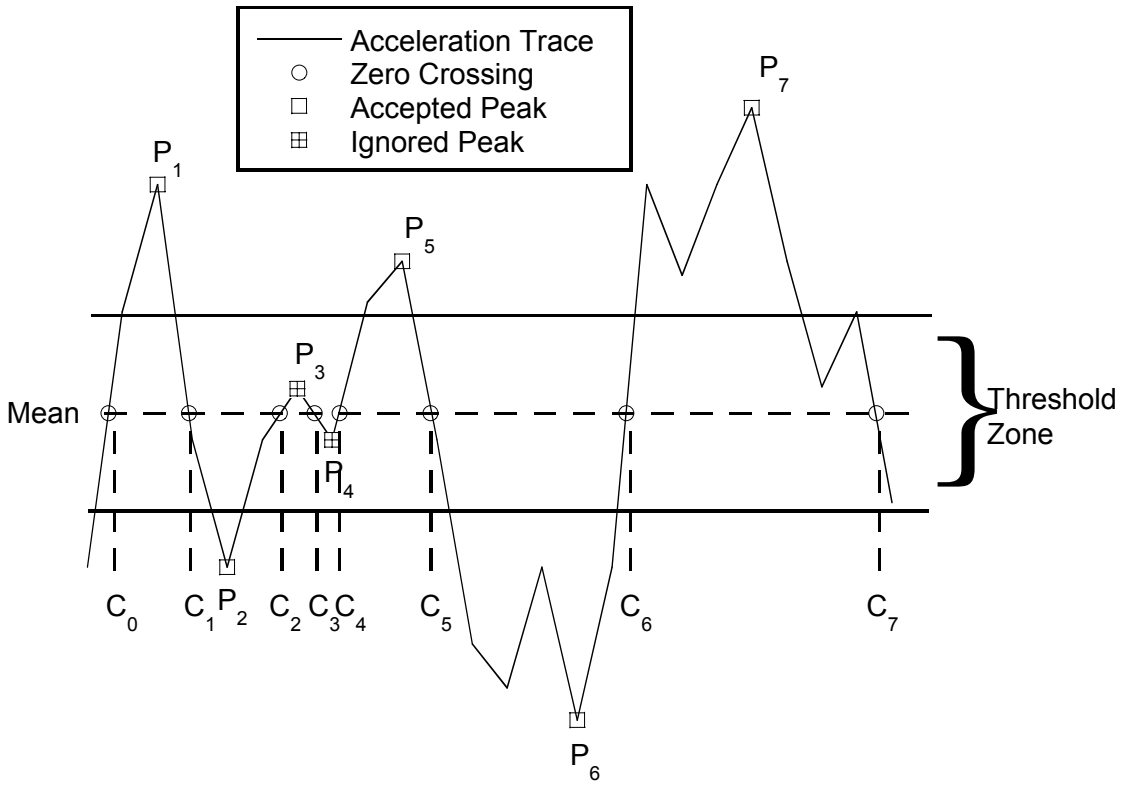


FIGURE 7. THE PEAK-BETWEEN-MEANS CLASSIFICATION CRITERIA

4.4.5 Separation of Maneuver and Gust Load Factors.

Vertical acceleration, n_z, is measured at the center of gravity (c.g.) of the aircraft and incremental vertical acceleration, Δn_z, results from removing the 1-g condition from n_z. The incremental acceleration measured at the c.g. of the aircraft in flight may be the result of either maneuvers or gusts. In order to derive gust and maneuver statistics, the maneuver-induced acceleration ($\Delta n_{z_{man}}$) and the gust response acceleration ($\Delta n_{z_{gust}}$) must be separated from the total acceleration history. Reference 3 reported the results of a UDRI study to evaluate methods of separating maneuver and gust load factors from measured acceleration time histories. As a result of this study, UDRI uses a cycle duration rule to differentiate maneuver-induced acceleration peaks from those peaks caused by gust loading. Review of the A-320 response characteristics has shown that a cycle duration of 2.0 seconds is appropriate for the A-320 aircraft and thus was used.

4.4.6 Flap Detents.

When flaps are extended, the effective deflection is considered to be that of the applicable detent, as indicated in table 6. The flap deflection ranges and placard speeds reflect the flap operational limits, as provided by Airbus Industries 15 June 1999.

TABLE 6. FLAP DETENTS (AIRBUS A-320)

Flap Detent	Minimum Flap Setting	Maximum Flap Setting	Operational Airspeed Limit (KCAS)
0	0	0	230
10	> 0	≤ 10	215
15	>10	≤ 15.3	200
20	> 15.3	≤ 20	185
40	> 20	≤ 40	177

5. DATA PRESENTATION.

The statistical data presented in this section provide the FAA, aircraft manufacturers, and the operating airline with the information that is needed to assess how the A-320 aircraft is actually being used in operational service versus its original design or intended usage. The statistical data presented herein can be used by the FAA as a basis to evaluate existing structural certification criteria, to improve requirements for the design, evaluation, and substantiation of existing aircraft, and to establish design criteria for future generations of new aircraft. The aircraft manufacturer can use these data to assess the aircraft's structural integrity by comparing the actual in-service usage of the A-320 aircraft versus its originally intended design usage. It can also use these data to derive typical flight profiles and to update structural strength, durability, and damage tolerance analyses in order to establish or revise maintenance and inspection requirements for critical airframe and structural components. The airline/aircraft operator can use these data to evaluate the aircraft's current usage with respect to established operational procedures and placard limitations. It can also use these data to identify where changes in current operational procedures could provide additional safety margins, increase the service life of structural components, and improve on the economics of its operations.

Table 7 lists all the statistical data formats for which data were processed. The various data formats have been grouped together within the table in an attempt to categorize the A-320 data being presented on the basis of whether it pertains to aircraft usage, ground or flight loads data, or systems operational data. The aircraft usage data section describes the aircraft's operational usage in terms of distributions of flight lengths, flight duration, flight phase, flight altitudes, flight speeds, takeoff and landing gross weights, fuel flows, etc. The loads and system data section describes the flight and ground environment and the induced system cyclic loadings experienced by the aircraft while the aircraft performs its intended usage.

TABLE 7. STATISTICAL DATA FORMATS

Data Description	Figure
AIRCRAFT USAGE DATA	
WEIGHT AND FLIGHT DISTANCE DATA	
Cumulative Probability of Takeoff Gross Weight	A-1
Cumulative Probability of Landing Gross Weight	A-2
Cumulative Probability of Flight Length	A-3
Correlation of Flight Length and Integrated Flight Distance	A-4
Correlation of Takeoff Gross Weight and Great Circle Flight Length	A-5
Correlation of Takeoff Gross Weight and Great Circle Flight Length, Percent of Flights	A-6
Correlation of Takeoff and Landing Gross Weight, Percent of Flights	A-7
Percent of Integrated Flight Distance in Altitude Bands	A-8
ALTITUDE AND SPEED DATA	
Correlation of Maximum Altitude and Flight Duration	A-9
Cumulative Probability of Maximum Ground Speed During Taxi	A-10
Maximum Mach Number and Coincident Altitude, All Flight Phases	A-11
Maximum Calibrated Airspeed and Coincident Altitude, All Flight Phases	A-12
Cumulative Probability of Airspeed at Liftoff	A-13
Cumulative Probability of Airspeed at Touchdown	A-14
ATTITUDE AND RATE DATA	
Cumulative Probability of Pitch Angle at Liftoff	A-15
Cumulative Probability of Pitch Angle at Touchdown	A-16
Cumulative Probability of Maximum Pitch Angle During Departure and Approach	A-17
Probability Distributions of Maximum Pitch Rate at Nose Gear Touchdown	A-18
GROUND LOADS DATA	
LATERAL LOAD FACTOR, n_y	
Cumulative Frequency of Maximum Lateral Load Factor During Ground Turns	A-19
Cumulative Frequency of Maximum Lateral Load Factor at Touchdown	A-20
Frequency Distributions of Maximum Lateral Load Factor During Runway Turnoff	A-21
Maximum Lateral Load Factor and Coincident Incremental Vertical Load Factor at Touchdown	A-22
Probability Distributions of Turning Angle During Runway Turnoff	A-23
Maximum Lateral Load Factor and Coincident Ground Speed during Runway Turnoff, 0-60 Degree Turns	A-24
Maximum Lateral Load Factor and Coincident Ground Speed during Runway Turnoff, 60-120 Degree Turns	A-25
Maximum Lateral Load Factor and Coincident Ground Speed during Runway Turnoff, 120-240 Degree Turns	A-26
Maximum Lateral Load Factor at Touchdown vs. Maximum Yaw Angle Before Touchdown	A-27
Maximum Lateral Load Factor at Touchdown vs. Mean Yaw Angle Before Touchdown	A-28
Maximum Lateral Load Factor at Touchdown vs. Maximum Bank Angle Before Touchdown	A-29
Maximum Lateral Load Factor at Touchdown vs. Mean Wind Speed Before Touchdown	A-30
LONGITUDINAL LOAD FACTOR, n_x	
Cumulative Frequency of Longitudinal Load Factor During Taxi Operations	A-31
Cumulative Frequency of Longitudinal Load Factor at Touchdown and During Landing Roll	A-32
VERTICAL LOAD FACTOR, n_z	
Cumulative Frequency of Incremental Vertical Load Factor During Taxi Operations	A-33
Cumulative Frequency of Incremental Vertical Load Factor During Takeoff Roll	A-34
Cumulative Frequency of Incremental Load Factor at Spoiler Deployment and at Touchdown	A-35

TABLE 7. STATISTICAL DATA FORMATS (Continued)

Data Description	Figure
Cumulative Frequency of Incremental Vertical Load Factor During Landing Roll	A-36
Maximum Incremental Vertical Load Factor vs. Maximum Angle of Attack During Lift off, 130-140 Knots	A-37
Maximum Incremental Vertical Load Factor vs. Maximum Angle of Attack During Lift off, 140-150 Knots	A-38
Maximum Incremental Vertical Load Factor vs. Maximum Angle of Attack During Lift off, 150-160 Knots	A-39
Maximum Incremental Vertical Load Factor vs. Maximum Angle of Attack During Lift off, 160-170 Knots	A-40
Maximum Incremental Vertical Load Factor vs. Maximum Angle of Attack During Lift off, 170-180 knots	A-41
Maximum Incremental Vertical Load Factor vs. Maximum Angle of Attack During Lift off, 180-190 knots	A-42
Maximum Incremental Vertical Load Factor at Touchdown vs. Maximum Yaw Angle Before Touchdown	A-43
Maximum Incremental Vertical Load Factor at Touchdown vs. Mean Yaw Angle Before Touchdown	A-44
Maximum Incremental Vertical Load Factor at Touchdown vs. Maximum Bank Angle Before Touchdown	A-45
Maximum Incremental Vertical Load Factor at Touchdown vs. Mean Wind Speed Before Touchdown	A-46
Maximum Incremental Vertical Load Factor at Touchdown vs. Mean Inertial Vertical Velocity Before Touchdown	A-47
Maximum Incremental Vertical Load Factor vs. Coincident Airspeed at Touchdown	A-48
Aircraft Runway Acceleration Response	A-49
FLIGHT LOADS DATA	
GUST VERTICAL LOAD FACTOR DATA	
Cumulative Occurrences of Incremental Vertical Gust Load Factor per 1000 Hours by Flight Phase	A-50
Cumulative Occurrences of Incremental Vertical Gust Load Factor per 1000 Hours, Combined Flight Phases	A-51
Cumulative Occurrences of Incremental Vertical Gust Load Factor per Nautical Mile by Flight Phase	A-52
Cumulative Occurrences of Incremental Vertical Gust Load Factor per Nautical Mile, Combined Flight Phases	A-53
DERIVED GUST VELOCITY DATA	
Cumulative Occurrences of Derived Gust Velocity per Nautical Mile, < 500 Feet Above Airport	A-54
Cumulative Occurrences of Derived Gust Velocity per Nautical Mile, 500-1,500 Feet Above Airport	A-55
Cumulative Occurrences of Derived Gust Velocity per Nautical Mile, < 500 Feet	A-56
Cumulative Occurrences of Derived Gust Velocity per Nautical Mile, 500-1,500 Feet	A-57
Cumulative Occurrences of Derived Gust Velocity per Nautical Mile, 1,500-4,500 Feet	A-58
Cumulative Occurrences of Derived Gust Velocity per Nautical Mile, 4,500-9,500 Feet	A-59
Cumulative Occurrences of Derived Gust Velocity per Nautical Mile, 9,500-19,500 Feet	A-60
Cumulative Occurrences of Derived Gust Velocity per Nautical Mile, 19,500-29,500 Feet	A-61
Cumulative Occurrences of Derived Gust Velocity per Nautical Mile, 29,500-39,500 Feet	A-62
Cumulative Occurrences of Derived Gust Velocity per Nautical Mile, Flaps Extended	A-63
Cumulative Occurrences of Derived Gust Velocity per Nautical Mile, Flaps Retracted	A-64
CONTINUOUS GUST INTENSITY DATA	
Cumulative Occurrences of Continuous Gust Intensity per Nautical Mile, Flaps Extended	A-65
Cumulative Occurrences of Continuous Gust Intensity per Nautical Mile, Flaps Retracted	A-66
GUST V-n DIAGRAM DATA	
Gust Load Factor and Coincident Speed vs. V-n Diagram for Flaps Retracted	A-67
Gust Load Factor and Coincident Speed vs. V-n Diagram for Flaps Extended, Detents 10, 15, 20, and 40	A-68
MANEUVER VERTICAL LOAD FACTOR DATA	
Cumulative Occurrences of Incremental Vertical Maneuver Load Factor per 1000 Hours During Departure by Altitude	A-69
Cumulative Occurrences of Incremental Vertical Maneuver Load Factor per 1000 Hours During Climb by Altitude	A-70
Cumulative Occurrences of Incremental Vertical Maneuver Load Factor per 1000 Hours During Cruise by Altitude	A-71
Cumulative Occurrences of Incremental Vertical Maneuver Load Factor per 1000 Hours During Descent by Altitude	A-72
Cumulative Occurrences of Incremental Vertical Maneuver Load Factor per 1000 Hours During Approach by Altitude	A-73
Cumulative Occurrences of Incremental Vertical Maneuver Load Factor per Nautical Mile During Departure by Altitude	A-74
Cumulative Occurrences of Incremental Vertical Maneuver Load Factor per Nautical Mile During Climb by Altitude	A-75
Cumulative Occurrences of Incremental Vertical Maneuver Load Factor per Nautical Mile During Cruise by Altitude	A-76
Cumulative Occurrences of Incremental Vertical Maneuver Load Factor per Nautical Mile During Descent by Altitude	A-77
Cumulative Occurrences of Incremental Vertical Maneuver Load Factor per Nautical Mile During Approach by Altitude	A-78

TABLE 7. STATISTICAL DATA FORMATS (Continued)

Data Description	Figure
Cumulative Occurrences of Incremental Vertical Maneuver Load Factor per 1000 Hours by Flight Phase	A-79
Cumulative Occurrences of Incremental Vertical Maneuver Load Factor per 1000 Hours, Combined Flight Phases	A-80
Cumulative Occurrences of Incremental Vertical Maneuver Load Factor per Nautical Mile by Flight Phase	A-81
Cumulative Occurrences of Incremental Vertical Maneuver Load Factor per Nautical Mile, Combined Flight Phases	A-82
MANEUVER V-N DIAGRAM DATA	
Maneuver Load Factor and Coincident Speed vs. V-n Diagram for Flaps Retracted	A-83
Maneuver Load Factor and Coincident Speed vs. V-n Diagram for Flaps Extended, Detents 10, 15, 20 and 40	A-84
COMBINED MANEUVER AND GUST VERTICAL LOAD FACTOR DATA	
Cumulative Occurrences of Incremental Vertical Load Factor per 1000 Hours by Flight Phase	A-85
Cumulative Occurrences of Incremental Vertical Load Factor per 1000 Hours, Combined Flight Phases	A-86
Cumulative Occurrences of Incremental Vertical Load Factor per Nautical Mile by Flight Phase	A-87
Cumulative Occurrences of Incremental Vertical Load Factor per Nautical Mile, Combined Flight Phases	A-88
COMBINED MANEUVER AND GUST LATERAL LOAD FACTOR DATA	
Cumulative Occurrences of Lateral Load Factor per 1000 Hours by Flight Phase	A-89
Maximum Lateral Load Factor vs. Coincident Gross Weight During Departure	A-90
Maximum Lateral Load Factor vs. Coincident Gross Weight During Climb	A-91
Maximum Lateral Load Factor vs. Coincident Gross Weight During Cruise	A-92
Maximum Lateral Load Factor vs. Coincident Gross Weight During Descent	A-93
Maximum Lateral Load Factor vs. Coincident Gross Weight During Approach	A-94
GROUND-AIR-GROUND CYCLE DATA	
Ground-Air-Ground Cycle Occurrences of Maximum and Minimum Incremental Vertical Load Factor	A-95
3-D Plot of Ground-Air-Ground Cycles	A-96
SYSTEMS OPERATIONAL DATA	
FLAP USAGE DATA	
Cumulative Probability of Maximum Airspeed in Flap Detent During Departure	A-97
Relative Probability of Maximum Airspeed in Flap Detent During Departure	A-98
Cumulative Probability of Maximum Airspeed in Flap Detent During Approach	A-99
Relative Probability of Maximum Airspeed in Flap Detent During Approach	A-100
Percent of Time in Flap Detent During Departure	A-101
Percent of Time in Flap Detent During Approach	A-102
SPEED BRAKE USAGE DATA	
Probability Distributions of Speed at Speed Brake Deployment	A-103
Probability Distributions of Maximum Speed During Speed Brake Deployment	A-104
Probability Distributions of Altitude at Speed Brake Deployment	A-105
Probability Distributions of Maximum Deployment Angle During Speed Brake Deployment	A-106
Total Hours of Coincident Speed Brake Deflection and Flap Detent	A-107
LANDING GEAR DATA	
Coincident Speed and Altitude above Airport at Landing Gear Retraction	A-108
Coincident Speed and Altitude above Airport at Landing Gear Extension	A-109
Cumulative Probability of Speed at Landing Gear Retraction and Extension	A-110
Cumulative Probability of Altitude above Airport at Landing Gear Retraction and Extension	A-111
Maximum and Minimum Incremental Vertical Load Factor and Coincident Airspeed at Landing Gear Extension	A-112
Maximum and Minimum Incremental Vertical Load Factor and Coincident Airspeed at Landing Gear Retraction	A-113
THRUST REVERSER DATA	
Cumulative Probability of Time with Thrust Reversers Deployed	A-114
Cumulative Probability of Speed at Thrust Reverser Deployment and Stowage	A-115
BRAKE APPLICATION DATA	
Probability Distributions of Time to Initial Brake Application after Touchdown	A-116
Probability Distributions of Duration of Brake Application During Landing Roll	A-117
PROPULSION DATA	
Cumulative Probability of Percent of N_1 During Takeoff, at Thrust Reverser Deployment, and During Thrust Reverser Deployment	A-118

Figures A-1 through A-118 are presented in appendix A. For ease of understanding, most of the figures in appendix A are presented in graphical form with a minimum of numerical summaries. In an effort to make the data presentation of a more comprehensive nature, some figures include both cumulative and relative probability or frequency distribution histograms as well as line plots. Where appropriate, scatter plots are also included to show the relationship between coincident parameters that are considered to be of interest and to show visible evidence of relationships, outliers, or suspicious data. The scatter plots presented in this report show that many of the plotted parameters are not related but occur in an independent random nature.

It should also be noted that the data presented in these figures are not always based on an identical number of flights or flight hours. During data reduction, it was discovered that some data frames and/or parameters exhibited random errors and were thus judged to be unacceptable for use. When this occurred, those "questionable data" were eliminated from the statistical database for any application, either directly or indirectly, of the other data measurements. As a result, not all figures are based on data from identical numbers of flights, hours, or nautical miles.

5.1 AIRCRAFT USAGE DATA.

Figures A-1 through A-18 provide statistical data on the aircraft's operational usage. Information on takeoff and landing gross weights, operational flight speeds and altitudes, aircraft attitude, and flight lengths based on normal everyday flight operations are presented. These data are primarily useful in defining typical flight profiles including gross weight, speed, and altitude and the number of flights associated with each type profile.

5.1.1 Weight and Flight Distance Data.

This section presents statistical data on operational takeoff and landing gross weights, flight distances, and plots showing the correlation between weight and flight distance. With the exception of figure A-4, the flight distances in figures A-1 through A-18 are based on the great circle distance (sometimes referred to as stage length) between departure and arrival points.

The cumulative probability distributions of gross weight during takeoff and landing are presented in figures A-1 and A-2. The occurrences of takeoff gross weight show a wide variation that one would expect due to differing fuel weights for different length flights and variable passenger and baggage loading. The landing weight distribution shows some tendency to group within a narrower range that could indicate use of fuel management that results in more consistent landing weights. However, the wide variations of both distributions could also result because some of the flights may not be refueled at each landing site. It is noteworthy that the maximum landing gross weight observed is very close to the maximum design landing gross weight of 142,195 lbs., listed in table 1.

Figure A-3 shows the cumulative probability distribution of the flight length from takeoff to landing for all A-320 flights. The distribution of flight length occurrences indicates that the flights tend to fall into three distinct groups. There is a grouping of short range flights of less than about 1000 nautical miles, a mid-range grouping of flights between 1000 and 1750 nautical miles, and a longer range group of flights between 1750 and about 2350 nautical miles.

Figure A-4 presents a scatter plot comparison of the differences in the great circle flight length and the integrated flight distance. The great circle flight length reflects the calculated straight-line flight distance between two points in still air. The integrated flight distances represents the airborne distance flown relative to the ambient air and accounts for the impact of winds, deviations from straight-line flight, and loiter on the total distance flown by the aircraft. These distances will always be different because of deviations that occur during the flight resulting from directional flight changes directed by air traffic control center, increased distance flown due to holding patterns, wind direction, and to a much lesser extent, the climb and descent distances that are slightly larger than the level flight distance. The figure 4 plot indicates, for operation of the A-320, that the integrated flight distance tends to be slightly longer than the great circle flight length. Hence, the aircraft is subjected to the loading environment for a longer period of time than if only the great circle flight length was considered. The flights shown with no change in great circle flight length were probably test flights or flights that turned back because they returned to the same takeoff location.

Figures A-5 and A-6 compare aircraft gross weight at takeoff with distance flown to determine whether there is any correlation between the two parameters. Figure A-5 compares the takeoff gross weight versus the distance flown for each individual flight as a scatter plot, whereas figure A-6 contains a tabular listing of the percent of flights that took off within the interval of gross weight shown and those that landed within the specified flight distance. While both figures indicate there is a wide variation in takeoff gross weights and flight lengths, the data show some correlation between gross weight and great circle flight length, although considerable scatter is evident. The data also indicate that the aircraft is being used for long, medium, and short flight distances.

Figure A-7 provides a tabular listing of the percent of flights that takeoff and land within the gross weight ranges indicated. The data indicate that about 87% of the flights takeoff in a gross weight range between 130-170 K lbs. and about 81% of the flights land at weights between 120-140 K lbs.

Figure A-8 shows the distribution, expressed in percent, of the integrated flight distance by pressure altitude bands. Each column represents 100% of the flights that fall within the specified distance range. The table shows that the aircraft consistently (>80% of the time) fly at the higher altitudes during the longest flights (>1500 nautical miles). However, for those flight distances less than 1500 nautical miles, the percent of flights operating at the middle to lower level altitudes between 4500 and 29,500 feet increases noticeably.

5.1.2 Altitude and Speed Data.

This section presents information about the altitudes and speeds at which the aircraft operate.

Figure A-9 shows the maximum altitude attained during each flight plotted versus the duration of the flight. The data indicate that as the flight length increases the aircraft consistently fly at the higher altitudes. The scatter plot also indicates that as the flight duration decreases to under an hour in length, these flights, which may include some training and/or test flights, tend to occur at the middle to lower altitudes. These trends indicate a probable correlation between flight duration and the maximum altitude attained.

The cumulative probabilities of ground speed for taxi in and taxi out operations are presented in figure A-10. The taxi in speed is somewhat higher than the taxi out speed, which agrees with what has been observed with other aircraft models. This probably occurs because ground movement of inbound traffic to the terminal after landing is generally accomplished faster due to less traffic than movement from the terminal to the takeoff position with traffic present. It should be noted for this report that the taxi in phase of operation begins after the first turnoff from the active runway as compared to previous UDRI reports that included the runway turnoff speeds as part of the taxi in phase of operation. The higher taxi-in speeds, as observed in these earlier reports, probably occurred as the aircraft was exiting the runway during the turnoff.

Figures A-11 and A-12 show measured speeds plotted versus Mach number and airspeed limits, M_{MO} or V_{MO}, as defined in the aircraft flight manual. Each plotted point represents the airspeed or Mach number that yielded the greatest difference between the observed airspeed or Mach number and the speed or Mach number limit at its coincident altitude regardless of flight phase. For example, in one flight, the maximum speed, with respect to the limit, might have been attained in the climb phase, while in another flight the maximum speed may have occurred in a different phase. Also, it should be noted that the Mach number and airspeed points as plotted do not necessarily occur simultaneously.

While both plots indicate there are many flights that operate at speeds or Mach number values approaching or slightly exceeding the airspeed limits, the A-320 aircraft's onboard computers should only allow these speed limits to be exceeded for a few seconds before automatically responding to reduce the aircraft's speed to acceptable levels. UDRI checked a few of the points that are over the airspeed limit at the lower altitudes and they occurred for several seconds either during descent or near the end of the descent phase. Also, except for one flight, there is an obvious absence of points anywhere near the Mach or airspeed limits for those flights shown operating below 10,000 feet. The flight point occurring from this flight in both plots nearest the limit at 5,000 feet was checked and represented a valid data point for a normal flight. All of the other points shown as occurring below 10,000 feet were also investigated and resulted during flights of very short duration. The reason there were no points in these flights near the airspeed limits is probably because other speed restrictions such as those imposed for flap and/or landing gear operations further restrict the aircraft's airspeed at these altitudes and flight distances.

Figures A-13 and A-14 show the cumulative probabilities of calibrated airspeed at liftoff and at touchdown. Figure A-13 shows that the majority of takeoffs occur at speeds between 150 and 165 knots. Figure A-14 separates the landing speeds at touchdown for flights that were landed under manual control and those using the autoland system. About 1% of the total number of flights recorded were landed using the autoland system. Although most landing speeds at touchdown vary between 115 and 140 knots, the speeds associated with autolandings are slightly higher than those during manually controlled landings. Comparison of the two figures also shows that the liftoff speeds for the A-320 are approximately 30 knots higher than the touchdown speeds.

5.1.3 Attitude and Rate Data.

This section presents statistical pitch angle data for selected phases of flight. Probability distributions showing the maximum pitch rate of the nose gear at touchdown are also included.

Figure A-15 provides the cumulative probability of maximum pitch angle at liftoff. The pitch angle data for figure A-15 were initially developed using the last pitch angle reading just before the squat switch indicated the aircraft had lifted off. However, these criteria resulted in many occurrences of pitch angle that exceeded the 10.5-11 degrees clearance necessary to avoid a tail strike. Thus, UDRI questioned its validity and initiated efforts to investigate the procedures and criteria it was using to identify pitch angle at liftoff. It became obvious from examining time histories of radio altitude and pitch angle at liftoff that the squat switch reading was not an accurate indicator of liftoff. Thus, UDRI changed its criteria and used radio altitude to determine when liftoff occurred. A new algorithm was developed that identified liftoff as the first reading in a series of increasing radio altitude values that were greater than 4 feet higher than the average radio altitude calculated during the takeoff roll. The curve shown in figure A-15 reflects the pitch angle at liftoff using radio altitude as the criteria. The data in this figure is based on 2458 flights because radio altitude was not provided on all flights. While this curve still shows an occurrence of pitch angle near 13 degrees, which could indicate a tail strike, the actual liftoff point could still be off by ±1 second due to the sampling rate associated with radio altitude.

Figure A-16 shows the cumulative probability distribution of pitch angle at touchdown/landing. The pitch angle during landing varied between 1 and 8 degrees with the most landings occurring at pitch angles between 5 and 6 degrees. Although the squat switch was not a reliable indicator of the instant of touchdown, it was considered to be adequate for purposes of determining the pitch angle during landing, because the pitch angle during the flare maneuver is usually held fairly constant until touchdown. Thus, the airplane's rotation, which significantly affected the reported pitch angle during liftoff, has a far lessor effect on the reported pitch angle at touchdown.

Figures A-17 presents the cumulative probability of the maximum pitch angle during the departure and approach phases of flight. The data shows that the pitch angle of the aircraft during departure varies between 14 and 24 degrees while during its approach, the pitch angle varies between about 4 and 10 degrees. Chai and Mason [4] attributed this difference to the fact that "with the flaps in the fully deflected position, the critical angle of attack of the wing during landing (and approach) is smaller than during takeoff (and departure). Consequently, the pitch angle during landing is smaller than that during takeoff."

Figure A-18 shows the probability and frequency distributions of the maximum pitch rate during touchdown of the nose gear following landing. Most touchdowns occur at pitch rates between -1.5 and +3.5 degrees/second.

5.2 GROUND LOADS DATA.

Figures A-19 through A-49 provide statistical loads data based on the A-320's ground operations. The ground loads data include frequency and probability information on vertical, lateral, and longitudinal accelerations during takeoff, landing, taxi, and turning operations. These loads primarily affect the landing gear and landing gear backup structure and, to a lesser extent, the wing, fuselage, and empennage. (Statistical ground loads data for other aircraft models can be found in reference 2.)

5.2.1 Lateral Load Factor Data.

This section presents lateral load factor statistical data during aircraft ground turning operations and at touchdown.

Figure A-19 shows the cumulative occurrences of maximum lateral load factor that occur during ground turning operations (excludes the runway turnoff). The information is presented per 1000 flights for both preflight and postflight taxi and contains data for both left and right turns. The magnitudes of lateral load factor are about equal during taxi in and taxi out. Data for the B-737-400, MD-82/83, and B-767-200 aircraft, as reported in references 5, 6, and 7, showed that during taxi in, the lateral load factors are a little higher probably because of the higher speeds associated with taxi in. Also, figure A-19 shows no significant difference between the number of left and right turns or their magnitudes.

Figure A-20 presents the cumulative occurrences of maximum lateral load factor that occur per 1000 flights at touchdown. Because of the delay in the squat switch indication of touchdown and to ensure that the maximum n_y load factor peak associated with touchdown was identified, UDRI scanned an interval of 5 seconds prior to squat switch closure to identify the maximum n_y load factor peak during touchdown. The data show that n_y peaks during the landing touchdown fall between approximately -0.26 to +0.3 g's. The relative frequency distribution does not exhibit a distinguishable mode frequency but increases as the side load factor approaches zero from either direction. There were 565 flights that did not contain an n_y peak at touchdown, so the number of peaks does not equate to the number of flights.

Figure A-21 presents the occurrences of the maximum lateral load factor that occurred per 1000 flights during the first turnoff from the active runway after landing. This figure shows there were 3,551 flights that turned right and 6,515 flights that turned left off the runway, which is more of a disparity than one would expect, but is a function of the airport/runway layout and traffic patterns. However, the magnitude of lateral load factor between about ±0.3 g's for right and left turns is very similar, as one would expect. These lateral load factor occurrences are not included in the taxi in data presented in figure A-19. Thus, when figures A-19 and A-21 are compared, it can be seen that values of lateral load factor are slightly higher during runway turnoff.

Figure A-22 presents the coincident incremental vertical load factor that occurs in conjunction with the maximum lateral load factor at touchdown (the same 5-second interval as defined above was used to identify touchdown). Some of the flights did not experience an n_y peak associated with touchdown; therefore, no coincident n_z values were plotted for these flights. The data show that the highest vertical load factor peaks occur in conjunction with the lower magnitude occurrences of lateral load factor. Similarly, when the highest lateral load factors occur, the vertical load factors tend to be at the lower end of their range.

Figure A-23 shows the probability of the turn angle (total angular measurement) experienced during 10,066 turnoffs from the active runway. The plot indicates that a significant number of turns are grouped in the 30, 90, and 180-degree range. The scatter plots, figures A-24 through A-26, show the maximum lateral load factor experienced during each turnoff versus its corresponding ground speed. The range of turn angles in each of these figures was selected in

order to span the three turn angles, which occurred most frequently. While the data show there is considerable variation in ground speeds during the runway turnoff, there does not appear to be any correlation between speed during the turn and the magnitude of the lateral load factor.

Figures A-27 through A-30 contain scatter plots showing the maximum lateral load factor at touchdown versus the yaw angle, bank angle, and wind speed before touchdown. Since yaw angle was not a recorded parameter, it had to be derived for each landing. This was accomplished by assuming that the calculated average magnetic heading of the aircraft on the runway after landing represented the direction of the runway. Then, the calculated difference in the aircraft heading prior to touchdown with the magnetic heading of the aircraft on the runway after landing resulted in the estimated yaw angle. The maximum yaw angle reflects the highest value that was calculated during an interval from -10 seconds to -3 seconds prior to the squat switch indication of touchdown. (The interval was terminated at -3 seconds prior to touchdown to ensure that data from touchdown were not included.) The mean yaw angle was determined by averaging the maximum yaw angles that occurred during the 10- to 3-second interval just prior to touchdown. At most, a minimal correlation exists between yaw angle and lateral acceleration at touchdown. The maximum bank angle reflects the maximum value recorded during the 50-second interval prior to touchdown. The mean wind speed was determined by taking the difference between the calculated mean airspeed and the calculated mean ground speed during a 40-second interval from 50 seconds to 10 seconds prior to touchdown. The 10-second cutoff was selected in order to avoid any possible effects of the aircraft's proximity to the ground. A positive difference indicates a head wind and a negative difference a tail wind. A statistical analysis of the data showed that 1 percent of the landings occur with tail winds (-speeds) greater than 10 knots, while 10 percent of the landings occur with tail winds greater than 5 knots.

5.2.2 Longitudinal Load Factor Data.

Longitudinal load factor statistics are presented for pre- and postflight taxi, at touchdown, and during the landing roll phases of ground operations.

Figure A-31 presents the cumulative occurrences of longitudinal load factor during pre- and postflight taxi operations per 1000 flights. The occurrences of longitudinal load factor during taxi occur primarily due to braking and throttle changes. The magnitude of longitudinal load factors observed during taxi vary between -0.47 and +0.41 g's.

Figure A-32 shows the cumulative frequency of the maximum and minimum longitudinal load factor measured at touchdown and during the landing rollout with and without thrust reverser deployment. It appears that additional braking, which results from deployment of the thrust reversers, increases the negative longitudinal load factor spectra by approximately 0.1 g over the values seen when the thrust reversers are not in use. The maximum longitudinal load factor observed was -0.56 g, which occurred during operation of the thrust reversers. The occurrence of positive longitudinal load factors, even though very small, probably occurs due to the variations in retardation forces caused by the thrust reversers, hydraulic brakes, and rolling friction.

5.2.3 Vertical Load Factor Data.

This section presents vertical load factor statistics during ground operations involving touchdown, taxi, and takeoff and landing roll (with and without thrust reverser), and at spoiler deployment; scatter plots showing the maximum vertical load factor versus the maximum angle of attack during liftoff for various selected speed ranges; and the aircraft's acceleration response due to operations on runways within this operator's system.

Figure A-33 presents cumulative occurrences of incremental vertical load factor per 1000 flights for the taxi in and taxi out phases of ground operations. The data show that the distribution of vertical load factor during taxi-in is slightly higher than for taxi out. This slight difference was also observed on the B-737-400, MD-82/83, and B-767 aircraft [5, 6, and 7] and is probably due to the slightly higher taxi in speeds shown in figure A-10.

Figure A-34 presents the cumulative occurrences of positive and negative incremental vertical load factors per 1000 flights that occurred during the takeoff roll. While the magnitudes of load factor appear to be consistent with what one would expect during the takeoff roll, these values are primarily a function of the condition or "roughness" of the runway.

Figure A-35 presents the cumulative occurrences of the minimum and maximum incremental vertical load factor per 1000 flights associated with touchdown and deployment of the ground spoilers. This figure shows that approximately the same minimum and maximum load factor peaks, -0.5 g and +1.0 g, respectively, are attributable to each event. These identical readings probably occur because the sampling rate for each event indicator is only once per second and deployment of the ground spoilers occurs very quickly after touchdown. Thus, when this occurred, it was impossible to determine which event actually caused the minimum and maximum load factor peaks. So, unless the peaks were separated by several seconds, the same minimum or maximum peak was probably identified and assigned as having occurred both at touchdown and during deployment of the spoilers.

Figure A-36 presents the cumulative occurrences of incremental vertical load factor per 1000 flights during the landing roll for operations with and without thrust reversers. These curves may also include the effects of ground spoiler usage on vertical load factor because the spoilers are normally used during the landing rollout concurrently with the thrust reversers.

Figures A-37 through A- 42 contain scatter plots that show the maximum incremental vertical load factor that occurred during the takeoff rotation versus the maximum angle of attack attained within a 10-second interval after liftoff and the coincident airspeed/range at which they occurred. While the plots show that the maximum angle of attack during liftoff tends to decrease with increasing airspeed, there doesn't appear to be any correlation between angle of attack and vertical acceleration. The airspeed ranges of 150-160 knots in figures A-39 and 160-179 knots in figure A- 40 generate the largest number of acceleration peaks because they are the speeds most frequently used during liftoff.

Figures A-43 through A-47 contain scatter plots that show the maximum incremental vertical load factor at touchdown versus the yaw angle, bank angle, wind speed, and inertial vertical velocity before touchdown. The values of yaw angle, bank angle, and wind speed values used

here are the same as those derived and used previously in figures A-27 through A-30. The values of mean inertial vertical velocity contained in figure A-47 were obtained by averaging the recorded values between -50 seconds and -10 seconds prior to aircraft touchdown. The final 10 seconds of flight data were not used because of concerns about the accuracy of these measurements due to ground effects.

Figure A-48 is a scatter plot that shows the maximum incremental vertical load factor versus the coincident computed airspeed at touchdown. The negative values shown indicate that the vertical load factor response during a few of the landing touchdowns was higher than the positive load factor due to landing impact.

Figure A-49 compares the roughness of different runways used by the airline involved with this program (see page xi for a list of airport codes). A Root Mean Square (RMS) vertical acceleration was calculated using the takeoff and landing roll vertical acceleration data from each airport. However, because of the close proximity of parallel runways at some airports and the questionable accuracy involved with presenting these data by runway, the RMS data presented reflect the average of all runways used at each airport. The data show that in terms of A-320 acceleration response, the roughest runway location (PVD) is about twice as rough as the smoothest runway location (BIL).

5.3 FLIGHT LOADS DATA.

The statistical flight loads data in this section, figures A-50 through A-96, describe the aircraft's operational gust, maneuver, and combined maneuver and gust load environment.

The gust loads data are presented in the form of incremental vertical load factors, derived gust velocity U_{de}, and continuous gust intensity U_{σ}. Gust vertical factor data are plotted as either cumulative occurrences per 1000 hours or as cumulative occurrences per nautical mile and may be plotted by phase of flight, altitude, flap position, etc. The derived gust velocity and continuous gust intensity are computed values as described in section 4.2.

Maneuver loads data are presented as either cumulative occurrences of incremental load factor per 1000 hours or as cumulative occurrences per nautical mile and may be plotted by phase of flight, altitude, flap position, etc.

This section also presents the combined total vertical and lateral load factor occurrences, due to the maneuver and gust environment, presented per 1000 hours or per nautical mile by phase of flight; and, for vertical load factor for all flight phases combined. V-n diagrams showing the coincident gust and maneuver vertical load factor versus speed for the flaps retracted and extended conditions are presented. Cumulative occurrences of maximum lateral load factor versus gross weight are presented by phase of flight. Also, the excursion, between the largest negative and highest positive load factor that occurs once per flight, are paired together and presented as the Ground-Air-Ground or GAG cycle data in this section.

5.3.1 Gust Vertical Load Factor Data.

Cumulative occurrences of incremental vertical gust load factor are plotted as either cumulative occurrences per 1000 hours or per nautical mile by phase of flight.

Figure A-50 shows the cumulative occurrences of incremental vertical gust load factor per 1000 hours by phase of flight, and figure A-51 shows the cumulative occurrences of incremental vertical gust load factor for all the airborne phases combined per 1000 hours. The maximum incremental vertical gust load factor encountered by the A-320 was 1.0 g and occurred, as shown in figure A-50, during the approach phase of flight.

Figure A-52 presents the cumulative occurrences of incremental vertical gust load factor per nautical mile by phase of flight, and figure A-53 shows the cumulative occurrences of incremental vertical gust load factor for all the airborne phases combined per nautical mile.

5.3.2 Derived Gust Velocity Data.

The magnitudes for the gust velocities were derived from the measured accelerations in accordance with the procedures presented in section 4.2.4. In figures A-54 and A-55, derived gust velocity, U_{de}, is plotted as cumulative occurrences per nautical mile for altitudes above the airport; in figures A-56 through A-62, U_{de}, is plotted as cumulative occurrences per nautical mile for pressure altitudes from sea level to 39,500 feet. In each figure, the derived gust velocities are compared to the gust velocity distributions presented in reference 8, which is an established standard that is often used in establishing structural design criteria for repeated gust loads.

Figures A-63 and A-64 present derived gust velocity, U_{de}, per nautical mile for the flaps extended and retracted conditions, respectively.

5.3.3 Continuous Gust Intensity Data.

The magnitudes of the continuous gust intensities, U_{σ}, were derived from the measured accelerations in accordance with the procedures presented in section 4.2.5. The cumulative occurrences of continuous gust intensity per nautical mile for the flaps extended and retracted conditions are presented in figures A-65 and A-66, respectively.

5.3.4 Gust V-n Diagram Data.

In order to display the coincident speed and gust accelerations, representative V-n diagrams were developed for the flaps retracted and extended configurations for illustration purposes only. Since V-n diagrams are a function of altitude and gross weight, the maximum takeoff gross weight of 162,083 pounds for the flaps retracted configuration and a landing gross weight of 130,000 pounds for the flaps extended configuration were selected at an altitude of sea level. The landing gross weight was selected as representing a median value based on the data as shown in figure A-2.

Figures A-67 and A-68 show the coincident gust acceleration and airspeed measurements plotted on the V-n diagrams for the flaps retracted and extended configurations, respectively. All flap

detent positions for which data were available (10, 15, 20, and 40), are shown in order to provide a range of flap extension conditions. Figure A-68 shows, for the flaps extended cases, that a few gust acceleration points fall outside the gust V-n diagram. These results are similar to those observed on other aircraft [5, 6, and 7] with the flaps extended. One must also keep in mind that the V-n diagram shown here is for only one gross weight and altitude condition. If the measured gust acceleration data were plotted against the V-n diagram for the actual gross weight and altitude conditions that existed at the time the acceleration was measured, the data might fall within the V-n diagram. Furthermore, the V-n diagram reflects only one static strength design requirement. The actual structure is designed to several different strength and rigidity design requirements, including static strength, durability, and damage tolerance. While the exceedance of a single design requirement may indicate a shortcoming in the design requirement, it does not necessarily translate into a deficiency in the overall design strength of the aircraft.

5.3.5 Maneuver Vertical Load Factor Data.

The maneuver loads data are presented in the form of incremental vertical load factors, either per 1000 hours or per nautical mile by phase of flight and altitude, or as combined phases.

Figures A-69 through A-73 provide the cumulative occurrences of incremental maneuver load factor per 1000 hours by altitude for each of the airborne flight phases, i.e., departure, climb, cruise, descent, and approach.

Figures A-74 through A-78 display the cumulative occurrences of incremental maneuver load factor by altitude per nautical mile (instead of per 1000 hours) in the airborne phases of flight.

Figure A-79 shows the total cumulative occurrences of incremental maneuver load factor per 1000 hours for each phase of flight, regardless of altitude. Figure A-80 contains the total cumulative occurrences of incremental maneuver load factor per 1000 hours for all flight phases combined.

Figure A-81 shows the total cumulative occurrences of incremental maneuver load factor per nautical mile for each phase of flight, regardless of altitude. Then, figure A-82 contains the total cumulative occurrences of incremental maneuver load factor per nautical mile for all flight phases combined.

The maximum incremental vertical maneuver load factor encountered by the A-320 was 0.8 g and occurred during the descent and approach phases of flight.

5.3.6 Maneuver V-n Diagram Data.

Maneuver strength is required for three different aircraft design speeds: flaps down speed (V_F), cruising speed (V_C), and dive speed (V_D). For the maneuver V-n diagram, the required limit load factors are specified in FAR 25.337. The positive limit maneuvering load factor (n) may not be less than 2.5, and the negative limit maneuvering load factor may not be less than -1.0 at speeds up to V_C, varying linearly with speeds to zero at V_D. FAR 25.345 specifies that the positive limit maneuver load factor is 2.0 g when the flaps are extended. As with the V-n diagram for gust loads, the maximum takeoff gross weight of 162,083 pounds for the flaps retracted configuration

and the maximum landing gross weight of 130,000 pounds for the flaps extended configuration were selected to develop representative maneuver V-n diagrams.

Figures A-83 and A-84 show the maneuver V-n diagrams with flaps retracted and extended with the coincident acceleration and speed measurements. All flap detent positions for which data were available (10, 15, 20, and 40), are shown in figure A-84 to provide a range of flap extension conditions. Figure A-84 shows, for the flaps extended cases, that a few maneuver acceleration points occur at speeds outside the maneuver V-n diagram. These results are similar to those observed on other aircraft [5, 6, and 7] with the flaps extended.

5.3.7 Combined Maneuver and Gust Vertical Load Factor Data.

Figure A-85 shows the cumulative occurrences of the combined maneuver and gust incremental vertical load factor per 1000 hours by phases of flight, and figure A-86 shows the incremental vertical load factor occurrences for all flight phases combined.

Figures A-87 and A-88 contain the same vertical load factor data as figures A-85 and A-86, but are plotted as occurrences per nautical mile by phases of flight and for all flight phases combined. The 1-g incremental gust load factor encountered during the approach phase of flight is still the highest load factor recorded for the A-320's operation.

5.3.8 Combined Maneuver and Gust Lateral Load Factor Data.

Figure 89 presents the cumulative occurrences of lateral load factor per 1000 hours by phase of flight. Maximum lateral load factor values between approximately -0.32 and +0.19 g's were observed during flight operations of the A-320.

Figures A-90 through A-94 contain scatter plots that show the maximum lateral load factor versus the coincident gross weight of the aircraft during the airborne phases of flight.

5.3.9 Ground-Air-Ground Cycle Data.

Figures A-95 and A-96 display occurrences of the maximum and minimum incremental vertical load factor that occurs once per flight. The load excursion between the largest negative and highest positive load factor is often referred to by aircraft design engineers as the Ground-Air-Ground or GAG cycle. Figure A-95 presents the number of GAG cycle occurrences in tabular form and figure A-96 shows the number of GAG cycle occurrences plotted as a three-dimensional (3-D) bar chart. The GAG cycle usually contributes the most damaging fatigue cycle experienced by the aircraft wing and carry through structural assemblies. The GAG cycle that contained the widest range between negative and positive occurred between -0.95 and +0.65 g's.

5.4 SYSTEMS OPERATIONAL DATA.

This section contains operational usage data for the flaps, speed brakes, landing gear, thrust reversers, brakes, and the propulsion system. Although control surface position information was available for the aileron, rudder, and elevator systems, it was not processed because the sampling

rates were deemed to be too slow to provide reliable statistical usage information for these components.

5.4.1 Flap Usage Data.

Flap usage data showing airspeed and percent of time spent by flap detent and phase of flight are presented. These data can be used to characterize the sources of repeated loads on the flaps and backup structure and other flap components. The A-320 flap operational speed limits for each detent setting were listed in table 6.

Figures A-97 and A-98 present the probability of the maximum airspeed encountered in various flap detents during the departure phase of flight, and figures A-99 and A-100 present similar probability data for the approach phase of flight. Figure A-100 shows that the most probable speed at which the flaps are first deployed during the approach phase of flight for detent 10 occurs at about 186 knots, for detent 15 about 184 knots, for detent 20 about 170 knots, and for detent 40 the speeds vary between about 150-165 knots.

Figures A-101 and A-102 present the percent of time spent in each flap detent setting during the departure and approach phases of flight, respectively. Flap detent 10 is the most frequently used setting during the departure phase (70%); flap detents 15 (42%) and 40 (39%) are the most often used settings during the approach phase. The low amount of time shown in detent 10 during the approach phase may explain why the speeds discussed above for detents 10 and 15 occur so closely together. The pilot probably does not stop at detent 10 during the approach phase, so the small amount of time shown is probably the time associated with passing through the detent 10 setting.

5.4.2 Speed Brake Usage Data.

Statistics on speed brake usage as a function of speed, altitude, deployment angle, and time spent at coincident flap detent and speed brake settings are of major interest to both aircraft manufacturers and airline operators. These data are presented in figures A-103 through A-107.

Figure A-103 illustrates the probability distribution of the speed at the instant of speed brake deployment, and figure A-104 gives the probability distribution of the maximum speed encountered while the speed brakes were deployed in flight. These plots are very similar because the airspeed at speed brake deployment is usually the maximum airspeed that occurs while the speed brakes are deployed. Figure A-105 presents the probability and frequency distributions of the altitude when the speed brakes were deployed, and figure A-106 presents the probability and frequency distributions of the maximum deployment angle reached while the speed brakes were deployed.

The table in figure A-107 shows the number of flight hours the aircraft was flown at coincident flap detent and speed brake settings. The table shows that speed brake deflections of less than 1-degree at flap setting of zero detent account for approximately 80 percent of the time the speed brakes are deployed.

5.4.3 Landing Gear Data.

Statistical data showing the speeds, altitudes, and vertical load factor when the landing gear is started to be retracted or extended are shown in figures A-108 through A-113. This information characterizes the operational usage of the landing gear for the airline and also provides data for the aircraft manufacturer that can be used to assess the loading conditions for the landing gear and backup structure.

Figures A-108 and A-109 contain scatter plots showing the coincident speed and altitude above the airport at the start of gear retraction and extension. Although figure A-108 shows considerable scatter, the beginning of the landing gear retraction cycle most often occurs around 160 knots and about 700 feet in altitude above the airport. While figure A-109 also shows a lot of scatter between speed and altitude when the landing gear extension cycle begins, the landing gear extension appears to occur most often between 160-190 knots at altitudes ranging from around 1000 feet up to about 3000 feet.

Figures A-110 and A-111 contain the same data points used to generate the scatter plots shown in figures A-108 and A-109 but are plotted here as the probability of speed and altitude above the airport at the beginning of landing gear extension and retraction.

Figures A-112 and A-113 contain scatter plots that show the maximum and minimum incremental vertical load factor versus coincident airspeed at the beginning of landing gear extension and retraction.

5.4.4 Thrust Reverser Data.

The times and speeds associated with thrust reverser ground operations were derived from the measured data. Figure A-114 presents the cumulative probability of time during which the thrust reversers are deployed. The data show that for 90 percent of the flights the thrust reversers are deployed for less than 25 seconds. Figure A-115 presents the cumulative probability of the speed at the time the thrust reversers were deployed and stowed. Most thrust reverser deployment cycles begin at speeds between 100 and 120 knots and are stowed at speeds between 40 and 80 knots.

5.4.5 Brake Application Data.

The time from aircraft touchdown to initial application of the brakes and the time duration for which braking occurred during the landing roll are presented. Figure A-116 shows the probability of time to application of the brakes after touchdown. The most frequent time to initial brake application ranges from about 10 to 30 seconds. Figure A-117 shows the probability of the duration of brake application during the landing roll after landing. Typical brake applications last from about 5 to 30 seconds.

5.4.6 Propulsion Data.

Figure A-118 presents the cumulative probability of the maximum engine fan speed, N_1, during takeoff, at the instant of thrust reverser deployment during the landing roll, and during the time

that the thrust reverser is deployed. Most takeoffs occur at fan speed values ranging between 80% and 90%. The typical fan speed at thrust reverser deployment ranges between 30% and approximately 50% and then increases up to a maximum value of around 72% during the time the thrust reverser is deployed.

6. CONCLUSIONS.

This report provides valuable information about how the Airbus A-320 aircraft and its onboard systems are being used during normal flight and ground operations by a U.S. airline.

The participating airline fully supported this program and provided University of Dayton Research Institute (UDRI) with 10,066 flights representing 30,817 flight hours of useable A-320 data from typical revenue flights. Except for some gaps and repeated frames, the recorded data were of high quality and compatible with UDRI's data processing software. The 10,066 flights were judged as sufficient to provide a representative statistical baseline of the aircraft's ground, airborne, and systems operational usage.

The squat switch indication that was used to determine when liftoff and touchdown occurred for reducing data for other large transport aircraft programs previously did not provide an accurate indication of when these events occurred for the A-320. New criteria were developed, which used radio altitude to identify when liftoff occurred and time (5 seconds) prior to when the squat switch indicated touchdown provided the best results for the A-320.

The 118 statistical data formats presented in this report provides the Federal Aviation Administration, airline, and aircraft manufacturer with a detailed characterization concerning A-320's actual operational service usage. New criteria were developed and incorporated into the UDRI data processing software to provide more information about the A-320's flight and ground operations. These criteria were developed to (1) identify the start and completion of the turnoff from the active runway after landing, (2) identify the ground-air-ground cycle, (3) define coincident fuel flow rates at maximum values of N_1, and (4) provide data on additional parameters such as bank angle and glide slope.

The statistical data presented in this report demonstrated that the operational ground and airborne usage of the A-320 aircraft is similar to other large transports such as the B-767, B-737, and MD-82/83 aircraft. However, there were instances, such as shown in figures A-12, A-68, and A-84, where the A-320 appeared to be operating very close to or slightly exceeded its structural and operational limits.

7. REFERENCES.

1. de Jonge, B., "Reduction of Incremental Load Factor Acceleration Data to Gust Statistics," DOT/FAA/CT-94/57, August 1994.

2. Tipps, Daniel O., John W. Rustenburg, and Donald A. Skinn, "Study of Side Load Factor Statistics From Commercial Aircraft Ground Operations," University of Dayton Research Institute Report UDR-TR-2001-00005, January 2001.

3. Rustenburg, John W., Donald A. Skinn, and Daniel O. Tipps, "An Evaluation of Methods to Separate Maneuver and Gust Load Factors From Measured Acceleration Time Histories," DOT/FAA/AR-99/14, April 1999.

4. Chai, Sonny T. and William H. Mason, "Landing Gear Integration in Aircraft Conceptual Design," Virginia Polytechnic Institute and State University Report MAD 96-09-01, September 1996 (rev. March 1997).

5. "Statistical Loads Data for Boeing 737-400 in Commercial Operations," FAA Report DOT/FAA/AR-98/28, August 1998.

6. "Statistical Loads Data for MD-82/83 in Commercial Operations," FAA Report DOT/FAA/AR-98/65, February 1999.

7. "Statistical Loads Data for B-767-200ER Aircraft in Commercial Operations," FAA Report DOT/FAA/AR-00/10, March 2000.

8. Press, Harry and Roy Steiner, "An Approach to the Problem of Estimating Severe and Repeated Gust Loads for Missile Operations," National Advisory Committee for Aeronautics Technical Note 4332, Langley Aeronautical Laboratory, Langley Field, Virginia, September 1958.

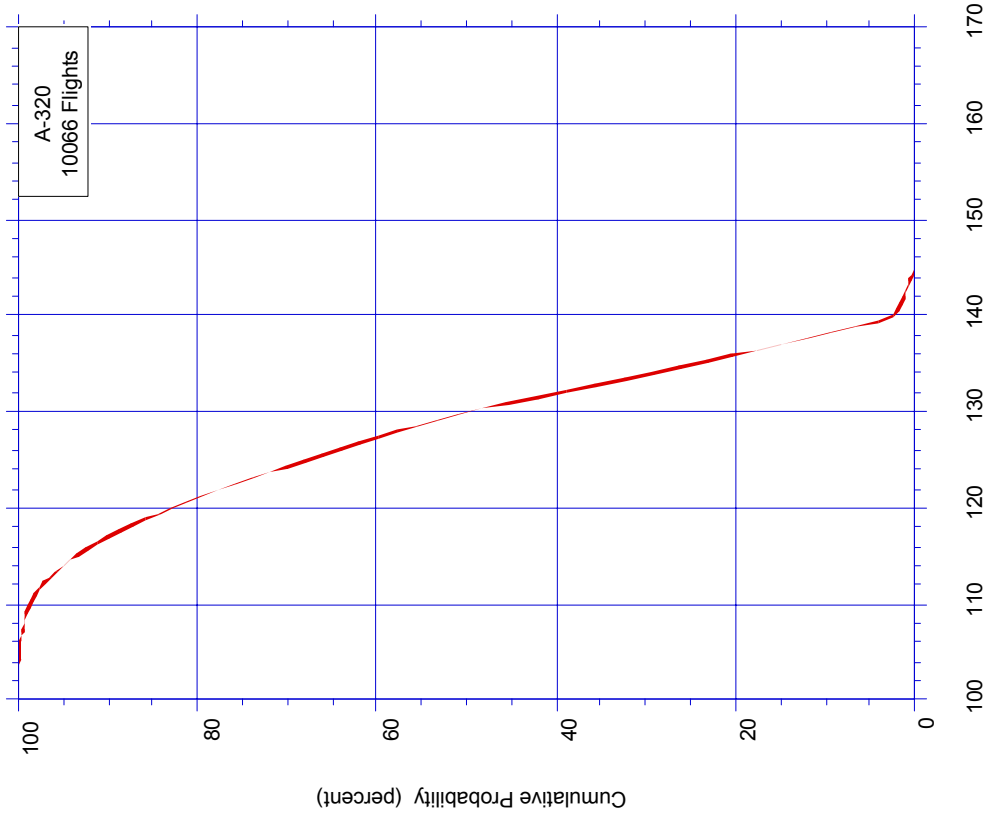


FIGURE A-2. CUMULATIVE PROBABILITY OF LANDING GROSS WEIGHT

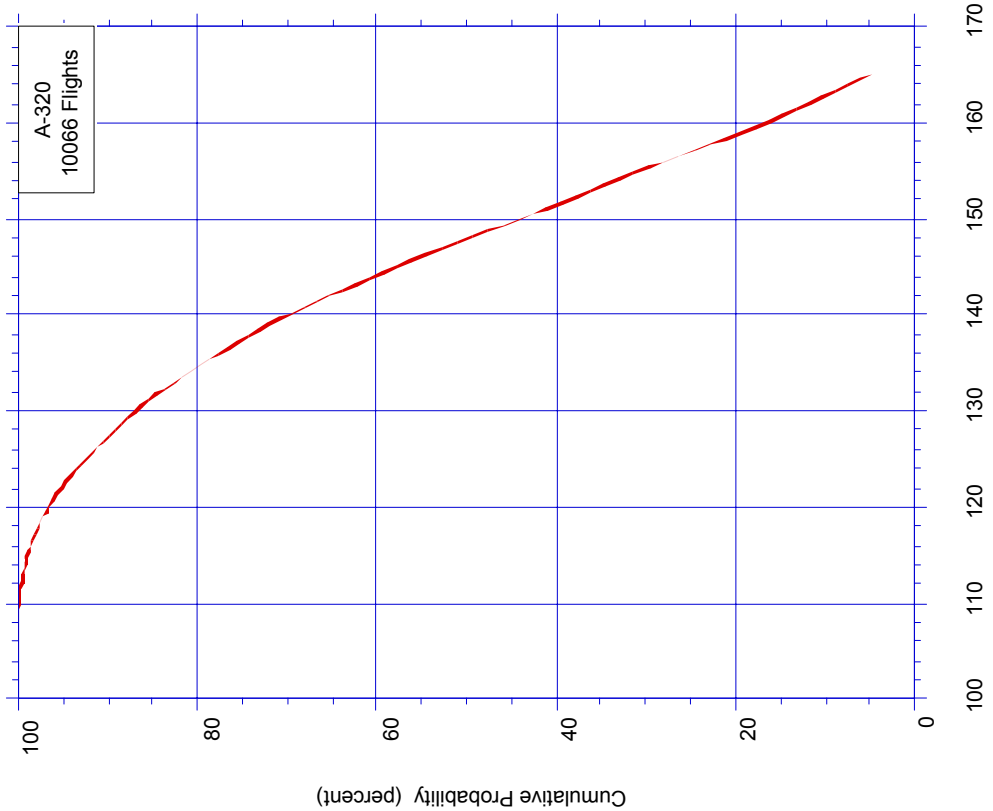


FIGURE A-1. CUMULATIVE PROBABILITY OF TAKEOFF GROSS WEIGHT

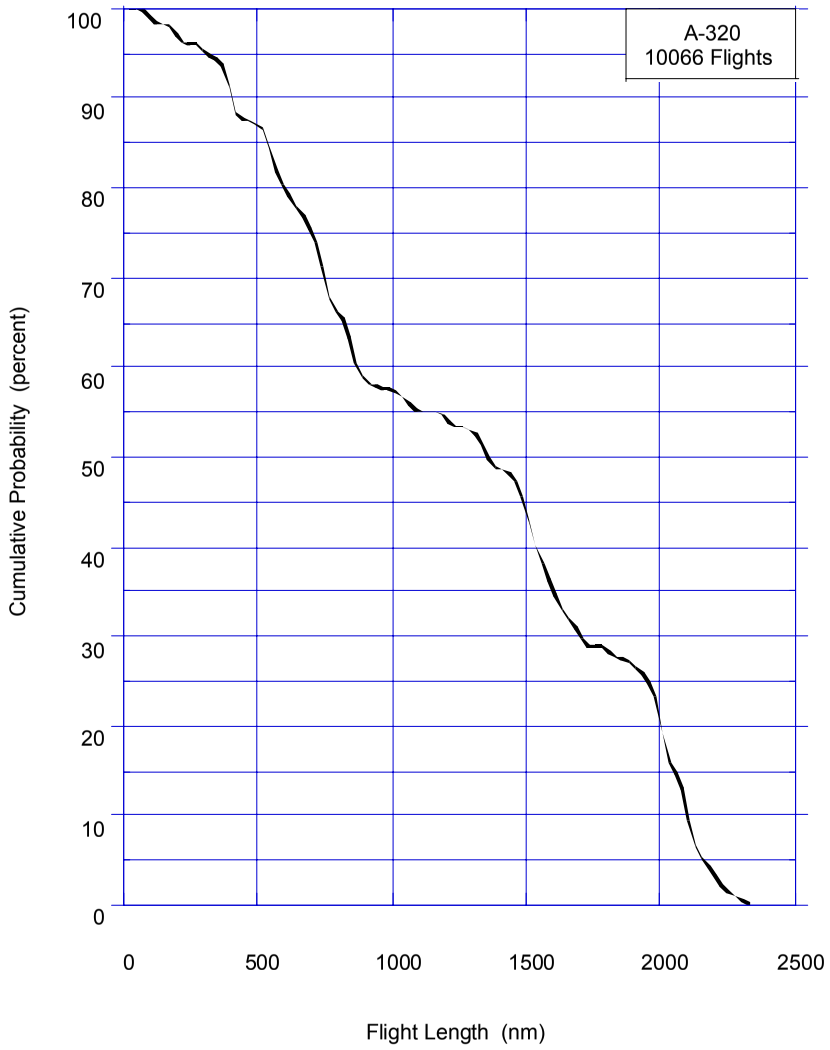


FIGURE A-3. CUMULATIVE PROBABILITY OF FLIGHT LENGTH

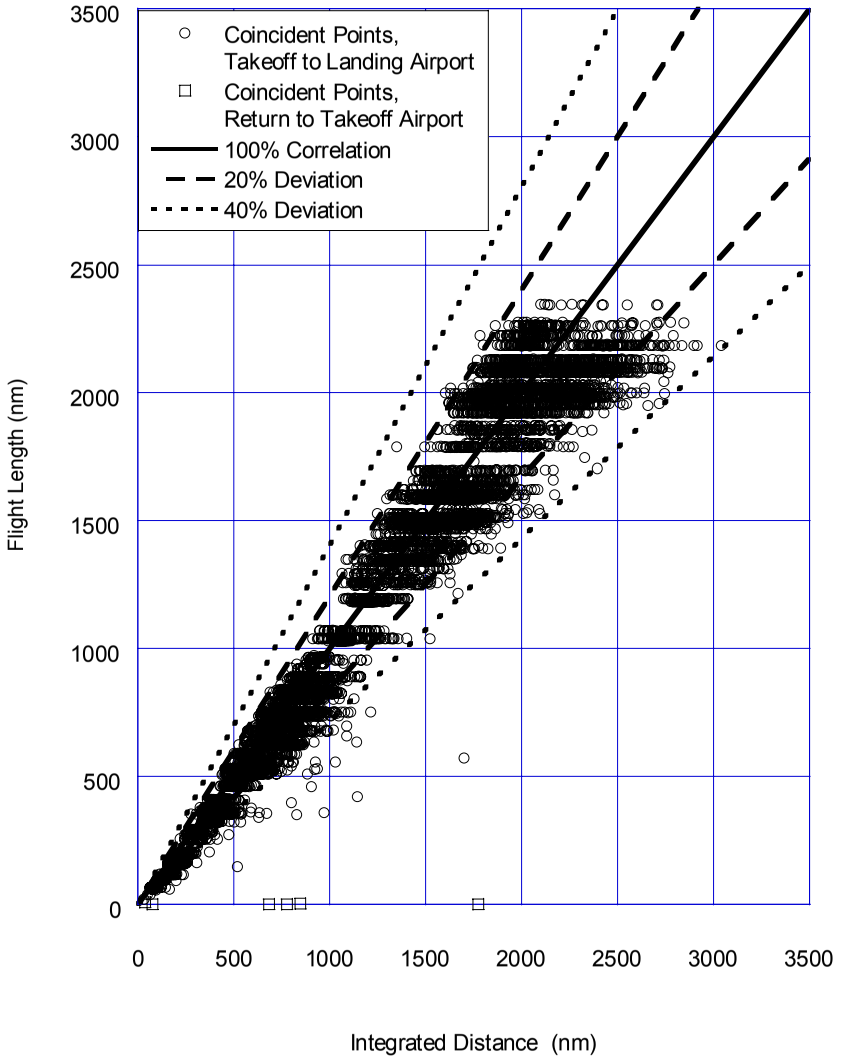


FIGURE A-4. CORRELATION OF FLIGHT LENGTH AND INTEGRATED FLIGHT DISTANCE

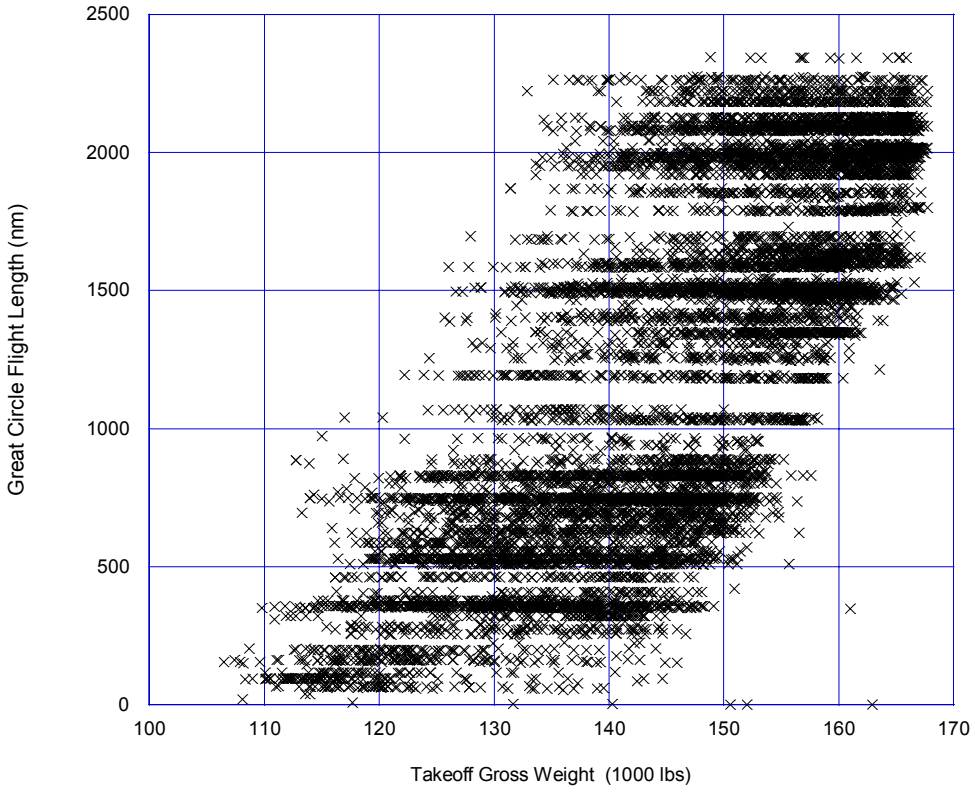


FIGURE A-5. CORRELATION OF TAKEOFF GROSS WEIGHT AND GREAT CIRCLE FLIGHT LENGTH

Takeoff Gross Weight (1000 lbs)

Great Circle Flight Length (nm)

10066 Flts	100-110	110-120	120-130	130-140	140-150	150-160	160-170	Total
0- 250	0.089	1.838	1.321	0.487	0.139	0.020	0.010	3.904
250- 500	0.010	0.864	2.752	3.924	2.086	0.010	0.010	9.656
500- 750		0.368	4.371	6.338	7.510	0.825		19.412
750-1000		0.139	0.944	2.424	4.947	1.371		9.825
1000-1250		0.010	0.228	1.033	1.212	1.431	0.020	3.934
1250-1500			0.109	1.202	2.861	6.666	1.331	12.170
1500-1750			0.070	0.874	2.503	6.030	2.643	12.120
1750-2000				0.437	2.444	4.729	5.037	12.647
2000-2250				0.209	2.027	5.722	7.252	15.210
2250-2500				0.099	0.278	0.457	0.288	1.123
Total	0.099	3.219	9.795	17.028	26.008	27.260	16.591	100.000

FIGURE A-6. CORRELATION OF TAKEOFF GROSS WEIGHT AND GREAT CIRCLE FLIGHT LENGTH, PERCENT OF FLIGHTS

Takeoff Gross Weight (1000 lbs)

Landing Gross Weight (1000 lbs)

10066 Flts	100-110	110-120	120-130	130-140	140-150	150-160	160-170	Total
100-110	0.099	0.984	0.169	0.030				1.282
110-120		2.235	7.500	3.209	2.434	0.417		15.796
120-130			2.126	11.862	9.160	9.011	1.053	33.211
130-140				1.927	14.206	16.759	14.385	47.278
140-150					0.209	1.073	1.142	2.424
150-160								
160-170							0.010	0.010
Total	0.099	3.219	9.795	17.028	26.008	27.260	16.591	100.000

FIGURE A-7. CORRELATION OF TAKEOFF AND LANDING GROSS WEIGHT, PERCENT OF FLIGHTS

Integrated Flight Distance (nautical miles)

Altitude Band (feet)

10066 Flts	0-500	500-1000	1000-1500	1500-2000	2000-2500	2500-3000	3000-3500
29500-39500	29.230	63.420	77.340	82.410	85.700	89.320	89.720
19500-29500	32.190	19.650	12.740	10.200	8.240	5.460	3.920
9500-19500	23.360	10.260	6.170	4.390	3.560	3.160	4.200
4500-9500	8.820	4.010	2.280	1.710	1.380	1.160	1.460
1500-4500	5.010	2.010	1.110	0.960	0.800	0.600	0.460
500-1500	1.000	0.470	0.260	0.240	0.210	0.180	0.150
0-500	0.380	0.170	0.100	0.100	0.110	0.110	0.090
Total	100.000	100.000	100.000	100.000	100.000	100.000	100.000

FIGURE A-8. PERCENT OF INTEGRATED FLIGHT DISTANCE IN ALTITUDE BANDS

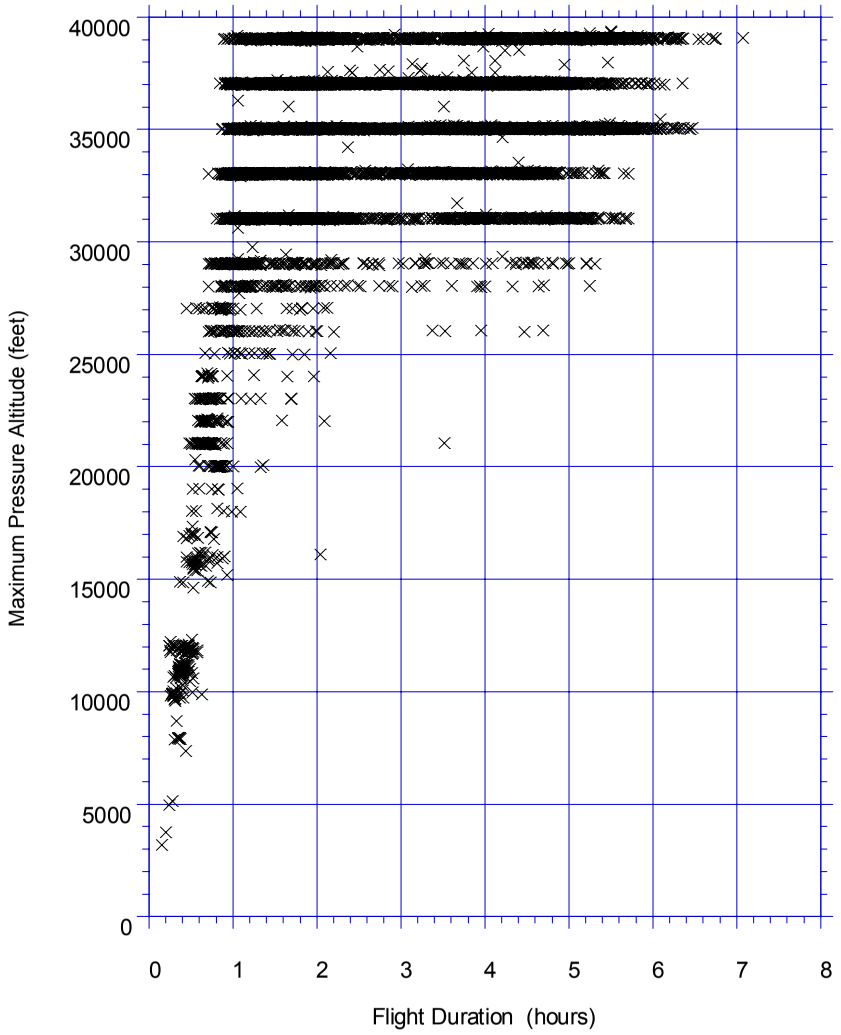


FIGURE A-9. CORRELATION OF MAXIMUM ALTITUDE AND FLIGHT DURATION

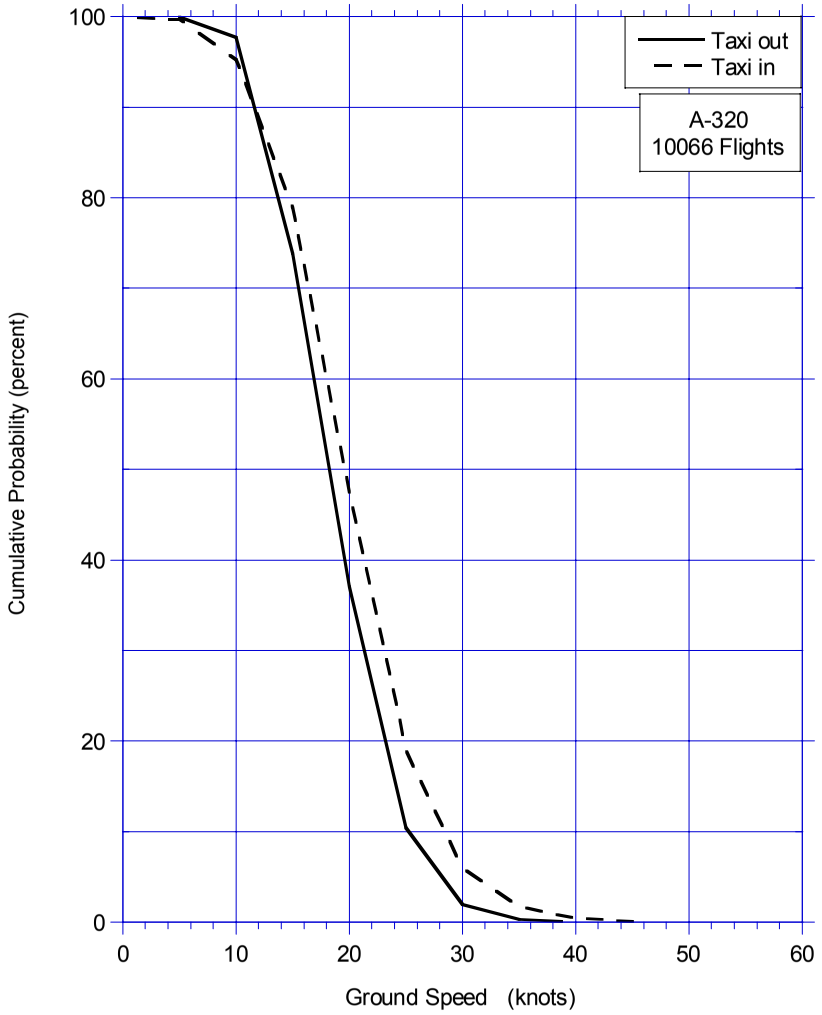


FIGURE A-10. CUMULATIVE PROBABILITY OF MAXIMUM GROUND SPEED DURING TAXI

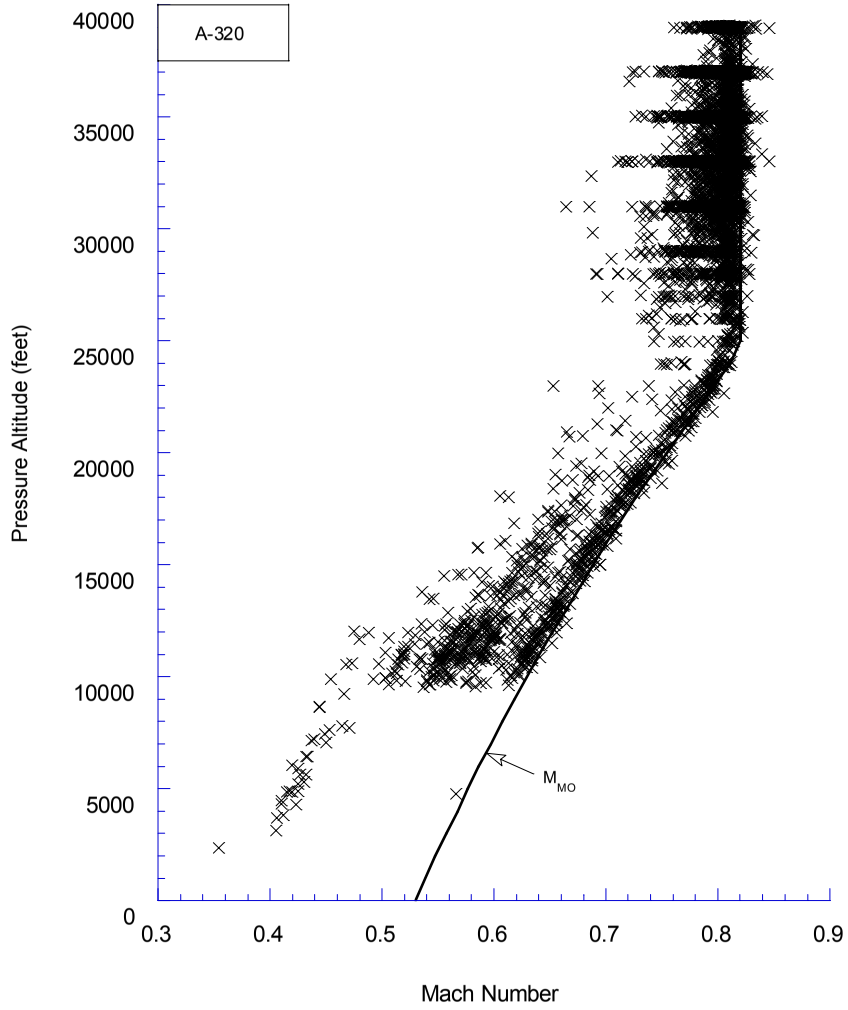


FIGURE A-11. MAXIMUM MACH NUMBER AND COINCIDENT ALTITUDE, ALL FLIGHT PHASES

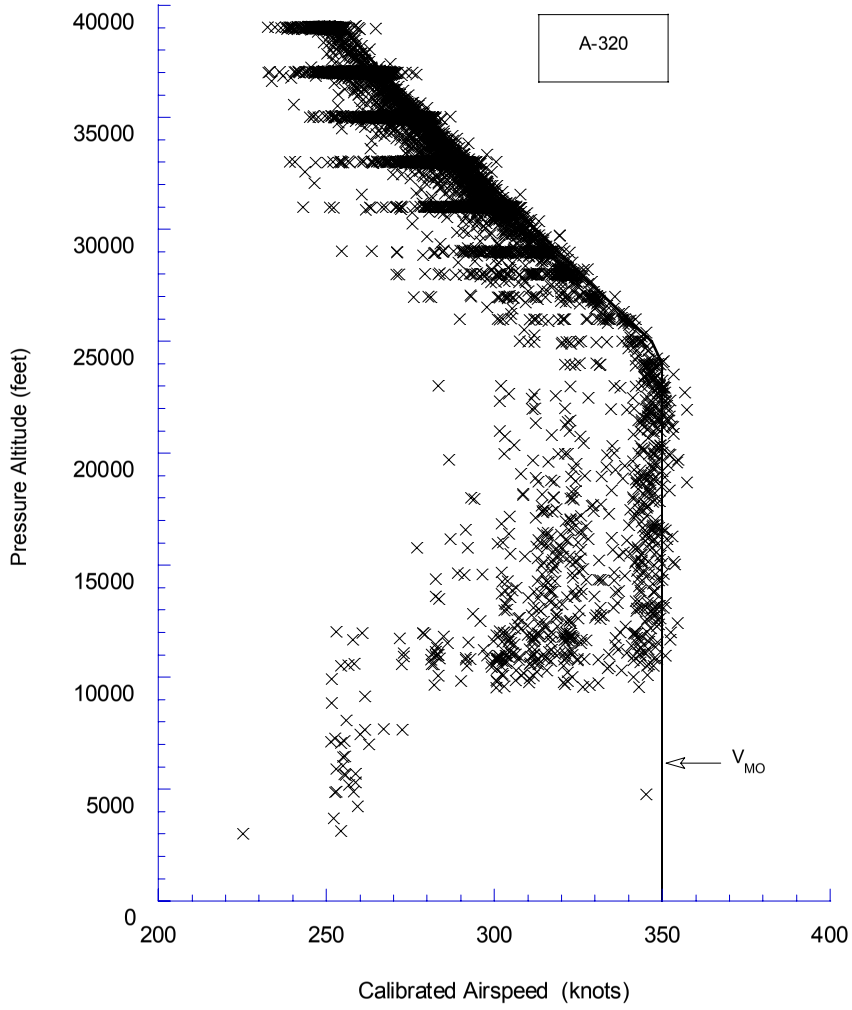


FIGURE A-12. MAXIMUM CALIBRATED AIRSPEED AND COINCIDENT ALTITUDE, ALL FLIGHT PHASES

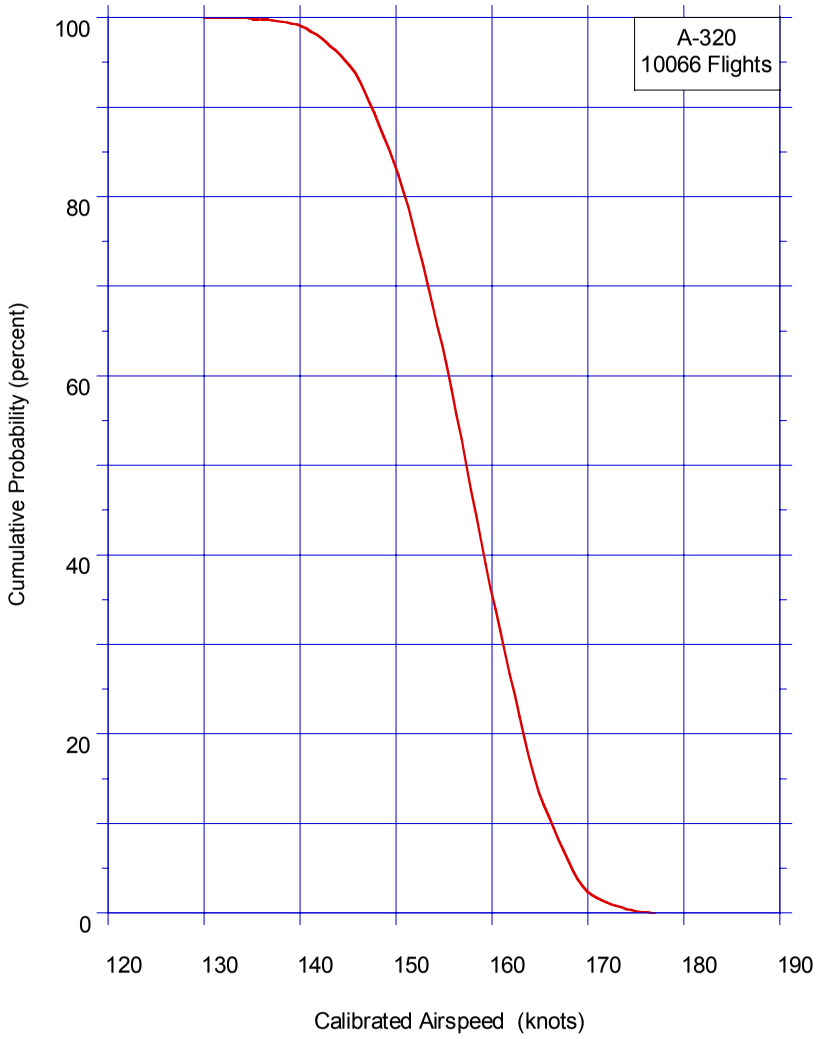


FIGURE A-13. CUMULATIVE PROBABILITY OF AIRSPEED AT LIFTOFF

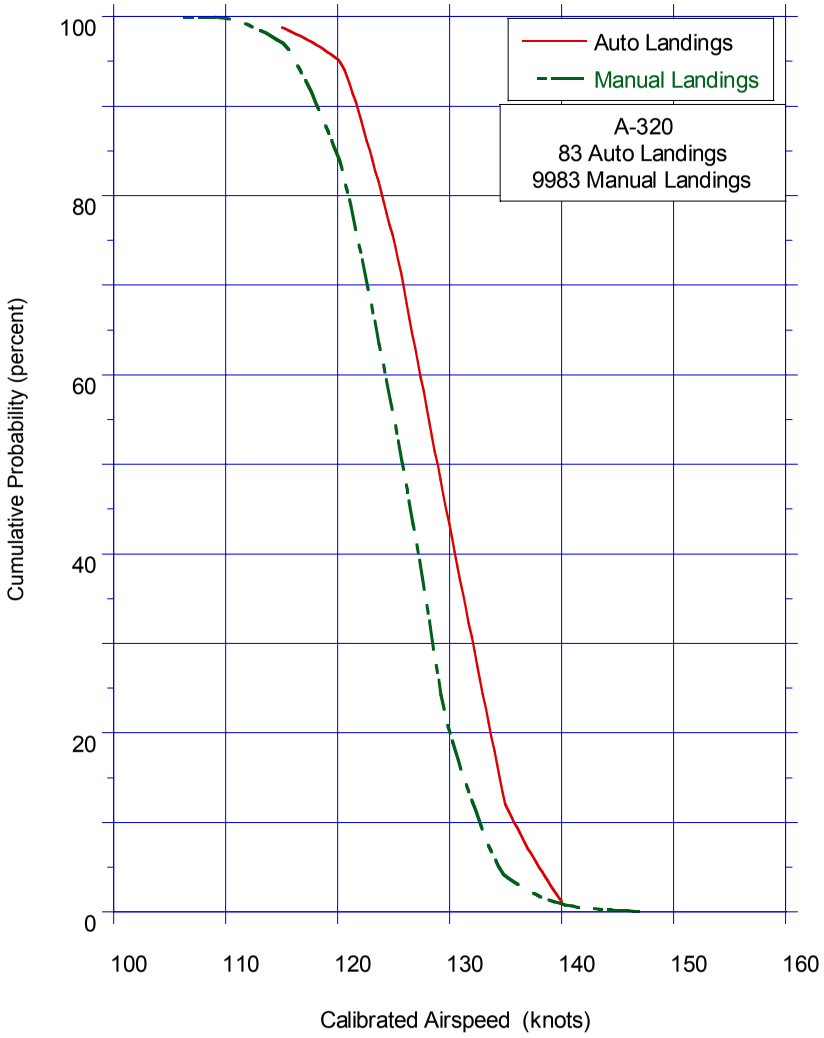


FIGURE A-14. CUMULATIVE PROBABILITY OF AIRSPEED AT TOUCHDOWN

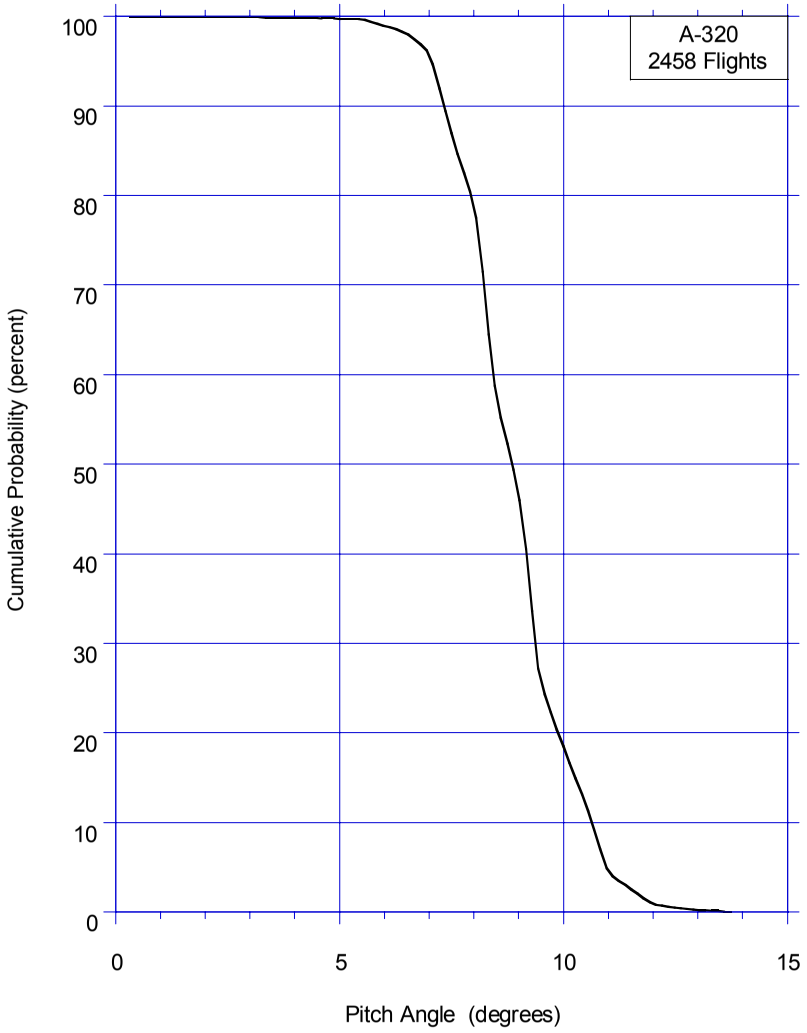


FIGURE A-15. CUMULATIVE PROBABILITY OF PITCH ANGLE AT LIFTOFF

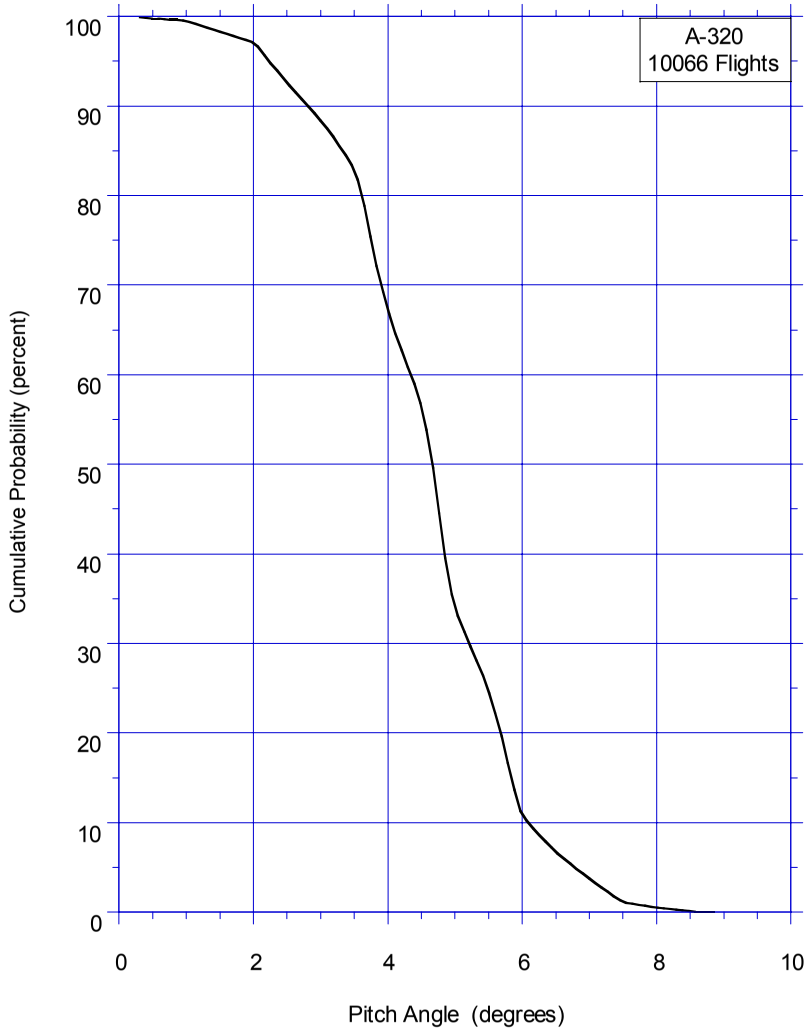


FIGURE A-16. CUMULATIVE PROBABILITY OF PITCH ANGLE AT TOUCHDOWN

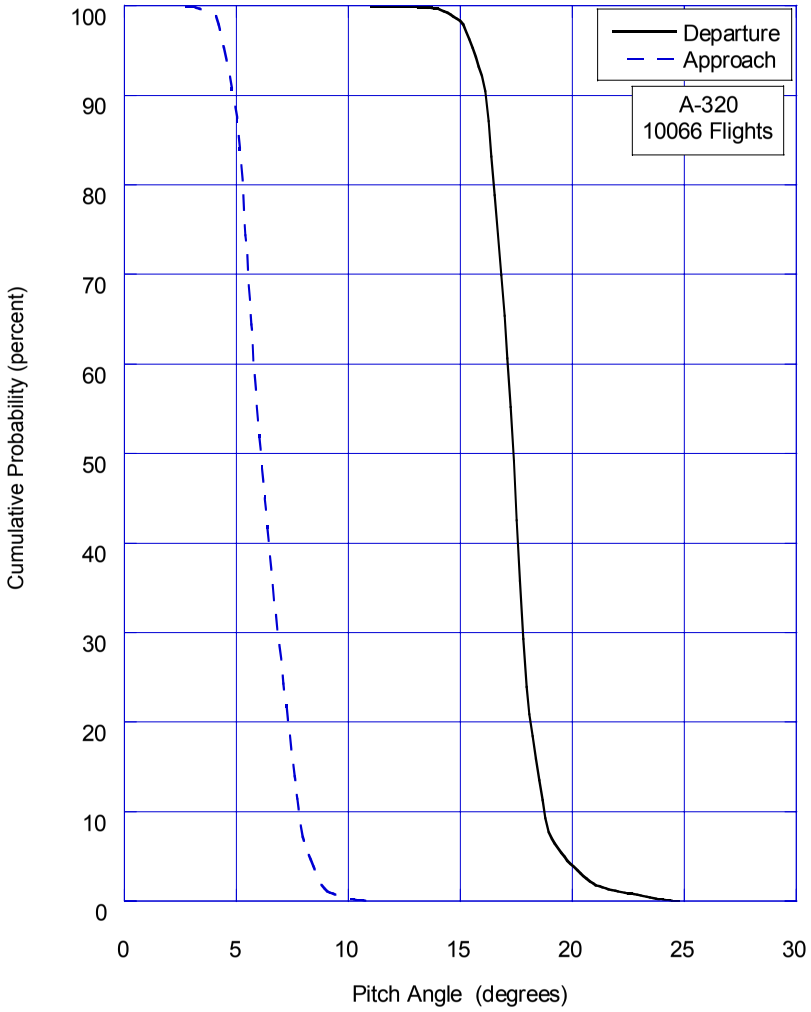


FIGURE A-17. CUMULATIVE PROBABILITY OF MAXIMUM PITCH ANGLE DURING DEPARTURE AND APPROACH

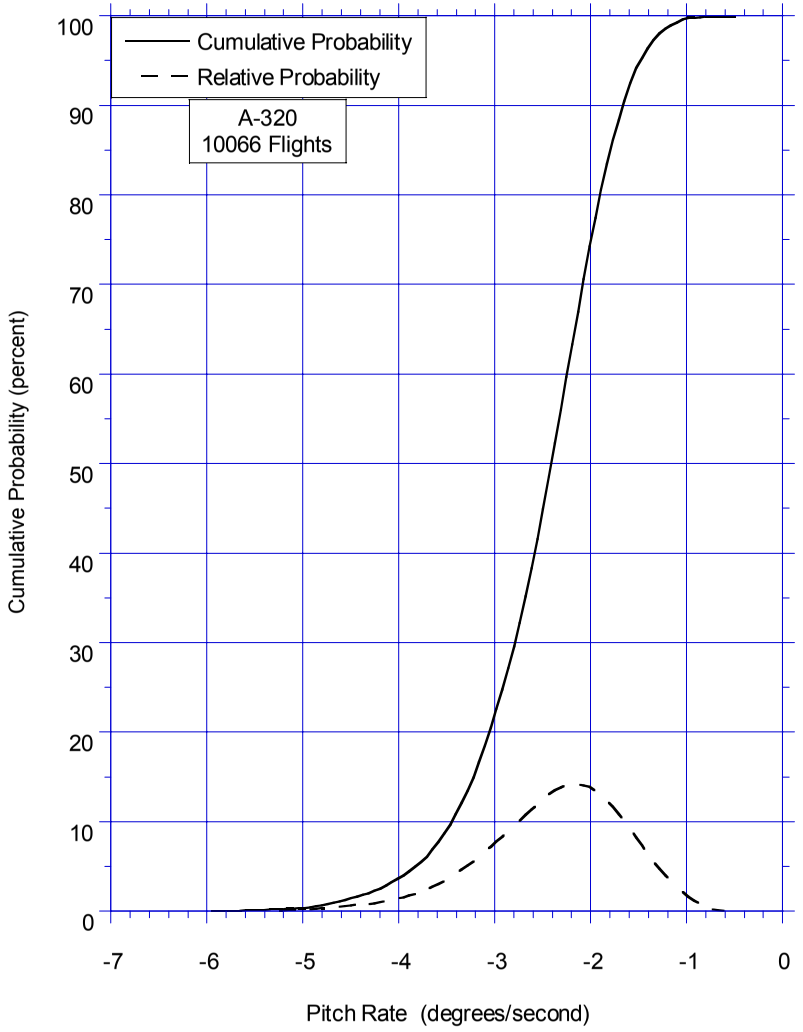


FIGURE A-18. PROBABILITY DISTRIBUTIONS OF MAXIMUM PITCH RATE AT NOSE GEAR TOUCHDOWN

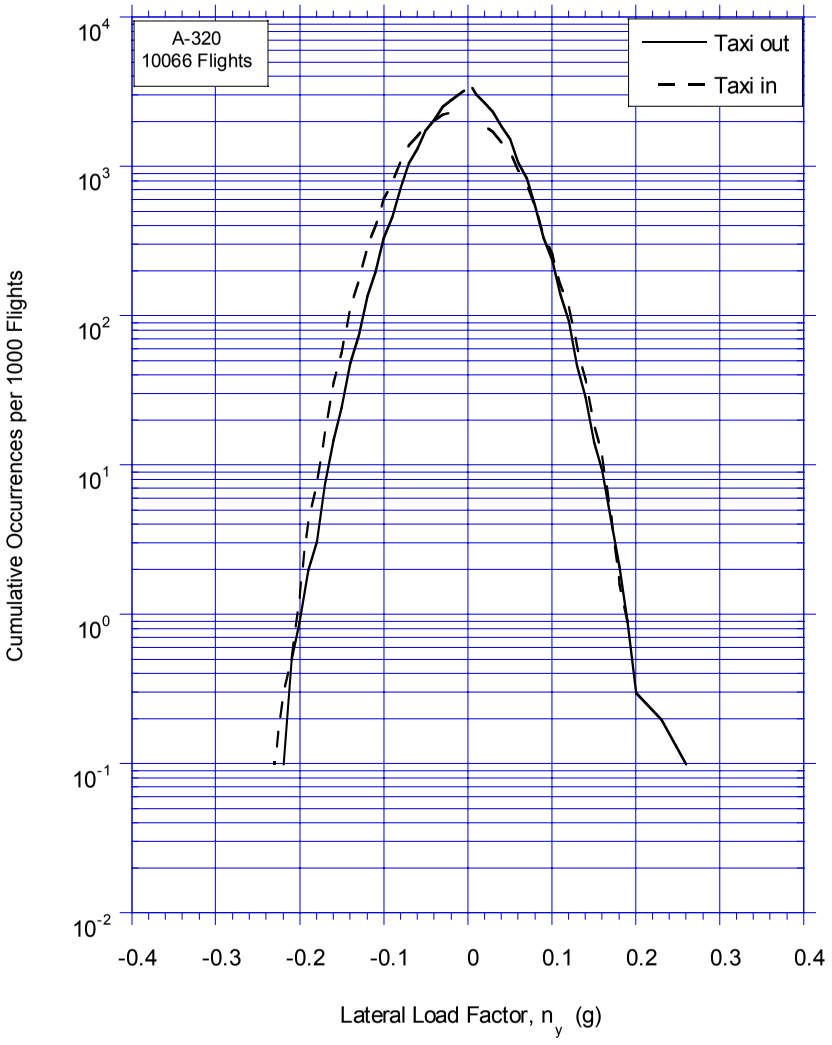


FIGURE A-19. CUMULATIVE FREQUENCY OF MAXIMUM LATERAL LOAD FACTOR DURING GROUND TURNS

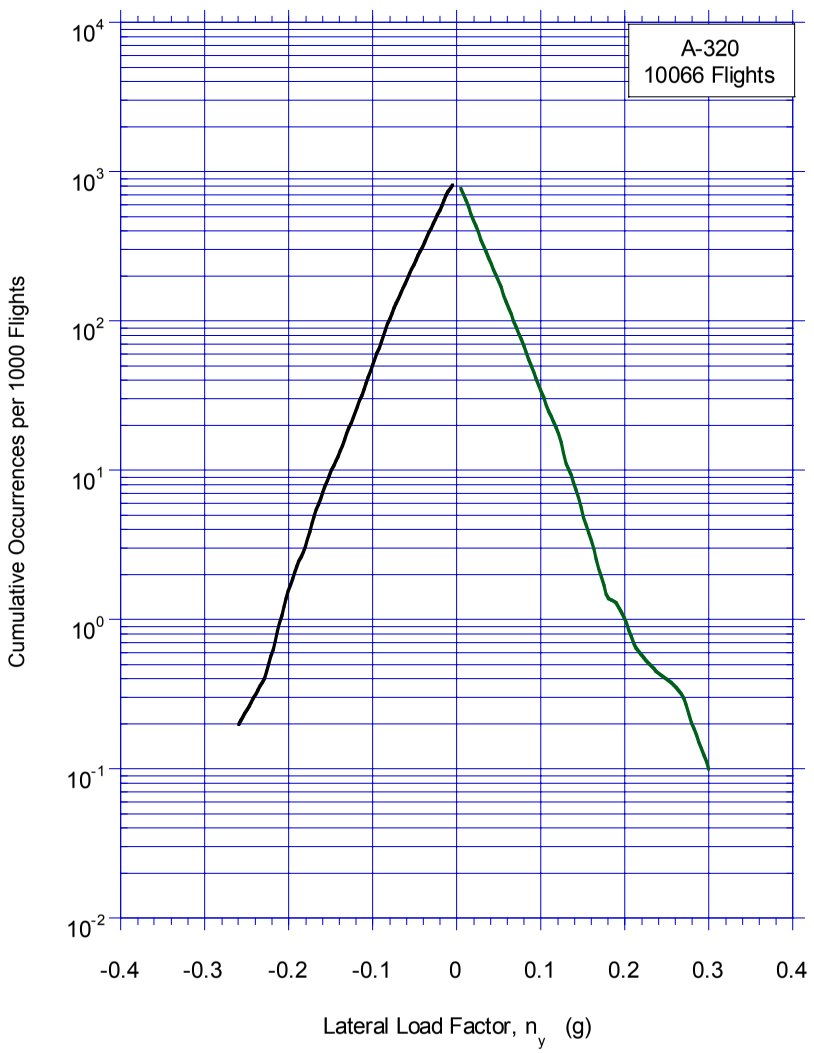


FIGURE A-20. CUMULATIVE FREQUENCY OF MAXIMUM LATERAL FACTOR AT TOUCHDOWN

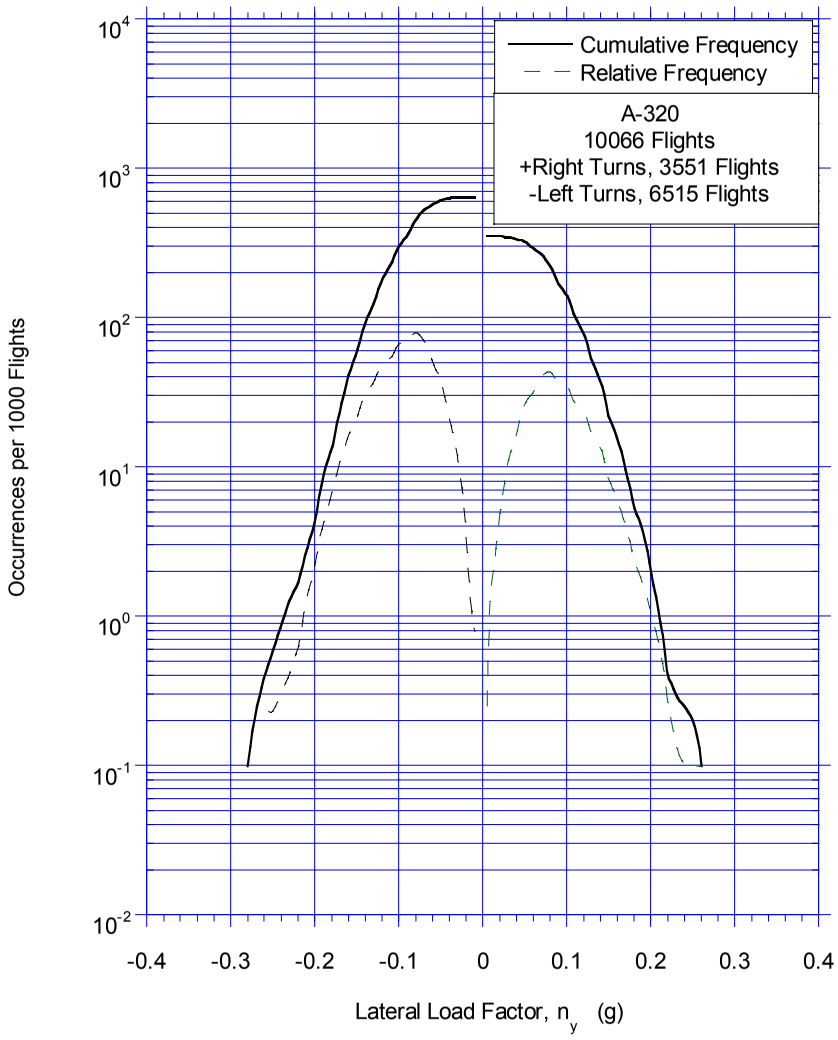


FIGURE A-21. FREQUENCY DISTRIBUTIONS OF MAXIMUM LATERAL LOAD FACTOR DURING RUNWAY TURNOFF

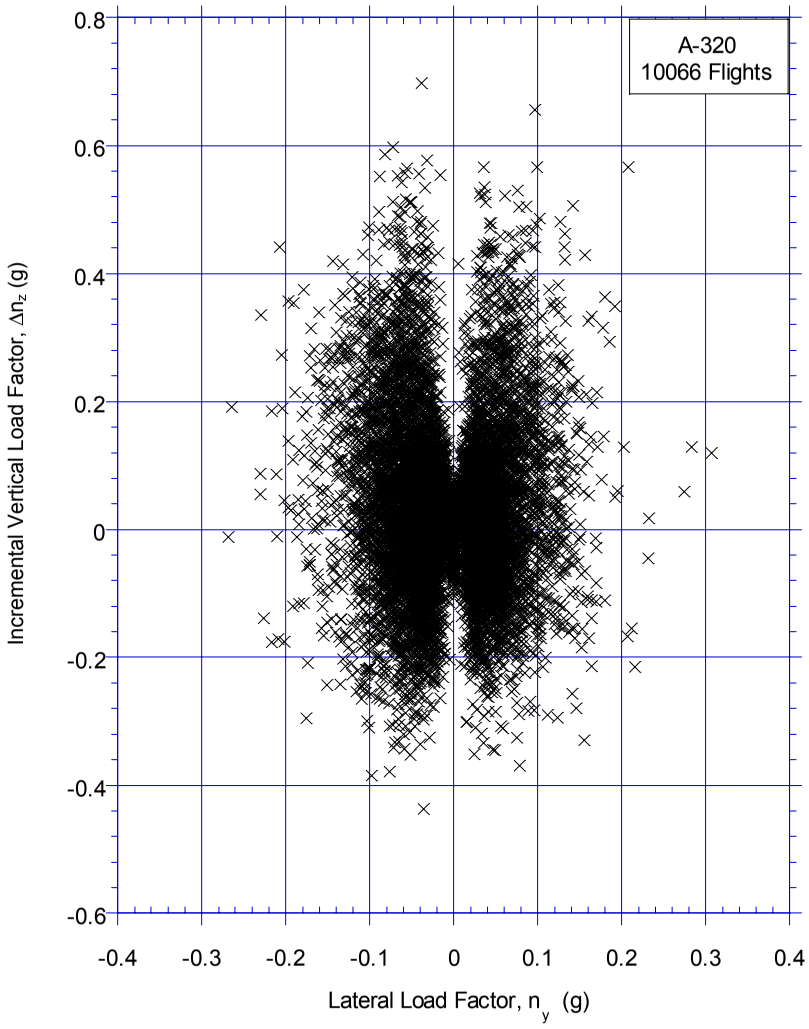


FIGURE A-22. MAXIMUM LATERAL LOAD FACTOR AND COINCIDENT INCREMENTAL VERTICAL LOAD FACTOR AT TOUCHDOWN

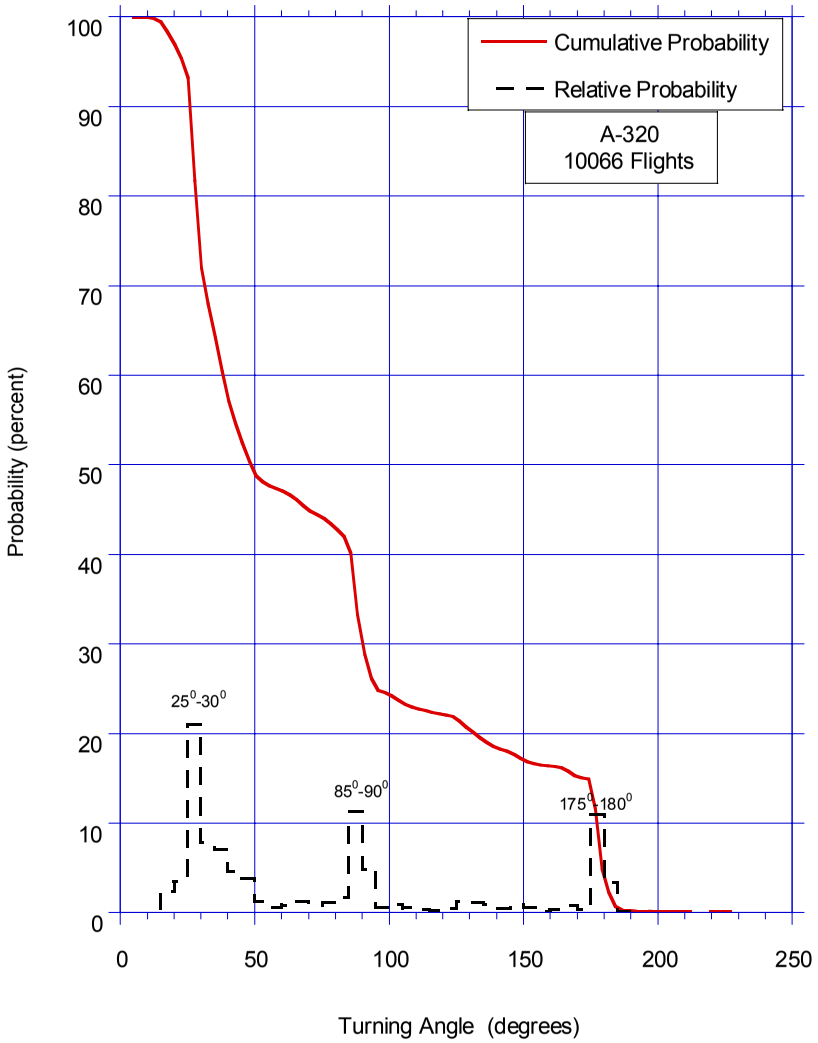


FIGURE A-23. PROBABILITY DISTRIBUTIONS OF TURNING ANGLE DURING RUNWAY TURNOFF

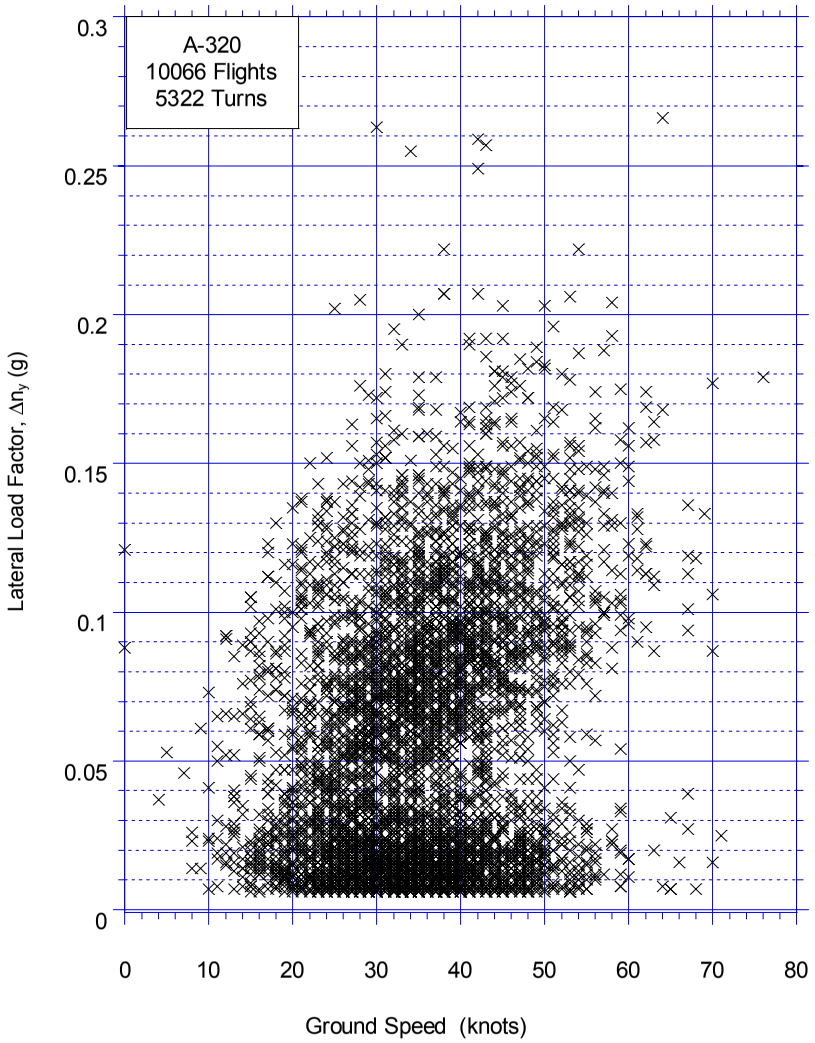


FIGURE A-24. MAXIMUM LATERAL LOAD FACTOR AND COINCIDENT GROUND SPEED DURING RUNWAY TURNOFF, 0-60 DEGREE TURNS

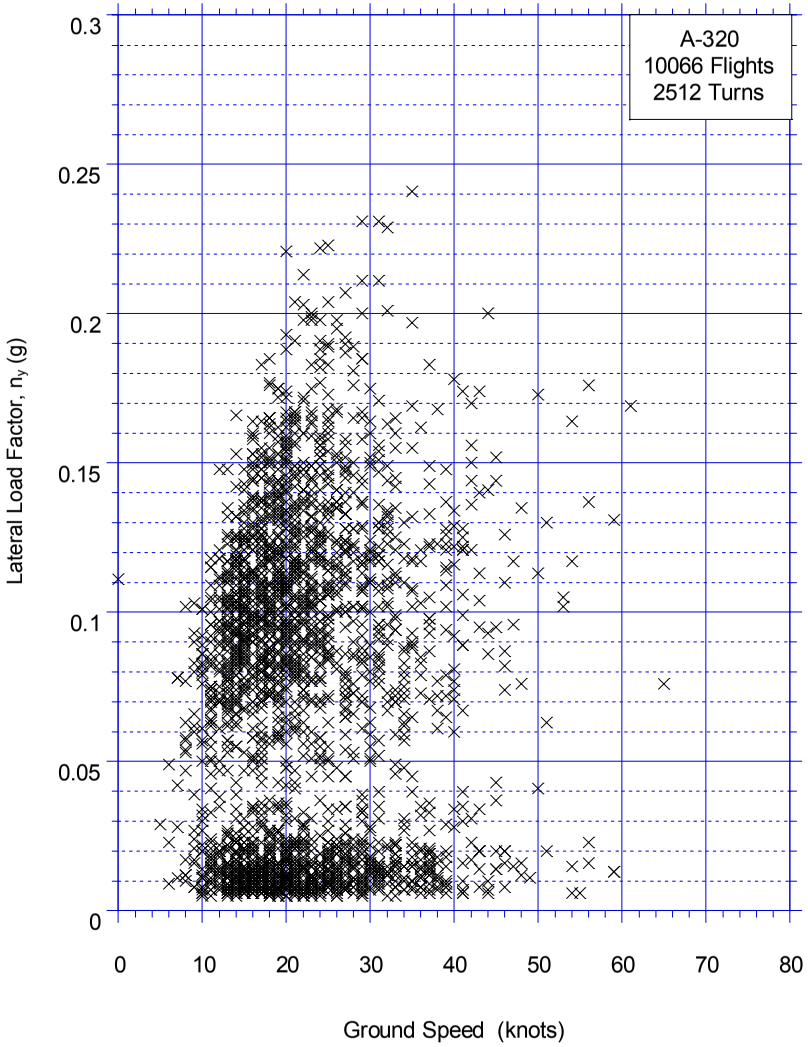


FIGURE A-25. MAXIMUM LATERAL LOAD FACTOR AND COINCIDENT GROUND SPEED DURING RUNWAY TURNOFF, 60-120 DEGREE TURNS

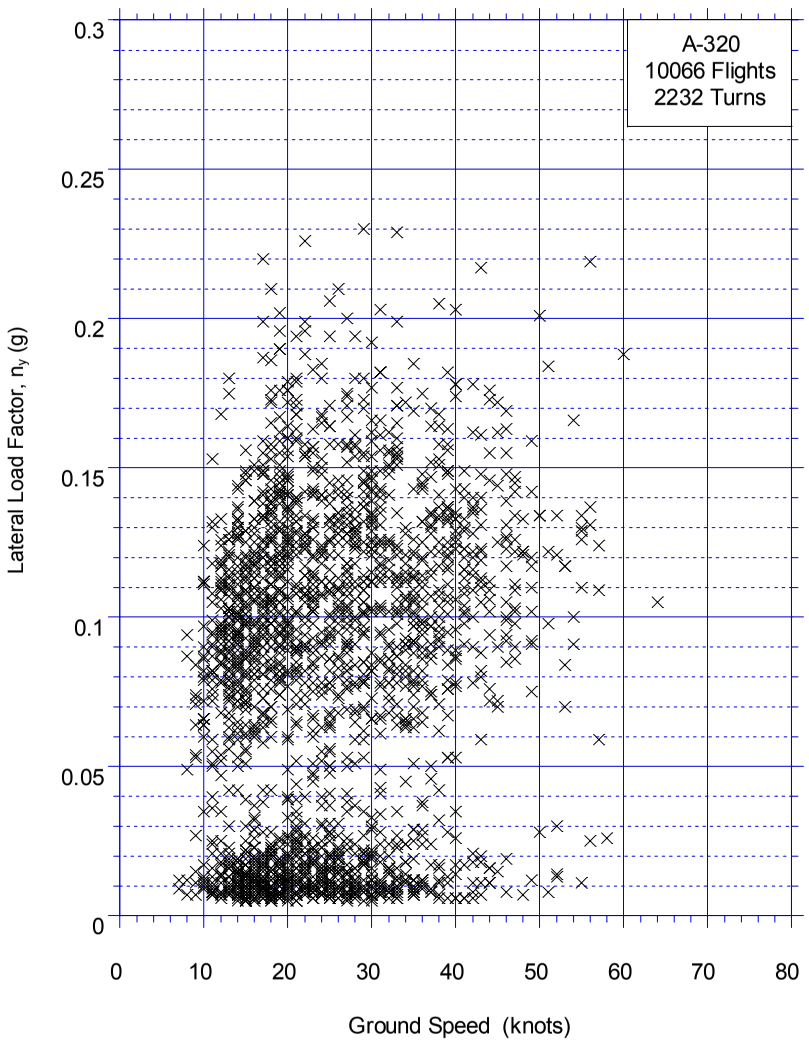


FIGURE A-26. MAXIMUM LATERAL LOAD FACTOR AND COINCIDENT GROUND SPEED DURING RUNWAY TURNOFF, 120-240 DEGREE TURNS

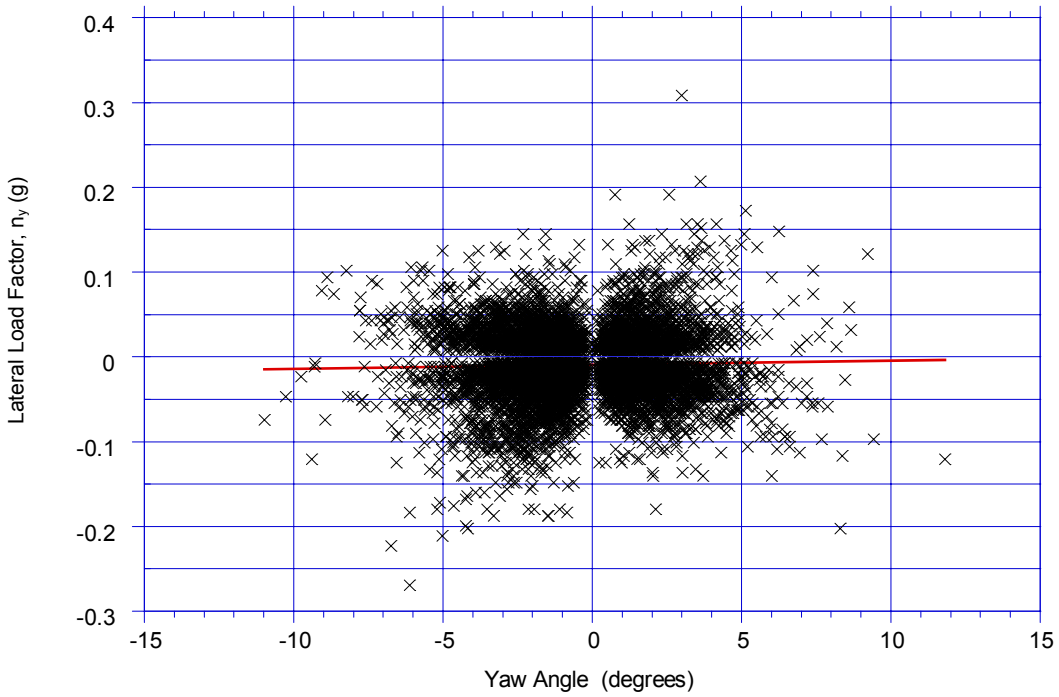


FIGURE A-27. MAXIMUM LATERAL LOAD FACTOR AT TOUCHDOWN VS MAXIMUM YAW ANGLE BEFORE TOUCHDOWN

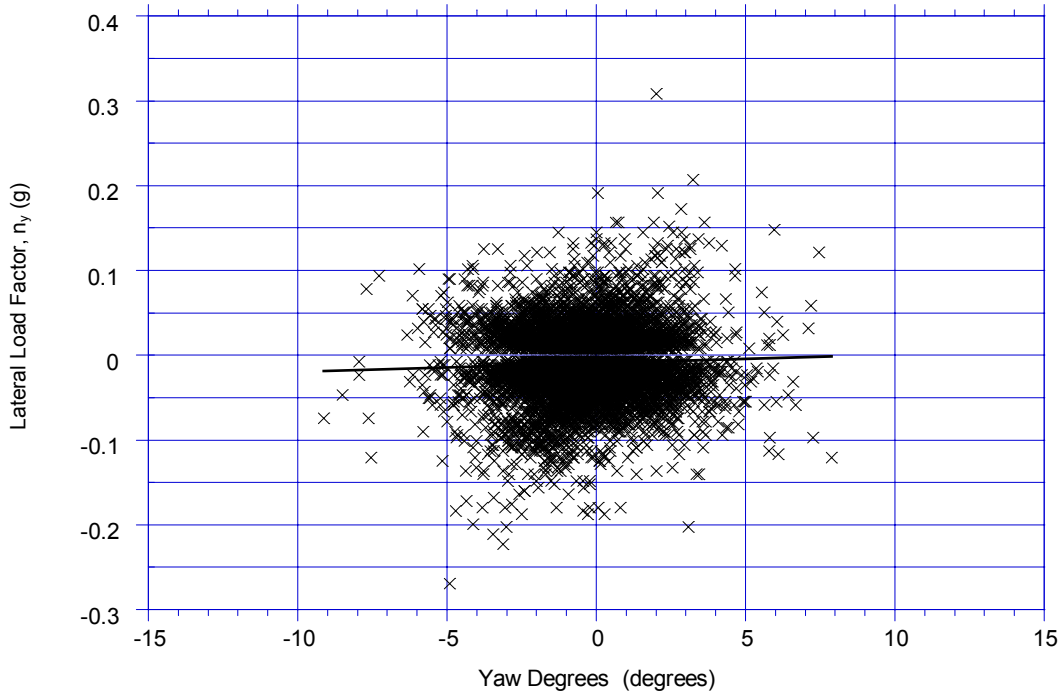


FIGURE A-28. MAXIMUM LATERAL LOAD FACTOR AT TOUCHDOWN VS MEAN YAW ANGLE BEFORE TOUCHDOWN

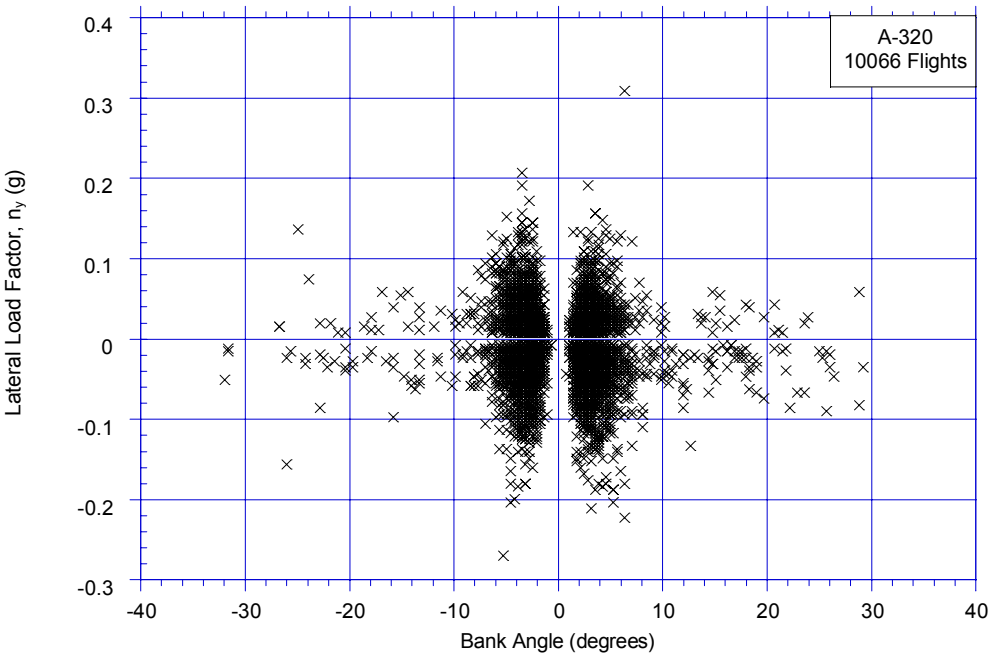


FIGURE A-29. MAXIMUM LATERAL LOAD FACTOR AT TOUCHDOWN VS MAXIMUM BANK ANGLE BEFORE TOUCHDOWN

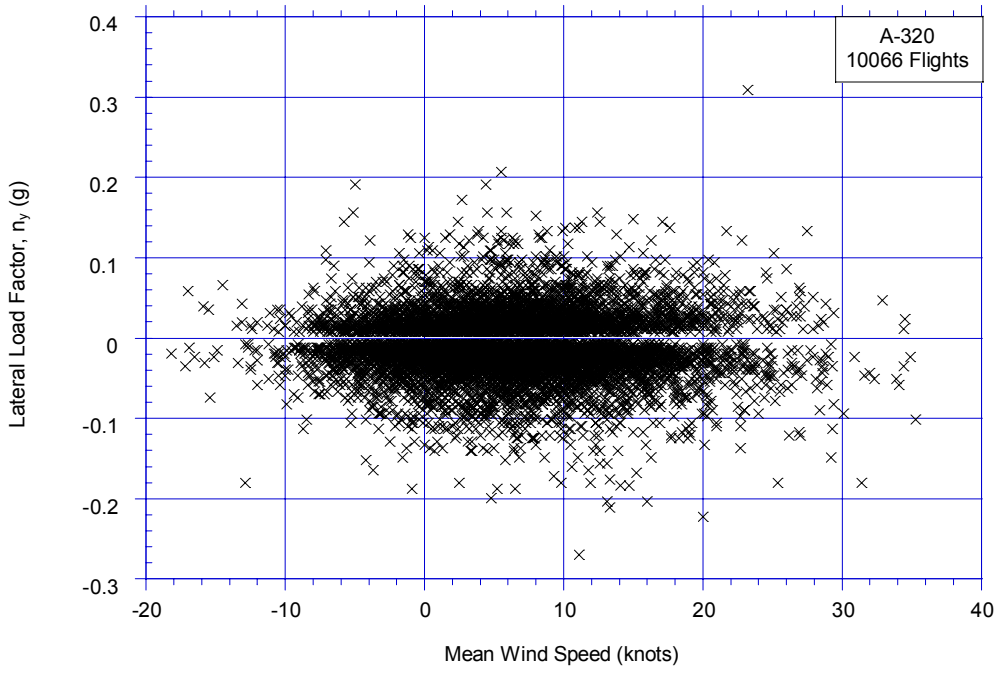


FIGURE A-30. MAXIMUM LATERAL LOAD FACTOR AT TOUCHDOWN VS MEAN WIND SPEED BEFORE TOUCHDOWN

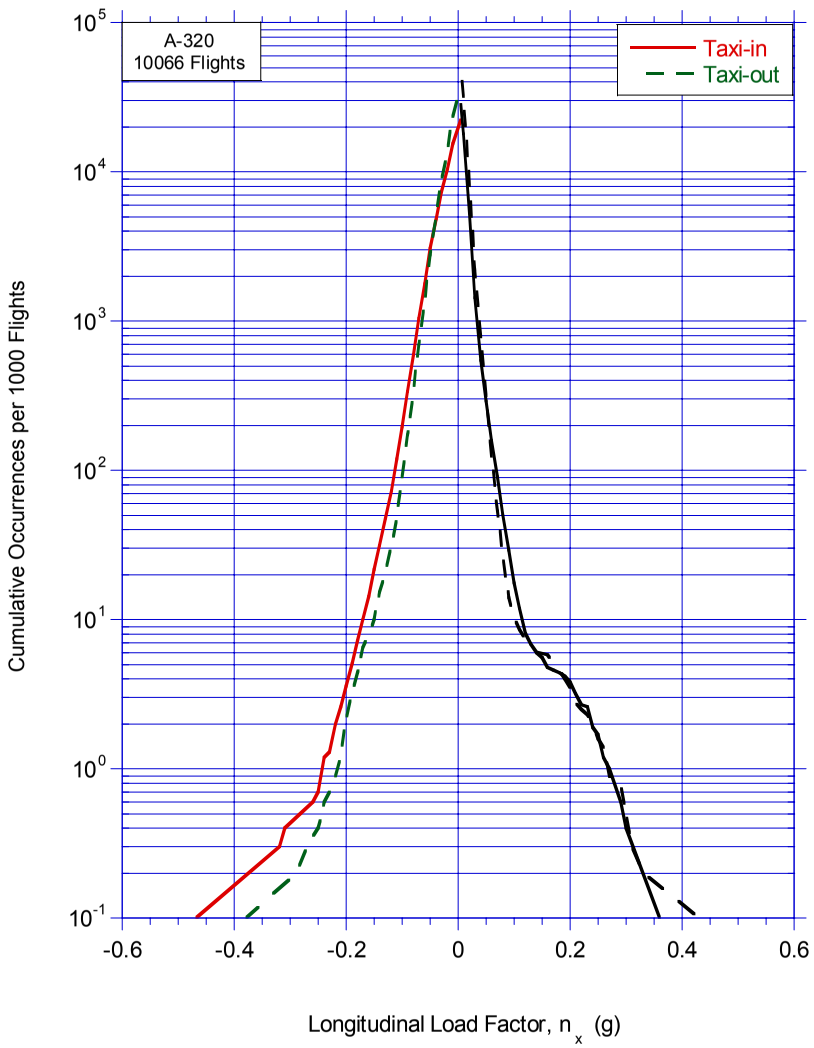


FIGURE A-31. CUMULATIVE FREQUENCY OF LONGITUDINAL LOAD FACTOR DURING TAXI OPERATIONS

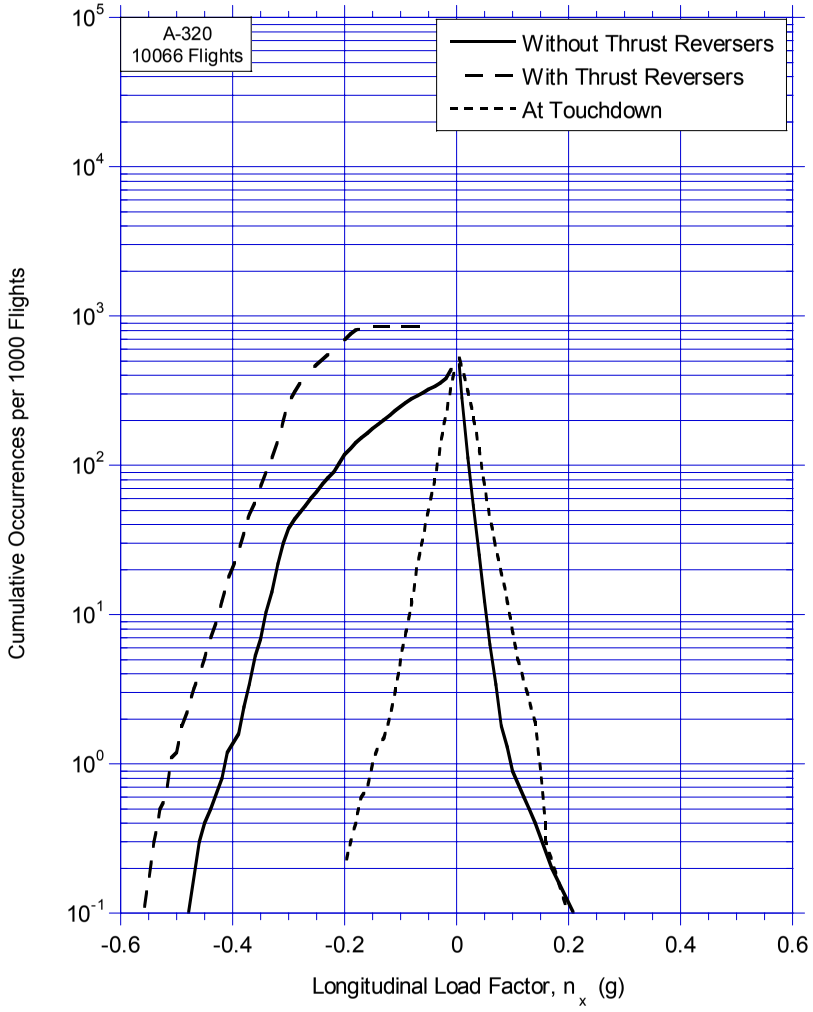


FIGURE A-32. CUMULATIVE FREQUENCY OF LONGITUDINAL LOAD FACTOR AT TOUCHDOWN AND DURING LANDING ROLL

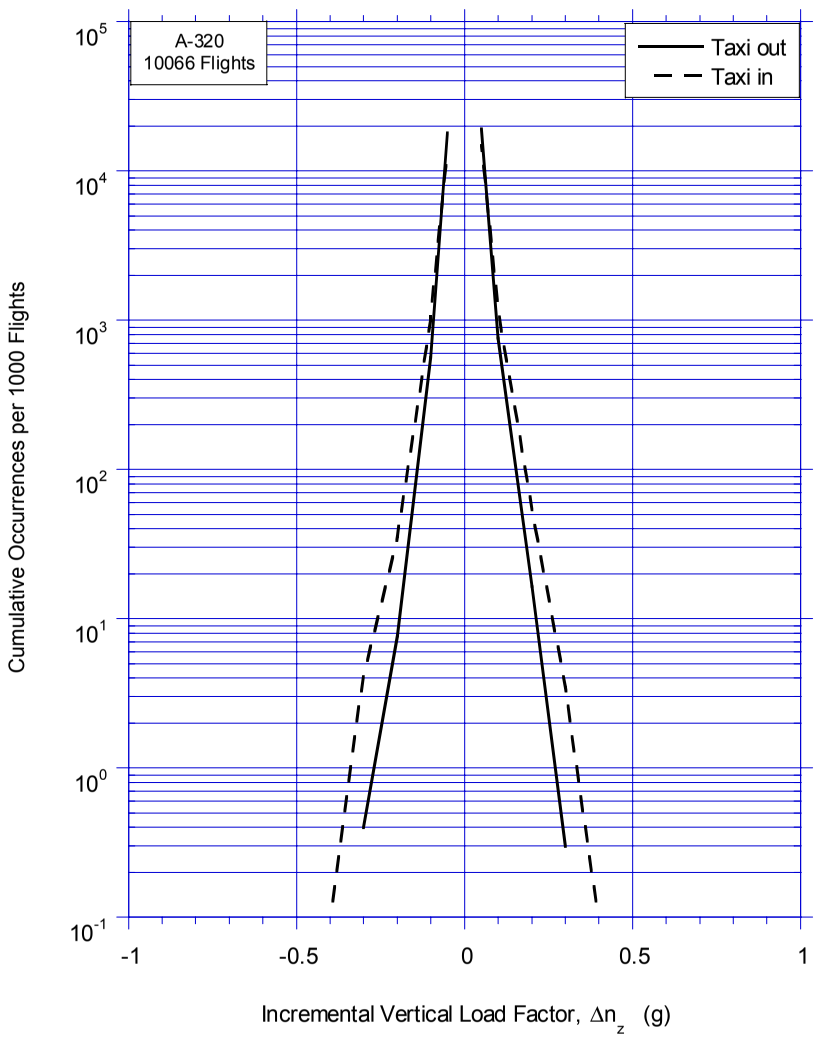


FIGURE A-33. CUMULATIVE FREQUENCY OF INCREMENTAL VERTICAL LOAD FACTOR DURING TAXI OPERATIONS

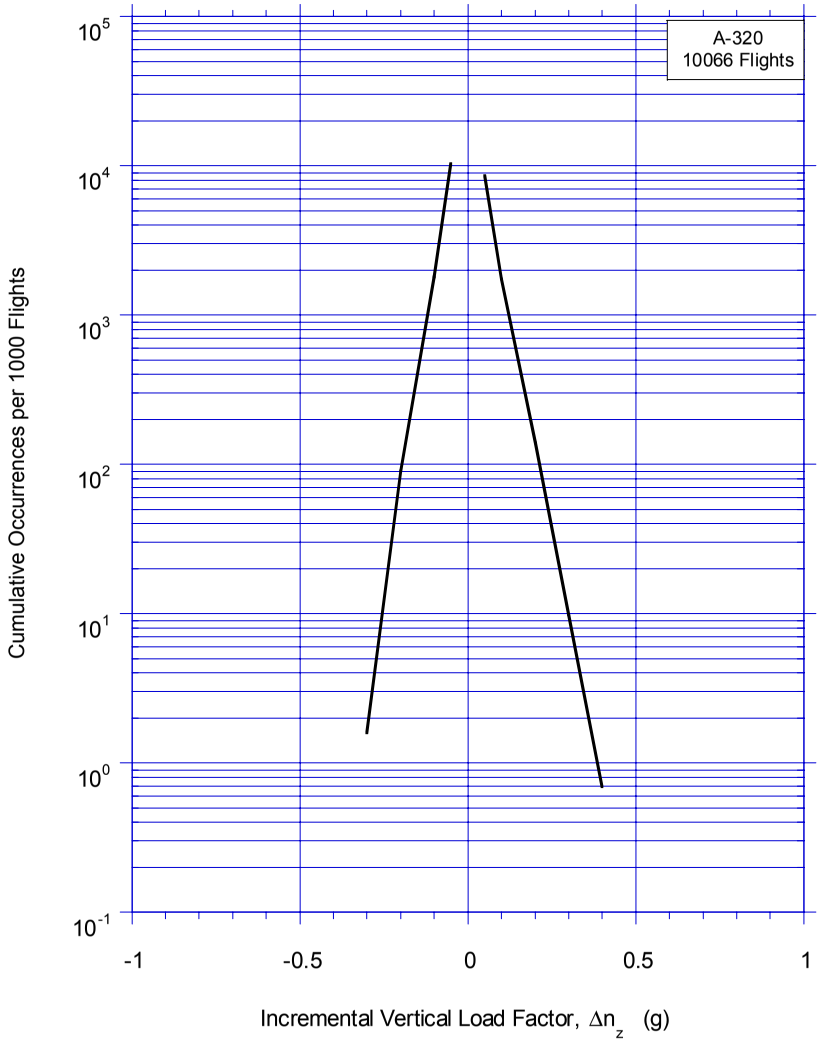


FIGURE A-34. CUMULATIVE FREQUENCY OF INCREMENTAL VERTICAL LOAD FACTOR DURING TAKEOFF ROLL

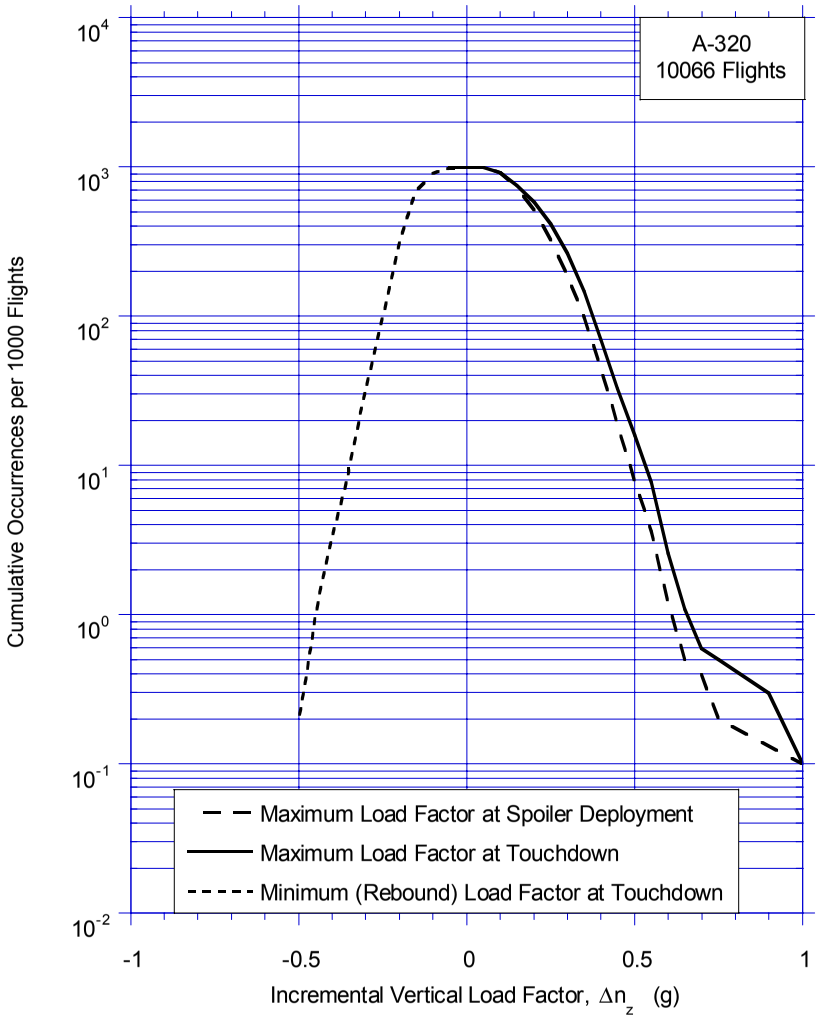


FIGURE A-35. CUMULATIVE FREQUENCY OF INCREMENTAL VERTICAL LOAD FACTOR AT SPOILER DEPLOYMENT AND AT TOUCHDOWN

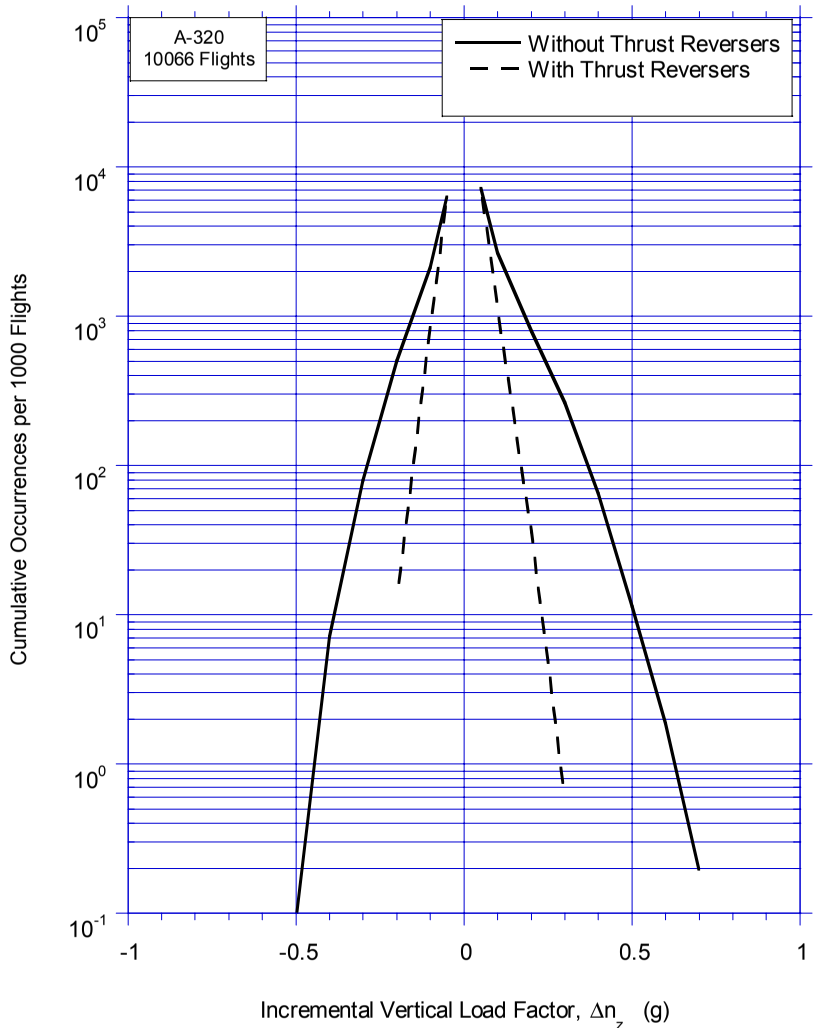


FIGURE A-36. CUMULATIVE FREQUENCY OF INCREMENTAL VERTICAL LOAD FACTOR DURING LANDING ROLL

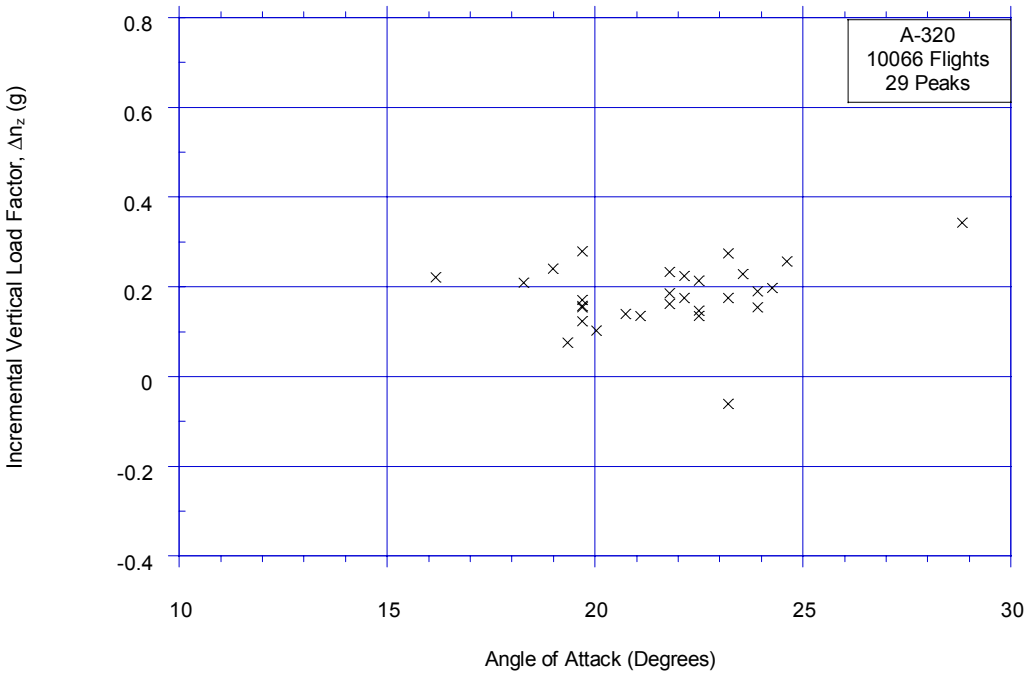


FIGURE A-37. MAXIMUM INCREMENTAL VERTICAL LOAD FACTOR VS MAXIMUM ANGLE OF ATTACK DURING LIFTOFF, 130-140 KNOTS

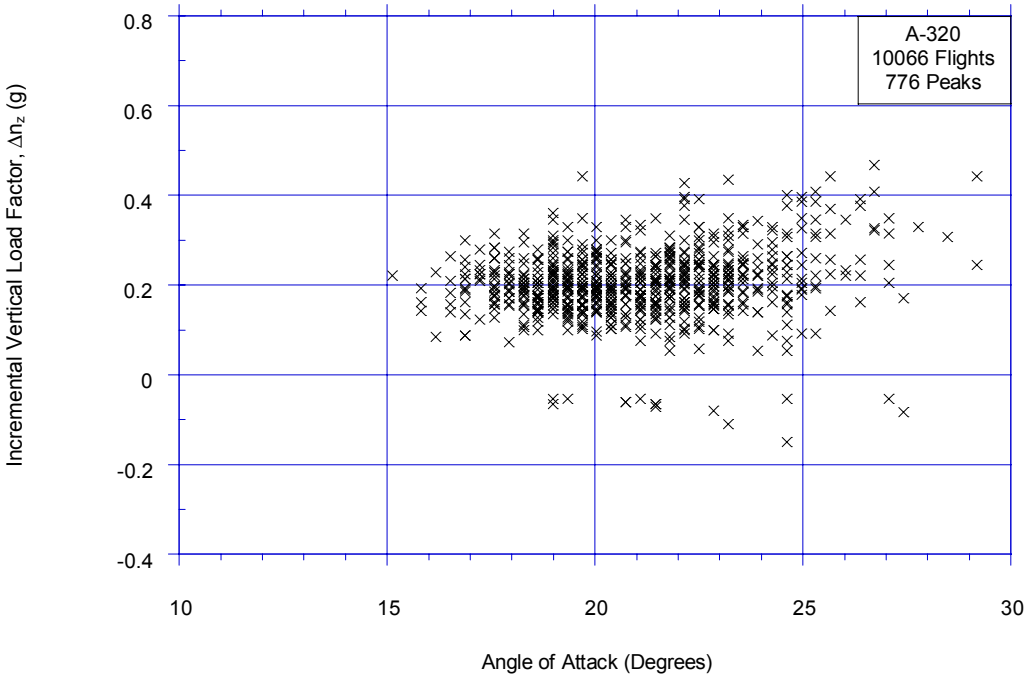


FIGURE A-38. MAXIMUM INCREMENTAL VERTICAL LOAD FACTOR VS MAXIMUM ANGLE OF ATTACK DURING LIFTOFF, 140-150 KNOTS

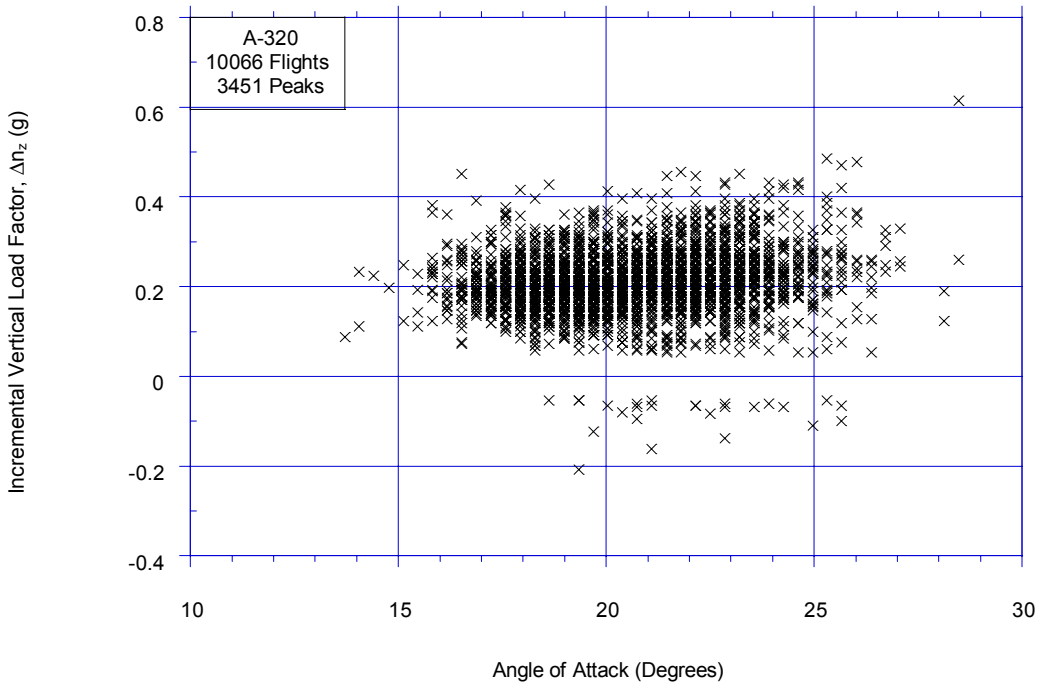


FIGURE A-39. MAXIMUM INCREMENTAL VERTICAL LOAD FACTOR VS MAXIMUM ANGLE OF ATTACK DURING LIFTOFF, 150-160 KNOTS

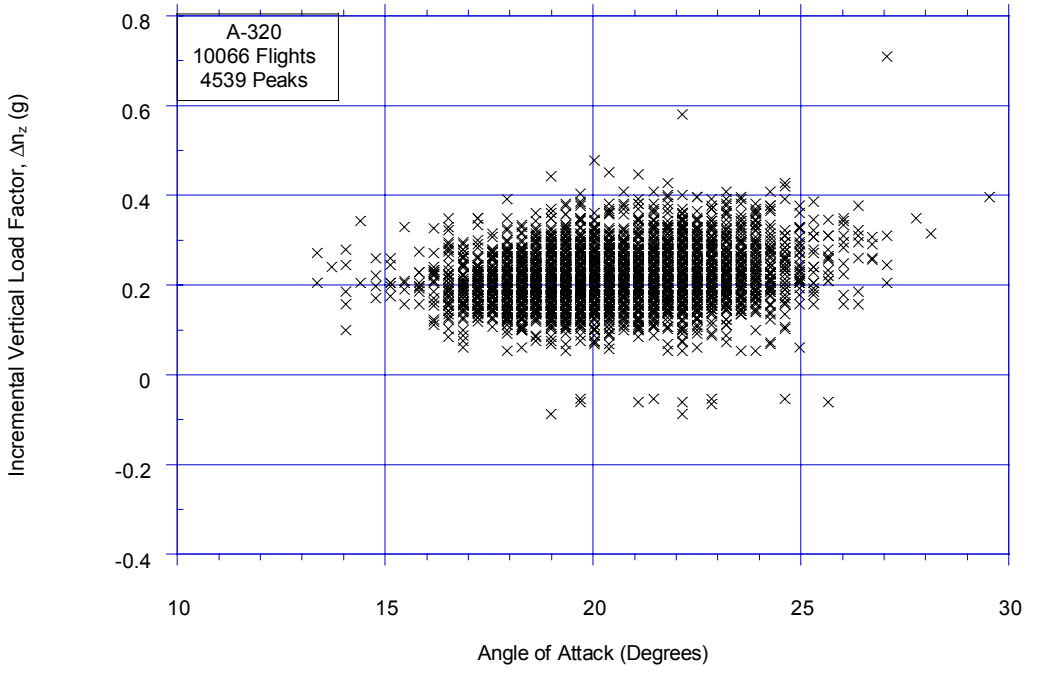


FIGURE A-40. MAXIMUM INCREMENTAL VERTICAL LOAD FACTOR VS MAXIMUM ANGLE OF ATTACK DURING LIFTOFF, 160-170 KNOTS

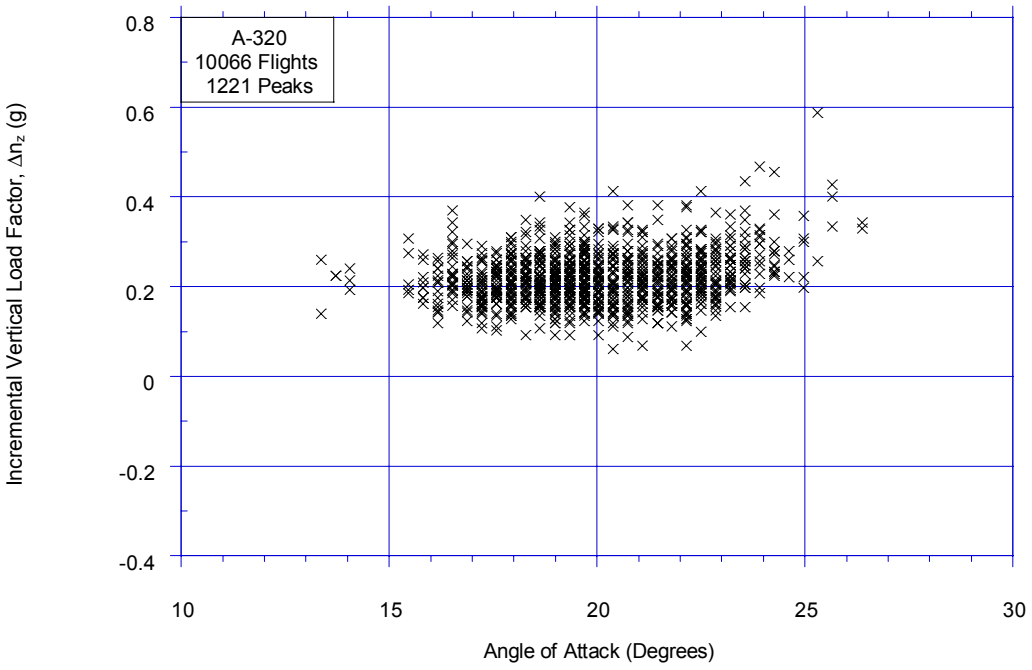


FIGURE A-41. MAXIMUM INCREMENTAL VERTICAL LOAD FACTOR VS MAXIMUM ANGLE OF ATTACK DURING LIFTOFF, 170-180 KNOTS

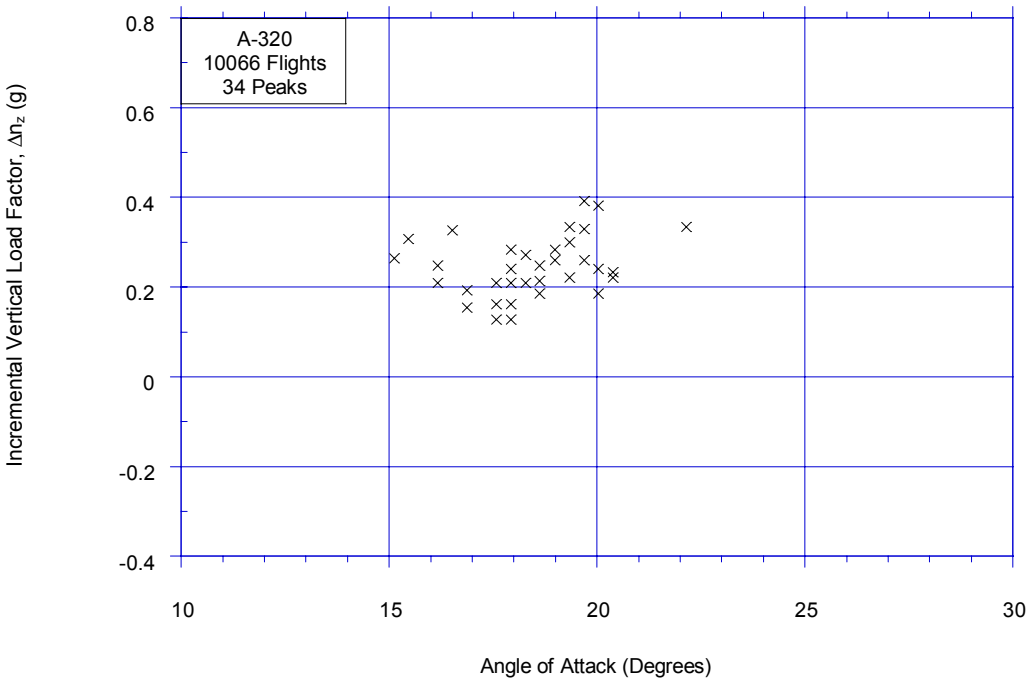


FIGURE A-42. MAXIMUM INCREMENTAL VERTICAL LOAD FACTOR VS MAXIMUM ANGLE OF ATTACK DURING LIFTOFF, 180-190 KNOTS

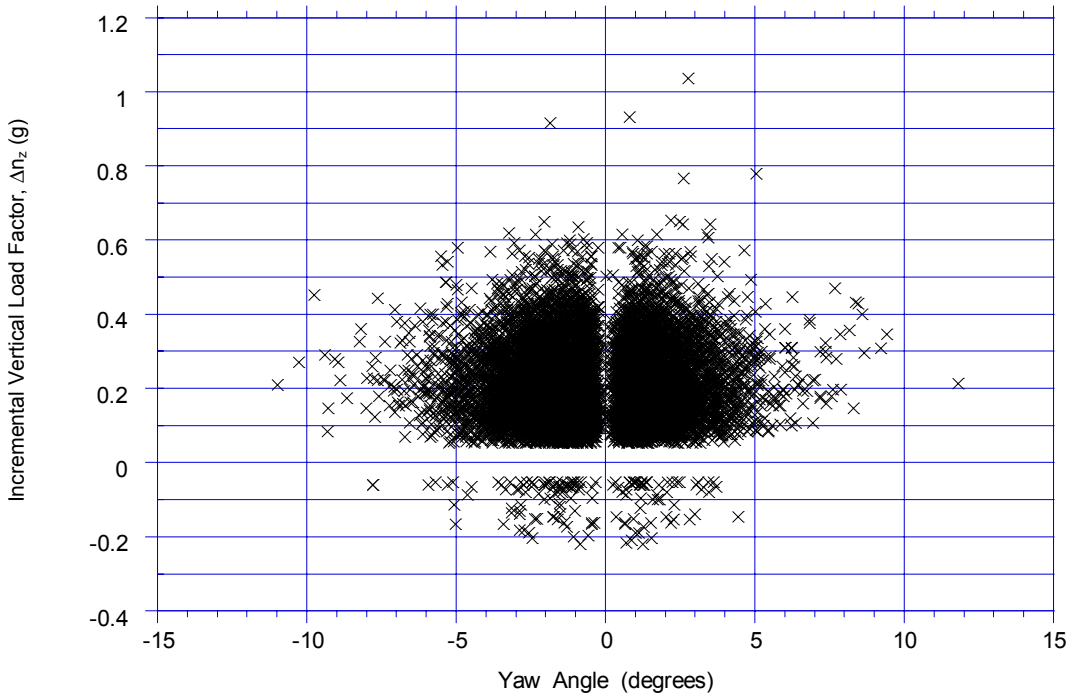


FIGURE A-43. MAXIMUM INCREMENTAL VERTICAL LOAD FACTOR AT TOUCHDOWN VS MAXIMUM YAW ANGLE BEFORE TOUCHDOWN

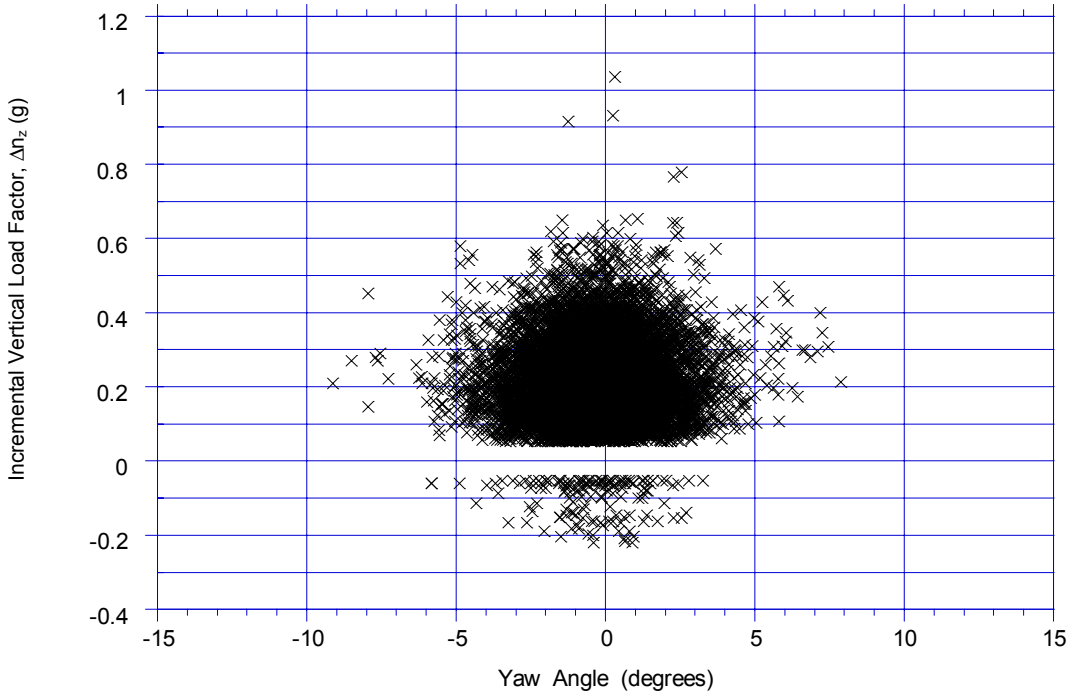


FIGURE A-44. MAXIMUM INCREMENTAL VERTICAL LOAD FACTOR AT TOUCHD0WN VS MEAN YAW ANGLE BEFORE TOUCHDOWN

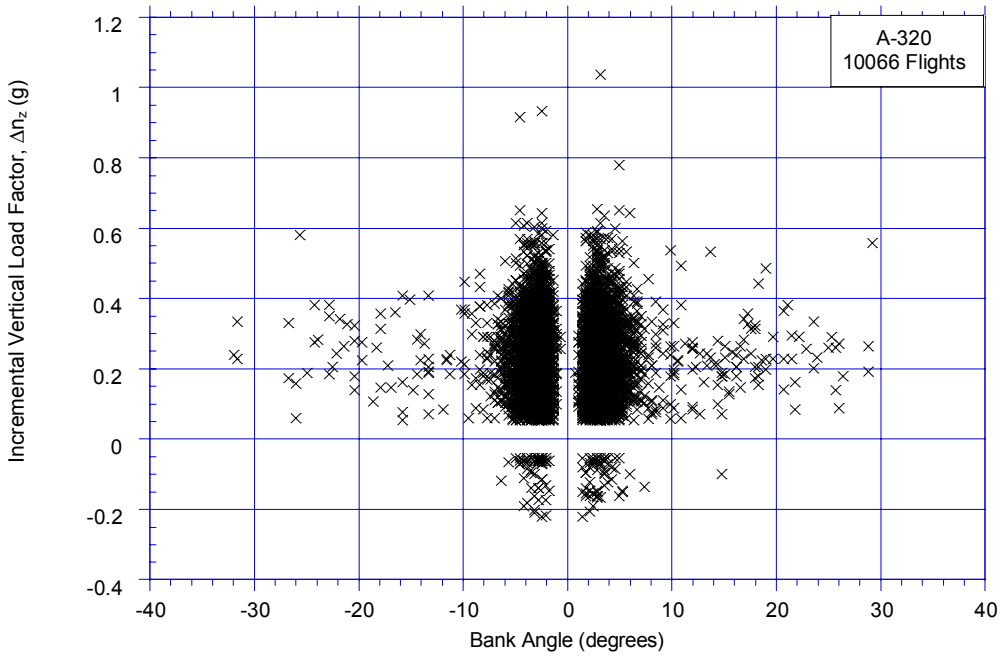


FIGURE A-45. MAXIMUM INCREMENTAL VERTICAL LOAD FACTOR AT TOUCHDOWN VS MAXIMUM BANK ANGLE BEFORE TOUCHDOWN

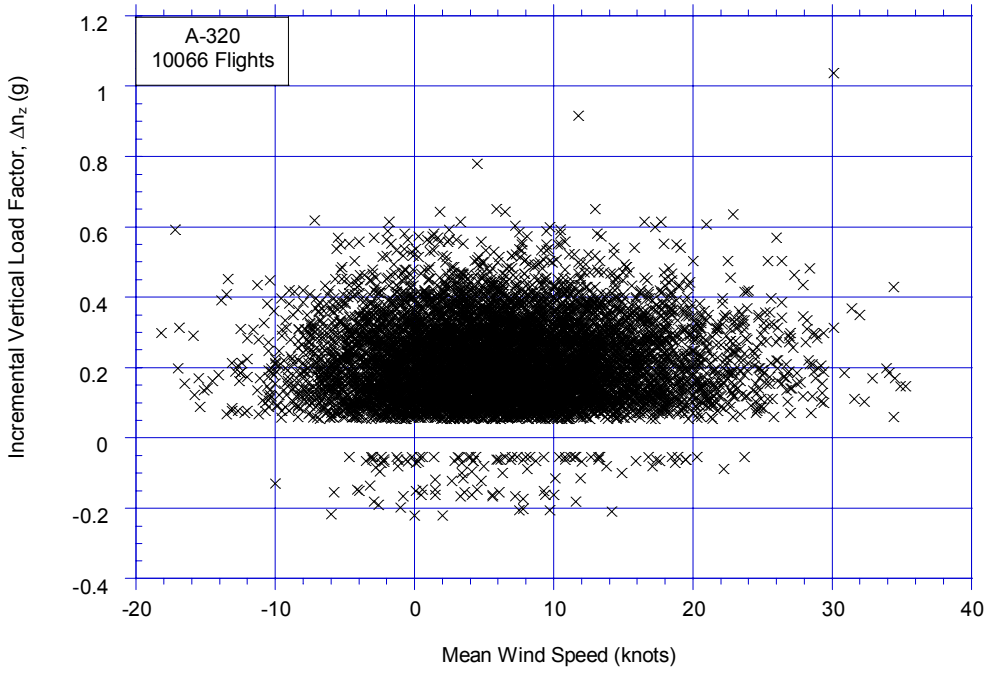


FIGURE A-46. MAXIMUM INCREMENTALVERTICAL LOAD FACTOR AT TOUCHDOWN VS MEAN WIND SPEED BEFORE TOUCHDOWN

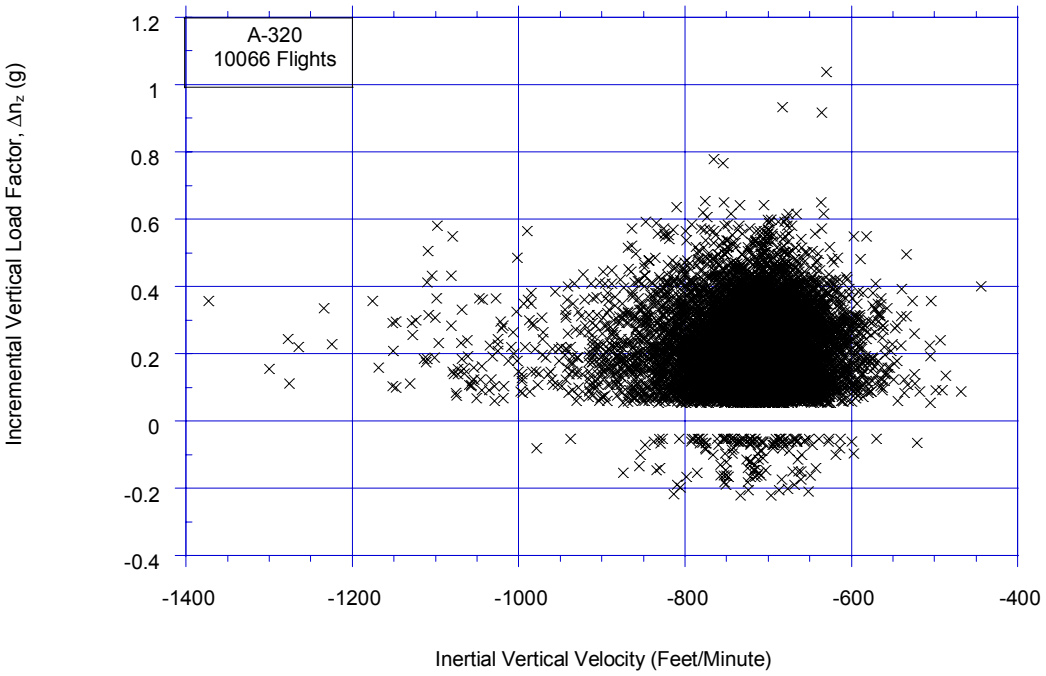


FIGURE A-47. MAXIMUM INCREMENTAL VERTICAL LOAD FACTOR AT TOUCHDOWN VS MEAN INERTIAL VERTICAL VELOCITY BEFORE TOUCHDOWN

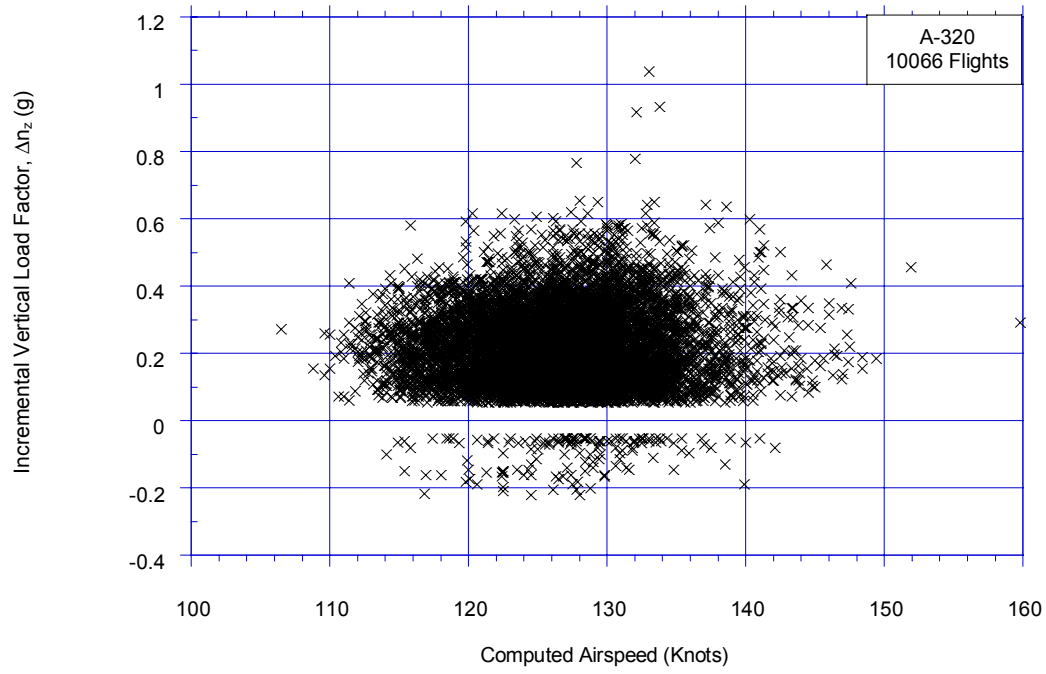


FIGURE A-48. MAXIMUM INCREMENTAL VERTICAL LOAD FACTOR VS COINCIDENT AIRSPEED AT TOUCHDOWN

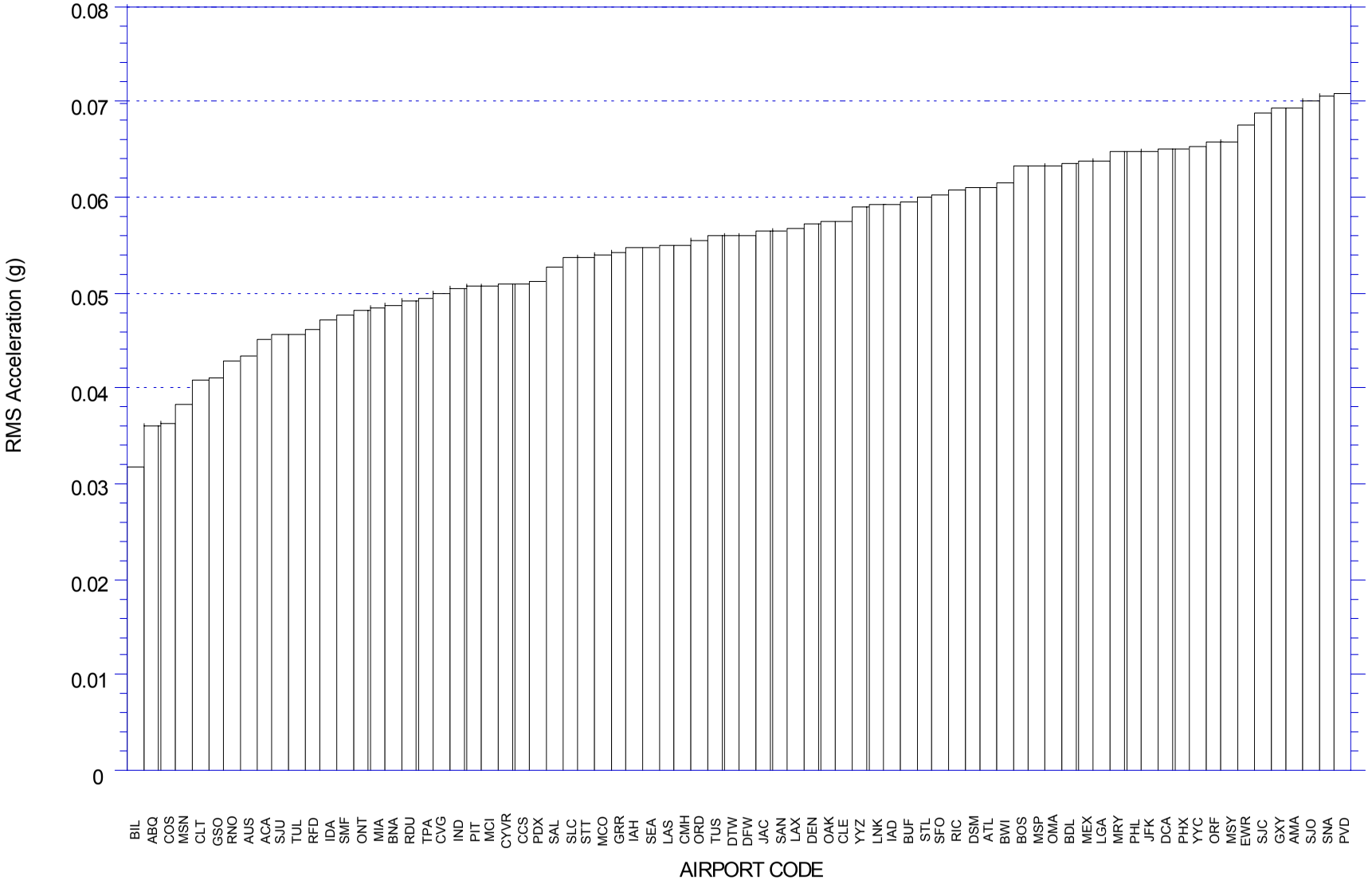


FIGURE A-49. AIRCRAFT RUNWAY ACCELERATION RESPONSE

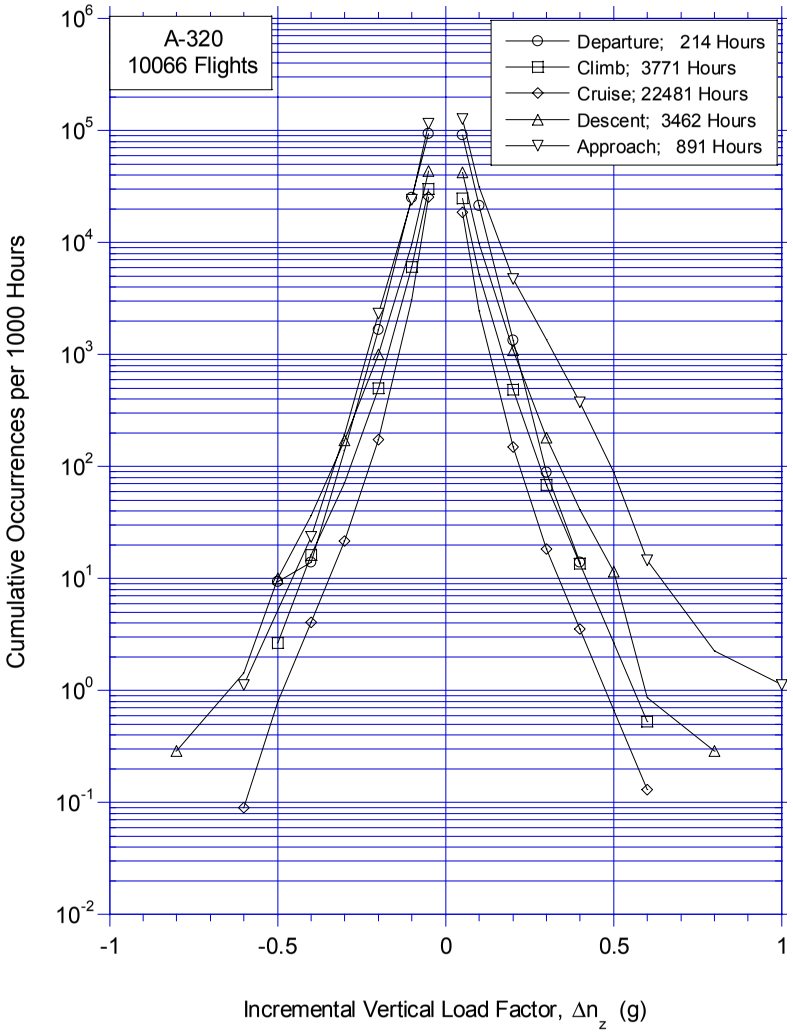


FIGURE A-50. CUMULATIVE OCCURRENCES OF INCREMENTAL VERTICAL GUST LOAD FACTOR PER 1000 HOURS BY FLIGHT PHASE

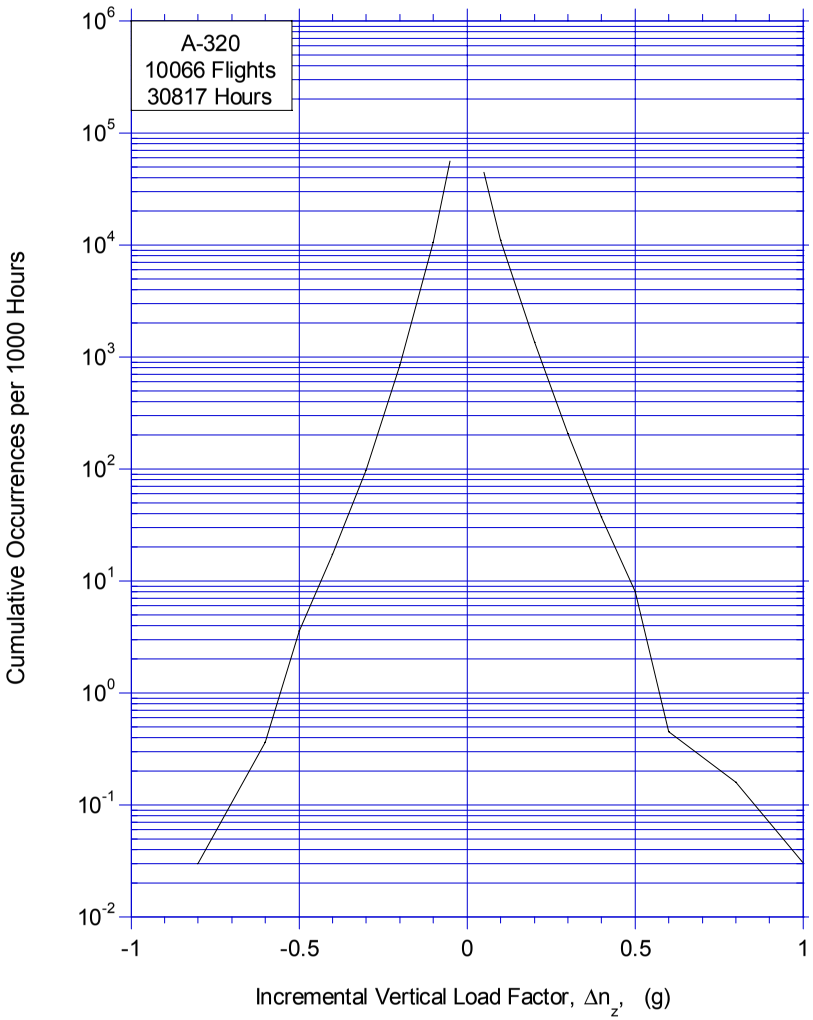


FIGURE A-51. CUMULATIVE OCCURRENCES OF INCREMENTAL VERTICAL GUST LOAD FACTOR PER 1000 HOURS, COMBINED FLIGHT PHASES

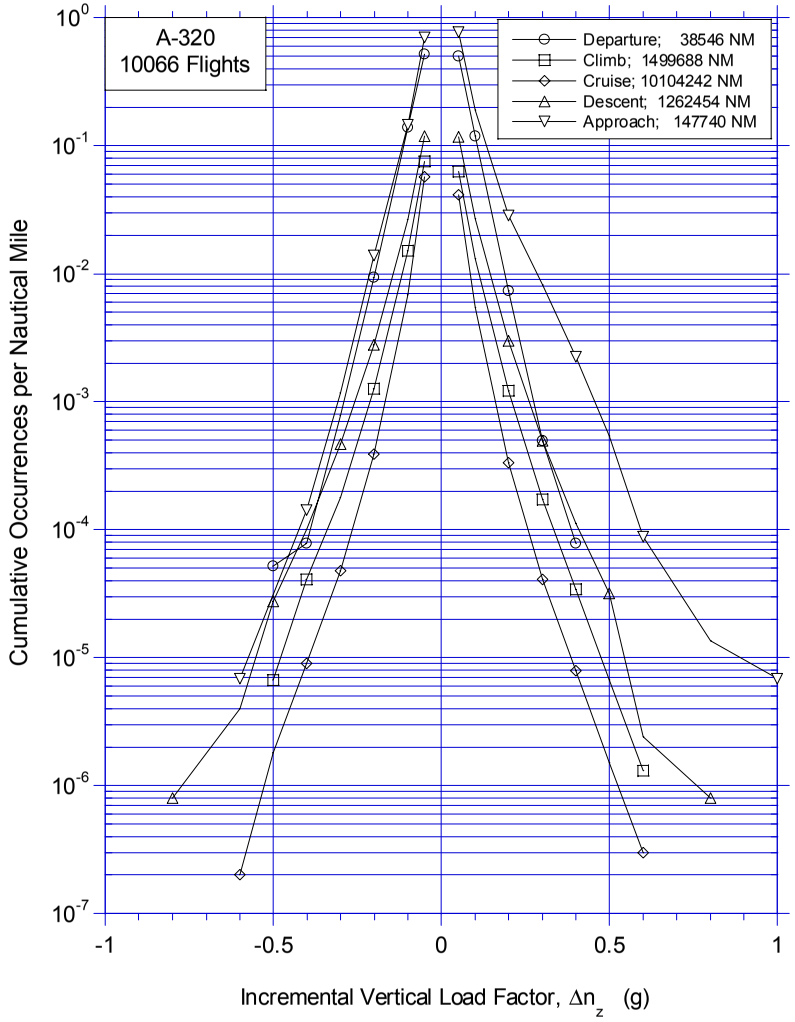


FIGURE A-52. CUMULATIVE OCCURRENCES OF INCREMENTAL VERTICAL GUST LOAD FACTOR PER NAUTICAL MILE BY FLIGHT PHASE

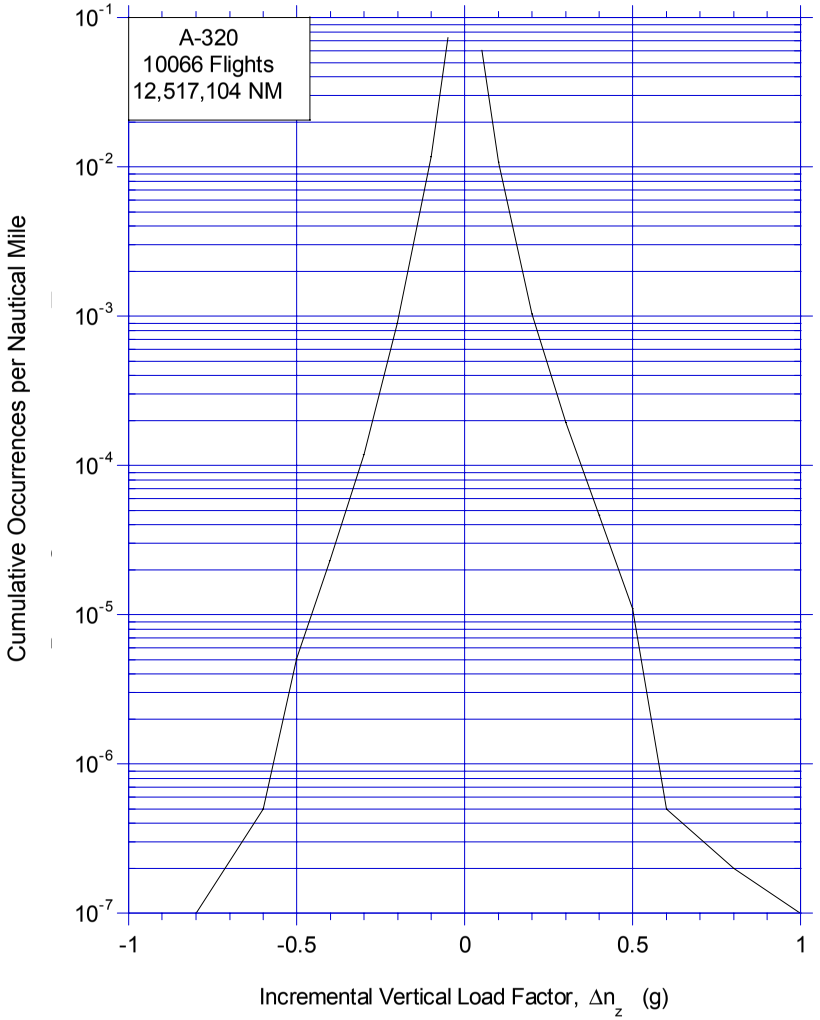


FIGURE A-53. CUMULATIVE OCCURRENCES OF INCREMENTAL VERTICAL GUST LOAD FACTOR PER NAUTICAL MILE, COMBINED FLIGHT PHASES

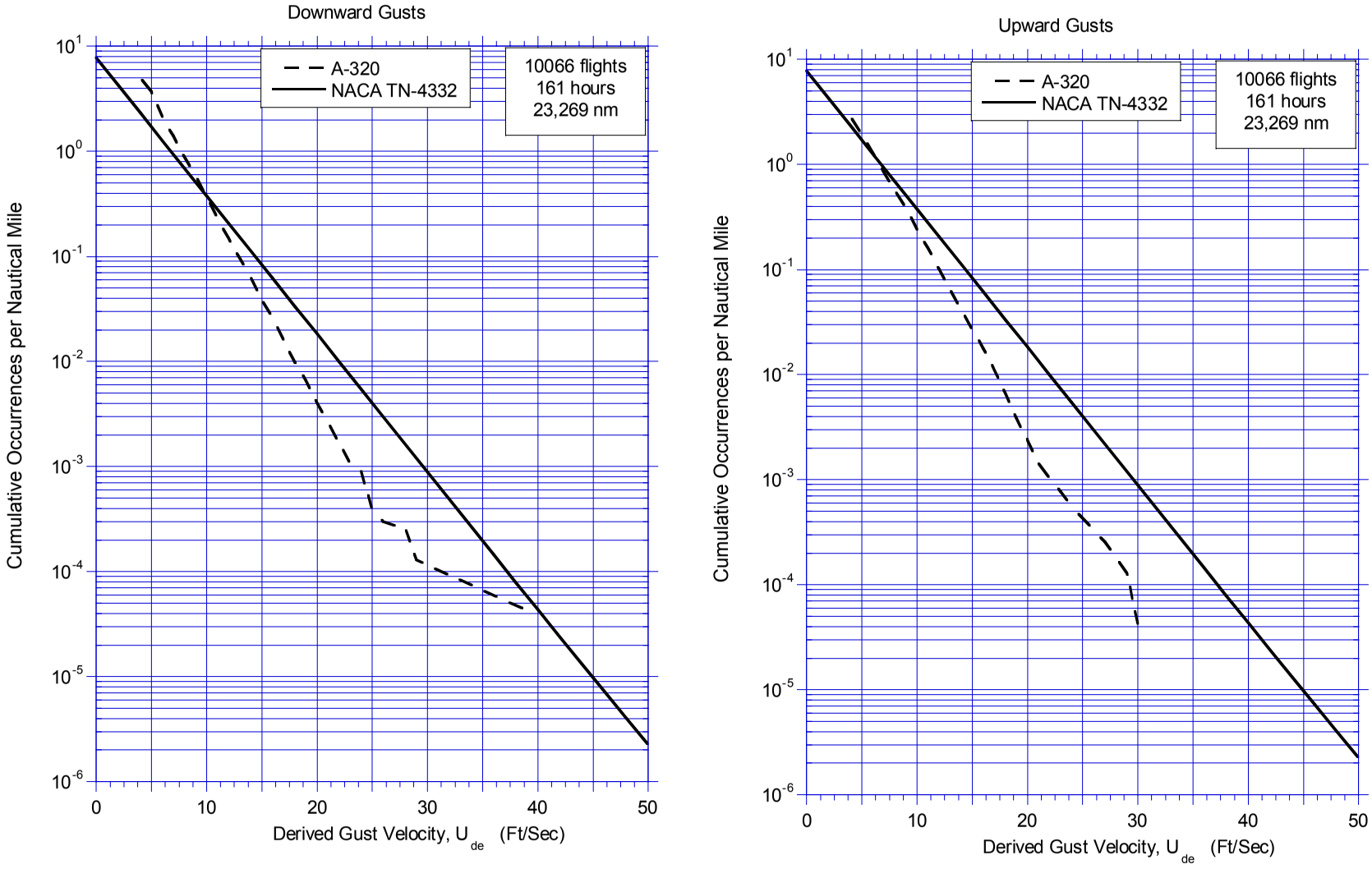


FIGURE A-54. CUMULATIVE OCCURRENCES OF DERIVED GUST VELOCITY PER NAUTICAL MILE, < 500 FEET ABOVE AIRPORT

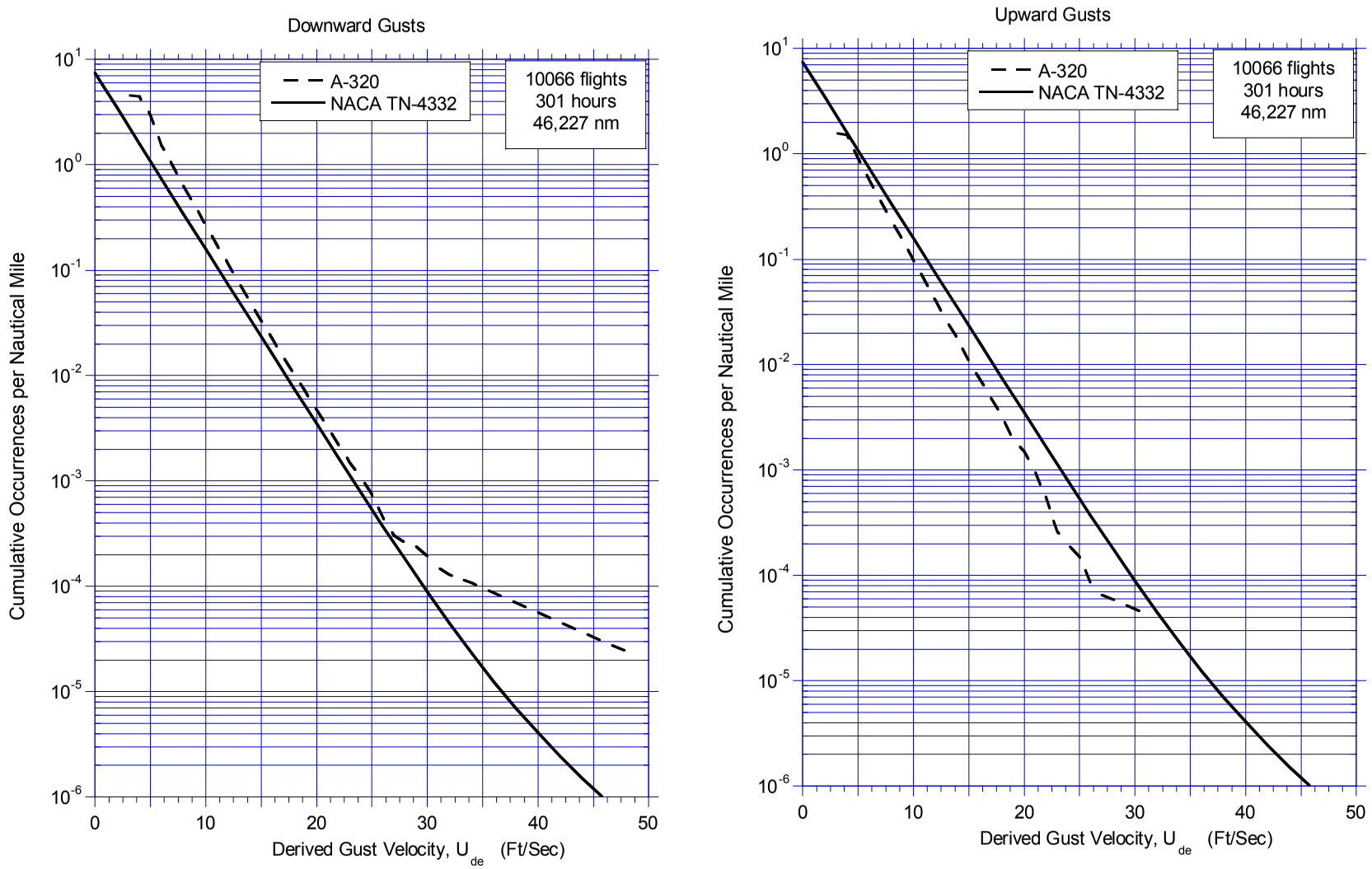


FIGURE A-55. CUMULATIVE OCCURRENCES OF DERIVED GUST VELOCITY PER NAUTICAL MILE, 500-1,500 FEET ABOVE AIRPORT

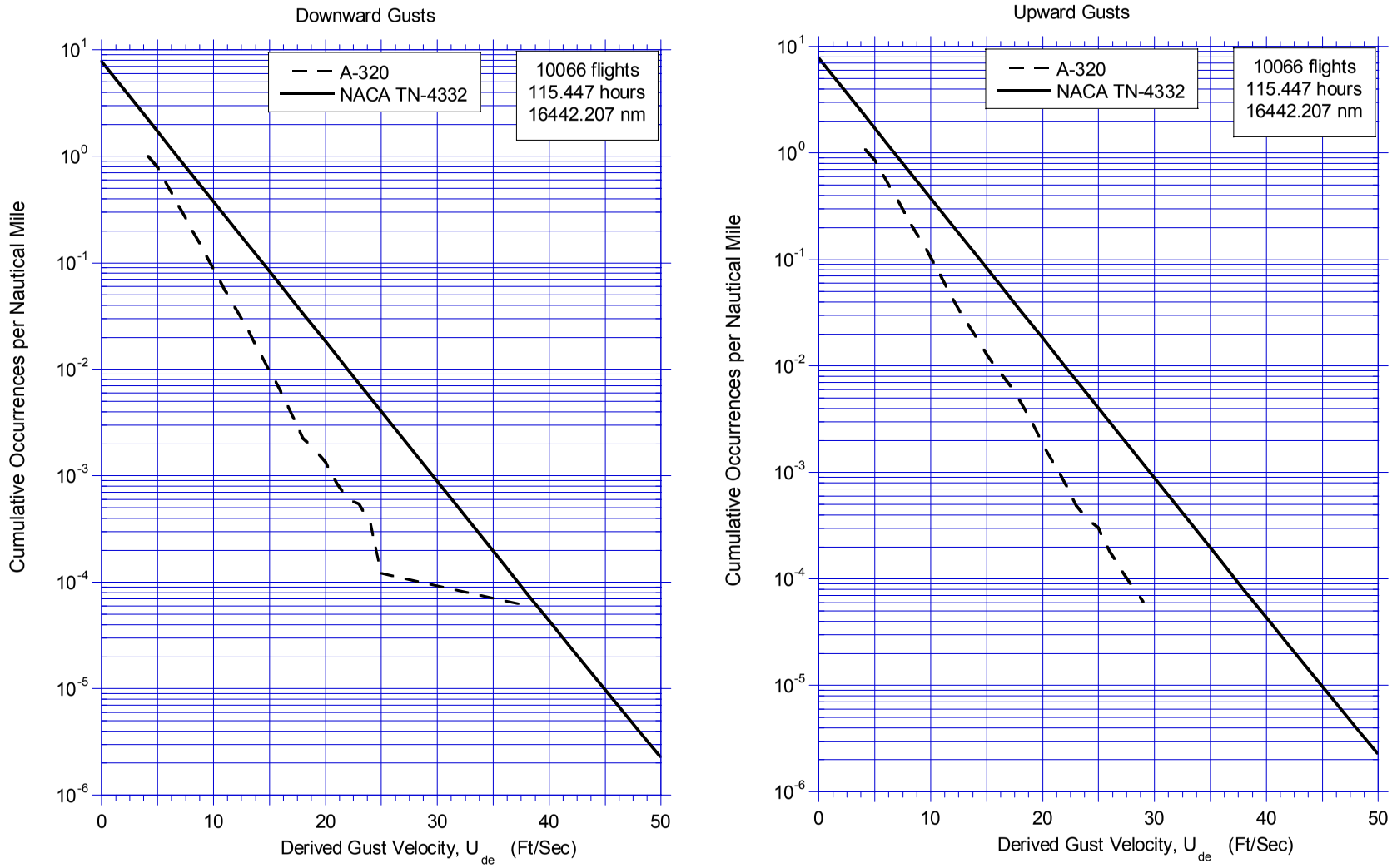


FIGURE A-56. CUMULATIVE OCCURRENCES OF DERIVED GUST VELOCITY PER NAUTICAL MILE, < 500 FEET

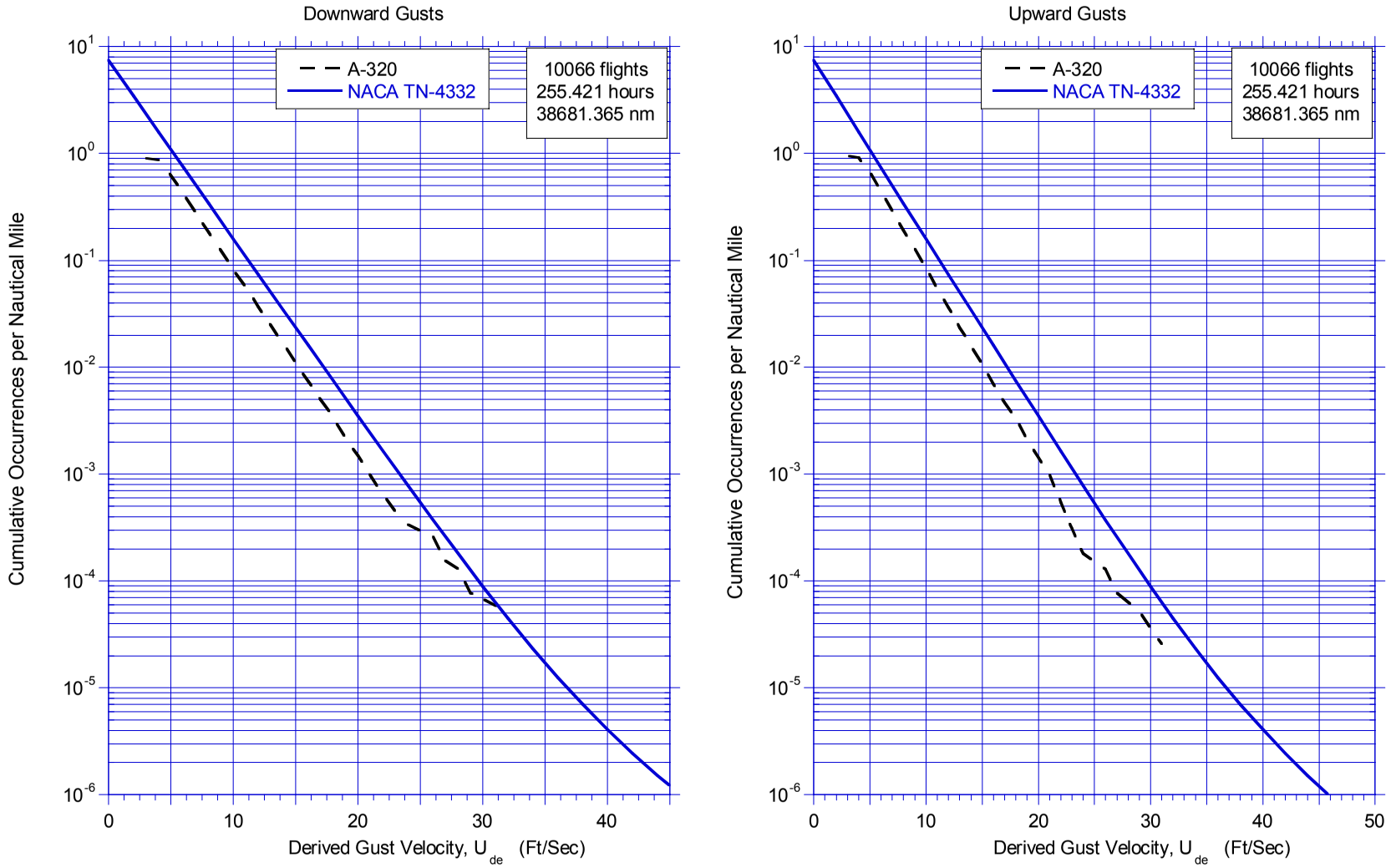


FIGURE A-57. CUMULATIVE OCCURRENCES OF DERIVED GUST VELOCITY PER NAUTICAL MILE, 500-1,500 FEET

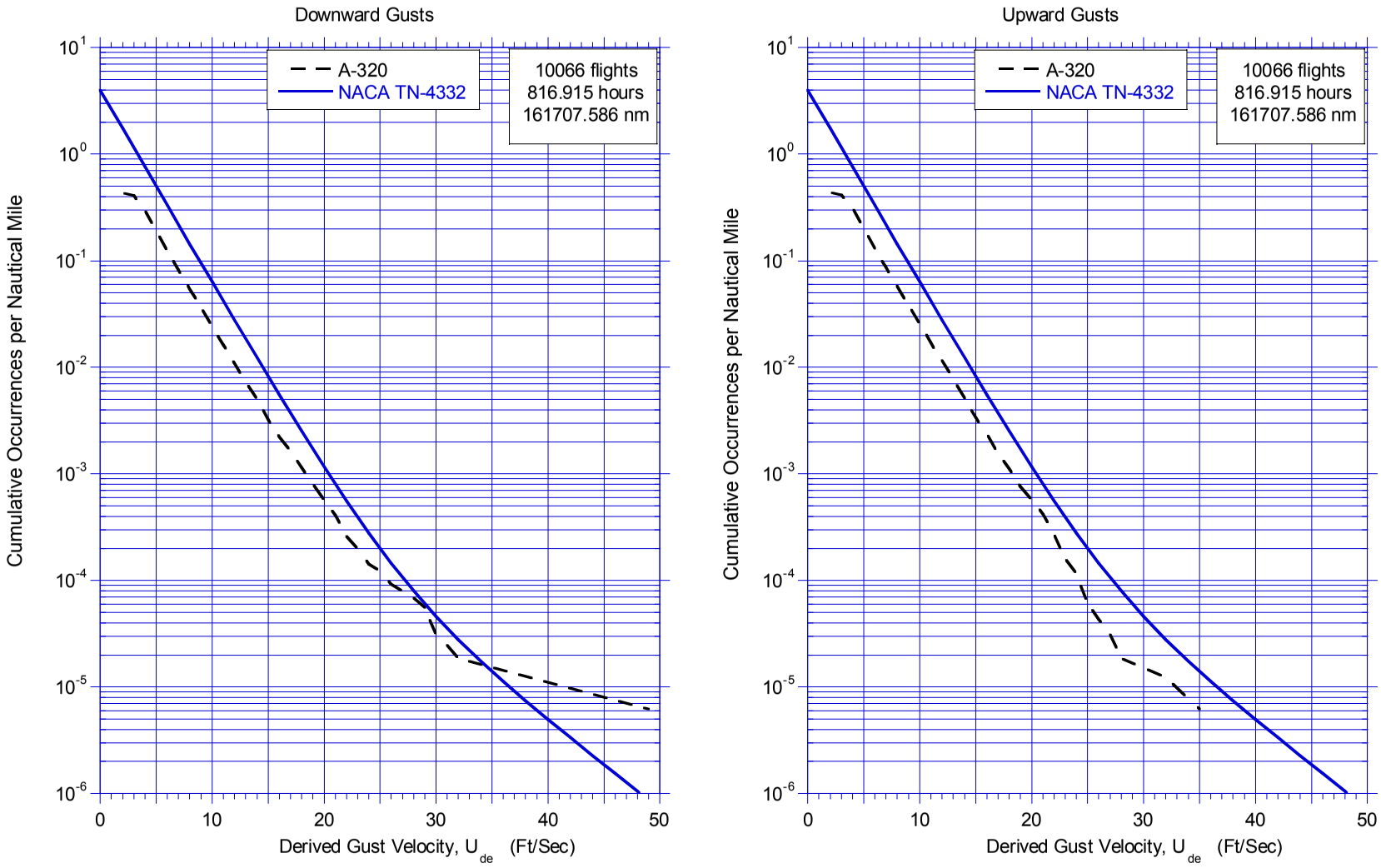


FIGURE A-58. CUMULATIVE OCCURRENCES OF DERIVED GUST VELOCITY PER NAUTICAL MILE, 1,500-4,500 FEET

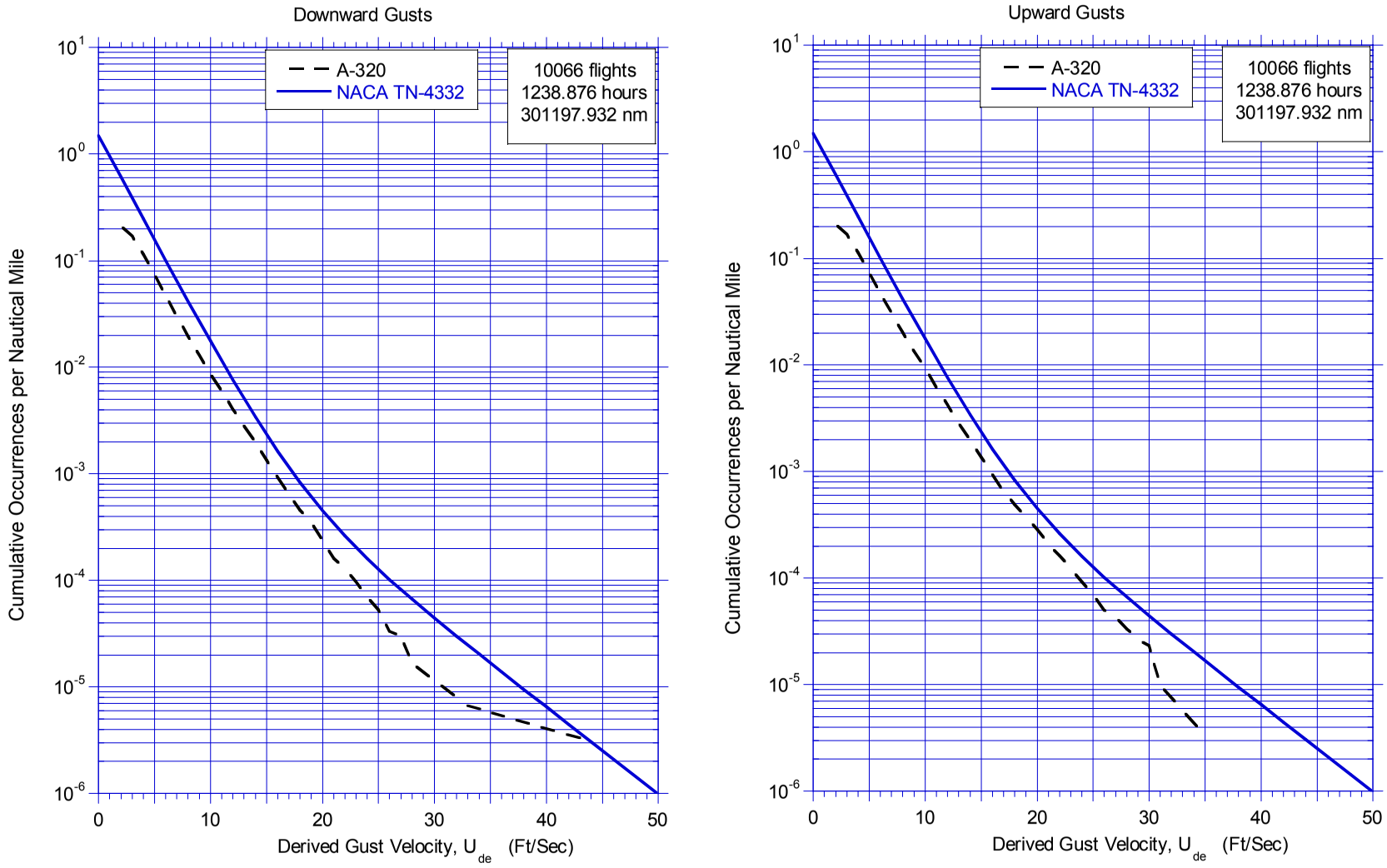


FIGURE A-59. CUMULATIVE OCCURRENCES OF DERIVED GUST VELOCITY PER NAUTICAL MILE, 4,500-9,500 FEET

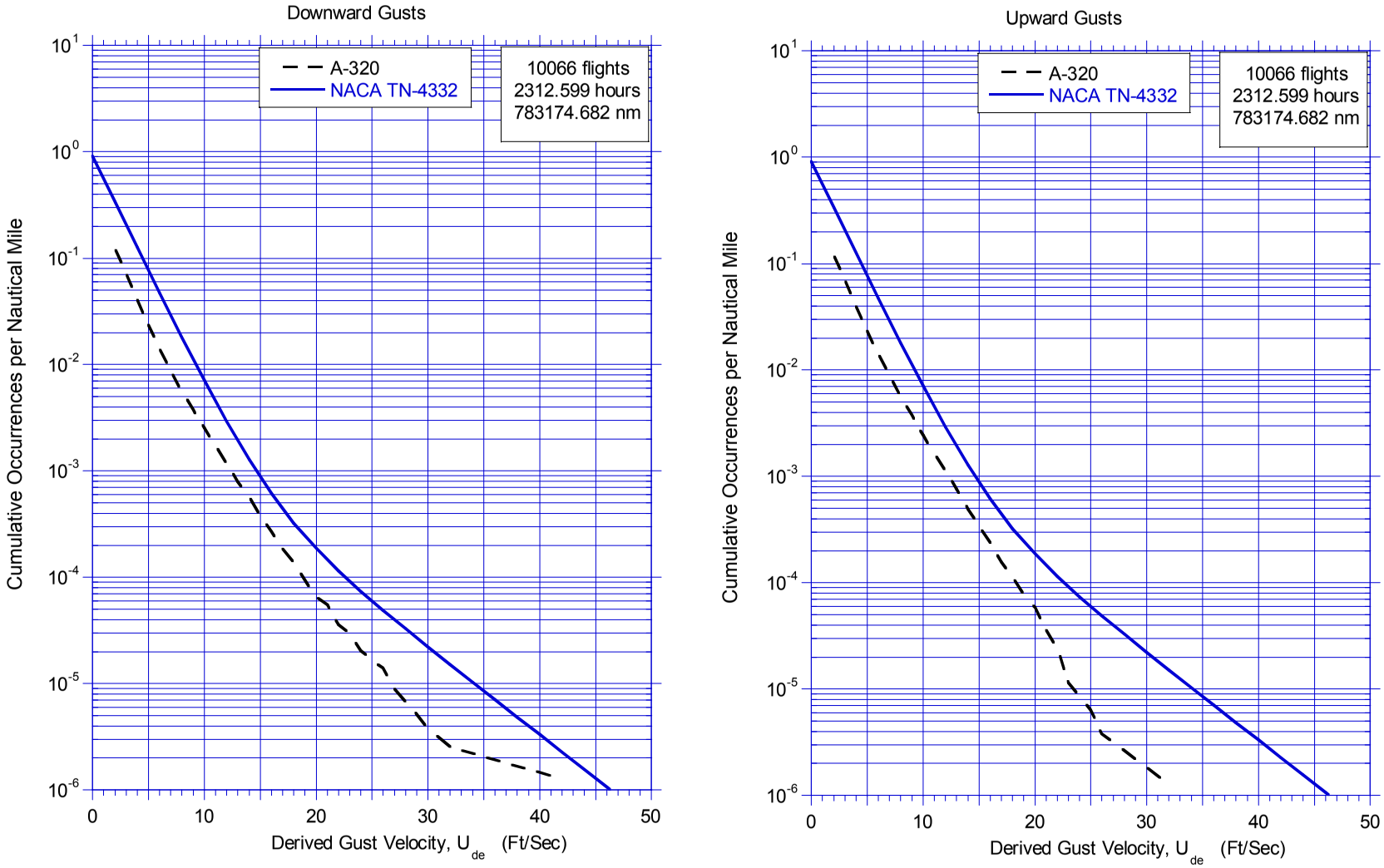


FIGURE A-60. CUMULATIVE OCCURRENCES OF DERIVED GUST VELOCITY PER NAUTICAL MILE, 9,500-19,500 FEET

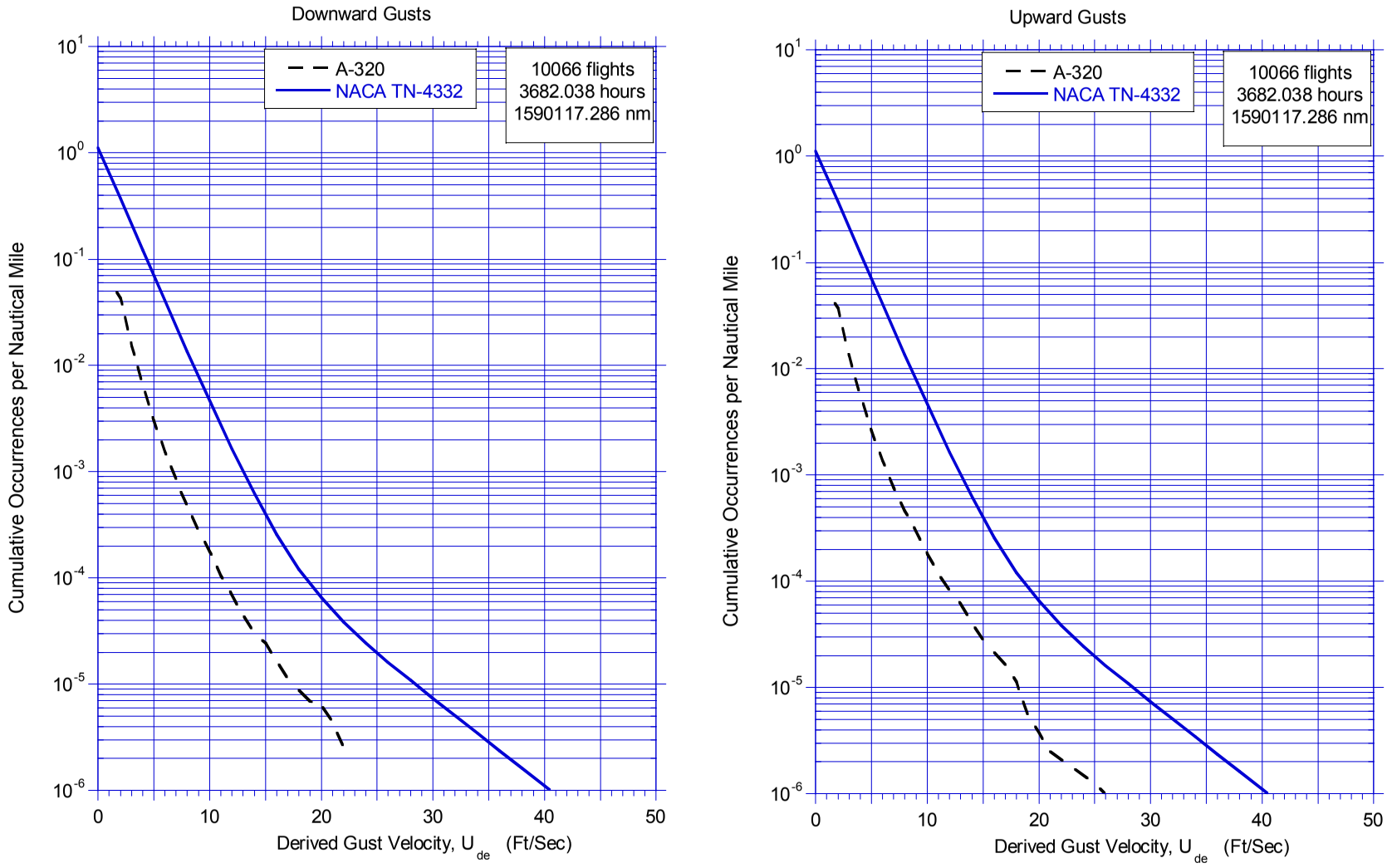


FIGURE A-61. CUMULATIVE OCCURRENCES OF DERIVED GUST VELOCITY PER NAUTICAL MILE, 19,500-29,500 FEET

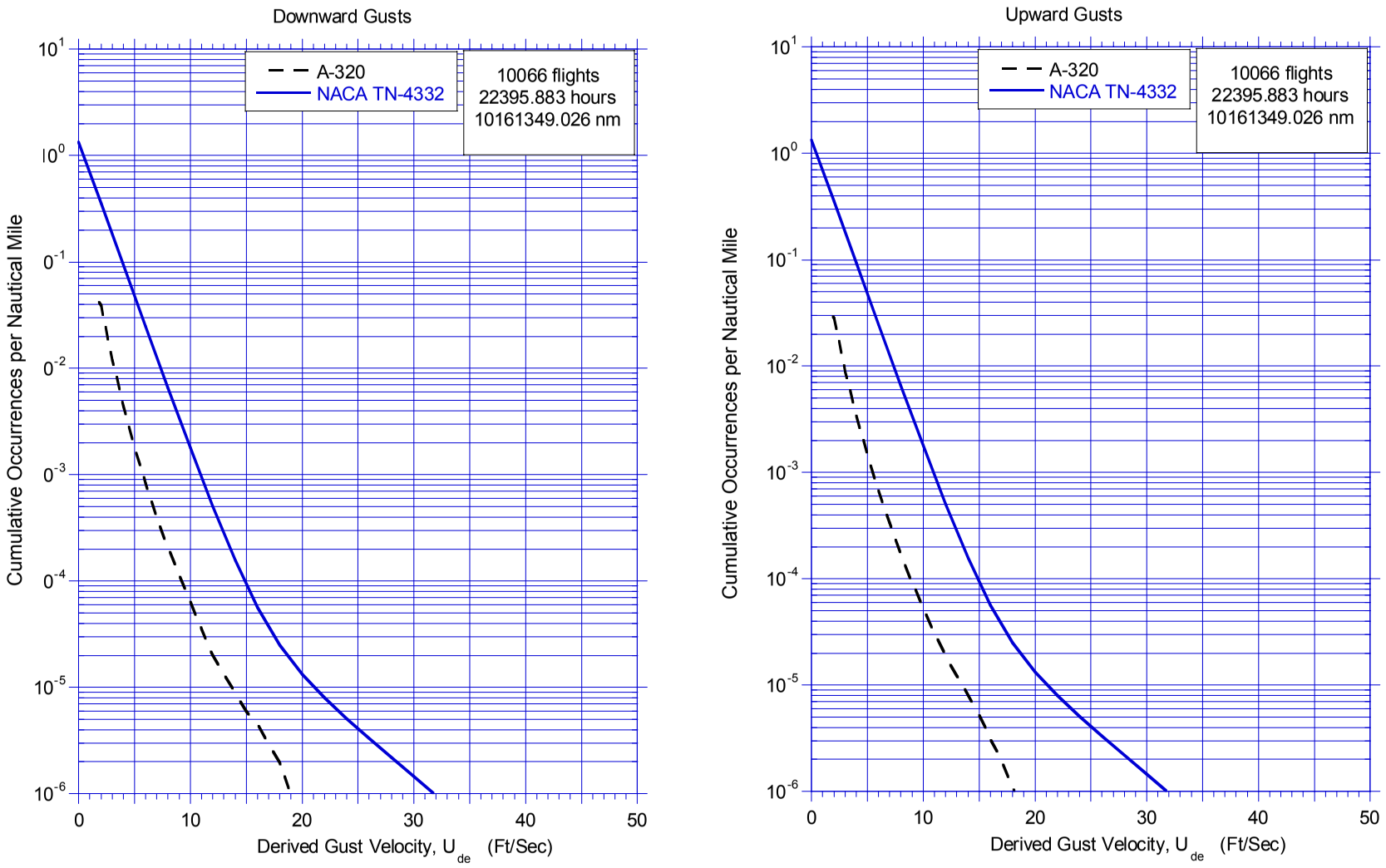


FIGURE A-62. CUMULATIVE OCCURRENCES OF DERIVED GUST VELOCITY PER NAUTICAL MILE, 29,500-39,500 FEET

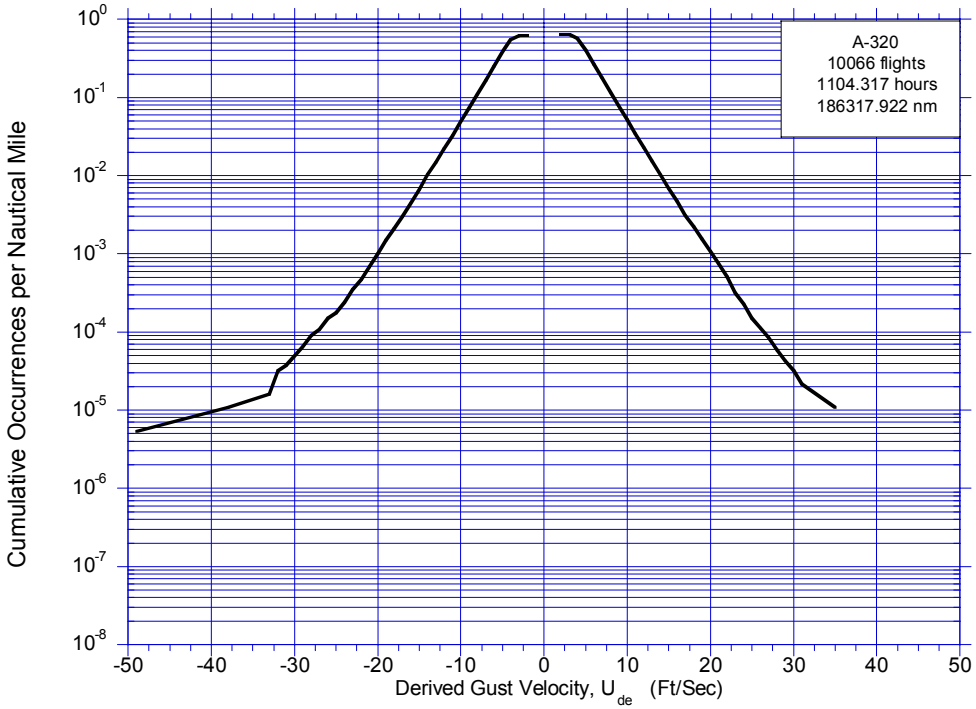


FIGURE A-63. CUMULATIVE OCCURRENCES OF DERIVED GUST VELOCITY PER NAUTICAL MILE, FLAPS EXTENDED

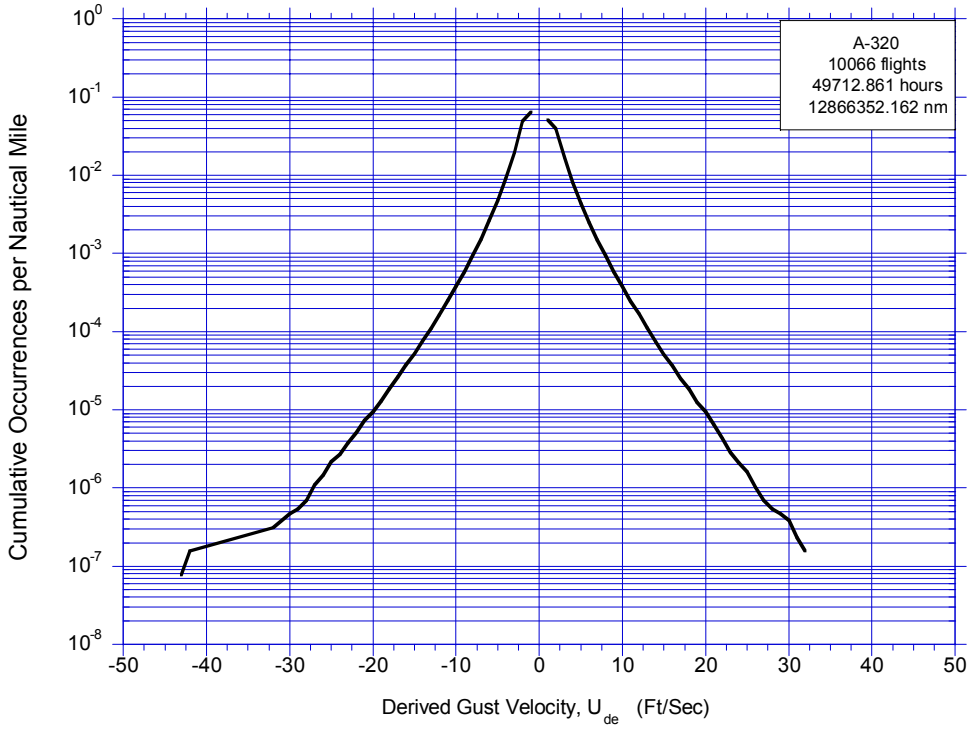


FIGURE A-64. CUMULATIVE OCCURRENCES OF DERIVED GUST VELOCITY PER NAUTICAL MILE, FLAPS RETRACTED

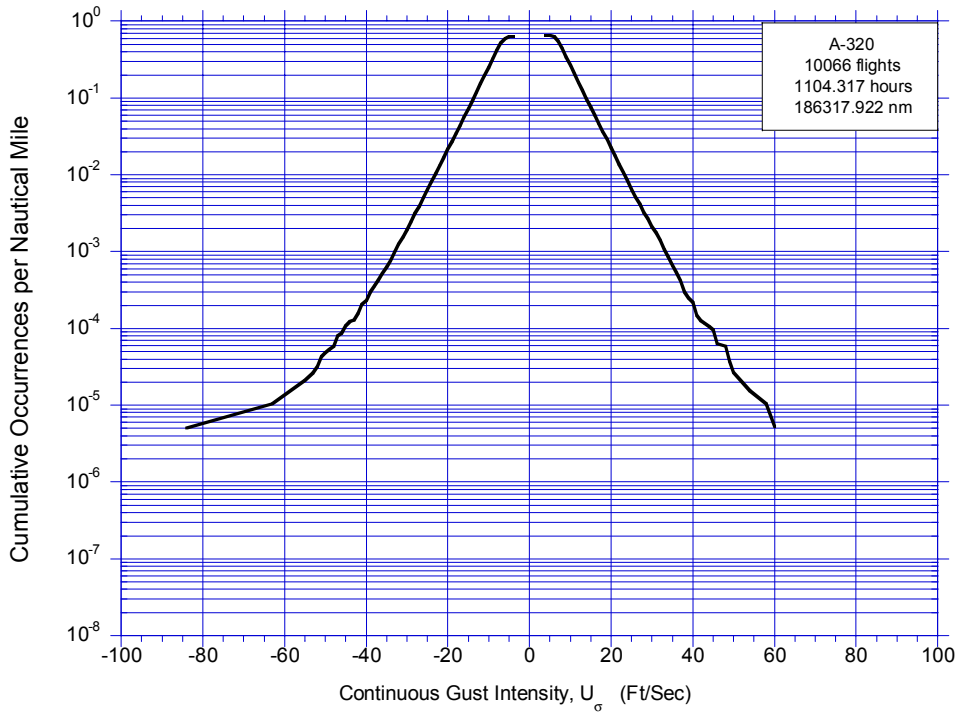


FIGURE A-65. CUMULATIVE OCCURRENCES OF CONTINUOUS GUST INTENSITY PER NAUTICAL MILE, FLAPS EXTENDED

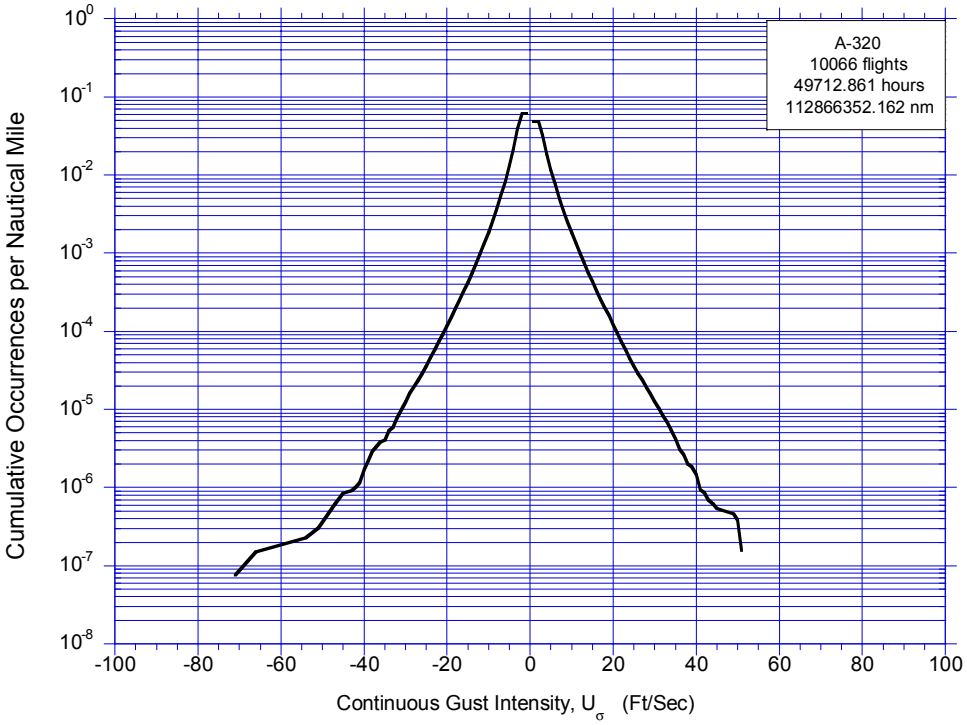


FIGURE A-66. CUMULATIVE OCCURRENCES OF CONTINUOUS GUST INTENSITY PER NAUTICAL MILE, FLAPS RETRACTED

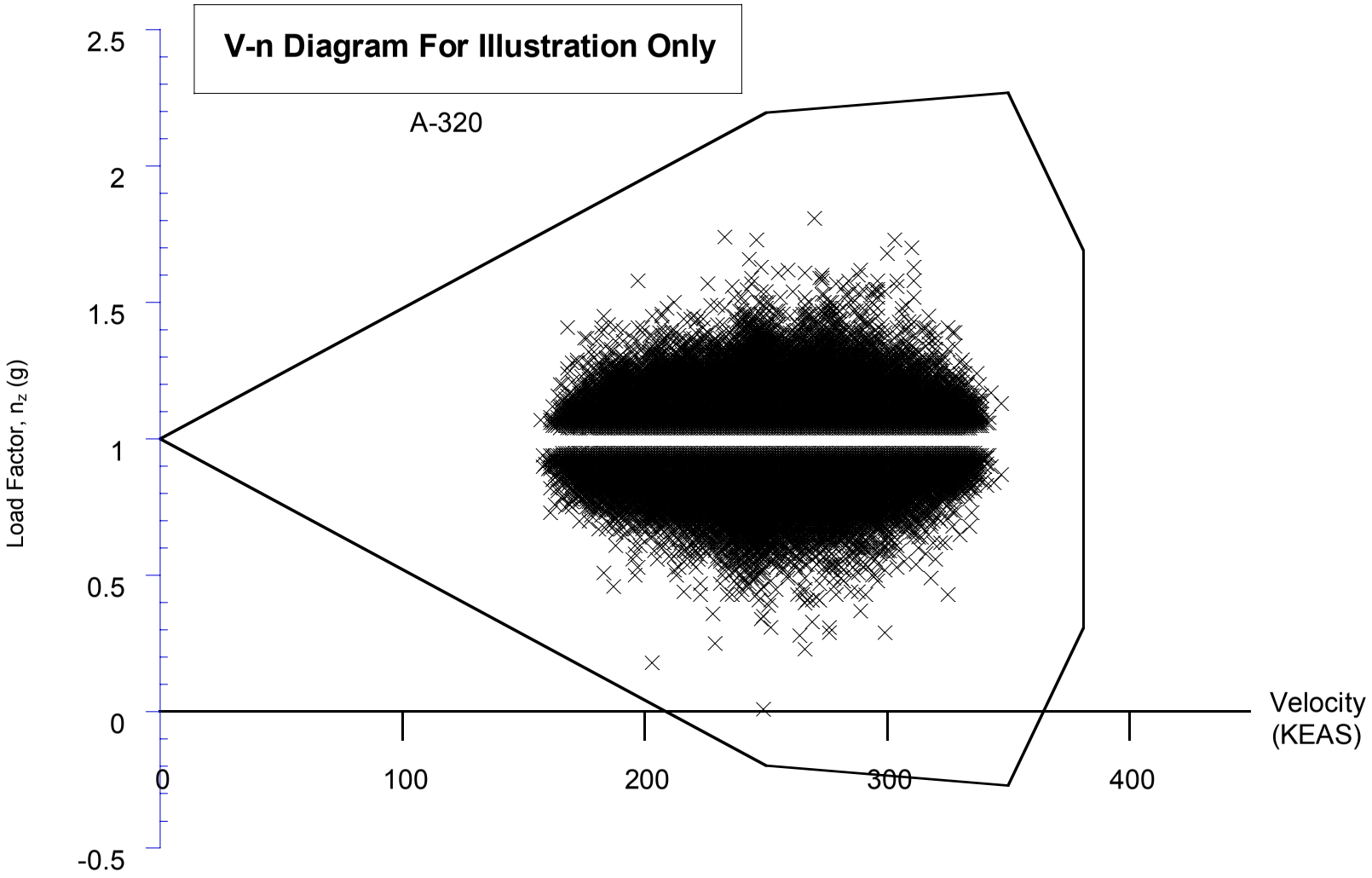


FIGURE A-67. GUST LOAD FACTOR AND COINCIDENT SPEED VS V-n DIAGRAM FOR FLAPS RETRACTED

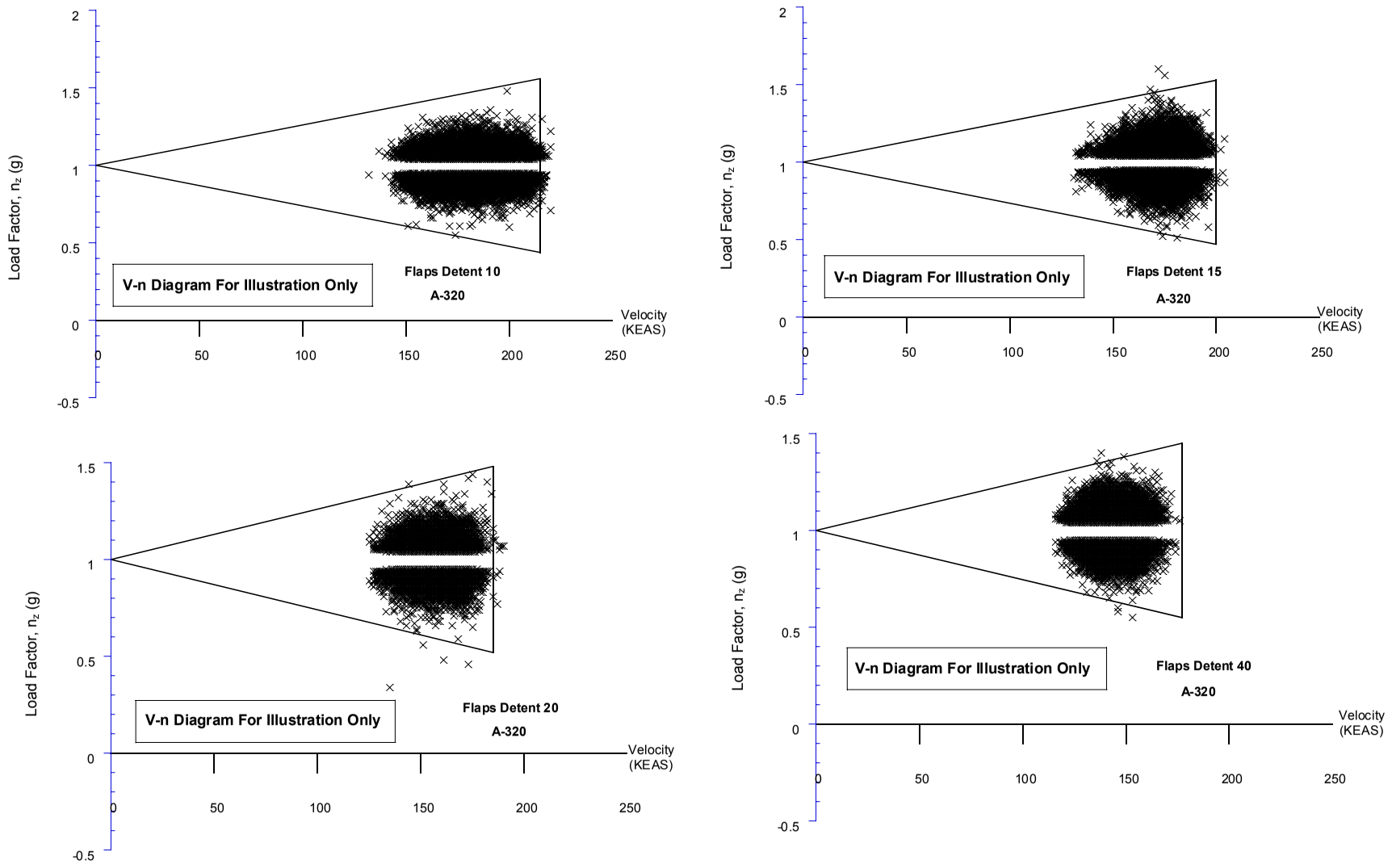


FIGURE A-68. GUST LOAD FACTOR AND COINCIDENT SPEED VS V-n DIAGRAMS FOR FLAPS EXTENDED, DETENTS 10, 15, 20, AND 40

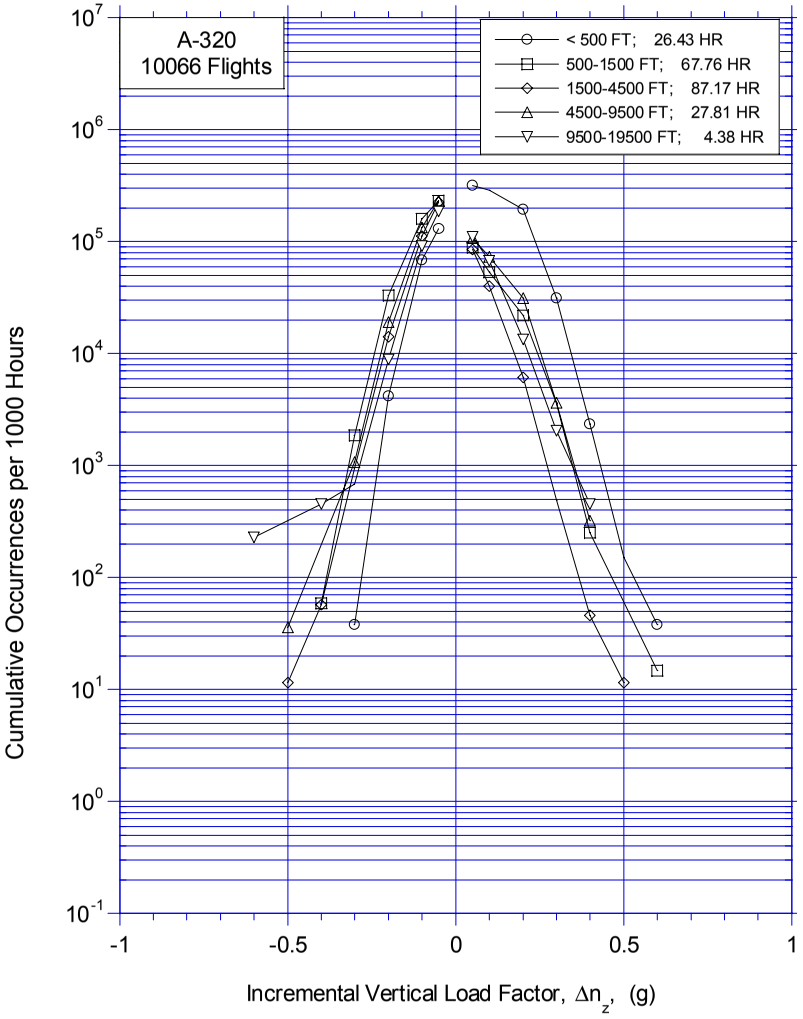


FIGURE A-69. CUMULATIVE OCCURRENCES OF INCREMENTAL VERTICAL MANEUVER LOAD FACTOR PER 1000 HOURS DURING DEPARTURE BY ALTITUDE

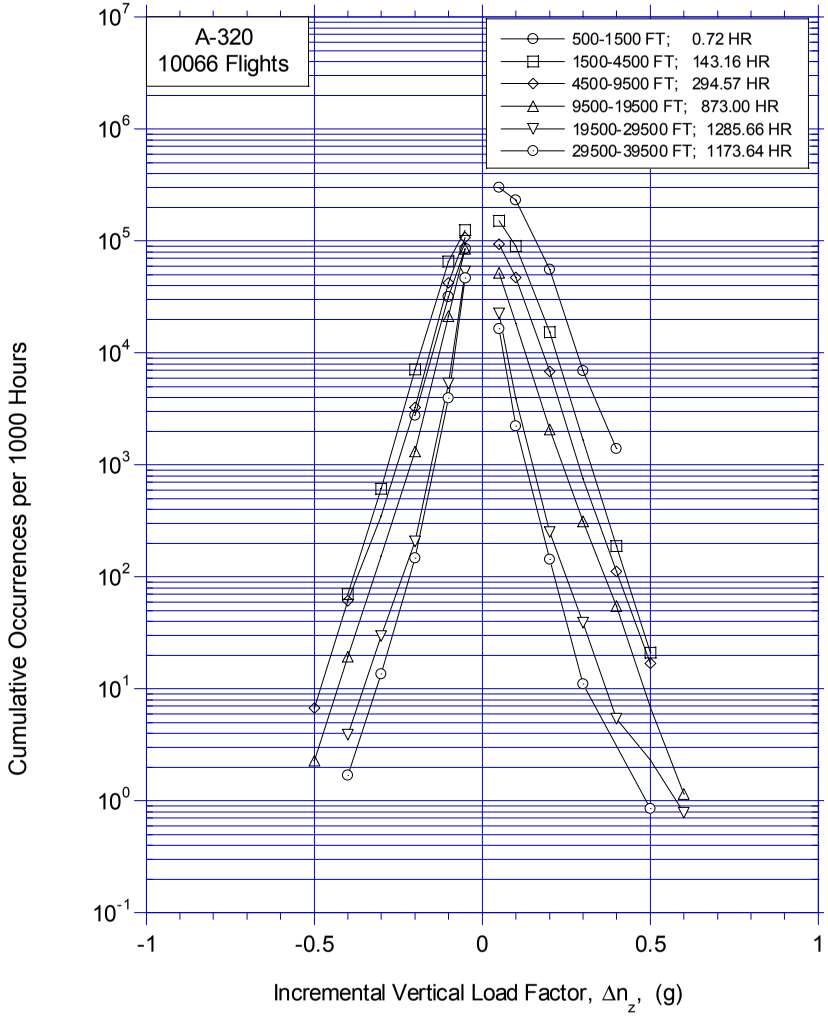


FIGURE A-70. CUMULATIVE OCCURRENCES OF INCREMENTAL VERTICAL MANEUVER LOAD FACTOR PER 1000 HOURS DURING CLIMB BY ALTITUDE

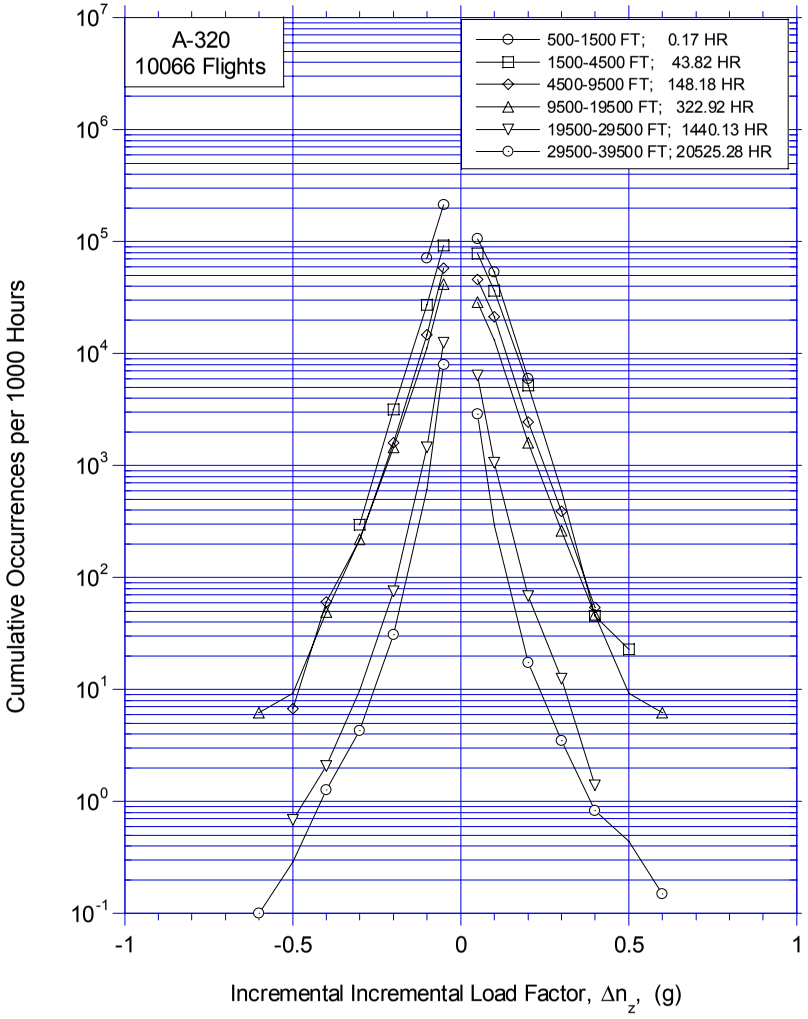


FIGURE A-71. CUMULATIVE OCCURRENCES OF INCREMENTAL VERTICAL MANEUVER LOAD FACTOR PER 1000 HOURS DURING CRUISE BY ALTITUDE

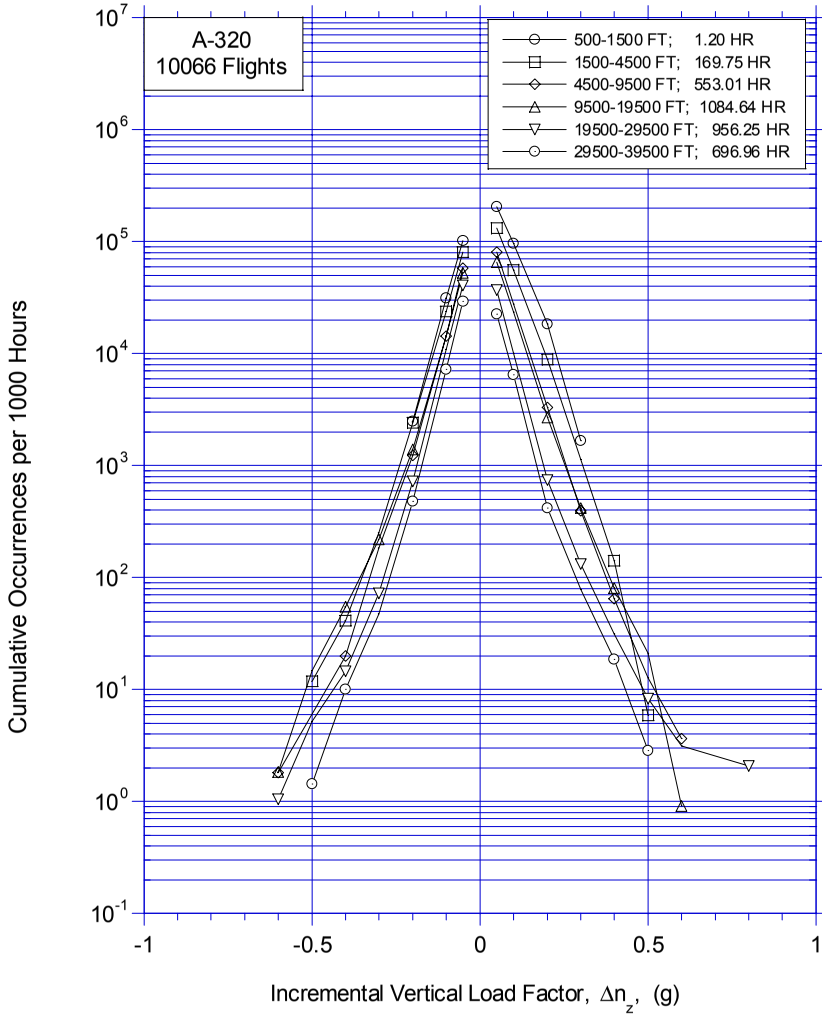


FIGURE A-72. CUMULATIVE OCCURRENCES OF INCREMENTAL VERTICAL MANEUVER LOAD FACTOR PER 1000 HOURS DURING DESCENT BY ALTITUDE

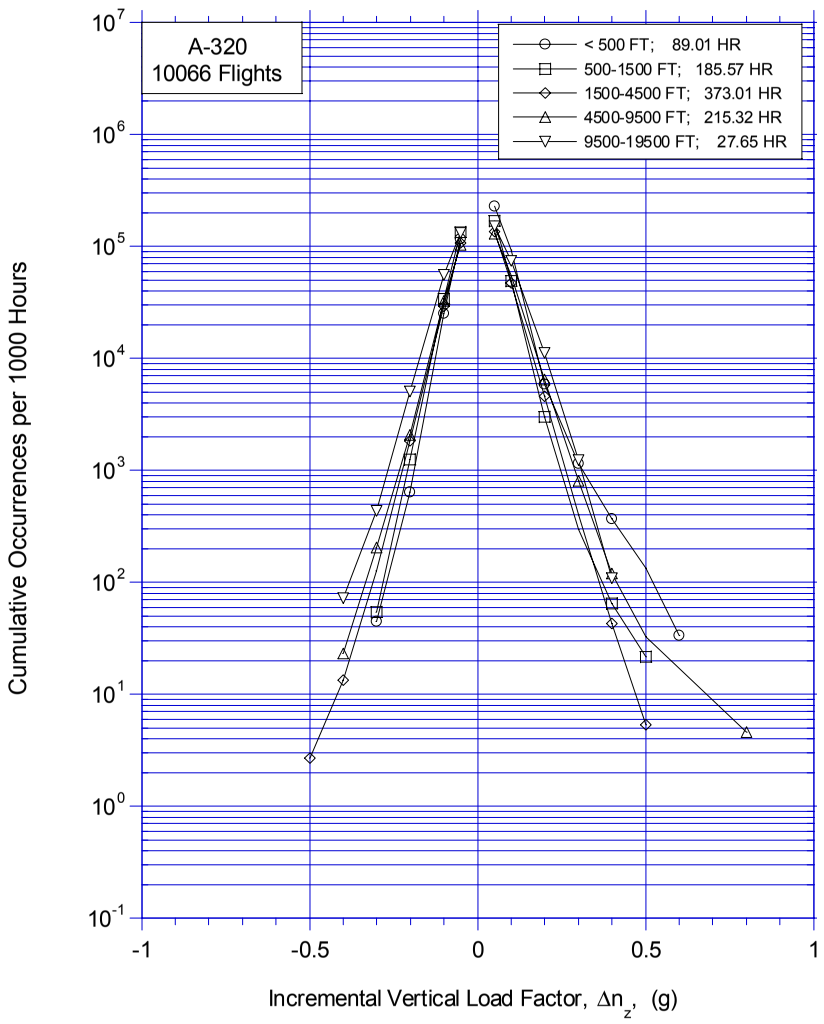


FIGURE A-73. CUMULATIVE OCCURRENCES OF INCREMENTAL VERTICAL MANEUVER LOAD FACTOR PER 1000 HOURS DURING APPROACH BY ALTITUDE

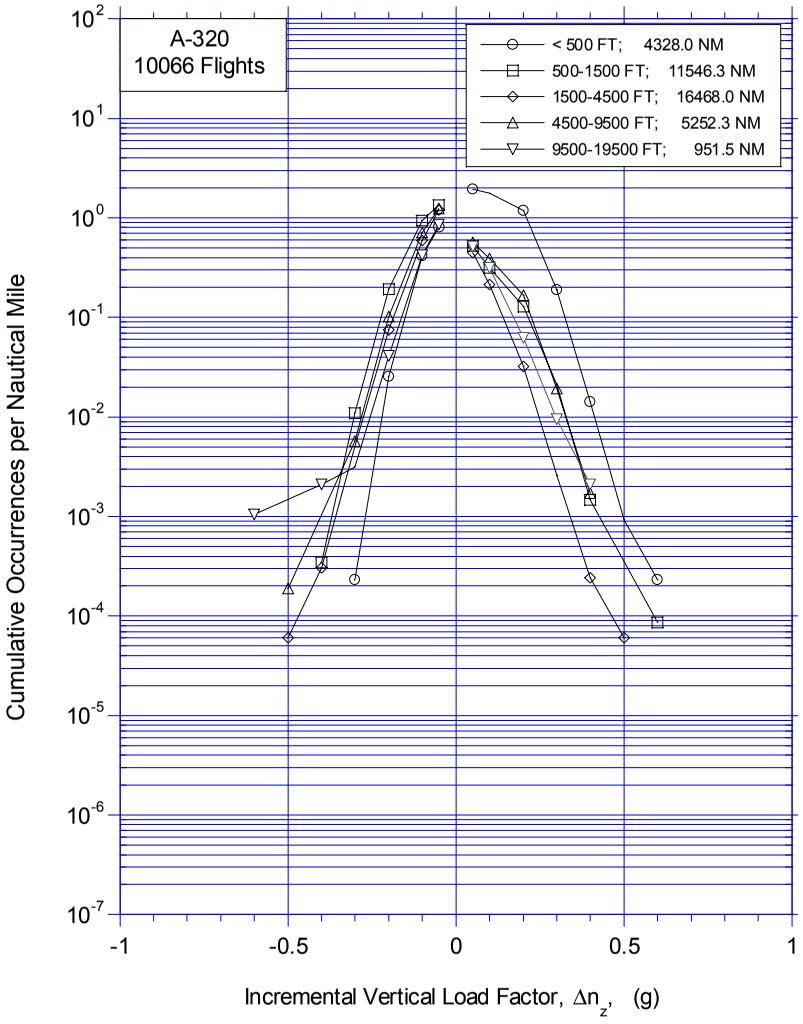


FIGURE A-74. CUMULATIVE OCCURRENCES OF INCREMENTAL VERTICAL MANEUVER LOAD FACTOR PER NAUTICAL MILE DURING DEPARTURE BY ALTITUDE

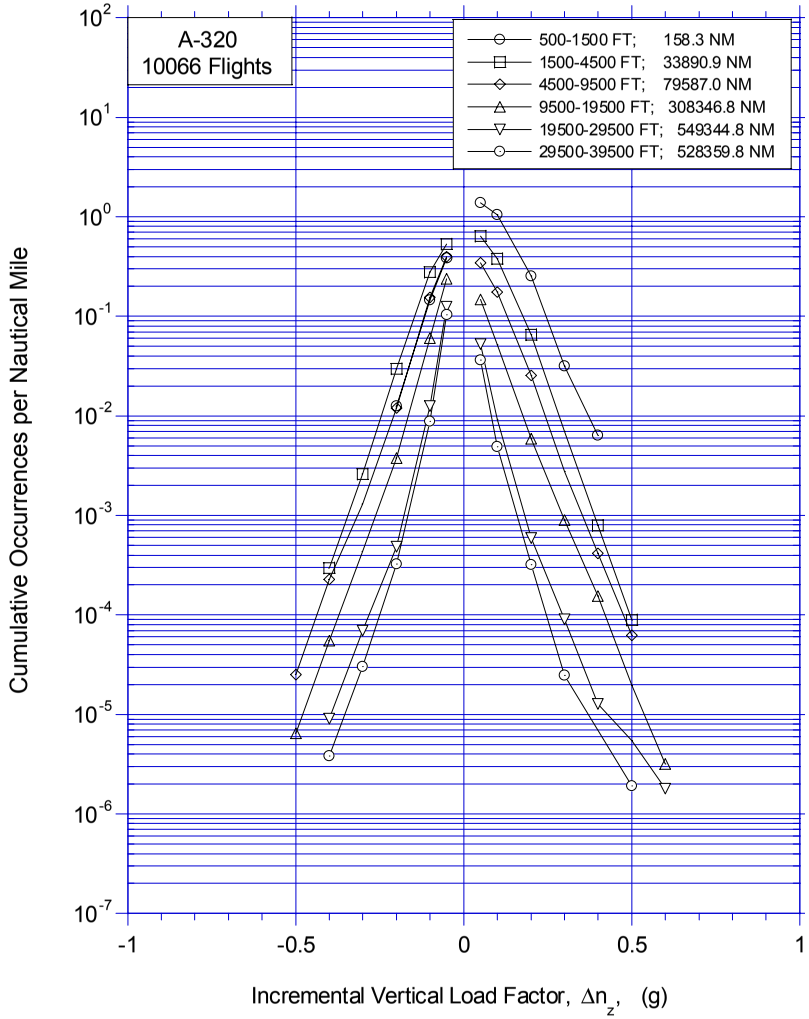


FIGURE A-75. CUMULATIVE OCCURRENCES OF INCREMENTAL VERTICAL MANEUVER LOAD FACTOR PER NAUTICAL MILE DURING CLIMB BY ALTITUDE

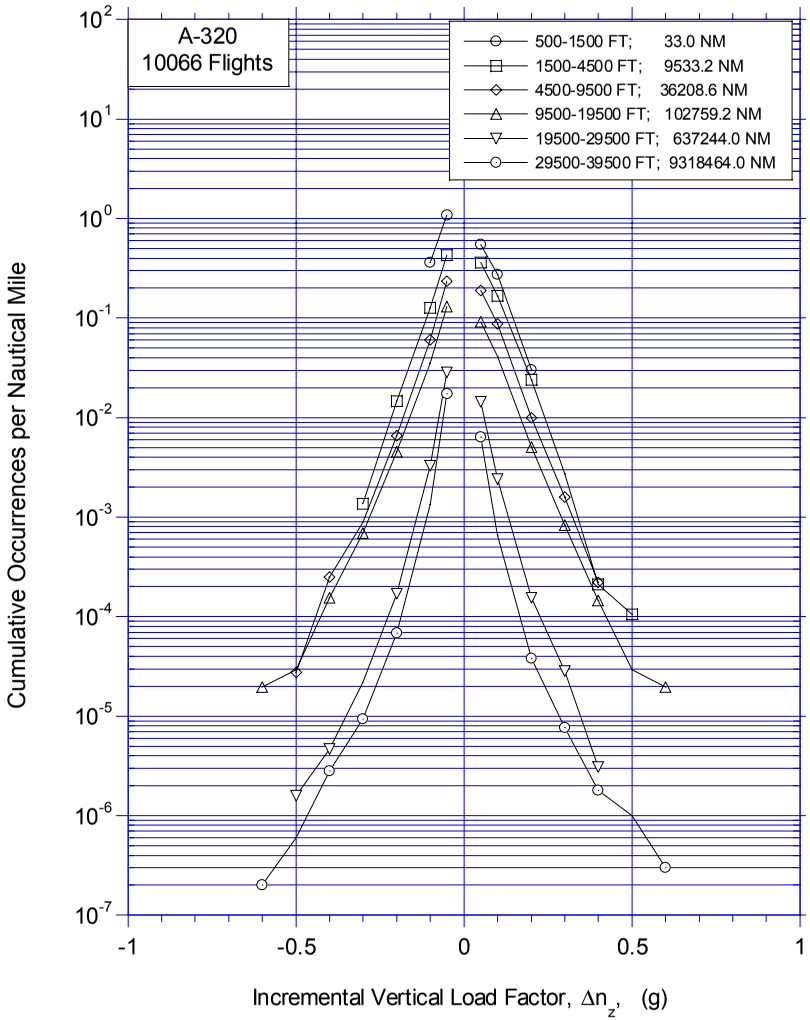


FIGURE A-76. CUMULATIVE OCCURRENCES OF INCREMENTAL VERTICAL MANEUVER LOAD FACTOR PER NAUTICAL MILE DURING CRUISE BY ALTITUDE

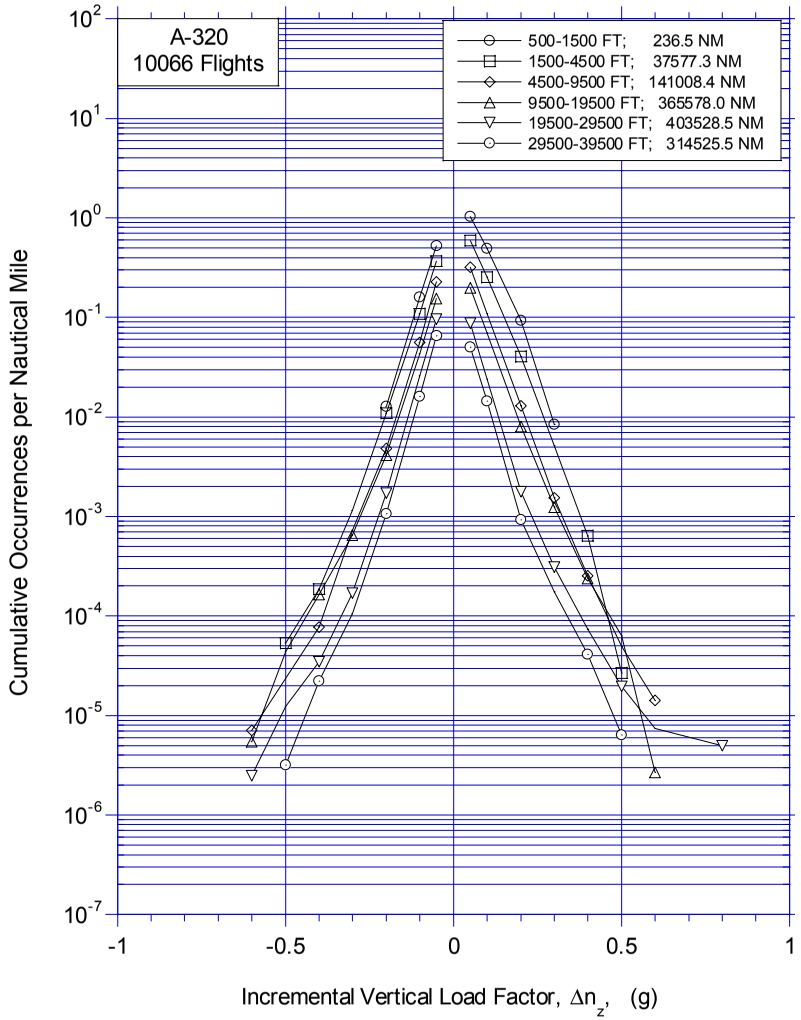


FIGURE A-77. CUMULATIVE OCCURRENCES OF INCREMENTAL VERTICAL MANEUVER LOAD FACTOR PER NAUTICAL MILE DURING DESCENT BY ALTITUDE

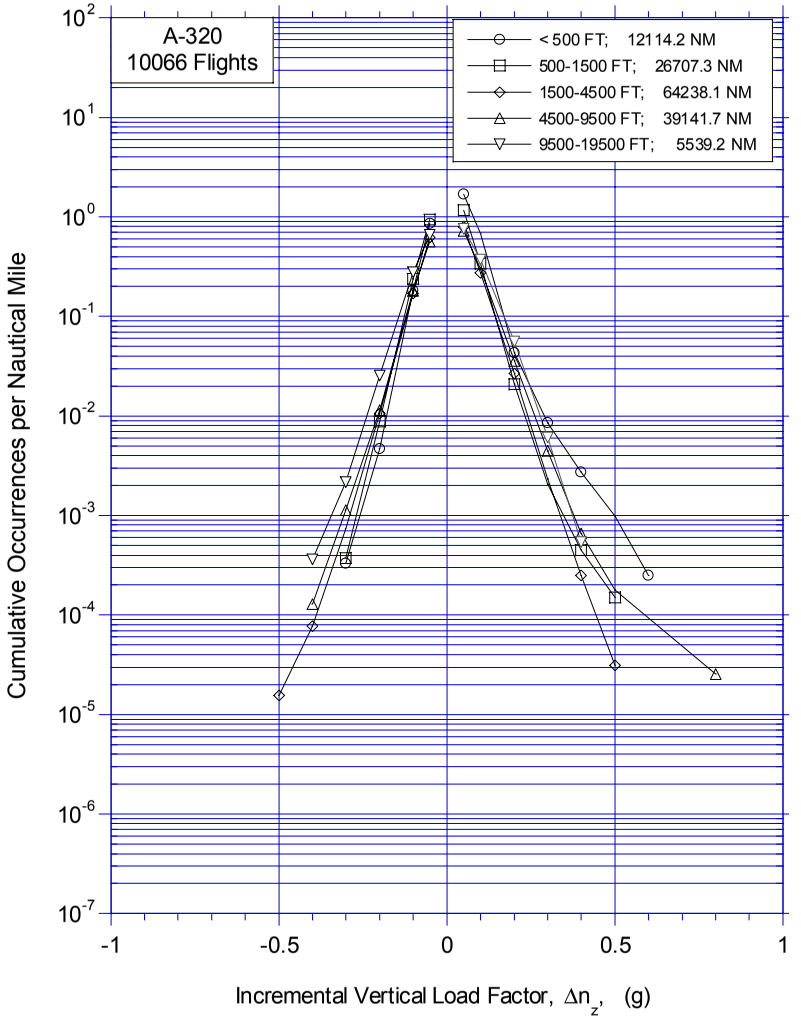


FIGURE A-76. CUMULATIVE OCCURRENCES OF INCREMENTAL VERTICAL MANEUVER LOAD FACTOR PER NAUTICAL MILE DURING APPROACH BY ALTITUDE

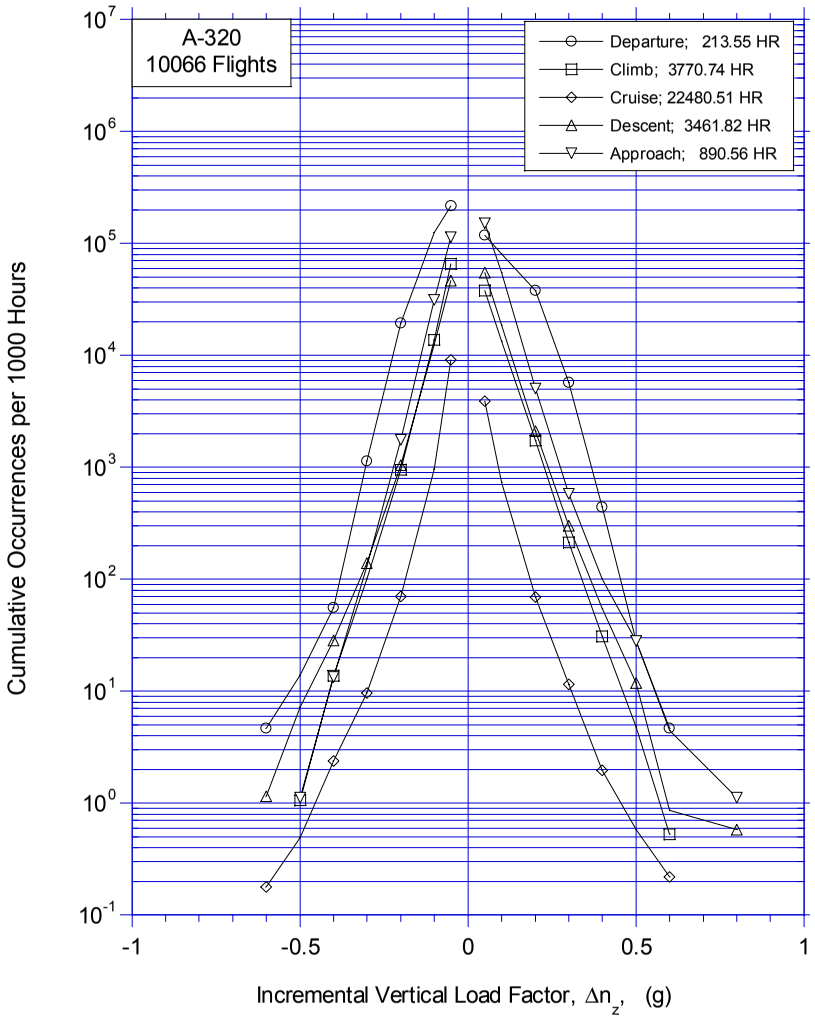


FIGURE A-79. CUMULATIVE OCCURRENCES OF INCREMENTAL VERTICAL MANEUVER LOAD FACTOR PER 1000 HOURS BY FLIGHT PHASE

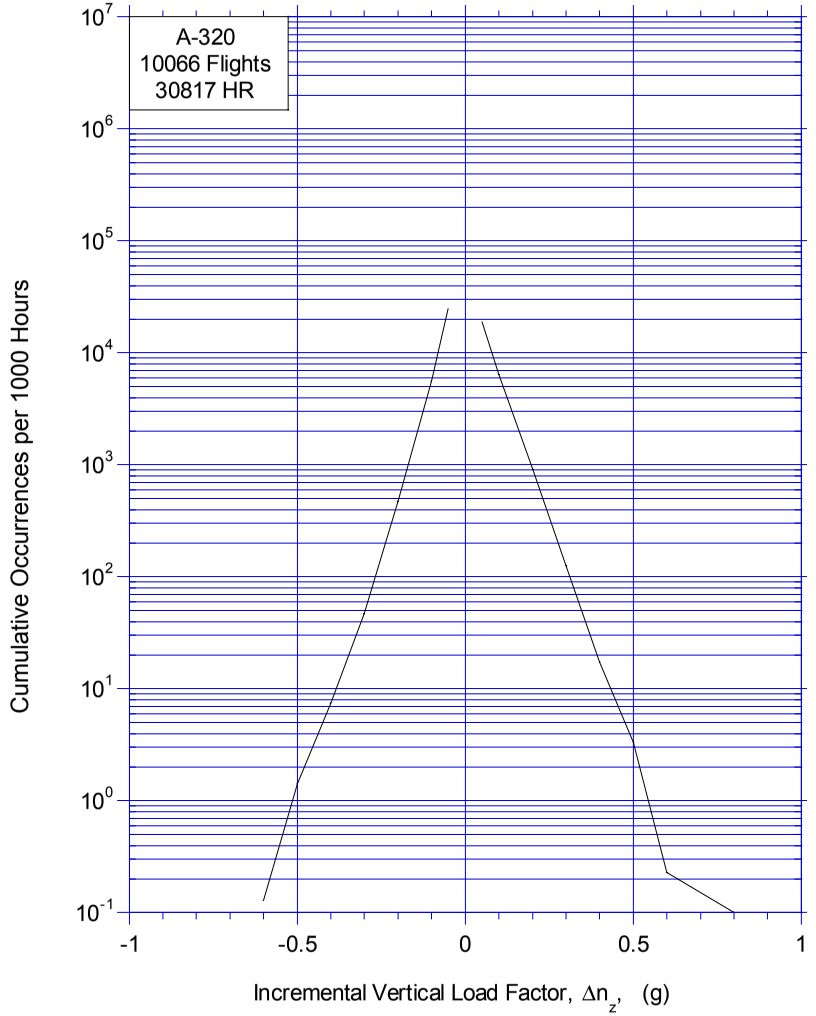


FIGURE A-80. CUMULATIVE OCCURRENCES OF INCREMENTAL VERTICAL MANEUVER LOAD FACTOR PER 1000 HOURS, COMBINED FLIGHT PHASES

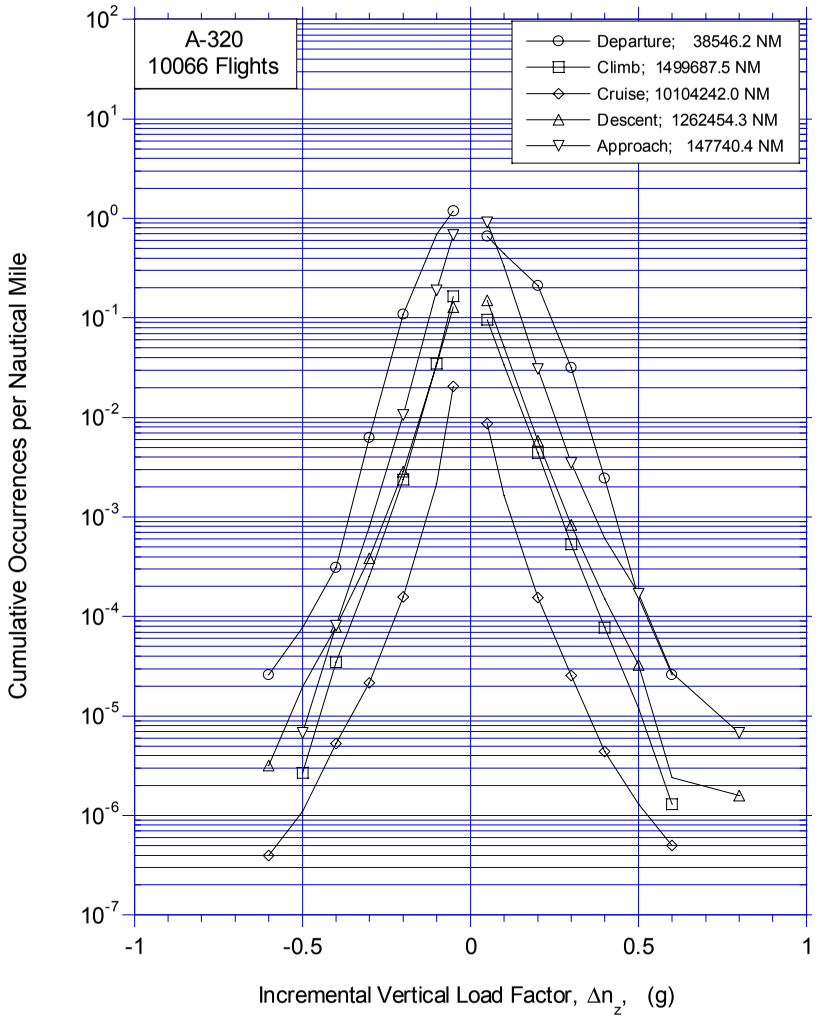


FIGURE A-81. CUMULATIVE OCCURRENCES OF INCREMENTAL VERTICAL MANEUVER LOAD FACTOR PER NAUTICAL MILE BY FLIGHT PHASE

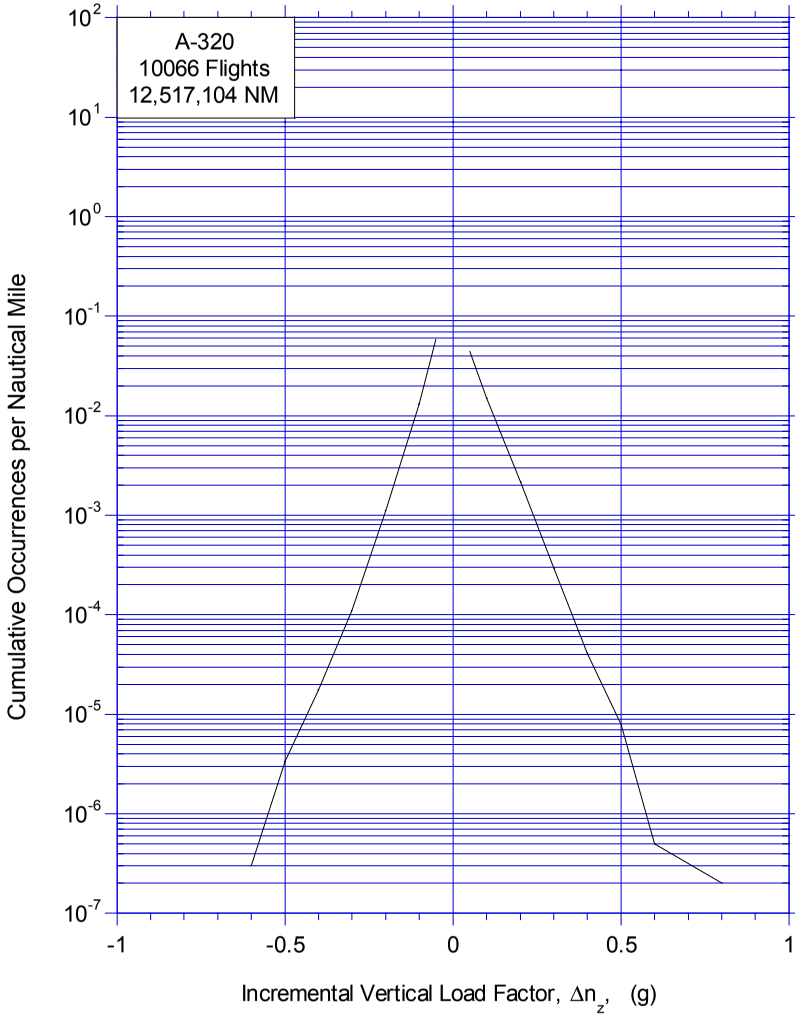


FIGURE A-82. CUMULATIVE OCCURRENCES OF INCREMENTAL VERTICAL MANEUVER LOAD FACTOR PER NAUTICAL MILE, COMBINED FLIGHT PHASES

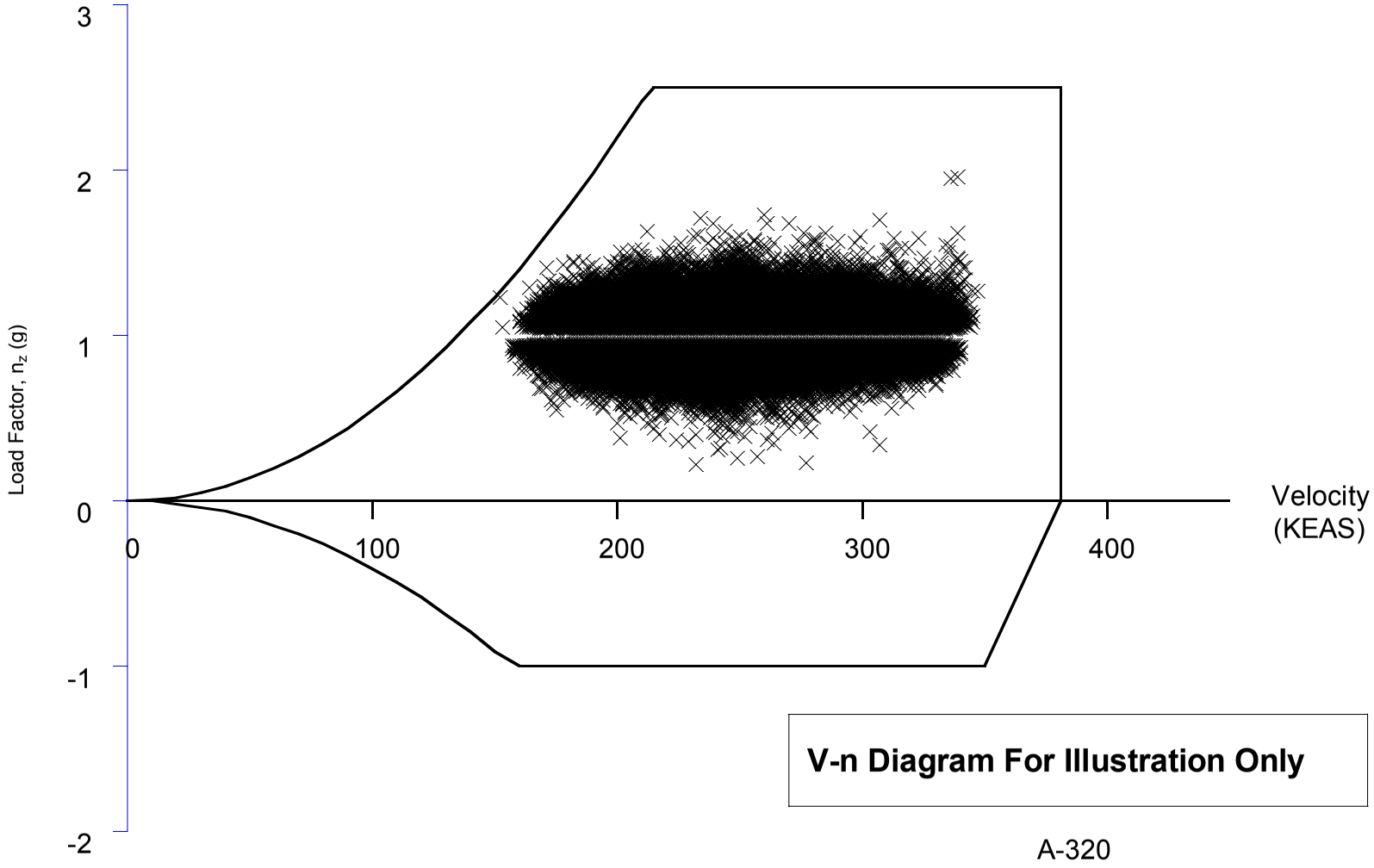


FIGURE A-83. MANEUVER LOAD FACTOR AND COINCIDENT SPEED VS V-n DIAGRAM FOR FLAPS RETRACTED

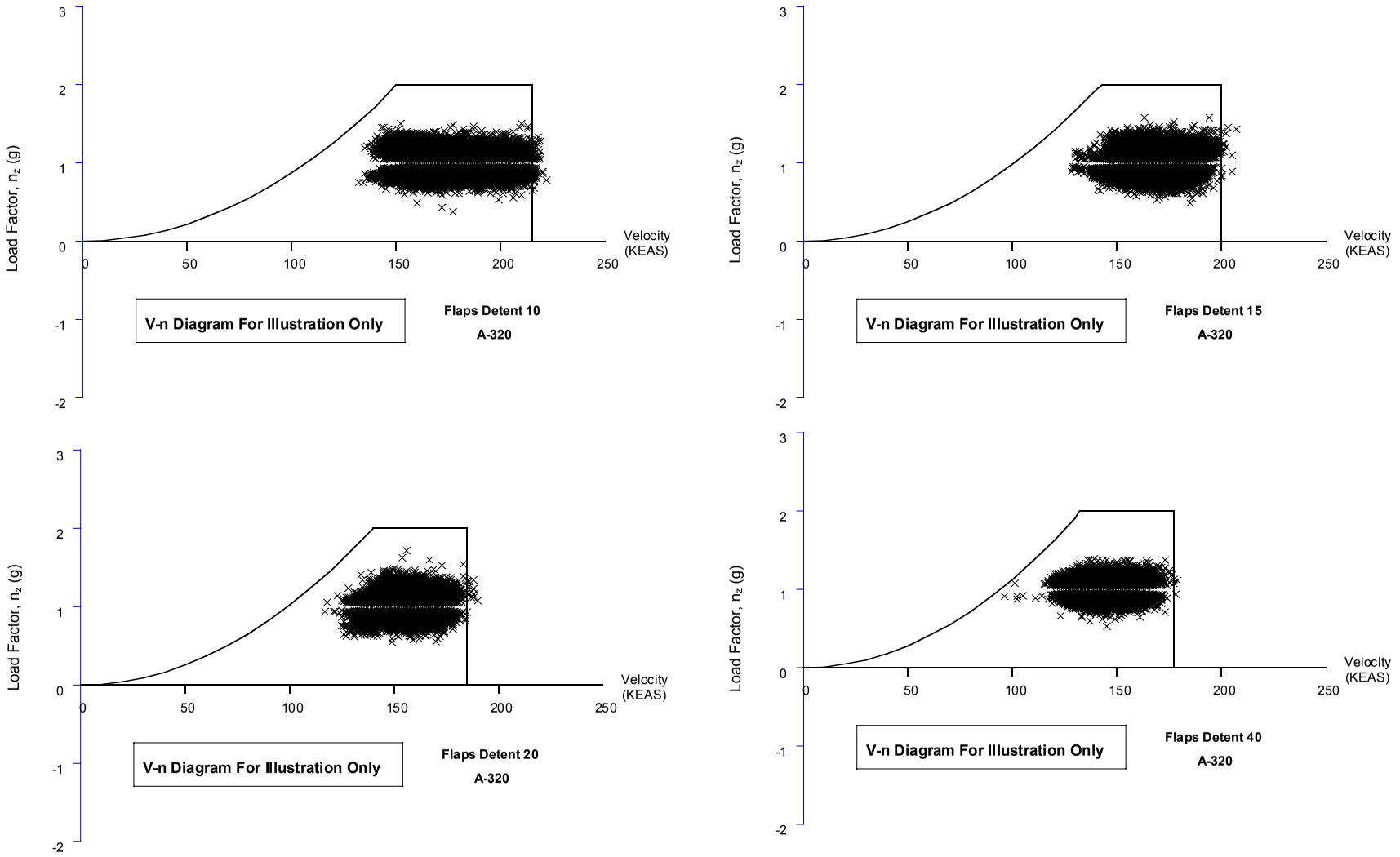


FIGURE A-84. MANEUVER LOAD FACTOR AND COINCIDENT SPEED VS V-n DIAGRAMS FOR FLAPS EXTENDED, DETENTS 10, 15, 20, AND 40

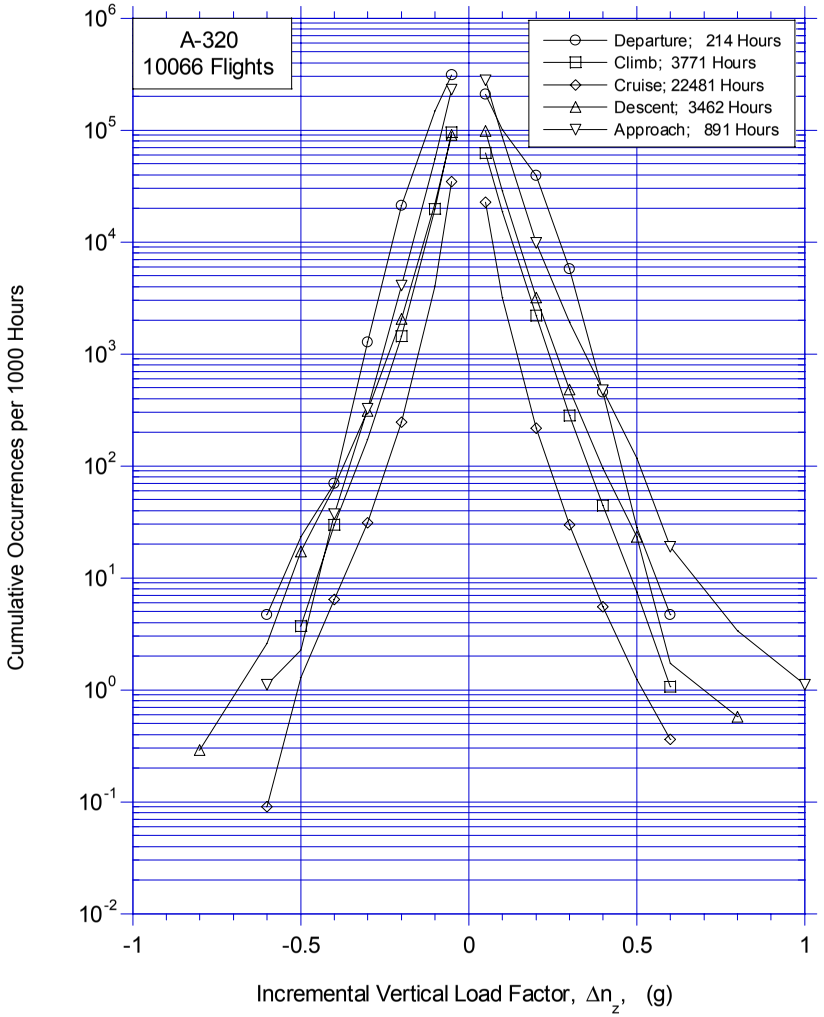


FIGURE A-85. CUMULATIVE OCCURRENCES OF INCREMENTAL VERTICAL LOAD FACTOR PER 1000 HOURS BY FLIGHT PHASE

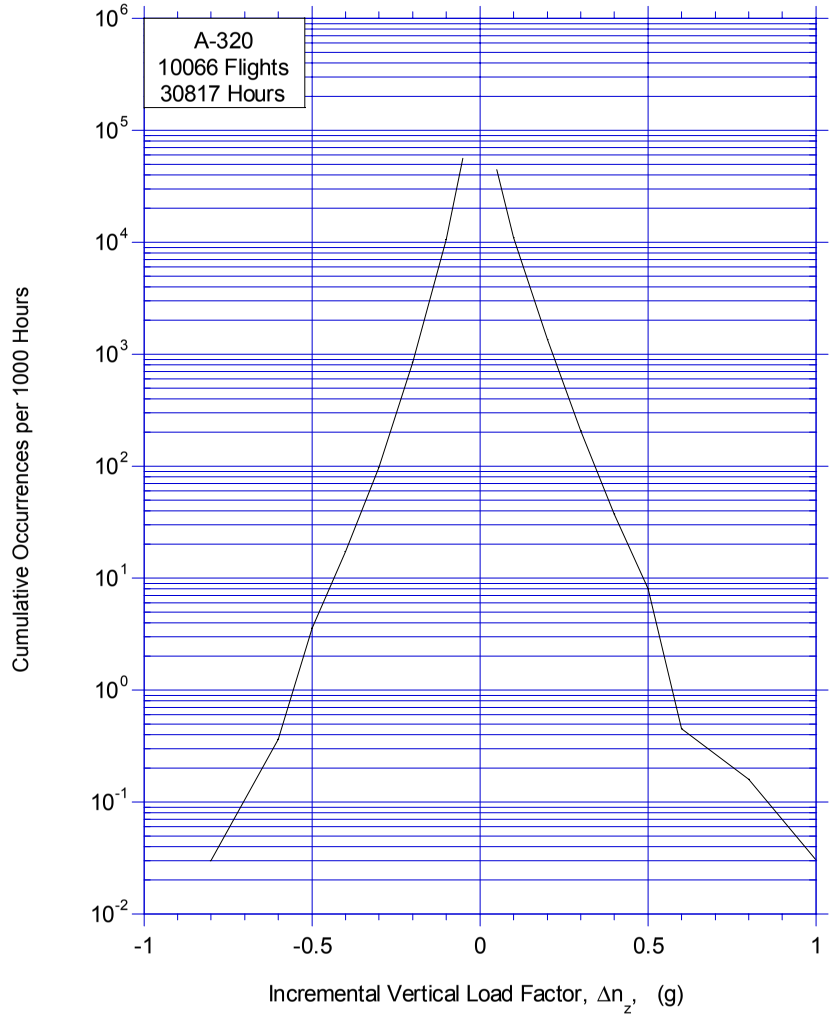


FIGURE A-86. CUMULATIVE OCCURRENCES OF INCREMENTAL VERTICAL LOAD FACTOR PER 1000 HOURS, COMBINED FLIGHT PHASES

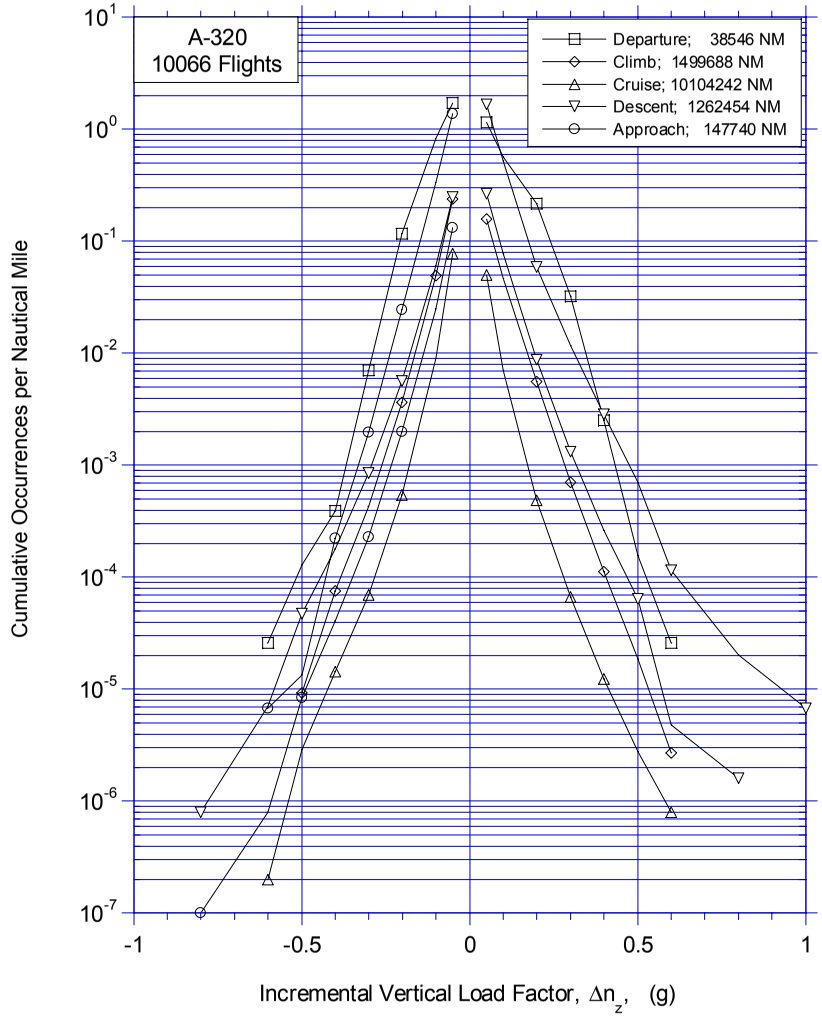


FIGURE A-87. CUMULATIVE OCCURRENCES OF INCREMENTAL VERTICAL LOAD FACTOR PER NAUTICAL MILE BY FLIGHT PHASE

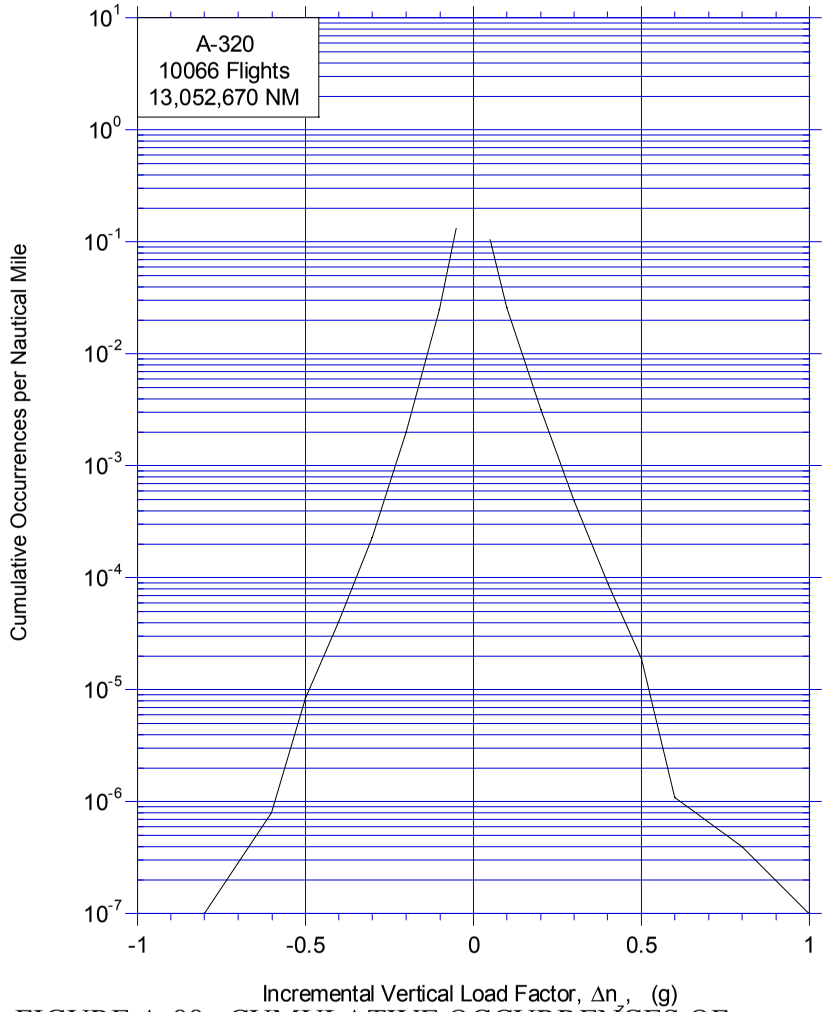


FIGURE A-88. CUMULATIVE OCCURRENCES OF INCREMENTAL VERTICAL LOAD FACTOR PER NAUTICAL MILE, COMBINED FLIGHT PHASES

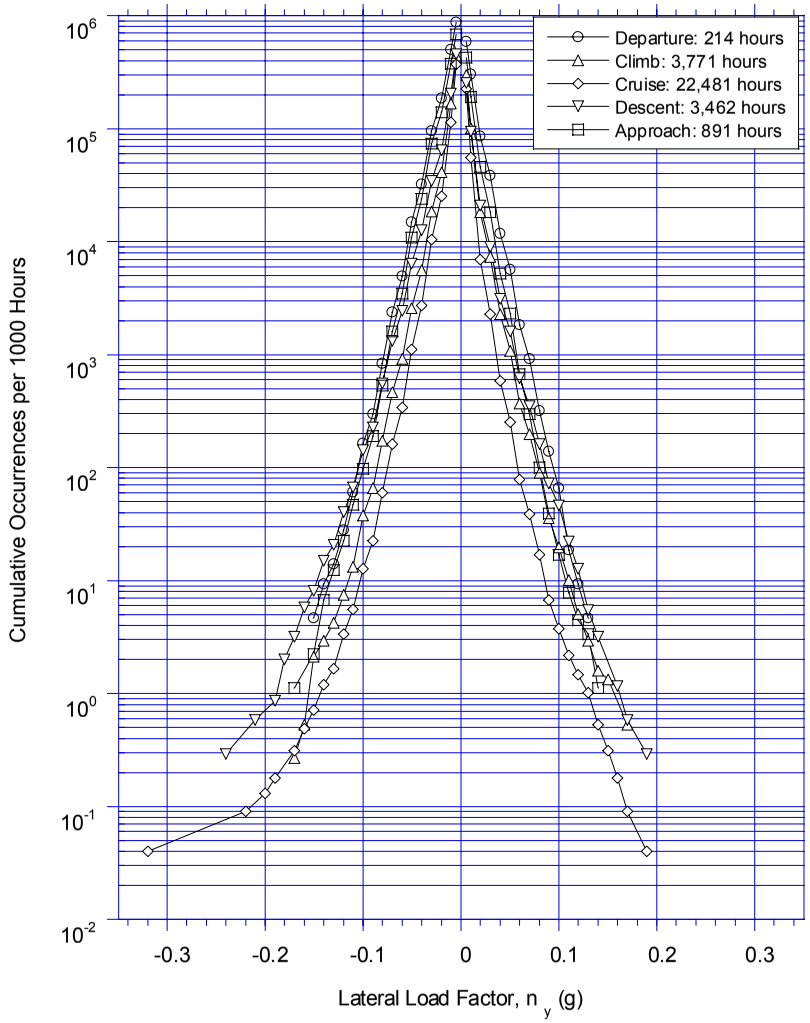


FIGURE A-89. CUMULATIVE OCCURRENCES OF LATERAL LOAD FACTOR PER 1000 HOURS BY FLIGHT PHASE

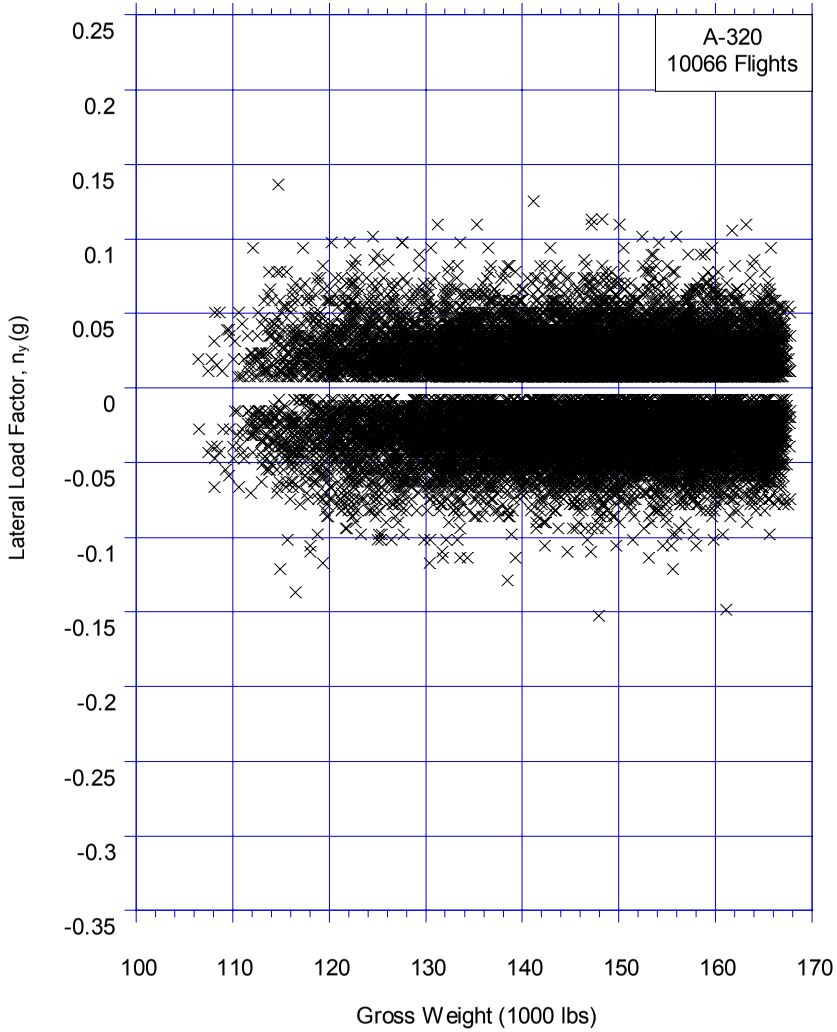


FIGURE A-90. MAXIMUM LATERAL LOAD FACTOR VS COINCIDENT GROSS WEIGHT DURING DEPARTURE

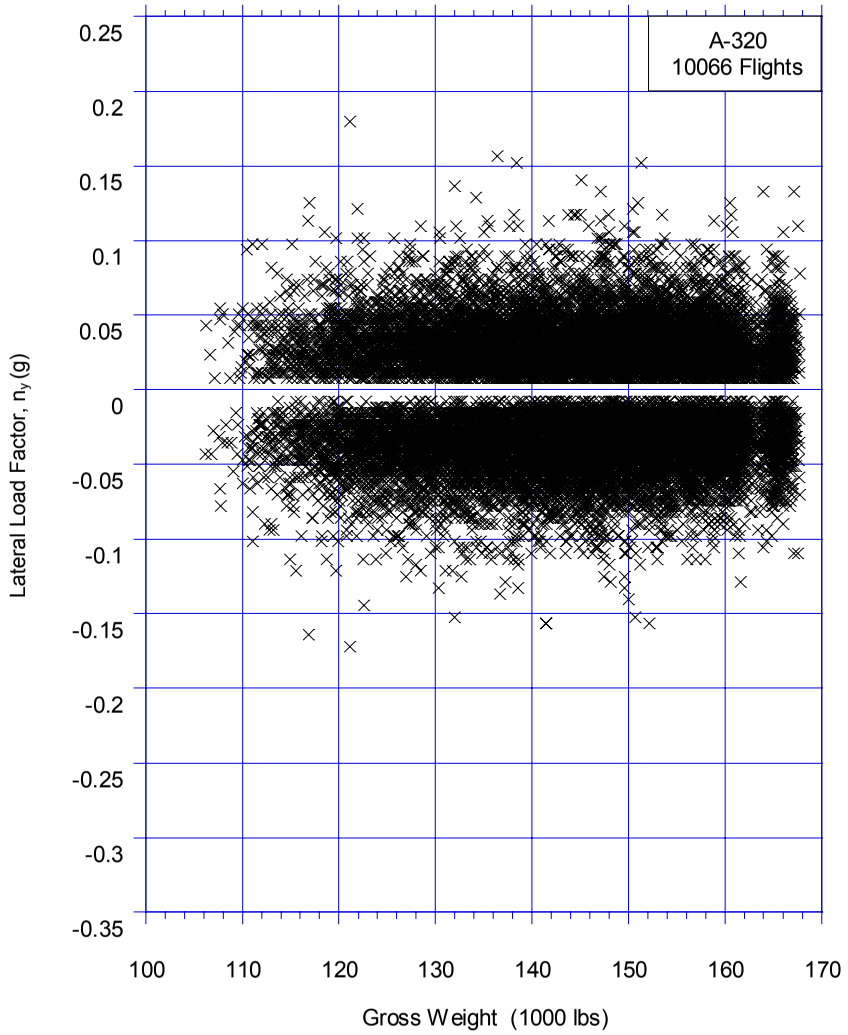


FIGURE A-91. MAXIMUM LATERAL LOAD FACTOR VS COINCIDENT GROSS WEIGHT DURING CLIMB

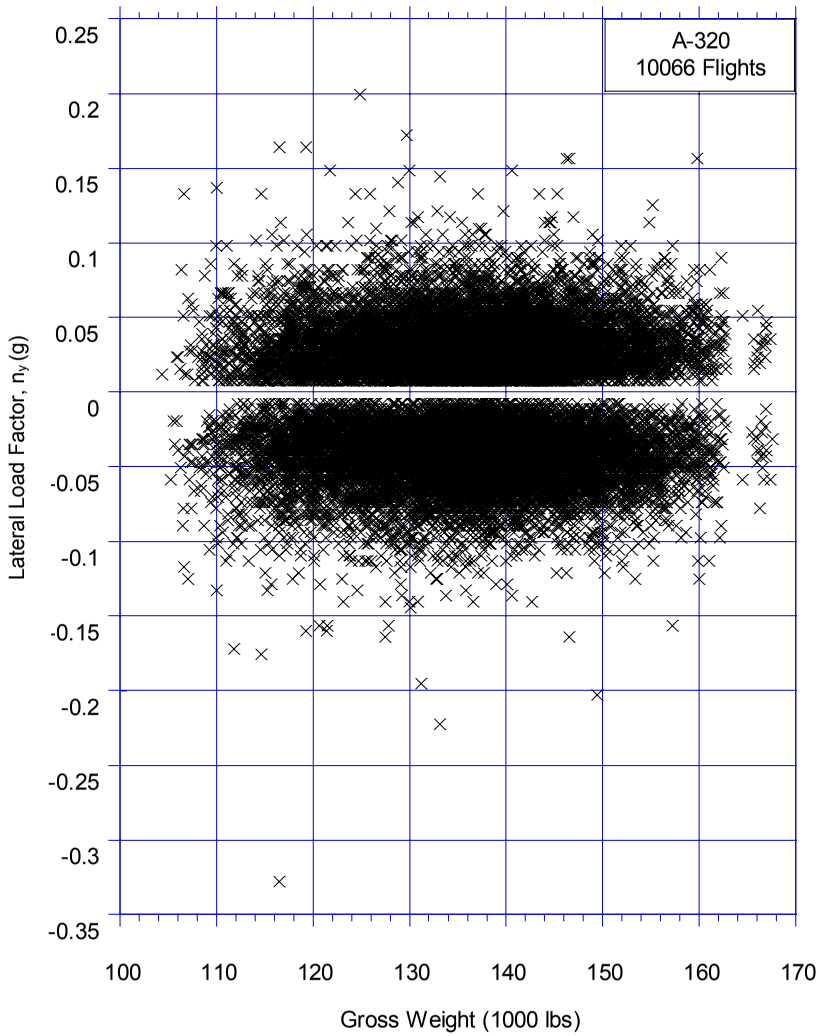


FIGURE A-92. MAXIMUM LATERAL LOAD FACTOR VS COINCIDENT GROSS WEIGHT DURING CRUISE

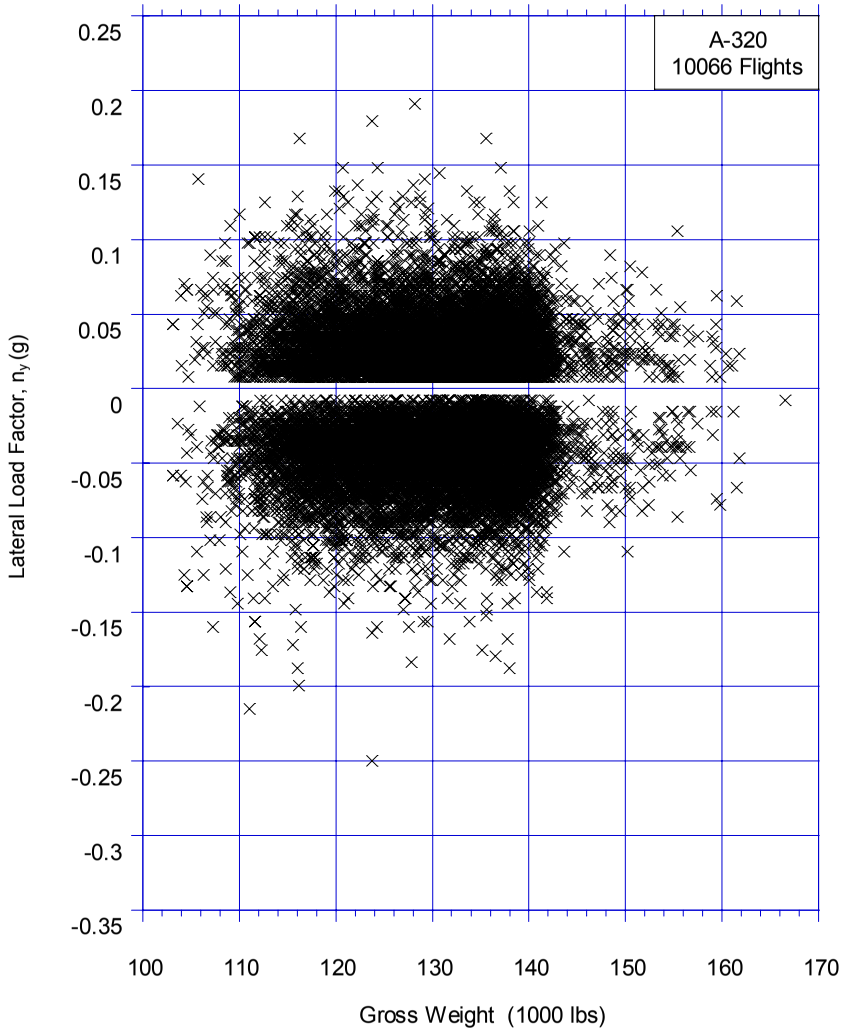


FIGURE A-93. MAXIMUM LATERAL LOAD FACTOR VS COINCIDENT GROSS WEIGHT DURING DESCENT

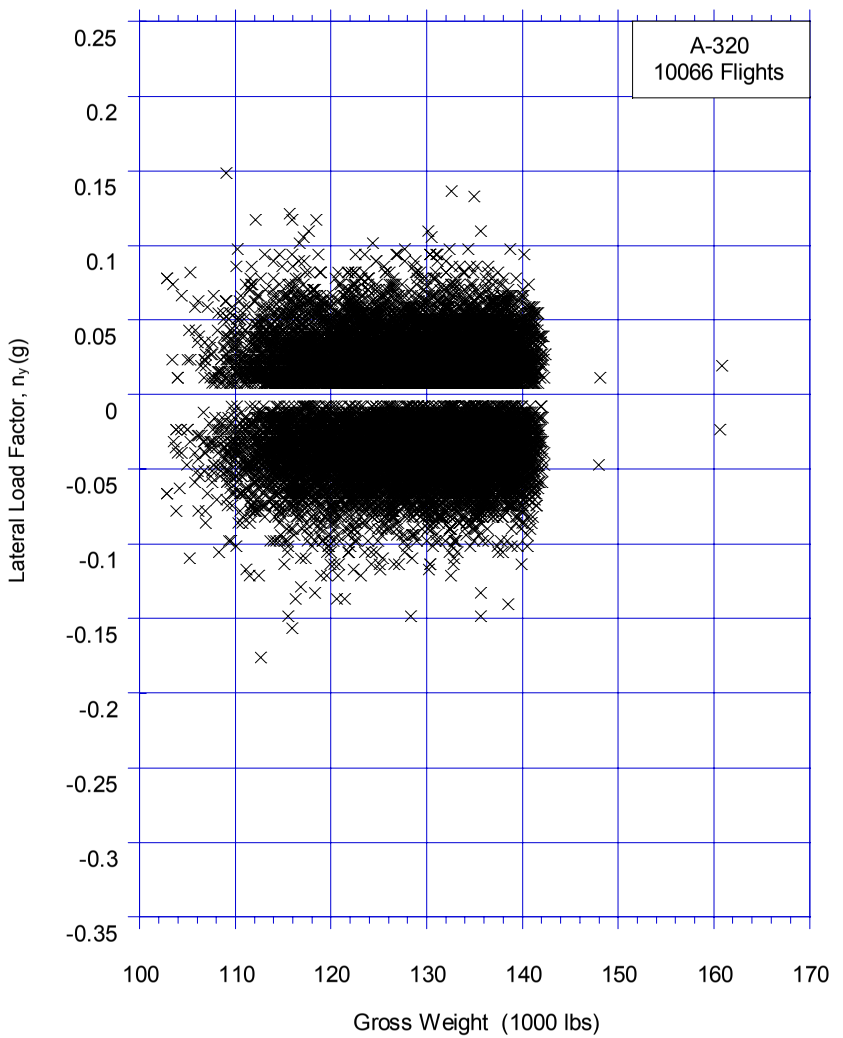


FIGURE A-94. MAXIMUM LATERAL LOAD FACTOR VS COINCIDENT GROSS WEIGHT DURING APPROACH

Maximum Incremental Vertical Load Factor, Δn_z (g)

Minimum Incremental Vertical Load Factor, Δn_z (g)

10066 Flights	0.1	0.15	0.2	0.25	0.3	0.35	0.4	0.45	0.5	0.55	0.6	0.65	0.7	0.75	0.8	0.85	0.9	0.95	1
-0.1		11	27	14	3		1												
-0.15	1	61	417	495	242	67	10	4	1										
-0.2		51	504	1167	1104	509	122	31	6	4	4			1					
-0.25	3	12	141	569	812	721	353	110	26	9	6			1				1	
-0.3		1	44	155	273	346	298	151	79	24	8	1	1						
-0.35			14	50	87	121	109	82	50	34	9	4							
-0.4			7	17	51	55	44	34	22	22	11	5	2		1		1		
-0.45				13	14	27	22	15	6	8	6	1	5	1			1		
-0.5			3	1	6	10	6	5	1	6	2	1	2						1
-0.55			2	3	6	6	3	5	4	2	1								
-0.6			2			3	2	1	4	2	1								
-0.65				2	2	1	2	2	2										
-0.7							1	2			1		1						
-0.75						1	2		1										
-0.8							1												
-0.85																			
-0.9																			
-0.95												1							

FIGURE A-95. GROUND-AIR-GROUND CYCLE OCCURRENCES OF MAXIMUM AND MINIMUM INCREMENTAL VERTICAL LOAD FACTOR

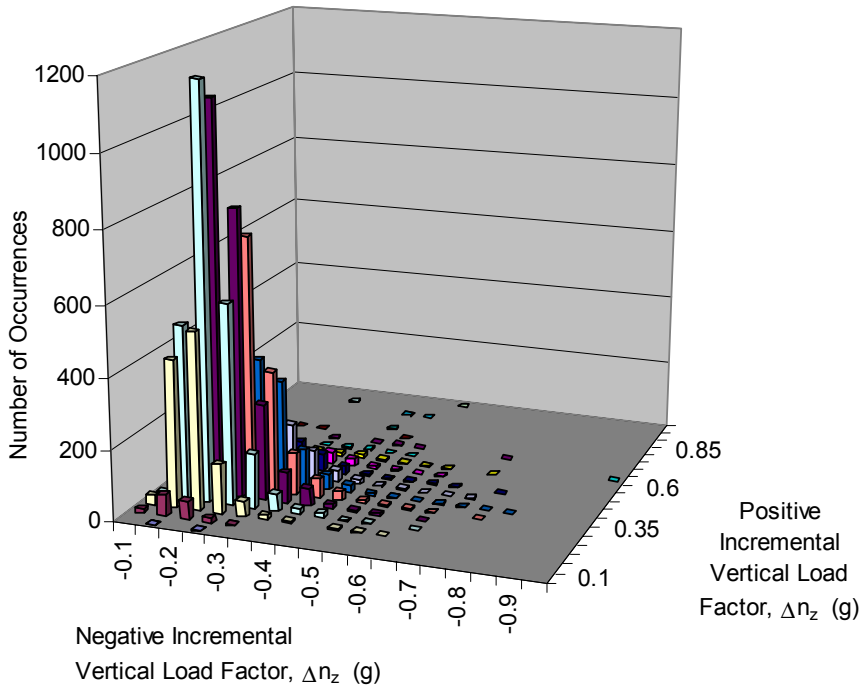


FIGURE A-96. 3-D PLOT OF GROUND-AIR-GROUND CYCLES

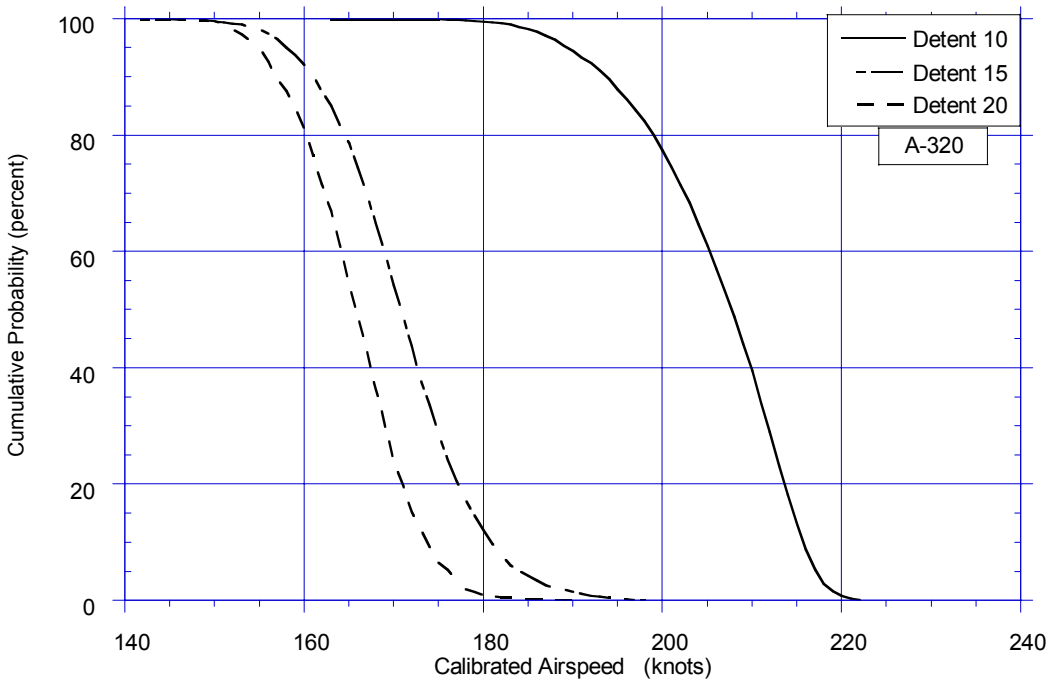


FIGURE A-97. CUMULATIVE PROBABILITY OF MAXIMUM AIRSPEED IN FLAP DETENT DURING DEPARTURE

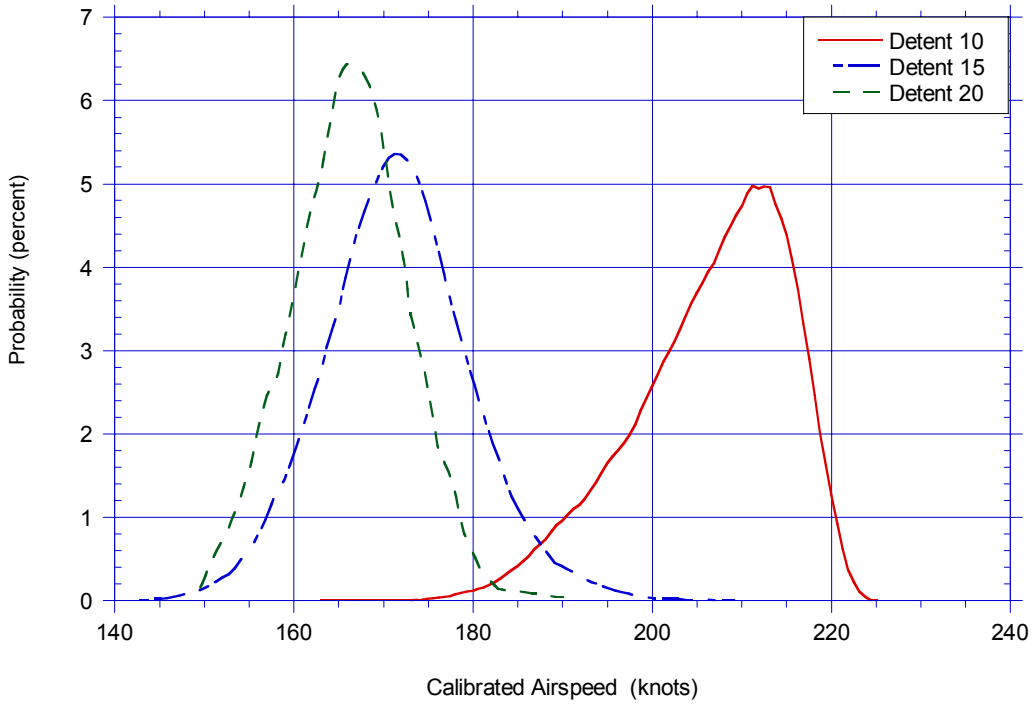


FIGURE A-98. RELATIVE PROBABILITY OF MAXIMUM AIRSPEED IN FLAP DETENT DURING DEPARTURE

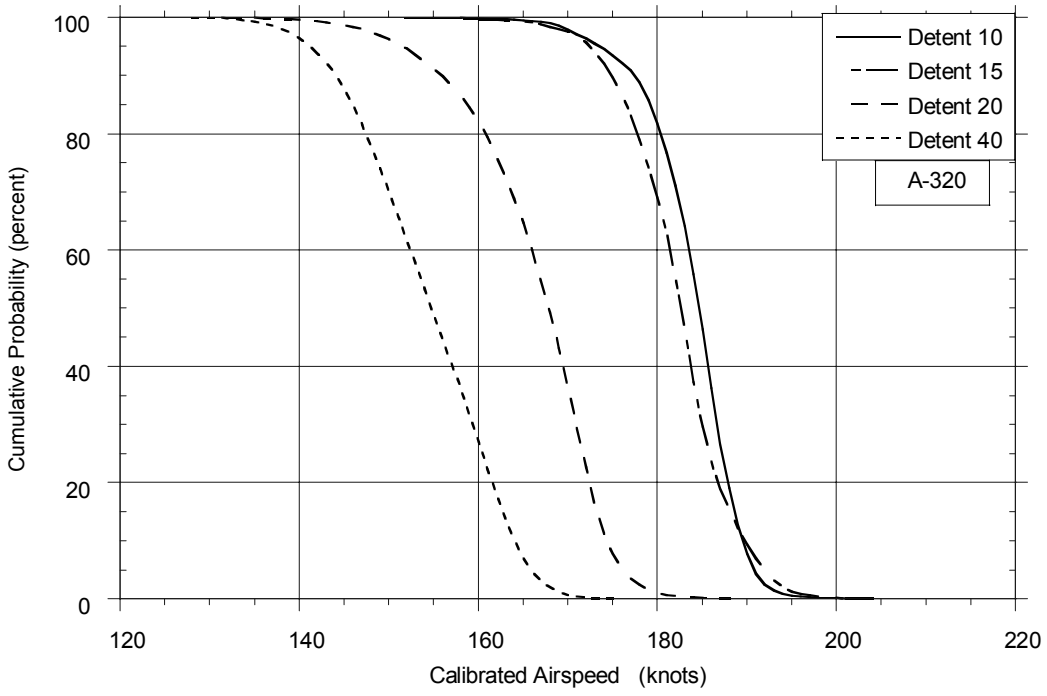


FIGURE A-99. CUMULATIVE PROBABILITY OF MAXIMUM AIRSPEED IN FLAP DETENT DURING APPROACH

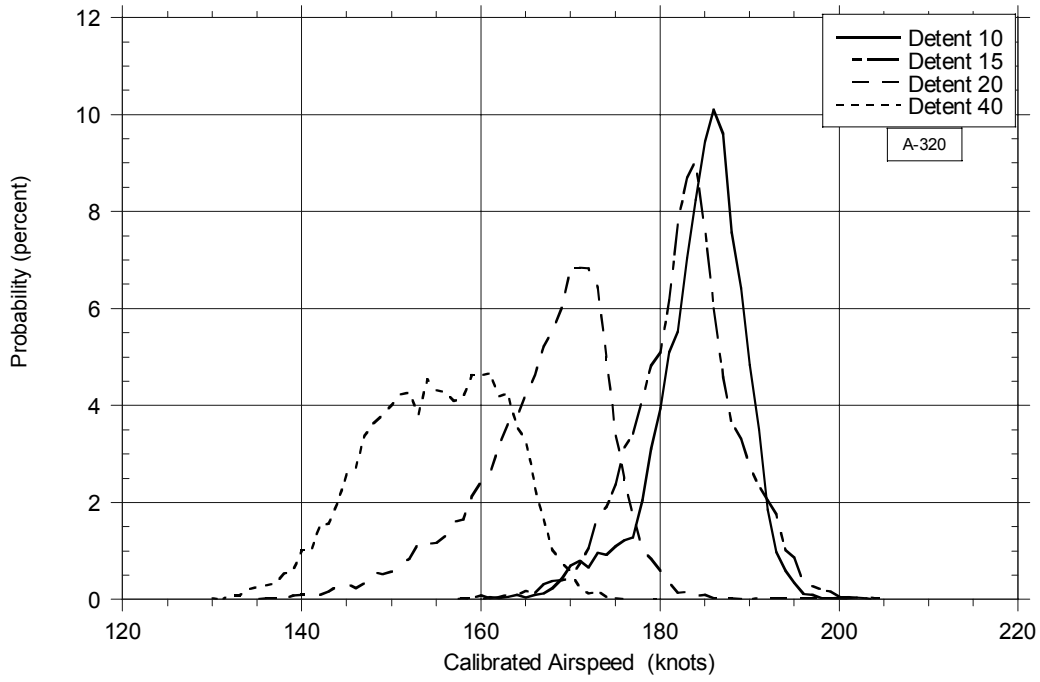


FIGURE A-100. RELATIVE PROBABILITY OF MAXIMUM AIRSPEED IN FLAP DETENT DURING APPROACH

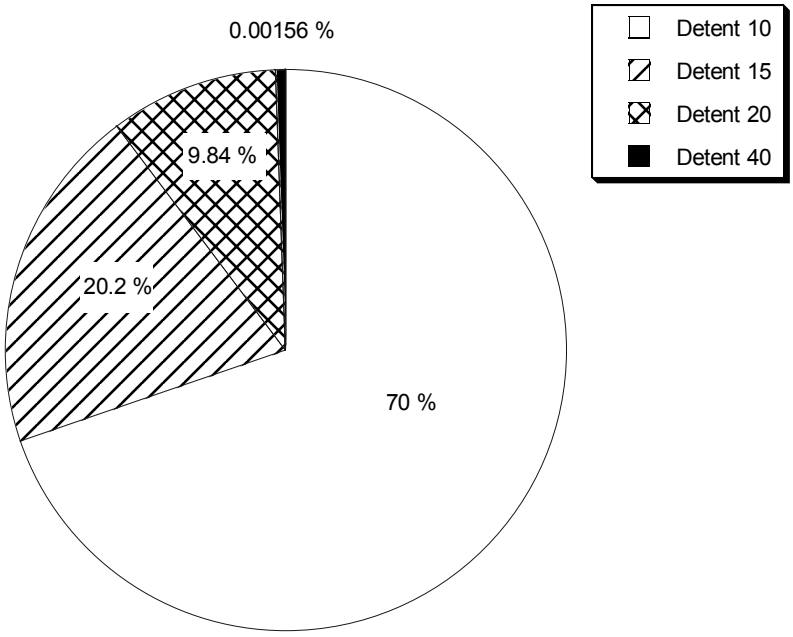


FIGURE A-101. PERCENT OF TIME IN FLAP DETENT DURING DEPARTURE

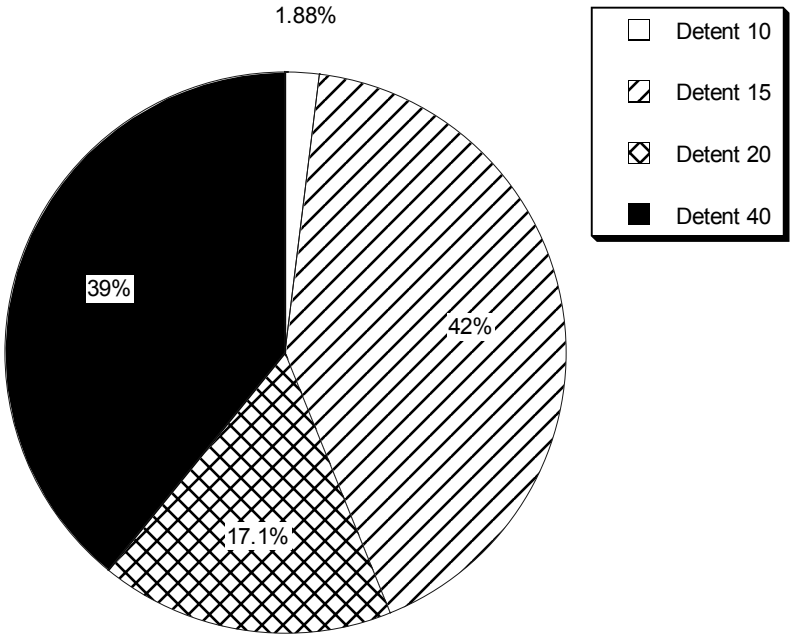


FIGURE A-102. PERCENT OF TIME IN FLAP DETENT DURING APPROACH

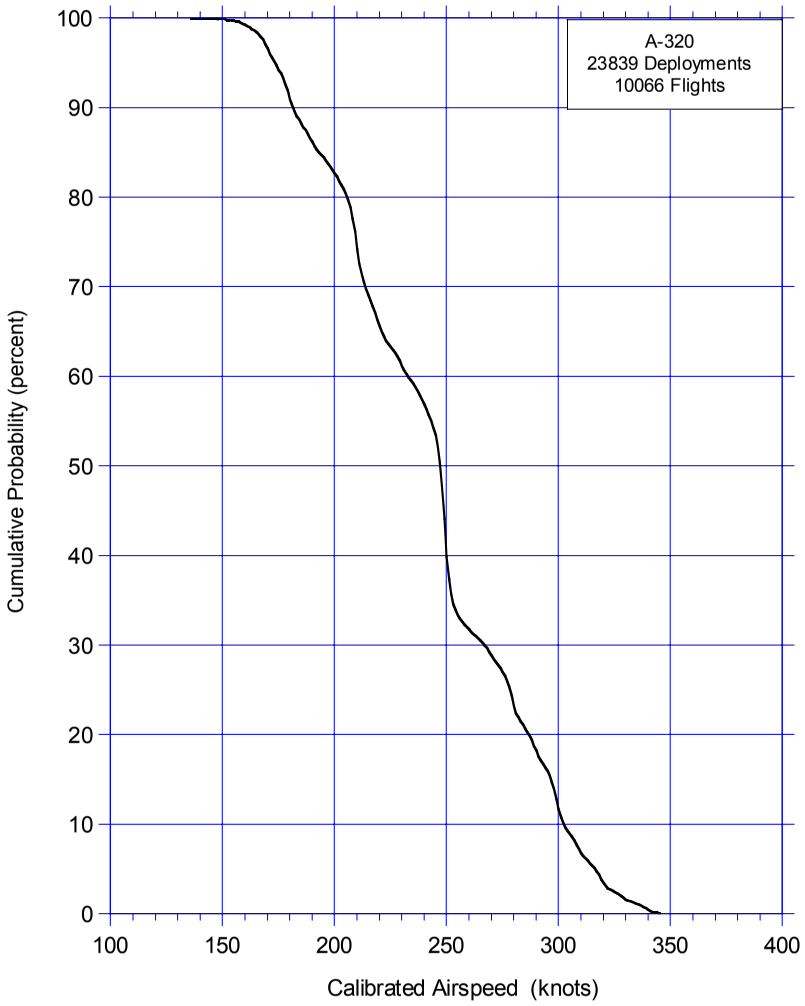


FIGURE A-103. PROBABILITY DISTRIBUTIONS OF SPEED AT SPEED BRAKE DEPLOYMENT

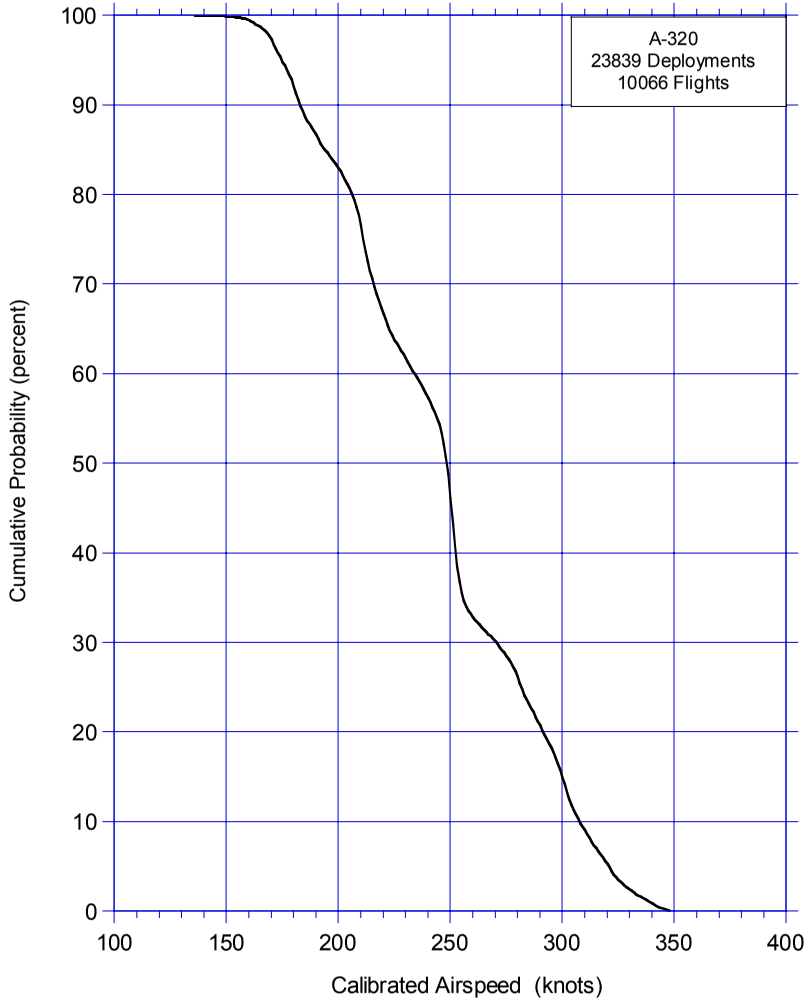


FIGURE A-104. PROBABILITY DISTRIBUTIONS OF MAXIMUM SPEED DURING SPEED BRAKE DEPLOYMENT

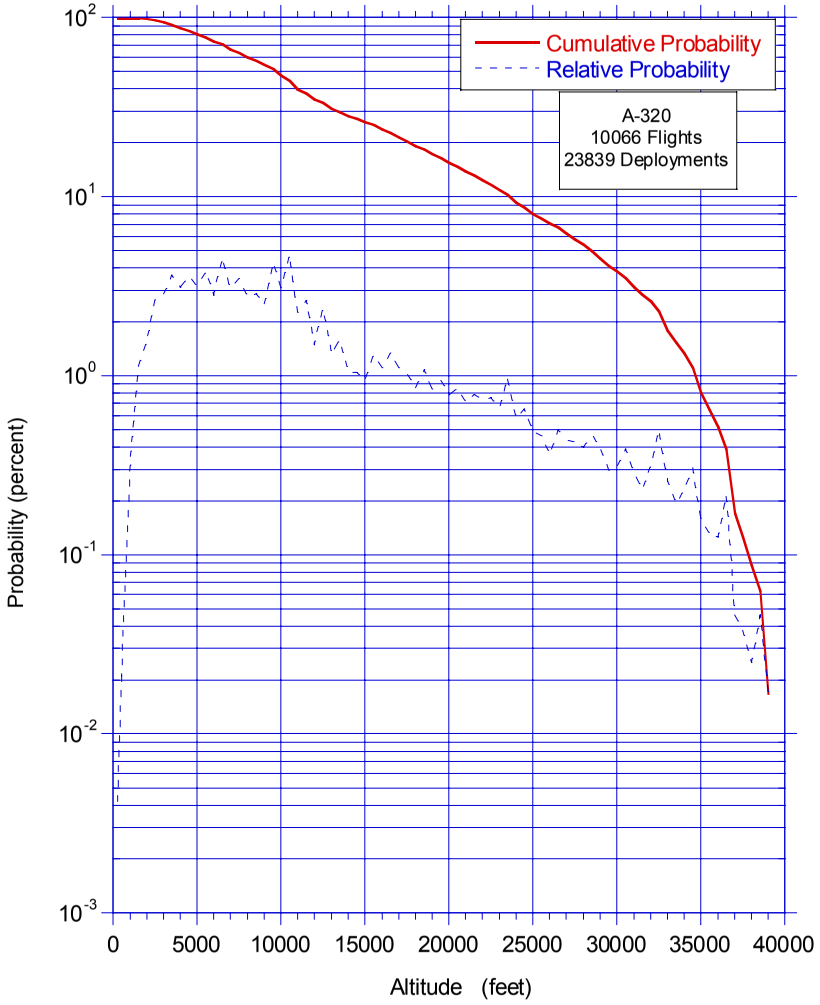


FIGURE A-105. PROBABILITY DISTRIBUTIONS OF ALTITUDE AT SPEED BRAKE DEPLOYMENT

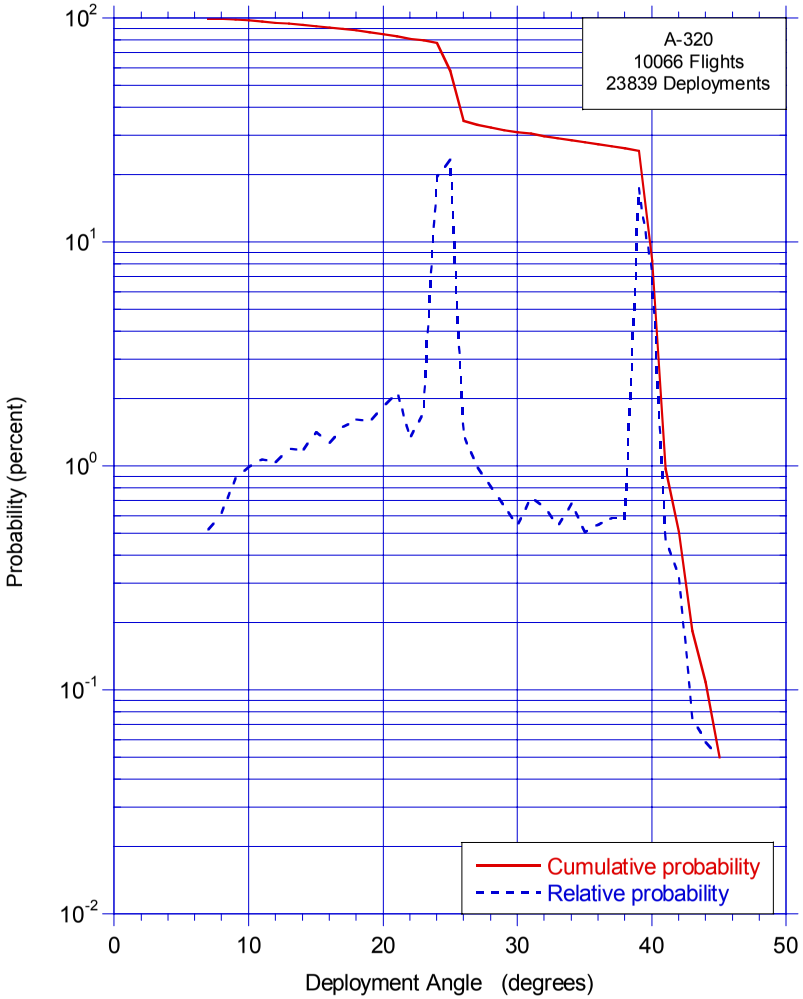


FIGURE A-106. PROBABILITY DISTRIBUTIONS OF MAXIMUM DEPLOYMENT ANGLE DURING SPEED BRAKE DEPLOYMENT

Flap Deflection

Speed Brake Deflection (degrees) 10066 Flights	Detent 0	Detent 10	Detent 15	Detent 20	Detent 40
0	23419.5	146.2	305.1	121.3	98.5
0-1	5820.4	14.1	56.8	32.9	204.6
1-2	8.2	0.5	1.9	2.1	32.4
2-3	4.6	0.3	1.4	1.0	9.4
3-4	3.7	0.2	0.8	0.5	1.9
4-5	4.0	0.1	0.6	0.3	0.4
5-10	30.3	0.3	3.2	1.2	0.2
10-15	46.9	0.3	3.9	1.2	0.1
15-20	47.0	0.3	4.6	1.3	0.1
20-25	148.2	1.1	14.2	3.7	0.1
25-30	97.8	1.0	10.4	2.8	0.0
30-35	13.4	0.3	2.5	1.0	0.0
35-40	57.9	1.2	9.5	3.4	0.0
40-45	10.9	0.2	2.0	0.6	0.0

FIGURE A-107. TOTAL HOURS OF COINCIDENT SPEED BRAKE DEFLECTION AND FLAP DETENT

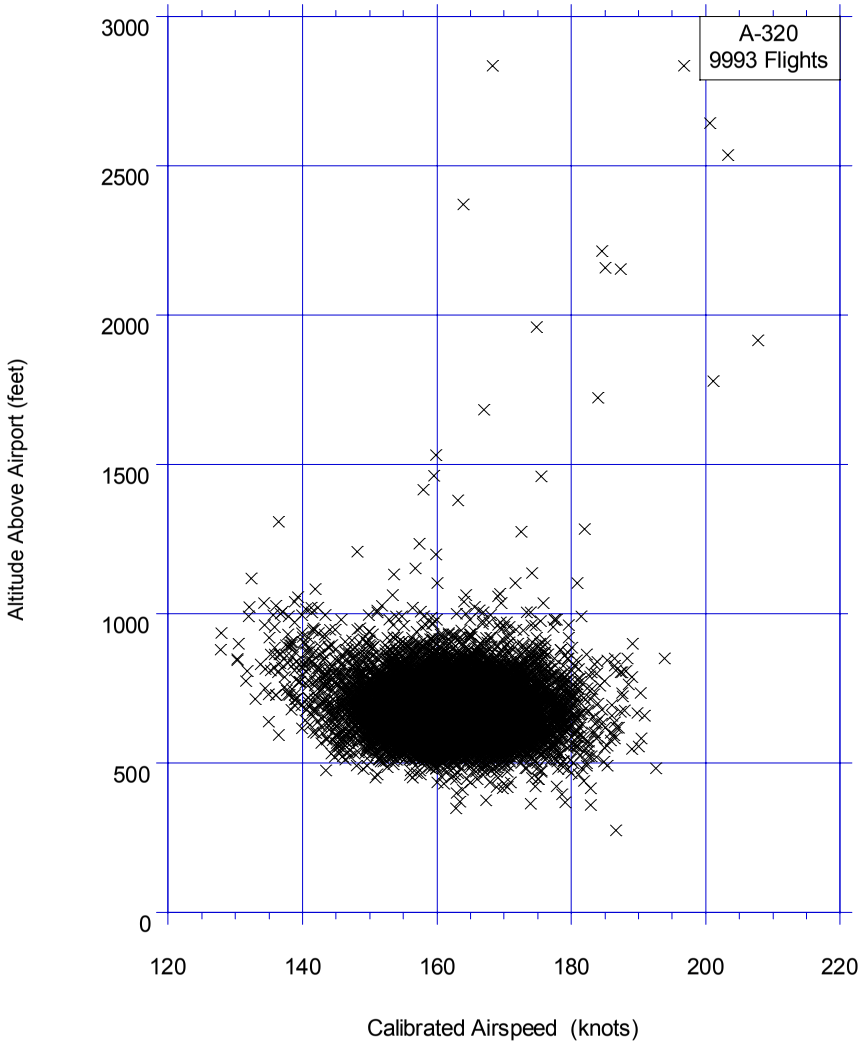


FIGURE A-108. COINCIDENT SPEED AND ALTITUDE ABOVE AIRPORT AT LANDING GEAR RETRACTION

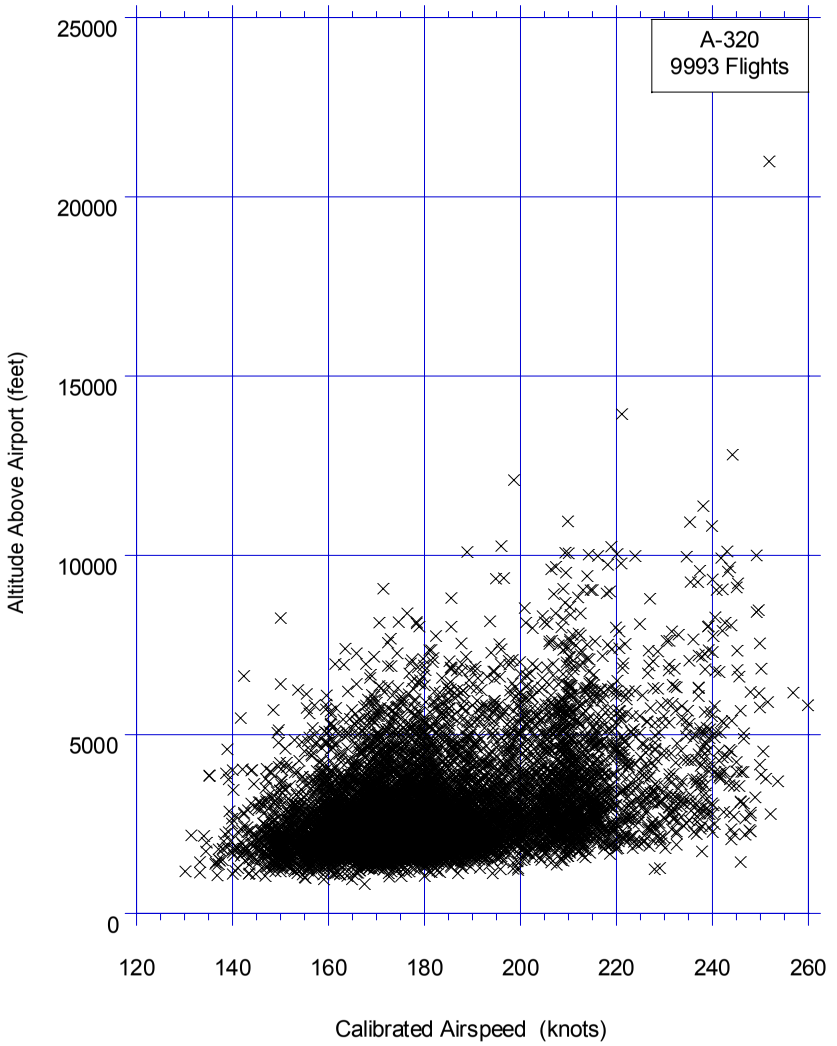


FIGURE A-109. COINCIDENT SPEED AND ALTITUDE ABOVE AIRPORT AT LANDING GEAR EXTENSION

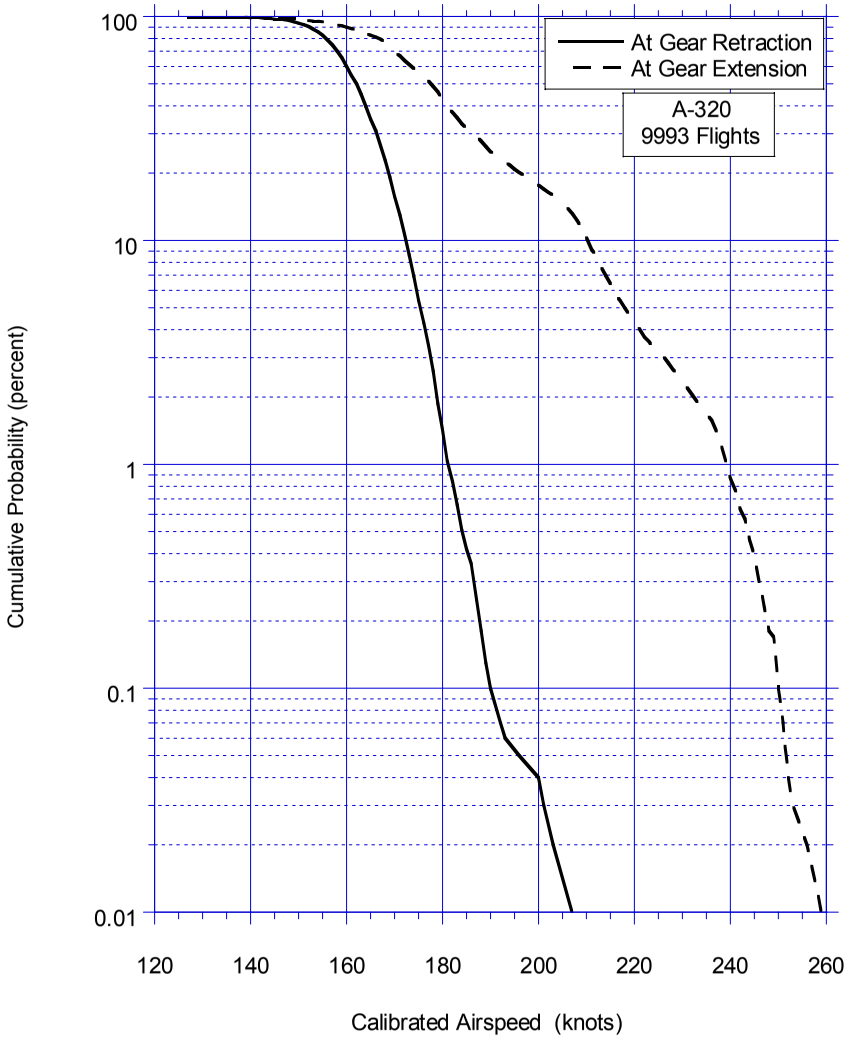


FIGURE A-110. CUMULATIVE PROBABILITY OF SPEED AT LANDING GEAR RETRACTION AND EXTENSION

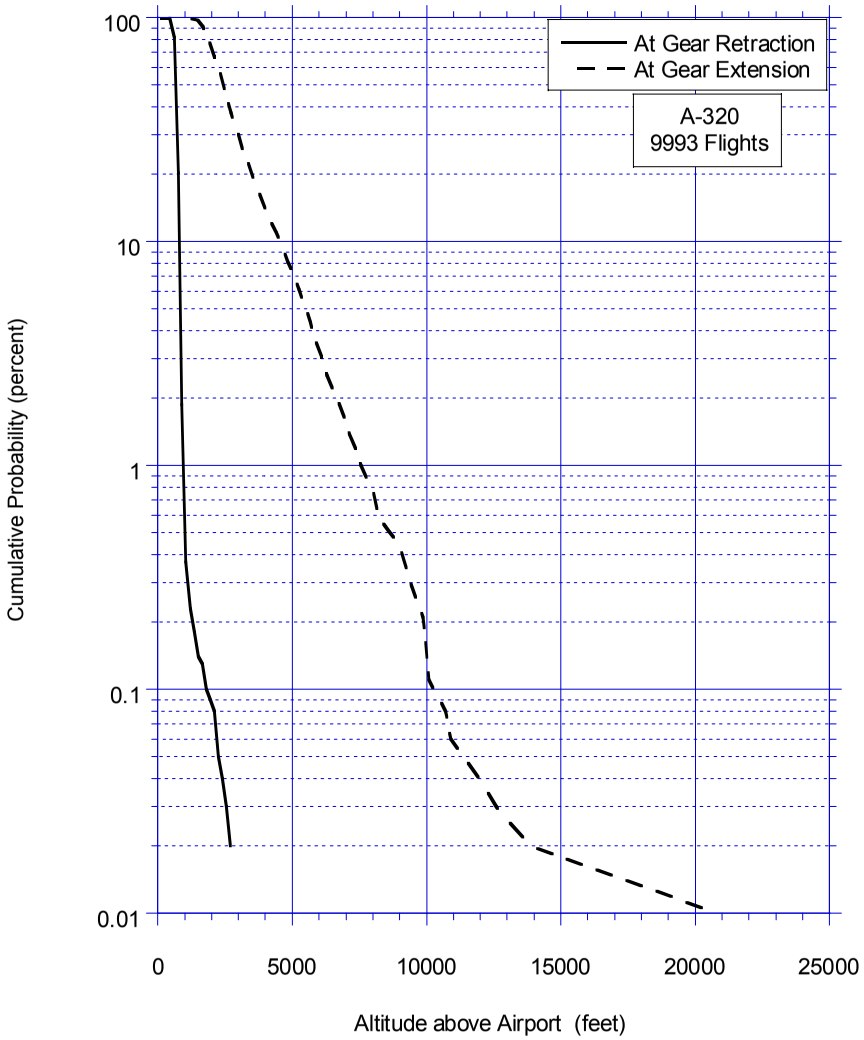


FIGURE A-111. CUMULATIVE PROBABILITY OF ALTITUDE ABOVE AIRPORT AT LANDING GEAR RETRACTION AND EXTENSION

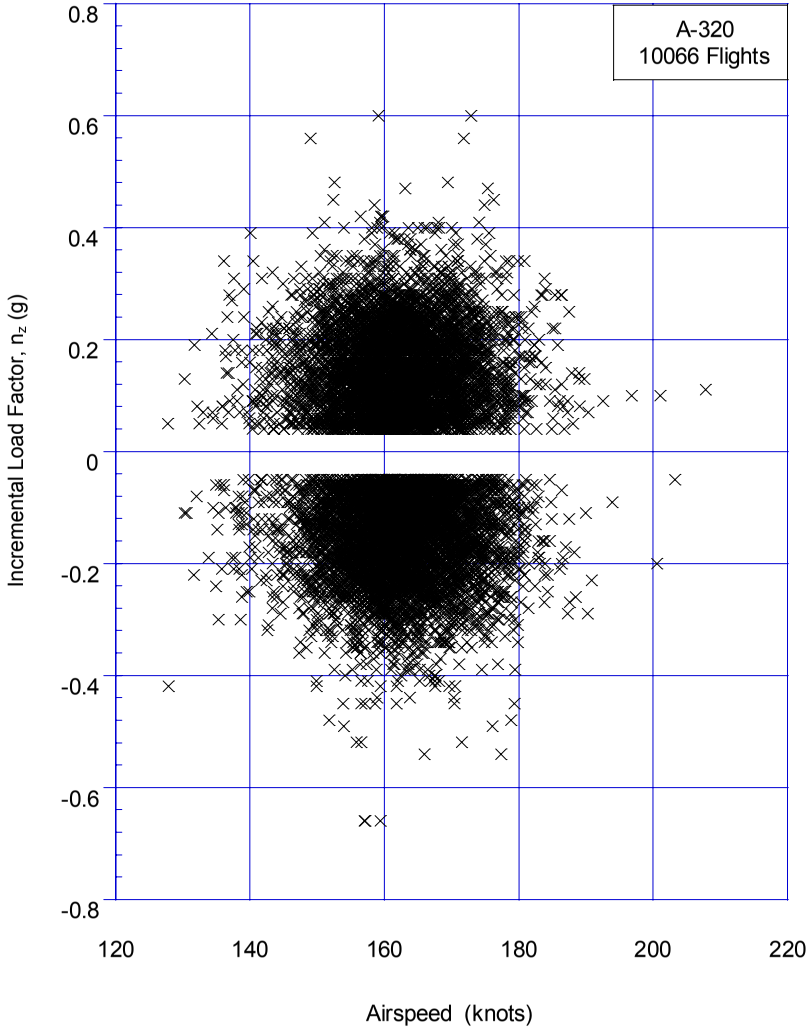


FIGURE A-112. MAXIMUM AND MINIMUM INCREMENTAL VERTICAL LOAD FACTOR VS COINCIDENT AIRSPEED AT LANDING GEAR RETRACTION

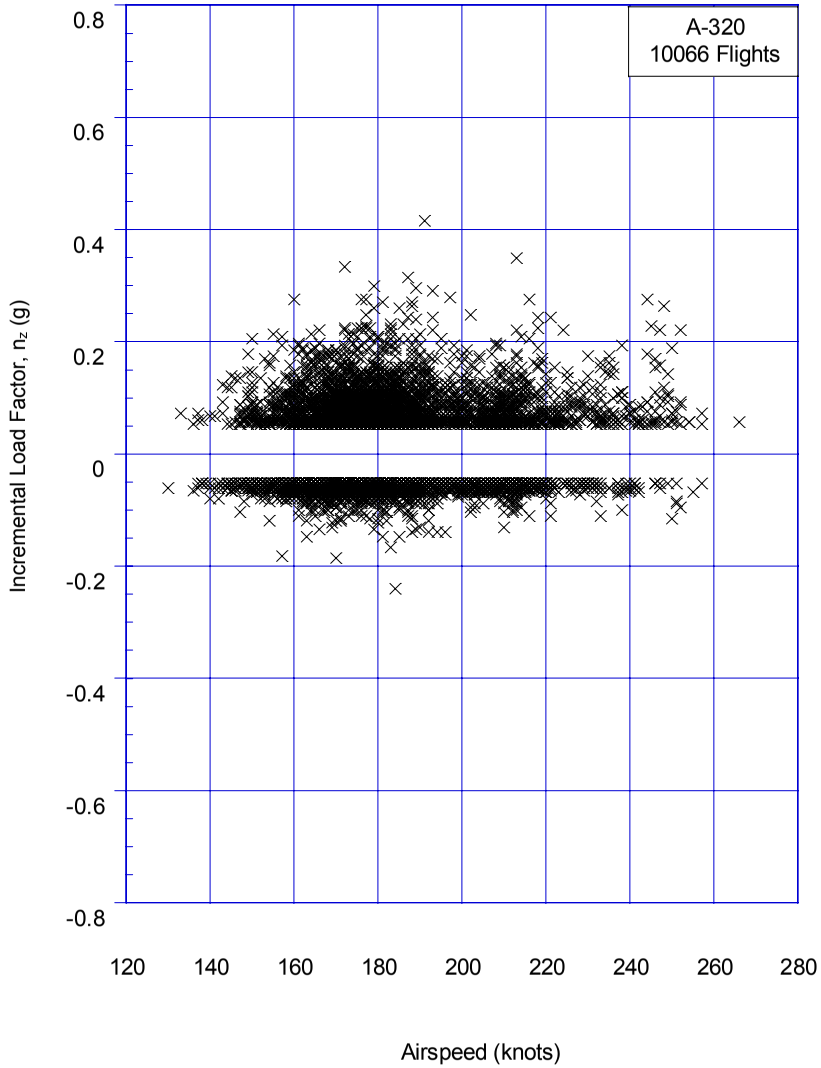


FIGURE A-113. MAXIMUM AND MINIMUM INCREMENTAL VERTICAL LOAD FACTOR VS COINCIDENT AIRSPEED AT LANDING GEAR EXTENSION

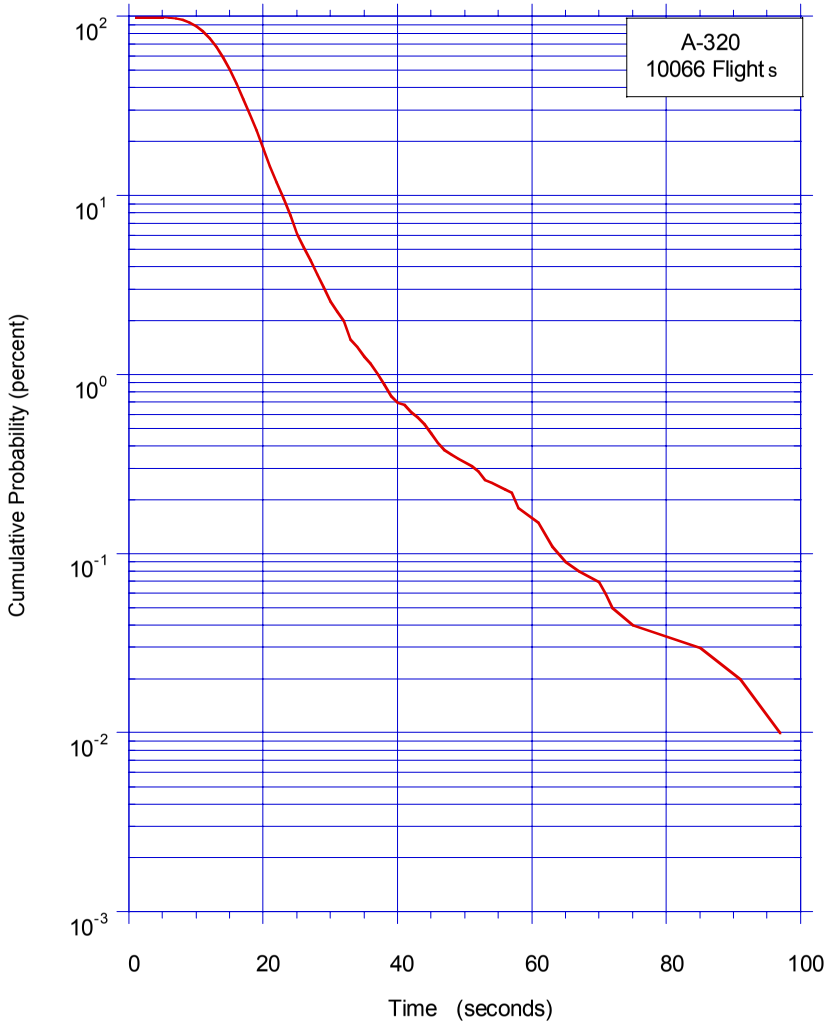


FIGURE A-114. CUMULATIVE PROBABILITY OF TIME WITH THRUST REVERSERS DEPLOYED

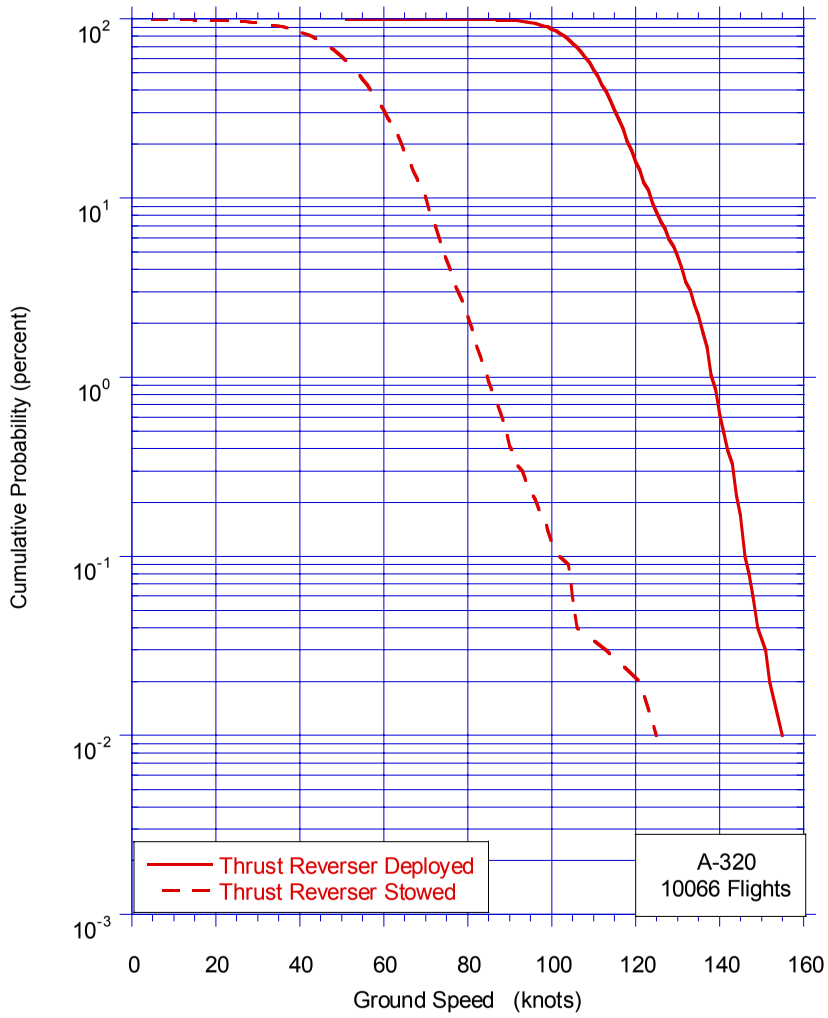


FIGURE A-115. CUMULATIVE PROBABILITY OF SPEED AT THRUST REVERSER DEPLOYMENT AND STOWAGE

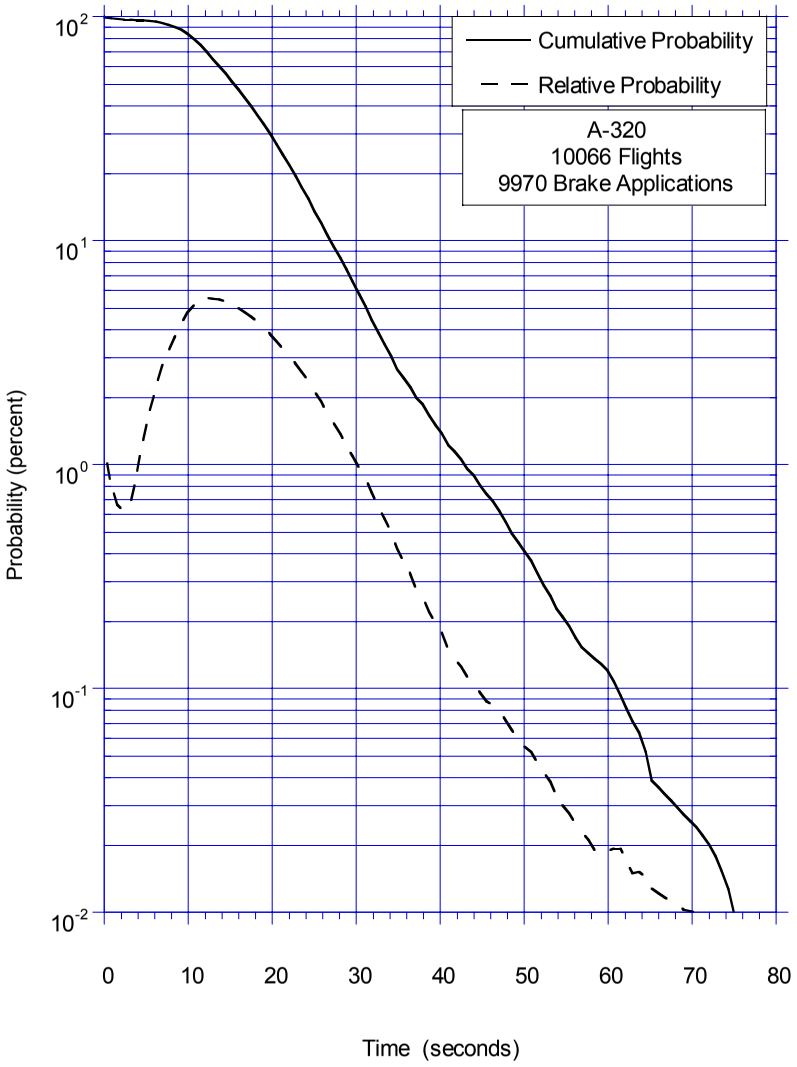


FIGURE A-116. PROBABILITY DISTRIBUTIONS OF TIME TO INITIAL BRAKE APPLICATION AFTER TOUCHDOWN

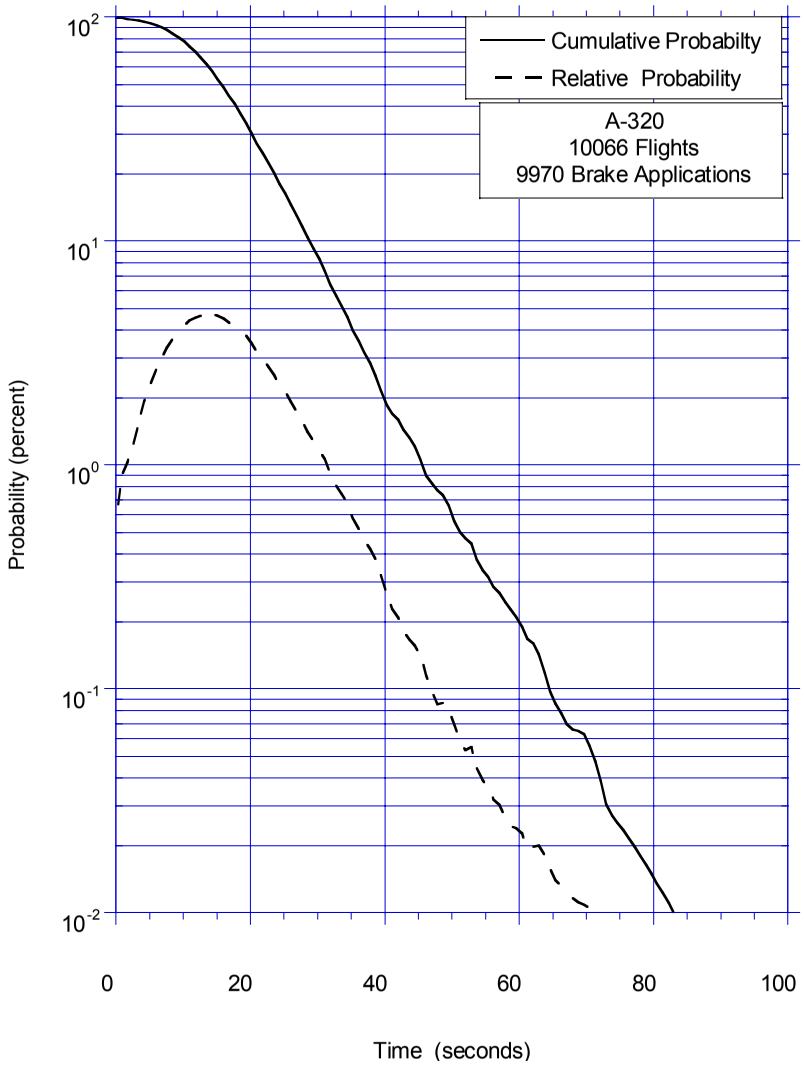


FIGURE A-117. PROBABILITY DISTRIBUTIONS OF DURATION OF BRAKE APPLICATION DURING LANDING ROLL

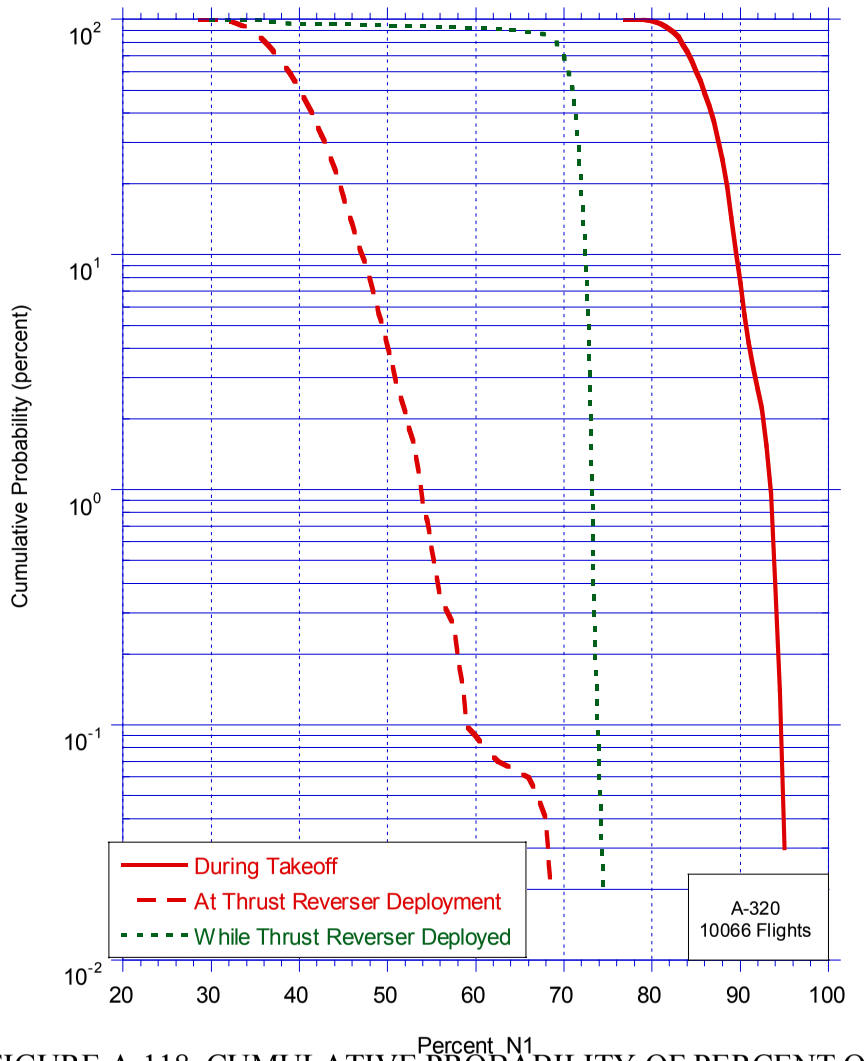
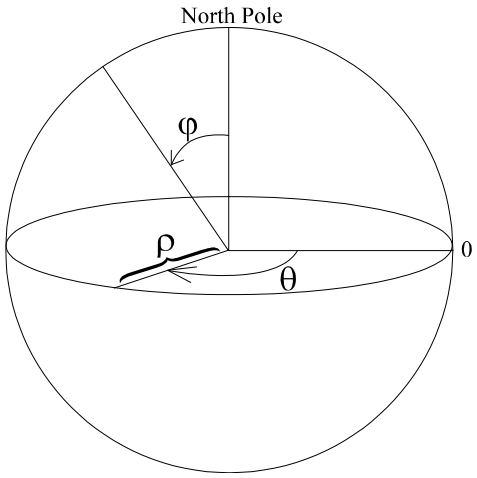


FIGURE A-118. CUMULATIVE PROBABILITY OF PERCENT OF N_1 DURING TAKEOFF, AT THRUST REVERSER DEPLOYMENT, AND DURING THRUST REVERSER DEPLOYMENT

APPENDIX B—GREAT CIRCLE DISTANCE CALCULATION



Given:

Latitude and Longitude	ρ = distance from center
of Departure and	φ = angle from North Pole
Destination Airports	θ = angle E/W of prime meridian

Procedure: (see sketch)

The standard mathematical system for spherical coordinates is shown, where three variables specify location: ρ, φ, and θ.

Let a = Great Circle Distance in angular measure.

Latitude is measured away from the Equator (0°) to the North Pole (+90°) and the South Pole (-90°); whereas in the standard spherical coordinate system, the North Pole, Equator, and South Pole lie at 0°, 90°, and 180°, respectively. Therefore,

$$\varphi = 90° - \text{latitude}$$

transforms latitude readings into equivalent angles (φ) in the standard spherical coordinate system.

Then

$$b = 90° - \text{Latitude}_{Dep}$$

$$c = 90° - \text{Latitude}_{Des}$$

where b and c are values of φ for the departure and destination locations, respectively.

Longitude is measured away from the prime meridian (0°). Longitudes to the east are positive and to the west negative. However, the standard spherical coordinate system measures its angles in the opposite direction. Therefore,

$$\theta = - \text{ longitude}$$

transforms longitude readings into equivalent angles (θ) in the standard spherical coordinate system.

Then

$$\begin{aligned} A &= (- \text{Longitude}_{Des}) - (- \text{Longitude}_{Dep}) \\ &= \text{Longitude}_{Dep} - \text{Longitude}_{Des} \end{aligned}$$

where A is the value of θ between the departure and destination locations.

The following equation, based on the spherical coordinate system, allows the computation of the Great Circle Distance, a. (Law of cosines for oblique spherical triangles)

$$\cos a = \cos b \cos c + \sin b \sin c \cos A$$

Substituting for b, c, and A from the above equalities,

$$\begin{aligned} \cos a = &\cos (90° - \text{Lat}_{Dep}) \cos (90° - \text{Lat}_{Des}) \\ &+ \sin (90° - \text{Lat}_{Dep}) \sin (90° - \text{Lat}_{Des}) \cos (\text{Lon}_{Dep} - \text{Lon}_{Des}) \end{aligned}$$

Since

$$\begin{aligned} \cos (90° - \text{Lat}_{Dep}) &= \sin \text{Lat}_{Dep} \\ \cos (90° - \text{Lat}_{Des}) &= \sin \text{Lat}_{Des} \\ \sin (90° - \text{Lat}_{Dep}) &= \cos \text{Lat}_{Dep} \\ \sin (90° - \text{Lat}_{Des}) &= \cos \text{Lat}_{Des} \end{aligned}$$

by replacement one obtains

$$\cos a = \sin (\text{Lat}_{Dep}) \sin (\text{Lat}_{Des}) + \cos (\text{Lat}_{Dep}) \cos (\text{Lat}_{Des}) \cos (\text{Lon}_{Des} - \text{Lon}_{Dep})$$

Thus a, the angular measure of the great circle arc connecting the departure and destination locations, is obtained as

$$a = \cos^{-1} [\sin (\text{Lat}_{Dep}) \sin (\text{Lat}_{Des}) + \cos (\text{Lat}_{Dep}) \cos (\text{Lat}_{Des}) \cos (\text{Lon}_{Des} - \text{Lon}_{Dep})]$$

So, for a expressed in radians

$$GCD = a \text{ radians} \left(\frac{180 \text{ deg.}}{\pi \text{ radians}} \right) \left(\frac{60 \text{ min.}}{1 \text{ deg.}} \right) \left(\frac{1 \text{nm}}{1 \text{ min.}} \right) = \left(\frac{10800a}{\pi} \right) \text{ nm}$$

and for a expressed in degrees,

$$GCD = a \text{ degrees} \left(\frac{60 \text{ min.}}{1 \text{ deg.}} \right) \left(\frac{1 \text{ nm}}{1 \text{ min.}} \right) = 60a \text{ nm}$$